National and Kapodistrian University of Athens

School of Sciences
Physics Department
Department of Environmental Physics and Meteorology

Ph.D. Thesis

Design, Development and Testing of Innovative Solar-Control Facade Systems

Tilmann E. Kuhn

Physicist (graduated at the University of Heidelberg),
born in Waiblingen, Germany

December 2015

National and Kapodistrian University of Athens

School of Sciences
Physics Department
Department of Environmental Physics and Meteorology

Supervising Committee

Prof M. Santamouris, NKUA, Supervisor
Prof C. Helmis, NKUA
Assist Prof M.N. Assimakopoulos, NKUA

Examination Jury

Prof M. Santamouris, NKUA
Prof H.-M. Henning, Karlsruhe Institute of Technology KIT
Prof C. Helmis, NKUA
Prof A. Papadopoulos, Aristotle University of Thessaloniki
Assoc Prof Aris Tsangrassoulis, University of Thessaly
Assist Prof D. Kolokotsa, Technical University of Crete
Assist Prof M. Assimakopoulos, NKUA
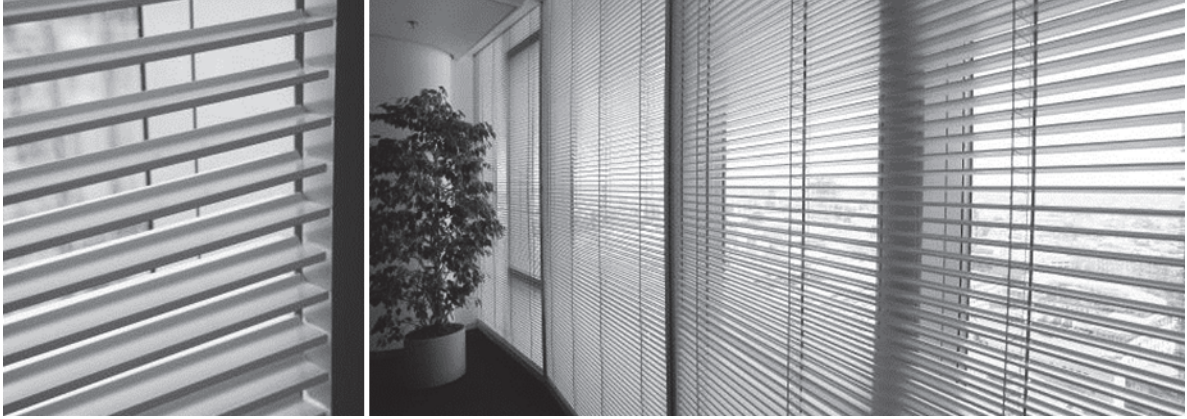
Figure 1: Internal venetian blind with 'Genius slats' in the 56-storey building Main-Tower in Frankfurt(Main), Germany. Pictures ©Warema.

Executive summary

The author of this thesis is a physicist from the Physics Department, University of Heidelberg, Germany, (1996) and is currently the head of the group Solar Facades at the Fraunhofer Institute for Solar Energy Systems ISE. In 29/2010 the Assembly of the Physics Department has appointed the supervising committee and the subject of this Ph.D. thesis entitled : Design, Development and Testing of Innovative Solar-Control Facade Systems. The supervising committee is composed by Prof. M. Santamouris (main supervisor), Prof M. Assimakopoulos and Prof C. Helmis. The experimental part of the thesis is mainly carried out in the Fraunhofer Institute for Solar Energy Systems ISE in Freiburg, Germany, while theoretical developments have been performed in close collaboration with the Laboratory of Building Energy Studies of the Physics Department under the European Research Project "Cost Effective".

The scientific subject of the thesis is related to the development, analysis and optimization of innovative solar control systems for the built environment. Solar-control systems can help to reduce the cooling energy consumption of buildings, to reduce the energy consumption of the artificial lighting system, to provide visual comfort, to ensure healthy natural lighting and to generate solar electricity and solar heat at the same time. All of these multifunctional aspects have to be assessed realistically and reliably when systems are chosen for specific buildings and when new systems are being developed. Well designed solar-control systems are therefore important elements that help to achieve the CO_2 reduction goals worldwide and especially in the European Union as defined in the Energy Performance of Buildings Directive (Directive 2002/91/EC and the recast (2010/31/EC), EPBD). It is important to note, that solar-control systems should not be regarded purely as an unavoidable energy-saving measure. Well designed solar-control systems can also contribute positively to the architecture of the buildings and to the well-being of the users. This thesis aims to contribute to achieving these goals by increasing the reliability of the corresponding performance assessment and by providing attractively designed high-performance solar-control systems.

This thesis comprises the **further development of performance criteria for solar-control systems**. The main contribution is the introduction of the "effective g-value g_{eff}", which is the first product characteristic that includes not only the static properties of the solar-control system but also the control, which is essential for a realistic performance evaluation. It is important to note that the "center-of-glazing" property g_{eff} is independent from the specific building. It only depends on the orientation and location and can therefore be used for a general performance characterization within a specific climatic zone. Another contribution is the new criterion for the color rendering of objects in the room, seen from an observer outside the building $Ra_{\text{out-in}}$. This performance aspect was not considered quantitatively until now. Contributions to performance criteria for BIPV or BIST solar-control systems with active photovoltaic or solar thermal energy conversion have been made, which also includes life-cycle-cost aspects. The chapter on performance criteria represents the background of the candidate for his contributions to the European Standards EN14500 (Blinds and shutters - Thermal and visual comfort - Test and calculation methods), and EN14501 (Blinds and shutters - Thermal and visual comfort - Performance characteristics and classification).

A **methodology for calorimetric g-value measurements** has been developed. The detailed documentation of this methodology together with the analysis of the measurement uncertainty was a major contribution the international standard ISO/CD 19467 (Thermal performance of windows and doors - Determination of solar heat gain coefficient using solar simulator). The author has contributed to the content of this standard with these results as a member of the committee ISO/TC163/SC1/WG17. The error analysis takes into account error contributions from differences between lab conditions and reference conditions, systematic biases due to imperfect sensor calibration and statistical errors. It also includes methods for the correction of significant differences between reference conditions and lab conditions.

The **mathematical-physics modeling of the interaction of the solar radiation with the building skin** is major part of the thesis. It ranges from the modeling of the transmission of daylight and the modeling of secondary heat gains to the modeling of photovoltaic or solar thermal energy conversion. This includes the modeling of the performance of the facade component itself (modeling of g_{eff}) and the modeling of the performance of the facade component in the building context (black-box model and virtual transparent solar thermal collector as component for dynamic building simulation programs).

Evaluation criteria for solar control systems have been further developed by introducing the **new criterion $Ra_{\text{out-in}}$** for color rendering of objects in the room, illuminated by daylight and viewed by an observer outside the building. The background for this new criterion is that it would be advantageous if the color of human skin were to be rendered with high quality when people are looking indoors from outdoors, so that occupants of a room do not look pale or ill. Color rendering of objects in the room viewed by an observer who is outdoors is also relevant for other cases such as internal "white venetian blinds" which are white for observers in the room and which should also appear white when the observer is outside. Instead, white venetian blinds often look greenish from the outside when they are mounted behind spectrally selective solar-control glazing and they are therefore sometimes rejected and replaced by less efficient blinds with gray slats. Application of the new criterion for several solar control systems showed that the quality of color rendering is lower in almost all cases, when the observer is looking from outdoors into the room. The difference is significant in many cases

Figure 2: The shape of the rods of the new stainless steel blind s_enn® has been developed by the author of this document, who is co-inventor of this system. Pictures ©clauss-markisen.

and can be much larger than 25%, with the effect that the quality of the color rendering changes from "very good" to "good" or it loses the attribute "good". The new criterion can therefore help to optimize the facade with respect to both, the solar-control performance and user acceptance.

The thesis provides a **detailed overview on the state of the art of solar-control systems including active solar energy conversion together with a general analysis of the design parameters for solar control systems**. Then it presents 6 new solar-control systems which have been invented and further developed with strong contributions of the author of this thesis. Some of them received national and international innovation prices and/or have been installed by famous architects in very large buildings. The patent list in the bibliography of the submitted document provides an overview on concepts for solar-control systems that have been invented or co-invented by the author of this thesis.

One of these systems is the **new stainless steel blind** s_enn®. The shape of the rods of the stainless steel blind s_enn® has been developed by the author, who is a co-inventor of this system. The system selectively shields certain regions of the sky. This leads to very good solar control and a transparent appearance while direct insolation of the room and the associated glare is prevented in most cases. This solar-control system has been used by several famous architects, e.g. by Murphy/Jahn (Chicago) for the building "Horizon Serono" in Geneva, where 6.500 m^2 of this blind have been installed in 2004.

The author is a co-inventor of an innovative venetian blind which is presented in chapter 7.3. The **special shape of the 'Genius slats'** of this new blind ensures good sun-shading properties which are relatively independent of the actual setting of the slat angle over broad ranges, which ensures robust performance despite so-called 'faulty operation'. The top-side is white with a high solar and light reflectance for good solar-control and light re-directing properties. The bottom side is light gray in order to reduce the luminance on the inner side of the screen for improved glare protection. Both side are matt with little gloss in order to minimize irritating light reflections and glare. The special shape provides people from looking onto the directly irradiated bright area on the top side of the slat, since this area is shielded in many cases by the "ridge" in the middle of the slat. Venetian blinds with this slats have been installed e.g. in the Roche-Tower, Basel, Switzerland. They also have been installed in the

Main-Tower in Frankfurt (Main), Germany, where the original internal venetian blinds with mirror-finished surface have been replaced since 2008 step by step by venetian blinds with 'Genius slats' in order to avoid overheating. The performance of the 'Genius slats' has been compared in detail with mirror-finished slats on the basis of the newly developed criterion g_{eff}.

The thesis presents a **daylighting roller shutter** which has been developed by the author of this thesis. It consists of translucent horizontal laths that are connected by hinges and can be retracted by a roller at the top. The laths are made of extruded polycarbonate. The inner and outer surfaces are transparent while the internal bars are translucent white. The translucent bars block the direct radiation. The new roller shutter is intended to be used in all offices or rooms, except bedrooms instead of conventional roller shutters. The idea behind the development is that the darkening function of conventional roller shutters is not needed in these cases and that the daylighting function of conventional roller shutters is very poor.

Additionally, the thesis presents **translucent slats for large scale external solar-control systems** which were co-invented by the author of this thesis. Each slat has a transparent ellipsoidal cover and integrated translucent and opaque sections to enhance the daylighting and glare-protection functionality. The slats have similar performance to the laths of the daylighting roller shutter. They are also made of extruded polycarbonate. The idea is to mount them externally on the facade of a building in front of and/or above the windows, preferably on south-oriented facades. They then provide solar-control and in some cases also glare protection. The advantage of the slats in comparison to conventional aluminum slats is the diffuse daylight transmission and the drastically reduced weight.

The new **angle-selective transparent BIPV-system PVShade®** was invented by the author of this thesis. This multifunctional facade system generates photovoltaic electricity and simultaneously provides solar-control and glare protection. It is especially designed to be used in the sill area of completely glazed facades. This area has very little effect on the daylighting conditions in the room. It therefore can be equipped with a static solar-control system in order to generate PV electricity and to reduce the cooling load of the building at the same time.

A new **angular selective transparent solar thermal collector** is presented which was co-invented by the author of this thesis. The basic idea is to introduce openings with angle-selective transmittance into an absorber and to integrate the absorber within a sealed glazing unit or a closed-cavity facade. The facade cavity with the absorber is continuously flushed with a very low flux of dry air in the case of closed-cavity facades. The multifunctional facade elements allow visual contact to the exterior, provide solar and glare control and generate useful solar thermal heat gains. In summer, during the cooling season, the collector is intended to be used as a heat source for thermally driven cooling systems or desiccant de-humidification systems. Desiccant de-humidification systems are particularly interesting since commercially available systems can already be operated at relatively low temperatures of e.g. $55°C$. The importance of de-humidification will increase, since energy-efficient cooling systems like thermally activated building systems (TABS) usually lower the temperature of the ceiling and since condensation has to be avoided under all circumstances. During the heating season the collector is intended to be used as a renewable heat source for low-temperature heating systems, like floor-heating systems.

Contents

Nomenclature

Angle definitions (numerical values of angles are specified in degrees throughout this thesis):

γ	facade orientation ($0°$:= south, west positive)
γ_s	solar azimuth angle ($0°$:= south, west positive)
γ_f	$\gamma_f := \gamma_s - \gamma$ (facade azimuth angle, $0°$ parallel to facade normal)
α_s	solar altitude angle
α_p	solar profile angle $\quad \alpha_p[\alpha_s, \gamma_f] = \arctan\left(\frac{\tan(\alpha_s)}{\cos(\gamma_f)}\right)$ [55]
α_{in}	angle of incidence $\quad \alpha_{in}[\alpha_s, \gamma_f] = \arccos\left(\cos(\alpha_s)\cos(\gamma_f)\right)$ [55]
β_k	tilt angle of the slats of a venetian blind or - in the case of facades with switchable properties - a parameter field which characterizes the switching state

Properties of glazing and blind:

$\mathcal{A}^x_{y, d, e\ z}$	$\mathcal{A} = [\ \tau\ /\ \rho\ /\ \alpha\ /\ g\ ]$ for transmittance / reflectance / absorptance / g-value (g-value = SHGC or Solar Factor or Total Solar Energy Transmittance TSET)]
	x = [$'$ / blank] when [radiation is incident on the indoor surface / otherwise]
	y = [e / v] for [solar / light] properties
	d = [$_{dif}$ / blank] for [diffuse irradiation / otherwise]
	e = [$_{eff\text{-}m}$ / $_{eff\text{-}h}$] for [monthly / hourly] effective (average) values
	z = [$_{gzg}$ / $_{bld}$ / $_{tot}$ or nothing] for [glazing / blind / combination]
λ	wavelength [nm] for spectral properties $\Rightarrow \mathcal{A}^x_{\lambda, d, z}$ or $\mathcal{A}^x_{d, z}[\lambda]$ respectively

Thermal properties:

U	U-value
$\mathbf{q}$	heat flux vector ($[W/m^2]$ resulting from radiative, convective or conductive heat transfer)
Q	heat flow rate ($[W]$ resulting from radiative, convective or conductive heat transfer)
R_x	x = [e / i] for [external / internal] convective and radiative surface heat transfer resistances and [s] for the thermal resistance of the sample. $1/U = R_e + R_s + R_i$
$h_x := \frac{1}{R_x}$	convective and radiative surface heat transfer coefficients
λ	thermal conductivity. The same greek letter λ is used for *wavelength* and *thermal conductivity* since this corresponds with the conventions in international standards and since it is improbable that they will be confused with each other.

Temperatures:

T_{int}	temperature indoors (internal/interior), behind the facade
$T_{int, rad}$	radiative temperature indoors, behind the facade
$T_{int, air}$	air temperature indoors, behind the facade
T_{ext}	temperature outdoors (external/exterior), in front of the facade
$T_{ext, rad}$	radiative temperature outdoors, in front of the facade
$T_{ext, air}$	air temperature outdoors, in front of the facade

2

Other:

A	area $[m^2]$
E	irradiance $[W/m^2]$ (Energy per unit area per unit time resulting from incident radiation)
:=	the equation defines the property on the left side of ":="
$\doteq$	the equation is a first order approximation

Examples using the nomenclature defined above

$\rho'_{v,\,\text{dif, gzg}}$	Diffuse light reflectance of the indoor surface of glazing without blind
$\rho'_{\text{gzg}}[\lambda]$	Spectral reflectance of the indoor surface of glazing without blind
$\alpha_{\text{tot}}[\alpha_s, \gamma_\text{f}]$	Total absorptance in the facade
$g_{\text{tot}}[\alpha_s, \gamma_\text{f}]$	Total Solar Energy Transmittance g of glazing and blind
$g_{\text{gzg}}[\alpha_{\text{in}}]$	Total Solar Energy Transmittance g of glazing without blind

1 Abstract

This thesis deals with performance criteria and measurements for the evaluation of solar-control systems. It also presents methods for the mathematical-physical modeling of the interaction of solar irradiation with the building skin, it provides an overview on the state of the art of solar-control systems and it introduces six new solar-control systems which have been invented and further developed with contributions of the author. A new methodology for calorimetric g-value measurements has been developed. The author contributed to the new international standard ISO/CD 19467 on g-value measurements on the basis of these results. Another major contribution is the introduction of the "effective g-value g_{eff}", which is the first product characteristic that includes not only the static properties of the solar-control system but also the operation/control strategy, which is essential for a realistic performance evaluation. The "center-of-glazing" property g_{eff} is independent of the specific building. It only depends on the orientation and location and can therefore be used for general performance characterization within a given climatic zone. Another contribution is the new criterion for the color rendering of objects in the room, seen from an observer outside the building $Ra_{\text{from outside}}$. This performance aspect was not considered quantitatively until now. Contributions to performance criteria for BIPV or BIST solar-control systems with building integrated photovoltaic or solar thermal energy conversion have been made. The mathematical-physical modeling of the interaction of the solar radiation with the building skin ranges from modeling of the transmission of daylight and the modeling of secondary heat gains to the modeling of photovoltaic or solar thermal energy conversion. This includes the modeling of the performance of the facade component itself (modeling of g_{eff}) and the modeling of the performance of the facade component in the building context.

Keywords: solar heat gain coefficient, g-value, total solar energy transmittance, TSET, solar factor, solar simulator, stationary, steady-state, calorimetric measurement, secondary inward flowing fraction, $SHGC$, g, q_i, passive solar gains, complex glazing, building-integrated, PV,

solar thermal collector, BIPV, BIST, dynamic facade, complex glazing, complex fenestration system, heat flux sensors, hot box, cooled plate, cooled box.

2 Background to this thesis

Solar-control systems can help to reduce the cooling energy consumption of buildings, to reduce the energy consumption of the artificial lighting system, to provide visual comfort, to ensure healthy natural lighting and to generate solar electricity and solar heat at the same time. All of these multifunctional aspects have to be assessed realistically and reliably when systems are chosen for specific buildings and when new systems are being developed. Well-designed solar-control systems are therefore important elements that help to achieve the CO_2 reduction goals worldwide and especially in the European Union as defined in the Energy Performance of Buildings Directive (Directive 2002/91/EC and the recast (2010/31/EC),EPBD). It is important to note, that solar-control systems should not be regarded purely as an unavoidable energy-saving measure. Well designed solar-control systems can also contribute positively to the architecture of the buildings and to the well-being of the users. This thesis aims to contribute to achieving these goals by increasing the reliability of the corresponding performance assessment and by providing attractively designed high-performance solar-control systems.

3 Introduction

The multi-functional performance of solar-control facade systems is determined by the interaction of several physical effects. The phenomenological discussion of these effects serves as an introduction and as a basis for the modeling and measurement chapters 5 and 6.

- **Transmission, reflection, refraction and absorption of solar radiation:** Transmission, reflection, refraction and absorption of radiation are the fundamental effects underlying all solar-control systems. These first-order effects initiate many other physical effects. These effects are often highly sensitive to the direction, spectral distribution and polarization state of the incident radiation. The reflected and transmitted light can be scattered or re-directed. In the case of nano-structured or micro-structured surfaces, it is important to consider the relation between the size of the structure/film thickness and the wavelength of the incident radiation.

- **Incidence-angle symmetry for glazing units and many other materials (Rotational symmetry with respect to the normal to the facade plane):** When the solar-control properties of glazing are required, the sun is usually high in the sky and the main share of the irradiation impinges on the facade with high angles of incidence. The performance of the glazing for off-normal angles of incidence is therefore very significant. The angular variation of the transmittance and the reflectance is determined only by the angle of incidence. It is relevant to note that the angular dependence of
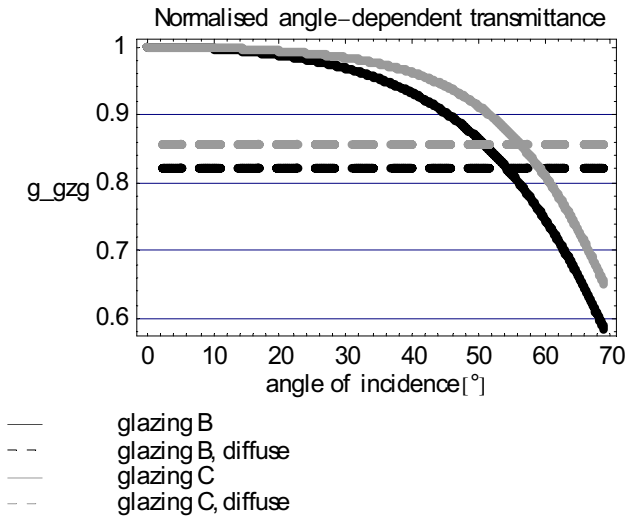
Figure 3: Normalized directional-hemispherical and diffuse-hemispherical transmittance for two different DGUs (double glazing units) [10].

the transmittance of insulating glazing units (IGUs) not only depends on the number of panes but also on the coating type [104], [79] and [10]. This is illustrated in figure 3.

- **Profile angle symmetry for horizontal 2D structures:** "Horizontal 2D structures" are defined as structures created by projection of a 2D cross-section in a horizontal direction within a plane parallel to the facade. Common examples are overhangs and venetian blinds. The seasonal variation of the position of the direct sun can be used to optimize the performance of facades equipped with such structures, by blocking the direct sun only during the cooling season. In the case of of horizontal 2D structures, the solar profile angle α_p can be used to simplify the 2-dimensional parameter field of the solar altitude angle α_s and the facade azimuth γ_f. It is important to note that horizontal 2D structures are well adapted only for south facing facades. For other orientations, the projection direction of the 2D cross-sections should be inclined [84]. For systems made of light-refracting materials (e.g. transparent glass-slats or prismatic structures), the profile-angle symmetry is no longer valid, because of the combined effects of refraction and the geometrical form of the structure, where the refraction varies with the angle of incidence α_{in} on the outer surface. In strict mathematical terms, this means that the profile-angle symmetry is also not valid for venetian blinds with colored slats, since light which is reflected by the slats also contributes to the solar transmittance and since the reflectance of the colored slats in general depends on the angle of incidence on the slat surface. However, this is only a second-order effect and the profile-angle symmetry is therefore a good and helpful approximation in the case of venetian blinds in most cases [10]. Figure 4 illustrates the difference between profile-angle symmetry and incidence-angle symmetry.

- **Light-scattering and light re-directing layers and surfaces** can have constant, switchable or self-adapting properties. Scattering layers are translucent or opaque. To
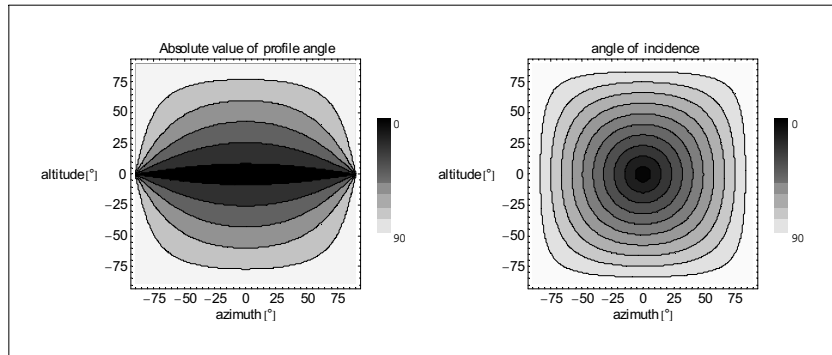
Figure 4: Difference between profile angle symmetry and (rotationally symmetric) incidence angle symmetry.

Figure 5: Examples of structured solar glass panes that have been investigated in round-robin tests within the framework of the International Commission on Glass ICG/TC10 [6]. The images in the lower two rows show that the angular distribution of the scattered light may differ depending on the position of the light beam on the sample which makes accurate measurements more difficult. See also http://www.icg-tc10.org. Picture ©ICG-TC10.

achieve a non-transparent appearance, where objects cannot be identified behind the layer, it is not necessary to scatter a large portion of the incident radiation. Some translucent layers therefore have little effect on the passive solar gains (g-value), they mainly create haze. The most important figure for the effect on passive solar gains is the fraction of back-scattered radiation. Rayleigh scattering by single molecules or air particles which are much smaller than the wavelength of the incident radiation creates the polarized blue skylight. Scattering processes by objects which are much larger than the wavelength of the incident irradiation follow the rules of geometrical optics. Other examples of scattering surfaces with characteristic dimensions larger than the wavelength of the incident radiation are patterned glass panes (see for example figure 5). The intermediate range, where the wavelength and the scatterer dimensions are similar, is described by Mie scattering (see e.g. [91]).

- **Thermal heat transfer within the facade:** Within the building skin, heat is transferred from one point to another by convection, conduction and thermal radiation (IR). The effective heat transfer is the sum of all of these transfer modes. In general, the effective thermal conductivity λ_{eff} depends on the temperature because of the temperature dependence of the underlying heat transfer mechanisms. It has to be taken into account that many materials are IR-transparent when they are thin, which is especially true for polymer materials. It is known that the effective thermal conductivity is thickness-dependent in the case of components that are composed of such IR-transparent sub-structures e.g. thin layers of polystyrene foam or transparent insulation materials. This thickness dependence is significant when the thickness of the material is similar to the *heat penetration depth* of the thermal radiation [99]. In the case of anisotropic solids, e.g. graphite, the thermal conductivity can be directionally dependent. An overview of the different heat transport modes is displayed in figure 6. The resulting insulation properties of building materials are compared in figure 7.

- **Thermal heat transfer to the surroundings:** The heat transfer from the facade to the external environment and the heat transfer from the facade to the room affects the solar-control properties of the facade. This can be seen for example in the simple case of a single-glazed window with a dark coated glass pane, where the inward flowing fraction of the absorbed radiation strongly depends on the internal and external wind conditions. The heat is transferred by convection/conduction and by thermal radiation. The heat transfer to the inside is dominated by radiation with typical values of 65% radiative heat transfer and 35% convective heat transfer (see chapter 6.1.3). The heat transfer to the exterior environment is dominated by convection with a typical share of 60% - 80% for the convective part of the heat transfer (see also chapter 6.1.3). Neither effect is *not* independent of the facade properties. Because of the radiative component, it is clear that the external and internal radiative heat transfer depends strongly on the internal and external emissivity of the facade $\varepsilon_{f,i}$ and $\varepsilon_{f,e}$. But the influence of the roughness and macroscopic geometrical patterns of the facade surface on the convective heat transfer is often neglected in product comparisons and product ratings, for example in the current standards for facade characterization (e.g. [58], [62] or [73]) and it is also neglected in current building simulation programs. But it is clear that the roughness effect is intrinsically included in calorimetric measurements of the g-value of the facade where test wind conditions are adjusted in the way that they correspond with standard heat transfer conditions on flat surfaces (see also chapter 5.1). In the discussion of the heat
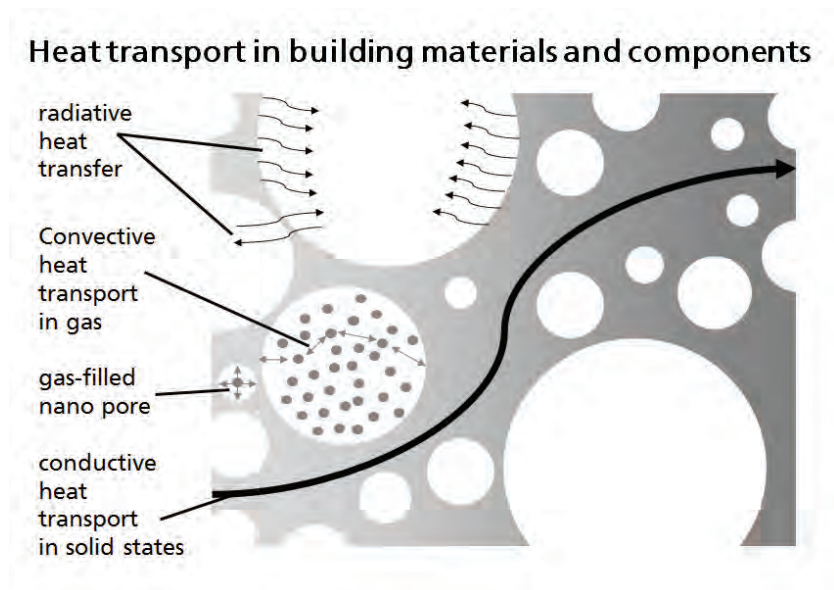
Figure 6: Heat transport phenomena in building materials: Thermal conduction via the solid skeleton/solid pore walls (blod black arrow), thermal conduction via the filling gases (small arrows) and thermal radiation heat transfer between the pore walls and through the pore walls in case of IR-transparent materials (curved arrows). In nanopores, with diameters comparable to or smaller than the mean free path of the air particles, the particles mainly interact with the pore walls and not with each other, which drastically reduces the thermal conductivity (Knudsen effect). A simplified version of this figure (without IR transparency and without nanopores) has already been presented in [36].

Thermal conductivity λ_{eff} [10^{-3} W/(m · K)]	0	5	10	15	20	25	30	35	40	45	50
filling gas air, not nanopourous											
Foam glass									⎯⎯⎯⎯		
Rockwool								⎯⎯⎯⎯			
Polystyrene foam							⎯⎯⎯⎯				
Heavy filling gases, not nanopourous											
Polyurethane foam					⎯⎯⎯⎯⎯⎯⎯						
Nanopourous, air filled											
Organic nanofoam				⎯⎯⎯⎯⎯							
Aerogel			⎯⎯⎯⎯⎯⎯								
Evacuated insulation panels		⎯⎯⎯⎯⎯⎯									
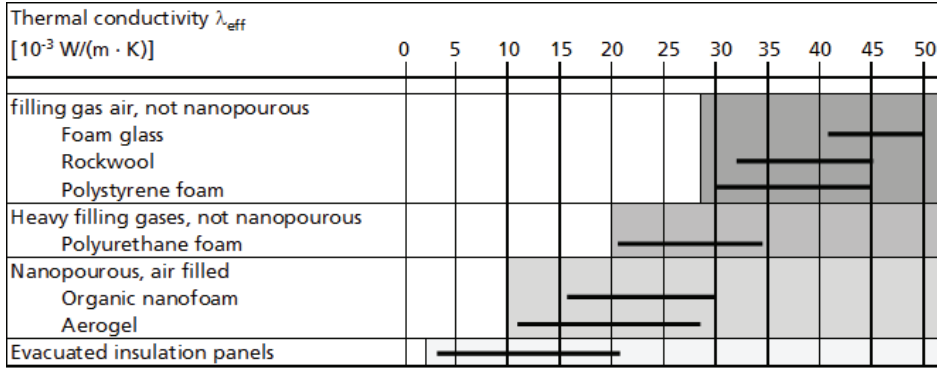
Figure 7: Effective thermal conductivity λ_{eff} of different building materials. Air-filled materials with macroscopic pores have $\lambda_{\text{eff}} \geq 0.030 W/m^2 K$. With filling gases heavier than air, the effective thermal conductivity can be reduced to $\lambda_{\text{eff}} \approx 0.022 W/m^2 K$. Further reduction can be achieved with nanoporous materials, where the size of the pores is smaller than the mean free path length of the filling gas under atmospheric pressure. This means that with pore-dimensions of less than some tenths of a micrometer $\lambda_{\text{eff}} \approx 0.015 W/m^2 K$ can be reached for example in aerogels. Further reduction can be achieved in vacuum insulation panels (VIP) where the pressure of the filling gas is reduced in order to minimize the mean free path length and therefore the thermal conductivity of the gas-fill. In VIPs the effective thermal conductivity can be reduced to $\lambda_{\text{eff}} \approx 0.002 W/m^2 K$ in the center of the material excluding edge effects.

transfer from the facade to the environment and the room it is important to distinguish between typical heat transfer conditions to be used for location independent product characterization and location specific heat transfer conditions for a specific facade in a specific building at a specific location to be used for the prediction of the performance of one concrete building.

- **Photovoltaic energy conversion (PV)** Absorbed energy can be converted into electricity with PV cells. The fraction of the absorbed energy that is converted into electricity does not contribute any more to the heating of the building skin. It has to be taken into account that the efficiency of the cells is temperature-dependent and that the actual operation mode of one cell is determined by the overall system operation (e.g. MPP tracking by the inverter). The overall system operation point is determined by the irradiation and shading conditions on the other cells and the electrical circuit configuration of the PV system, including the bypass and blocking diodes between the cells and modules. In the case of thin-film solar cells, seasonal variations of the efficiency caused by light soaking, annealing and other internal effects should also be taken into account. A detailed discussion can be found in [20], see also chapters 4.9 and 6.4

- **Extraction of heat with solar thermal collectors:** Solar thermal collectors can extract a share of the energy absorbed by the building skin. This lowers the passive solar gains and has to be taken into account in the room energy balance, especially in the case of low thermal insulation levels (high u-values). Heat transfer media can be liquid (e.g. water or water-glycol) or gaseous (e.g. air). In many cases, liquid heat transfer media may evaporate when the system is not operated while the irradiation level is high

www.cost-effective-renewables.eu

EUROPEAN / European / 7th Framework
COMMISSION / Research Area / Programme
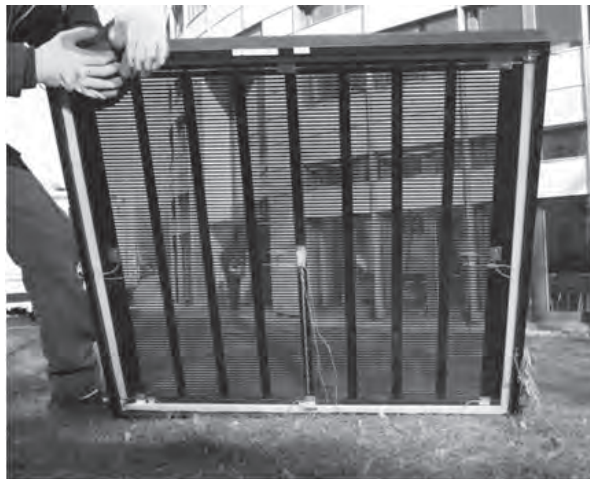
Figure 8: Prototype transparent solar thermal collector, developed in the European research project Cost-Effective. For details see chapter 7.6. Photo © Fraunhofer ISE

(= stagnation conditions). A stagnation-safe system configuration has to consider this effect. It is important to note that the solar-control properties of a glazing integrated solar thermal collector depend on the operation mode of the system: When the system is not operated (stagnation), no heat is extracted, which leads to absorber temperatures of typically more than 100°C. When the collectors are used for solar heating they can be operated with absorber temperatures of e.g. 45°C. This has an impact on the inward flowing fraction of the absorbed solar radiation (the secondary internal heat gains). The total solar energy transmittance g can therefore vary to a large amount. In case of the newly developed solar thermal collectors (see figure 8 and chapter 7.6), developed in the the EU research project Cost-Effective[1] it has been shown [17], that the g-value can vary by a factor of two because of this fact depending on the operation mode (see also figure 56 on page 127).

---

[1]see also http://www.cost-effective-renewables.eu. The research project has been co-ordinated by the author.
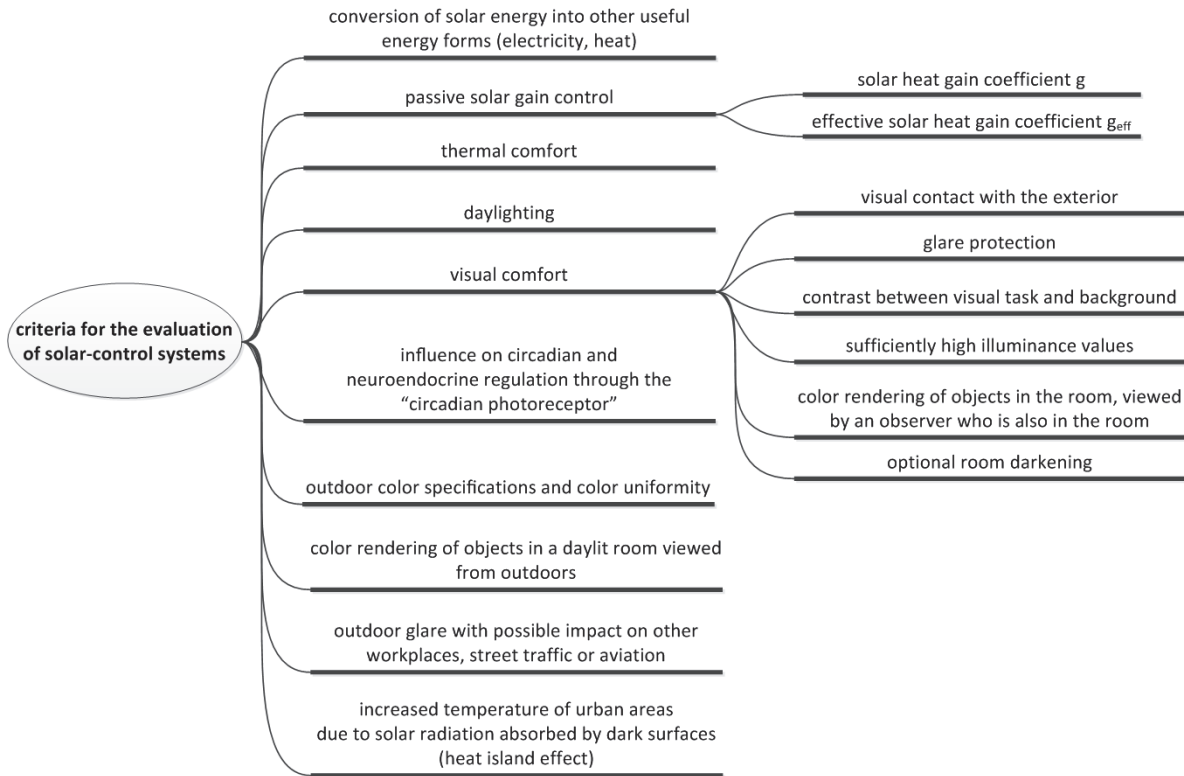
Figure 9: Evaluation criteria for solar-control systems.

4 Performance criteria for solar-control systems

Transparent components are essential to the design and performance of a building. They influence its indoor comfort and energy budget in many diverse ways [13]: daylight illuminates indoor rooms throughout the year [32], solar energy can be used to heat buildings passively, excessive solar gains can cause glare and overheating, transparent areas allow visual contact with the exterior and the transparent areas are also important for the architectural appearance of a building. The following sub-sections are providing an overview on the different criteria which are relevant for the evaluation of solar-control systems for the building skin. The criteria are summarized in figure 9.

4.1 Criteria for passive solar gain control

Passive solar gains, transmitted through the facade, are determined primarily by:

- the size of the glazed areas
- the orientation of the glazed areas with respect to the sun
- external obstructions by surrounding buildings and trees

- the insulation properties of the facade system (U-value)

- the solar heat gain coefficient g of the complex fenestration system / facade system

- the operation of the facade system.

The first three items are building-related / architectural criteria which are not discussed further in this chapter. The amount of heat which enters modern buildings by thermal heat transfer through the envelope is usually small in the summer/cooling season due to the small temperature differences in summer and the level of thermal insulation which is already common in many countries. Conductive gains may still be relevant in warmer climates with less need for thermal insulation. The solar heat gain coefficient g is defined and explained in chapter 4.1.1. Chapter 4.1.2 provides the criterion g_{eff} with which the operation mode or control strategy can be taken into account when the performance of passive solar gain control is evaluated.

4.1.1   Solar heat gain coefficient g

The solar heat gain coefficient g is the fraction of the incident solar radiation that enters a room after passing through the building skin, it quantifies the passive solar thermal gains. In other words: A solar heat gain coefficient of $g = 0.3$ means that 30% of the incident radiation enters the room in the form of transmitted radiation or as secondary heat gains due to the inward flowing fraction of the radiation that has been absorbed in different layers of the building skin. g therefore consists of two parts, the solar transmittance τ_{e} and the secondary internal heat transfer factor q_{i}. Figure 10 illustrates this. These solar gains passively heat the room, which is desired during the heating season and unwanted in the case of summer conditions. g is therefore a key parameter for minimization of the building's energy consumption and for correct dimensioning of the heating, ventilation and air-conditioning system (HVAC). g can be used to characterize transparent, translucent or opaque building components with or without integrated active solar energy conversion technologies such as building-integrated PV systems (BIPV) or building-integrated solar thermal collectors (BIST). Several names are used internationally for g: it is called the "solar heat gain coefficient (SHGC)", "g-value", "total solar energy transmittance (TSET)" or "solar factor". All of these terms are used synonymously in this thesis. From autumn 2016, it will be mandatory to include a statement on the solar-control performance in the CE labeling of all retractable solar-control systems as specified in EN13561 [63] and EN13659 [64]. The performance class to be stated in the CE conformity declaration is defined in EN14501 [2]. The determination of the performance class is based on the effect of the solar-control system in combination with a certain reference glazing as specified in EN14500 [1]. g can be used to describe the properties of the facade/roof as a whole, of parts of it (e.g. windows) or of sub-components (e.g. insulating glazing units (IGU)). For the case of components or combinations of components (e.g. combinations of glazing and venetian blind) it is important to know the *"center of glazing" value* which excludes the influence of frames, lateral losses and spacers at the glazing edges. The "center of glazing" value is especially meaningful since it is independent of the glazing area and therefore generally valid [14]. In many cases the influence of the frame etc. can be taken into account in a second step by calculation methods such as [74] or [31].
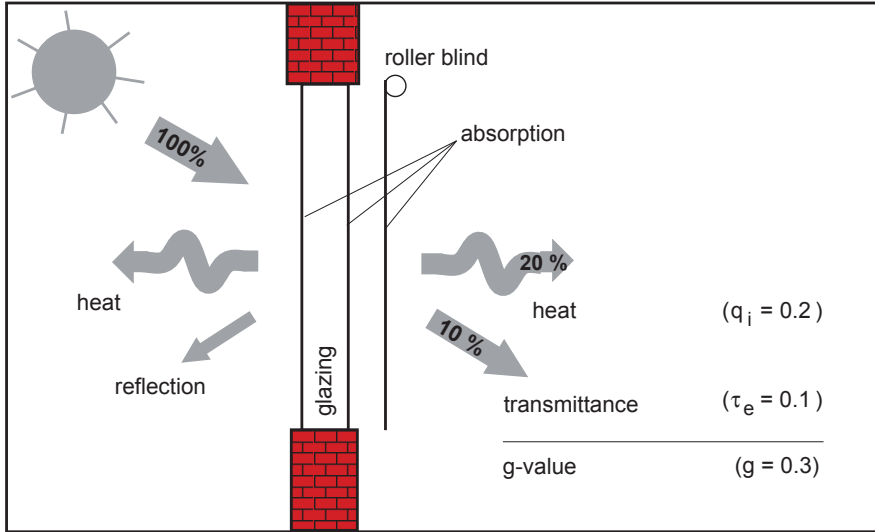
Figure 10: The meaning of the solar heat gain coefficient g. g is the sum of the solar transmittance τ_e and the secondary internal heat transfer factor q_i [8].

It is important to understand, that g is not a material constant. g is *influenced by several boundary conditions* such as the external and internal heat transfer (governed mainly by the wind conditions), the spectrum of the incident radiation and the internal and external temperature. The goal of measurements or calculations is to determine g for a certain set of reference boundary conditions. These reference boundary conditions can be national or international reference conditions for product comparisons or product ratings. However, the reference conditions can also be special conditions valid for a specific building and location under consideration. An example of special conditions are the very windy conditions in higher stories of some high-rise buildings.

The general quantity , $g_{\text{whole window}}$ for the whole window including frames is defined by the following equation:

$$g_{\text{whole window}} := \frac{Q_{\text{with sun}} - Q_{\text{without sun}}}{A_{\text{ref}}\, E_{\text{ref}}} \tag{1}$$

where $Q_{\text{with sun}}$ or $Q_{\text{without sun}}$ is the heat flow rate [W] through the window with or without sun, respectively. A_{ref} is the window area including frames. E_{ref} is the irradiance on the facade. The boundary conditions "without sun" are identical to the conditions with sun with the only difference that $E_{\text{ref}} = 0\ W/m^2$. The center of glazing (cog) value of g is defined by:

$$g := \frac{q_{\text{with sun}} - q_{\text{without sun}}}{E_{\text{ref}}} \tag{2}$$

where $q_{\text{with sun}}$ or $q_{\text{without sun}}$ is the heat flux density $[W/m^2]$ through the center of the glazing with or without sun, respectively. This document focuses mainly on the center of glazing value. g can either be measured directly (see chapter 5.1) or calculated based on the properties of the individual layers and components of the facade (see chapter 6). The fundamental differences between the two methods are described in table 1. Very often, a combination of calorimetric measurements and model calculations is appropriate for an efficient and reliable characterization of g.

Table 1: Comparison of different methods to determine the solar heat gain coefficient g.

	Calorimetric measurement	Calculation methods
Advantages	**Direct measurement** without model assumptions. g is therefore well defined also for very complex fenestration systems	When the model has been prepared and validated, the effect of modifications can be assessed quickly and easily. (e.g. different tilt angle or color of the slats).
	Since **real samples** are assessed, deviations from the ideal properties of the sample are included in the result (e.g. unequally tilted slats of venetian blinds).	Samples of the whole facade segment are not required.
Challenges	Many time-consuming measurements are necessary to cover all the required combinations of operation modes (e.g. tilt angle of slats) and directions of the incident radiation (considering different α_s and γ_f)	No standard models are available for very complex fenestration systems with e.g. thick absorbing and scattering layers with non-negligible thermal resistance.
	A sample of the fenestration system has to be constructed and sent to the laboratory.	Validation with calorimetric measurements is mandatory.
	In some cases, additional difficulties are raised by the not perfectly uniform and parallel light in laboratory measurements.	Models very often do not consider the angular dependence of g correctly.
	In some cases, additional difficulties are raised by the thermal capacity of the facade because of transient, constantly changing boundary conditions in the case of outdoor measurements.	

4.1.2 Effective Solar Heat Gain Coefficient g_{eff}

A comparison of the performance of different complex fenestration systems should be realistic and reliable. The standard conditions (e.g. from [58] or [74]) with normal incidence of the radiation are unrealistic, especially in the case of facades with venetian blinds. In addition to that they do not consider the usage/control strategy in the case of switchable facade systems. It is clear that the real usage can not be foreseen when the facade is controlled manually or when manual override is allowed. Based on experience from many real building projects, it can be stated that it is nevertheless very helpful to assess the performance for different assumed user modes in order to determine the *robustness* of a facade concept. This is especially true for buildings with large glazed areas of the facade. Especially in open-plan offices or rooms which are located at the corners of a building, careful design of solar-control systems is therefore essential. In some rooms of the fully glazed German high-rise building GALLILEO, in Frankfurt(Main), 70 % of the *peak* cooling load is caused by solar gains [34]. Solar gains can therefore have a huge impact on occupant comfort, building energy demand, CO_2 emissions, investment costs for HVAC systems and additional costs.

A realistic and reliable approach for the evaluation of the solar-control performance is based on the so-called "effective g-value" or "effective Solar Heat Gain Coefficient" g_{eff}. It is defined as

$$g_{\text{eff}} := \frac{\text{monthly (or hourly) solar gains}}{\text{monthly (or hourly) total incident irradiation}} \tag{3}$$

A detailed description of a method for the determination of g_{eff} is given in chapter 6.2. Chapter 6.2 shows that the method can also be used to determine hourly or daily effective g-values.

4.2 Criteria for thermal comfort

Thermal comfort in rooms is influenced by the following factors:

- the thermal energy balance on the surface of the person's body

  - the activity of the person and the resulting metabolic rate / heat generated by this task (see also [76]).
  - the convective heat exchange between the person and the surroundings, depending on the air movement and clothing conditions (see also [76]).
  - the radiative heat exchange between the person and the surroundings, depending on the infrared and solar radiation and on clothing conditions.

- uneven or asymmetric radiative temperature distribution (see also [76])

- local differences in the air temperature (e.g. cool air temperatures at floor level and hot temperatures at head height), (see also [76]).

- drafts, determined by the wind speed and the turbulence level (see also [76]).

- relative humidity of the air which determines the possibility of evaporative cooling by perspiration (see also [76]).

- individual aspects such as physical, physiological, psychological and cultural factors

Effective solar-control systems therefore do not only have to reduce the solar gains, they also have to prevent high local temperatures on the indoor surface of the facade in order to avoid high peaks and asymmetric radiative temperature distributions. In addition, solar-control systems should also be able to protect people against direct solar irradiation which causes strongly asymmetric radiative temperature distributions and high thermal gains. Detailed calculation formula and criteria are given in [76] and [65], but these criteria are only applicable to moderate differences in the local radiative temperature and therefore not valid for situations with direct insolation of persons with high irradiation levels. It seems to be clear nevertheless, that it is a mandatory requirement for facade systems that they should be able to protect people against direct solar irradiation with high irradiation levels, especially in summer conditions. But what about venetian blinds with perforated slats or electrochromic glazing that do not completely block the direct solar radiation? There are always asymmetric irradiation conditions when daylight enters a room (also in overcast situations) and these radiative gains in the solar spectral range are not taken into account in the calculation methods given in [76]. It is not clear how these radiative gains should be taken into account. In principle they could be simply added to the energy balance on the body of the person as given in e.g. [76] as contribution to the mean radiant temperature and to the local radiant temperature of the window. However, the solar radiation is not distributed diffusely into the room like the thermal radiation and has to be treated as directional radiation. also, it is not at all obvious that asymmetric daylight radiative gains are perceived in the same way as asymmetric thermal radiative gains from opaque walls. The reason is that people are accustomed to this type of asymmetric heat gain and that they probably expect and accept some asymmetry due to daylight, especially in winter. Further investigation of this topic by user assessments under daylight conditions is strongly recommended to further analyze this issue.

4.3   Criteria for daylighting

Electric lighting is often responsible for approximately one third of the total primary energy demand in energy-efficient buildings. The use of daylight by optimized facade systems (including optimized control strategies for these systems) is therefore an important measure to reduce the energy demand for the electric lighting. The daylight, transmitted through the facade, is determined primarily by:

- the climatic conditions / location

- the size of the glazed areas

- the position of the glazed areas (the parapet area is for example generally less efficient for daylighting than the upper parts of the facade)

- the orientation of the glazed areas with respect to the sun

- external obstructions by surrounding buildings and trees

- the light transmittance τ_{v} of the complex fenestration system / facade system including the light distribution function on the indoor surface of the facade

- the operation / control of the facade system.

Therefore, daylighting can not be evaluated independently of the building. In many countries (e.g. Germany), daylighting requirements are based on minimum requirements for the daylight factor D. D is defined by

$$D := \frac{E_{\mathrm{v,\ global,\ horizontal,\ indoor}}}{E_{\mathrm{v,\ global,\ horizontal,\ outdoor}}}\ 100\% \tag{4}$$

for overcast conditions. The main idea was already introduced early in the 20th century [122] and is still in use in many standards (see e.g. [54]). $E_{\mathrm{v,\ global,\ horizontal,\ indoor}}$ is the indoor global horizontal illuminance on the working plane [lux]. $E_{\mathrm{v,\ global,\ horizontal,\ outdoor}}$ is the outdoor global horizontal illuminance. Different definitions for the diffuse sky are used in different standards being either uniform or with lower luminance at the horizon [89]. In all cases the sky is assumed to be purely diffuse without direct sun and without differentiation between different orientations like e.g. south or north. In most cases the "CIE standard general sky" [75] is used. D can not be transformed directly into indoor illumination levels under real or typical weather conditions for a given location and a specific facade orientation. D can therefore not be used directly to assess how often the required illuminance levels, as specified in e.g. [60], are reached by daylight alone. It is therefore also not possible to determine the energy demand for artificial lighting based on D alone. A research program for the California Energy Commission CEC in the US [72] showed that there is almost no correlation between D and user satisfaction with the daylighting situation, which means that D is not a reliable metric. In addition to that, it is completely impossible to compare the daylighting performance of different moveable shading devices or different control strategies since blinds are usually fully retracted when the sky is overcast.

A dynamic metric is therefore necessary to evaluate the daylighting performance of switchable complex fenestration systems realistically and reliably. This is especially true for systems with venetian blinds or with other slatted or louvered devices with tiltable slats. Such an evaluation is based on time series of illuminance values for certain points on the working plane in a room. In many cases the hourly average illuminance is not representative for the quickly fluctuating daylighting conditions and the time step has to be decreased from one-hour to one-minute mean values by using validated interpolation algorithms to generate meteorological data for the intermediate time steps [123]. A discussion of different "dynamic daylight performance metrics" can be found in [102]. The "daylight autonomy" metric DA [101] is defined as

$$DA := \frac{t_{\mathrm{within\ working\ hours\ and\ with\ }E_v \geq \mathrm{threshold}}}{t_{\mathrm{total}}}\ 100\% \tag{5}$$

and is therefore the "percentage of the working hours of the year when the minimum illuminance requirement at the sensor point is met by daylight alone". In the case of facade systems with venetian blinds it has been shown that the illuminance values on the working plane in a room can be calculated reliably using the RADIANCE daylight simulation program [125],

[101], [103]. A discussion of different variants of daylighting simulation programs based on RADIANCE can be found in [103]. In 2012, the CEC-research program [72] showed good correlation between user satisfaction with the daylighting situation and the daylight autonomy DA. With DA, it is therefore possible to take the control strategy for the complex fenestration system into account and to evaluate the daylighting performance reliably. It is essential to use the same control strategy for the assessment of daylighting, visual comfort and passive solar gain control. In the case of "manual control" or possible "manual override", the control strategey is not known a priory. It is nevertheless possible to evaluate different control strategies to assess the robustness of the performance of a complex fenestration system against user interventions (see also the discussions in chapter 7.3 on page 135). In chapter 4.1.2, the effective solar heat gain coefficient g_{eff} has been defined for the evaluation of the solar-control performance. There are also ongoing activities to define an "effective daylight autonomy" DA_{eff} [103] which takes a reference control strategy for a venetian blind system into account. It is possible to calculate the daylight autonomy DA for many points in a room in order to analyze the distribution of the DA. It is an actual research topic to find metrics to evaluate the DA-distribution in the room with respect to overall user satisfaction with the daylighting situation in the room as a whole (not only at certain positions in the room). One of these approaches is the 'spatial Daylight Autonomy' sDA [72].

Conclusion on criteria for daylighting   Dynamic metrics are necessary to evaluate the daylighting performance of switchable complex fenestration systems realistically. Static metrics like the daylight factor D are not appropriate, especially because they are based on overcast sky conditions which are not relevant for the use of solar-control systems. Dynamic metrics exist together with validated modelling tools. The daylight autonomy DA seems to be the most appropriate metric. It has the additional advantage that the results can also be used to determine the energy demand for artificial lighting.

4.4   Criteria for visual comfort

Visual comfort is an important parameter that influences the well-being and performance of human beings. It becomes even more important in working environments that include computer monitors or other visual display terminals. The key aspects of visual comfort are:

- visual contact with the exterior

- glare protection and avoiding reflections on computer screens

- contrast between visual task and background.

- sufficiently high illuminance values

- color rendering of objects in the room.

Often conflicting aspects have to be optimized case for case, e.g. visual contact with the exterior and providing glare protection.

4.4.1 Criteria for visual contact with the exterior

Visual contact with the exterior is a very important aspect of visual comfort. User assessments with different venetian blinds in Freiburg, Germany [126] have shown, that many people even accept some disturbance by glare in order to be able to see the outside. Nevertheless, a validated and generally accepted metric for visual contact does not exist at present. Such a metric would at least have to address the rating of the following aspects:

- sufficiently large view of the exterior. It is obvious that the size of the view depends not only on the size of the window but also on the distance between observer and facade. User satisfaction also depends on the position of the image relative to the person's viewing direction (an observer will not be satisfied e.g. with a window behind himself).

- quality of the image. The quality of the image is influenced at least by the following aspects:

  - color rendering of the outside image. The color rendering index R_A [58] can be used as metric also for this criterion although it is intended to be used for the color rendering of objects inside the room which are illuminated by daylight which has passed through the facade. The reason is that the color stimulus (tristimulus value) of a colored surface is identical for both situations:

    1. colored surface and observer being in the room and
    2. colored surface being outside the room and the observer being in the room

    as can be seen from eq. (6) for the X_t-value of the tristimulus:

$$X_t := \frac{\int_{380 \text{ nm}}^{780 \text{ nm}} S_\lambda \, \tau_\lambda \, \rho_\lambda \, \overline{x}_\lambda \, d\lambda}{\int_{380 \text{ nm}}^{780 \text{ nm}} S_\lambda \, d\lambda} \tag{6}$$

    where S_λ is the spectrum of the incident daylight, $\overline{x}_\lambda$ is the spectral tristimulus x-value for the CIE 1931 colorimetric standard observer [58], τ_λ is the spectral transmittance of the facade and ρ_λ is the spectral reflectance of the colored surface. When the colored surface and the observer are inside the room, the surface is illuminated by $(S_\lambda \, \tau_\lambda)$ which means that the spectral tristimulus is $X_t(\lambda) = (S_\lambda \, \tau_\lambda) \, \rho_\lambda \, \overline{x}_\lambda$. When the object is outside, the illuminant is S_λ. The spectrum of the reflected light is therefore $S_\lambda \, \rho_\lambda$. The reflected light has to pass the facade with transmittance τ_λ before it can enter the room. The eye of the observer therefore receives the spectral tristimulus $X_t(\lambda) = (S_\lambda \, \rho_\lambda \, \tau_\lambda) \, \overline{x}_\lambda$ which is identical to the first case. Analogous reasoning can be used to prove the statement for the tristimulus Y_t- and Z_t-values.

  - sharpness and image distortion (the quality could be reduced e.g. in the case of some daylight re-directing glass patterns).

  - no disturbing reduction of contrast by haze (which can occur e.g. in the case of some light-scattering white fabrics) or sources with disturbingly high luminance in the viewing area (like the glossy edges of some perforated slats of venetian blinds when the sun is shining on the edges). It is important to note that all of these effects are generally irrelevant without direct irradiation. The effects are most

evident when relatively dark images are being observed (e.g. a park in the shadow of large trees) and when the facade is at the same irradiated directly by the sun with high illuminance values. This should be taken into account when such effects are evaluated.

4.4.2   Criteria for glare protection

Glare can be categorized in the following way:

- **glare causing ocular health problems** like temporary blinding or permanent damage of the eye. This can happen for example in the case, when people are observing a solar eclipse phenomenon using glasses with damaged filter or when they look into devices that concentrate solar radiation (like lenses or curved mirrors). A discussion of criteria for the evaluation of high glare levels, which can be produced e.g. by small concentrating heliostat fields in building facades, can be found in [49].

- **disability glare** impairs the visual perception of objects, in most cases by reducing the contrast between colors or black and white, but it is also possible that strong light sources (like the flash of a camera) disturb the visual perception by reducing the size of the pupil and therefore reducing the brightness of the rest of the image. Contrast reduction is mainly caused by stray light within the eye, within the air between the eye and the viewed object or by light reflections on surfaces (veiling glare, see below). The stray light in the eye can be caused by light scattering effects at the iris cornea, the lens or the vitrous humour. The intensity of stray light in the eye varies greatly from person to person and it generally becomes stronger when people get older. Stray light between the eye and the viewed object caused by scattering (e.g. by atmospheric particles) creates additional luminance in the field of view that reduces the contrast of the original image. Criteria for the evaluation of disability glare caused by contrast reduction are therefore directly linked to the evaluation of the minimum contrast requirements in a given scene (e.g. the contrast between black letters and white background on a computer screen or on paper). A discussion of minimum contrast requirements on computer screens can be found in [77], [88] or [109]. Moghbel [88] considers both, the contrast on the screen and the background luminance. [109] takes into account different direct and global illuminance levels on different types of computer screens and evaluates the effect not only for black and white but also for contrast ratios between different colors. The determination of the maximum allowable illuminance on the computer screen is a mandatory part the GS-certification [70] of the device, it therefore has to be determined for every visual display terminal. It can be concluded, that illuminance levels of up to 1500 lux are tolerable for ordinary screens and that illuminance levels above 3000 lux are difficult, even for advanced screens.

- **discomfort glare** is a subjective rating of a lighting situation. The glare level is in many cases below the level of disability glare. It has indirect consequences like fatigue or headaches. It is normally not directly measurable and is therefore determined by user assessments with questionnaires. It is generally rated into four different classes:

- – imperceptible

- – perceptible, but not disturbing

- – disturbing, but tolerable

- – intolerable

Since discomfort glare is a highly subjective and individual phenomenon, it is clear that it is not possible to predict, whether an unknown person will be disturbed by discomfort glare in a particular situation. All discomfort glare rating schemes therefore try to predict statistically the average glare rating of a large group of people. An overview of current work on discomfort glare for daylight conditions can be found in [126] and [45]. Discomfort glare rating schemes have the following general structure:

$$
\begin{aligned}
\text{discomfort glare} \quad &= \quad [\text{large glare source term}] + [\text{small glare source term}] \\
&= \quad \underbrace{\frac{f(\text{overall brightness of the scene})}{\text{adaptation level}}}_{\text{large glare source term}} \\
&\quad + \text{c } \log \left(1 + \sum_i \underbrace{\frac{(\text{brightness}_i)^y \times \text{solid angle}_i}{\text{adaptation level} \times \text{position rating}_i}}_{\text{term for all small glare sources } i} \right)
\end{aligned}
\tag{7}
$$

The term for small glare sources contains the constant c and takes into account how bright and how large a glare source is. It weights this result by the adaptation level of the eye and by the relative position in the field of view of the observer. This position rating has to take into account the direction and the angular displacement of the glare source from the observers line of sight. The human eye is more sensitive to light coming from below the horizontal plane that contains the eye, than from above. It should also take into account that the sensitivity to bright light depends on the position of the bright source in the field of view and that the eye is much more sensitive in the central region of the visual field than in the peripheral regions of the visual field. The large glare source term consists of a constant and a function depending on the overall brightness of the scene, weighted by the adaptation level. There are strong indications from the work in [126] that both, the experienced brightness of the room and the adaptation level are closely related to the global vertical illuminance at eye level $E_{\text{vert, glob}}$. If the response of the eye and the adaptation level would linearly depend on $E_{\text{vert, glob}}$ at the same time, the large glare source term would be a constant. However, this is not to be expected because of the logarithmic sensitivity of the eye. It is therefore probable that the large glare source term can be developed in a Taylor-series with the elements $(E_{\text{vert, glob}})^x / E_{\text{vert, glob}}$ with $x = 1, 2, 3, \ldots$. An approximation to equation (7)
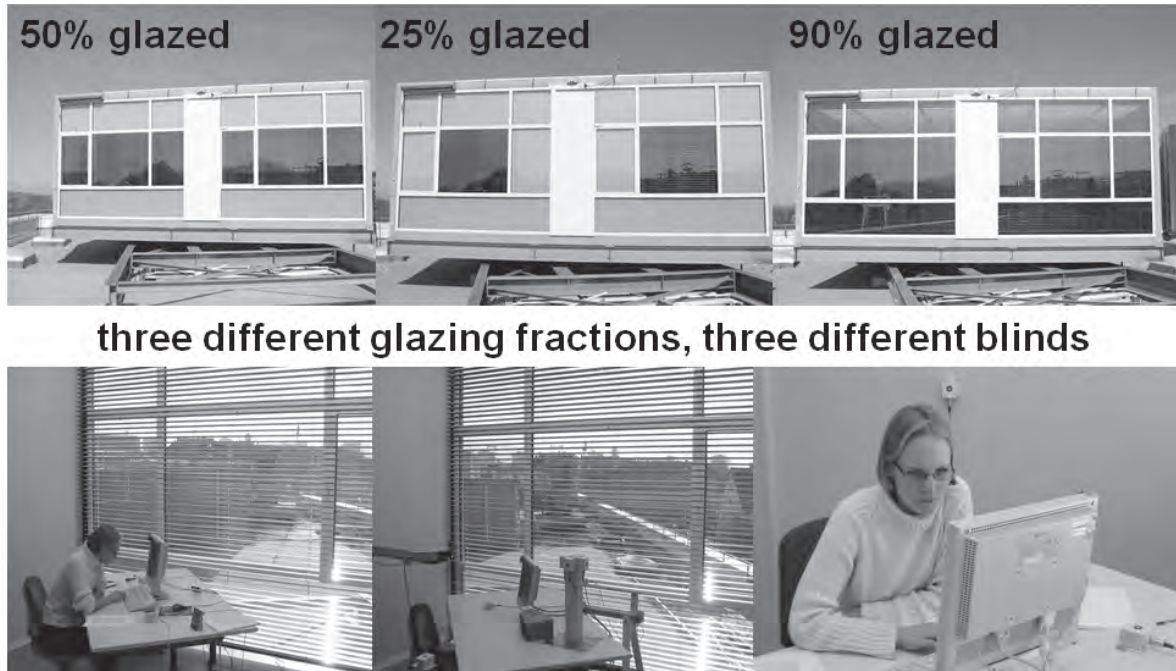
Figure 11: Rotatable test offices on the roof of the building of the Fraunhofer Institute for Solar Energy Systems ISE in Freiburg, Germany. This setup has been used for the extensive user assessments with 74 subjects, more than 110h tests and in total more than 349 different situations, which are the basis for the glare metric daylight glare probability DGP [126]. They have been carried out in the European research project Ecco-build. Ecco-build has been co-ordinated by the author of this document. Pictures ©Fraunhofer ISE.

is therefore:

$$\text{discomfort glare} = \underbrace{c_1 + c_2\,E_{\text{vert, glob}} + c_3\,(E_{\text{vert, glob}})^2 + \ldots}_{\text{large glare source term}}$$
$$+ c_4 \log\left(1 + \sum_i \underbrace{\frac{(\text{brightness}_i)^y \times \text{solid angle}_i}{\text{adaptation level} \times \text{position rating}_i}}_{\text{term for all small glare sources } i}\right) \quad (8)$$

Currently, the most widely accepted and best validated glare metric is the daylight glare probability DGP, developed by Wienold et. al. [126]. The DGP is based on extensive user assessments in Germany and Denmark with 74 subjects, more than 110h tests and in total more than 349 different situations. These user assessments have been carried out in the European research project Ecco-build.

$$DGP \quad := \quad c_1 \times E_{\text{vert, glob}} \; + \; c_2 \log \left(1 + \sum_i \frac{L_i^2 \times \omega_i}{(E_{\text{vert, glob}})^{1,87} \times P_i^2} \right) \; + \; c_3 \qquad (9)$$

$$= \quad \underbrace{c_3 \; + \; c_1 \times E_{\text{vert, glob}}}_{\text{large glare source term}} + c_2 \log \left(1 + \sum_i \underbrace{\frac{L_i^2 \times \omega_i}{(E_{\text{vert, glob}})^{1,87} \times P_i^2}}_{\text{small glare sources } i} \right) \qquad (10)$$

where ($c_3 +$ $c_1 E_{\text{vert, glob}}$) has been interpreted as a second order approximation to the large glare source term in equation (8). P_i is the Guth position index, L_i and ω_i are the luminance and the solid angle of each glare source respectively.

- **reflex glare or veiling glare** generally creates discomfort or disability glare. When the contrast of an object (e.g. on a visual display terminal) is reduced by additional light stemming from reflected radiation, this is called "reflex glare". In general reflex glare has a stronger impact on the contrast between different colors than on the contrast between black and white [109].

- **outdoor glare** with possible impact on workplaces in other rooms, street traffic or aviation. There are no generally accepted criteria for the evaluation of outdoor glare. In Germany there is only a guideline for plants (like e.g. photovoltaic power plants) [83] but it does not consider realistic weather conditions and it assumes ordinary flat glass surfaces into account . It therefore cannot take anti-reflective coatings, patterned glass or anti-gloss structures on the outer surface. Since some of the patterned glass surfaces create stronger glare effects than flat glass because of low-angle scattering, the guideline underestimates the glare situation for these cases. Since it neglects all existing anti-glare surface treatments, it overestimates glare effect drastically in many cases. It can be concluded that there is no valid criterion at the moment, there have only some initial attempts to improve the situation (see e.g. [127] or [38]).

It is important to understand that a specific glare phenomenon generally belongs to more than one of the categories mentioned above. Evaluation of glare protection can be divided into glare protection in the room and outdoor glare. Glare evaluation in the room can be limited to the evaluation of disability glare and discomfort glare in almost all practically relevant cases, since veiling glare creates discomfort or disability glare and since ocular health problems created by glare normally do not occur in offices or similar situations.

Conclusion: In situations like offices with computer screens, glare evaluation can be reduced in most cases to two tasks:

- **disability glare:** calculate the illuminance on the computer screen (e.g. with RADI-ANCE) using typical meteorological data for the whole year, to determine whether the illuminance is within the specifications for the screen. Assume 1500 Lux as maximum, if the type of the screen is not known. A carpet plot provides a good overview. If the data is analyzed statistically, it often makes sense to allow a certain number of hours with higher illuminance than required by the specification of the screen, e.g. 1-5% of the working hours.

- **discomfort glare:** calculate (e.g. with RADIANCE) with typical meteorological data for the whole year, whether the DGP is within the limits given in [126]. This means that DGP values below 0.35 are desirable and correspond in many cases to imperceptible glare. $0.35 \leq DGP < 0.40$ corresponds in many cases to perceptible, but not disturbing glare. $0.40 \leq DGP < 0.45$ corresponds in many cases to disturbing, but tolerable glare. Measures should be taken to prevent DGP values above 0.45 from occurring, since they correspond to intolerable glare in most cases. Again, a carpet plot provides a good overview and it often makes sense to allow a certain number of exceptions, e.g. 1-5% of the working hours.

4.4.3   Contrast between visual task and background

This section deals with the contrast between the visual task (e.g. computer screen or printed paper) and the ambient background behind the visual display terminal or the paper. The contrast between e.g. the black letters and the white paper on which the letters are printed is not covered here, as it has been discussed in chapter 4.4.2. In general, it is desirable for the background to have a lower luminance than the visual task itself in order to minimize reflex glare/veiling glare. The difference between the ambient luminance of the background behind the visual task and the luminance of the visual task should be limited in order to avoid tiring darkness-brightness re-adaptation of the eye. However, this does not mean that a monotonic, completely homogeneous and tedious luminance distribution is desirable. A good compromise has to be found and large differences in the adaptation level over the viewing field should be avoided.

4.4.4   Sufficiently high illuminance levels

Sufficiently high illuminance values are necessary in order to perform visual tasks accurately and effectively. The necessary illuminance value depends on the type of activity and the duration of the visual task. Necessary illuminance levels for indoor work places are specified in the EN12464-1 [60] standard. They range from 100 lux for corridors etc. up to 5000 lux for e.g. special medical tasks. The necessary illuminance values can be provided by daylight and/or artificial lighting. Artificial lighting has to be designed to ensure that the illuminance requirements can always be met, not only when the lighting system is new (maintenance factor). However, this does not mean that the artificial lighting has to be switched on automatically when the illuminance value falls below the required level in daylight situations. The requirement is only that the user must have the possibility to switch on additional artificial lighting in order to reach the required level. Experience shows that a large amount of energy can be saved when users manually switch on the additional artificial lighting instead of an automatic switch, without the user satisfaction with the lighting situation decreasing. This is especially relevant in the case of energy-efficient office buildings, where artificial lighting often accounts for approximately 1/3 of the total primary energy consumption of the building.

4.4.5 Colour rendering of objects in the room, viewed by an observer who is also in the room
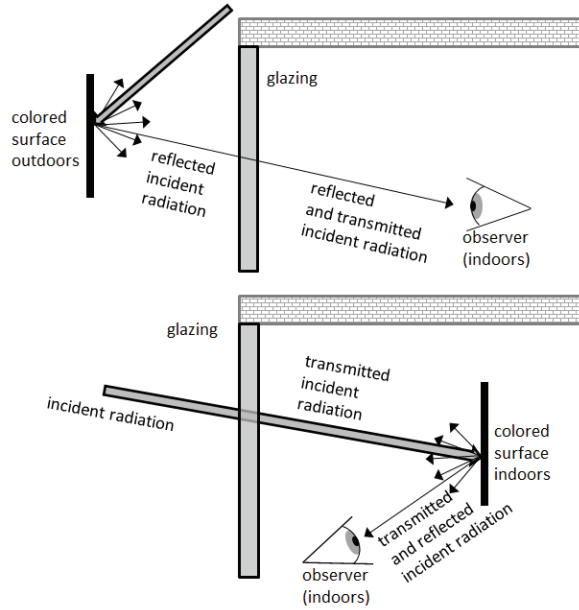
Figure 12: The general color rendering index Ra, defined in the European EN410 standard [58] or in [42] is suitable to evaluate the color rendering of indoor objects viewed by an observer who is in the room. In this case (lower illustration), the fenestration system may include scattering layers (like venetian blinds or roller blinds). Ra is also suitable for viewing outdoor objects, if the fenestration system does not contain scattering or light re-directing layers [15].

The color rendering of objects, viewed by an observer who is in the room (see Figure 12), is in general different from the color rendering of objects in the room viewed by an observer who is outdoors, looking through a spectrally selective glazing unit into the room (see section 4.7). The color rendering of objects within the room for an internal observer is evaluated by the general color rendering index R_a as defined in the EN410 standard [58] and CIE13.3 [42]:

$$R_a := \frac{1}{8} \sum_{i=1}^{8} R_i \tag{11}$$

where R_i is the specific color rendering index for each of eight different test colors. R_i is calculated for the CIE1931 colorimetric 2° standard observer within the CIE 1964 (U*, V*, W*) color vector space. It is related to the color difference $\Delta E_{i,\text{U*V*W*}}$ in this color vector space between the test color i illuminated directly by the reference illuminant D65 and by the D65 illuminant transmitted through glazing. The eight test colors are relatively weakly saturated colors distributed over the whole color range (chromaticity/hue range). The test colors 9 to 14 and the corresponding specific indices R_9 to R_{14} have been excluded from the general color rendering index R_a in EN410 [58]. Colors 9 to 12 are saturated red, yellow, green and blue. Color 13 is close to the color of Caucasian human skin and color 14 is a saturated green that is similar to the leaves of trees. It is therefore clear that R_a undervalues the rendering of saturated colors and light colored human skin. If these colors are important,

the color rendering index could be extended or the additional R_i can be evaluated separately. From the evaluation of the color rendering of LED lamps, it is known that the rendering of weakly saturated colors can be very different from the rendering of saturated colors, as conventional LEDs typically reach $R_a > 80$, but often $R_9 \ll 50$. In general, it can be stated that R_i or $R_a > 90$ corresponds to very good color rendering [58]. R_i or $R_a > 80$ corresponds to good color rendering [58].

4.4.6   Optional room darkening

In some situations it is necessary to darken the room to a certain extent. This ranges from darkening of bedrooms during daytime, up to high-level darkening of scientific laboratories or photographic studios. The darkening performance can be differentiated between the performance of the moveable part itself and the fixing or guiding system. Sometimes even the windowsill is relevant for the darkening performance, especially in the case of window sills made of e.g. marble, which is partly translucent and therefore allows some light to be transmitted through the stone itself. It is also important to note that the adaptation level of the eye in scotopic vision determines the level of darkening necessary. In bedrooms, if LCD displays of clocks, radios or TV are present, there is always a background illuminance of several 10^{-3} lux so that the eye does not reach the maximum sensitivity. The requirements are therefore much lower under such conditions than for laboratory-grade darkening and this background illuminance level of several 10^{-3} lux should be considered when darkening products for home applications are tested with human observers. For the moveable part of the curtain, possibly existing "pin-holes" are the most relevant aspect for laboratory-grade darkening. Both, the moveable part of the curtain and the complete system including the fixing system can be characterized with the criteria and methods specified in EN14500 [1] and EN14501 [2]. New versions of these standards with enhanced darkening performance evaluation are currently under preparation with the involvement of the author of this thesis. The new versions will be published at the end of 2015 or in 2016.

4.5   Influence on circadian and neuroendocrine regulation through the "circadian photoreceptor"

All mammals have an internal timing mechanism that co-ordinates biochemical, physiological and behavioral processes to maintain synchrony with the ambient cycles of light, temperature and nutrients. This also applies to human beings. Several studies have shown that light is the most potent cue to synchronize daily activities [80]. In mammals, light perception occurs only in the retina [80]. Three different types of photoreceptors are present within this part of the eye: cones, rods and the newly discovered circadian photoreceptor. The circadian photoreceptors were first discovered in 1991 in mouse eyes [66]. The circadian photoreceptor consists of intrinsically photosensitive retinal ganglion cells (*ip*RGCs) which are a kind of nerve cell [35]. Their existence and important role in the human eye have been verified and documented in 2007 by Zaidi et. al. in the outstanding paper [133]. The sensitivity of the human *ip*RGCs peaks in the blue area of the solar spectrum (at ≈ 481 nm) [133]. Researchers

believe that the classical photoreceptors (the rods and the cones) are responsible for image-forming vision, whereas the ipRGCs play a key role in the non-image forming vision [80]. This non-image-forming photoreceptive system communicates not only with the master circadian pacemaker located in the suprachiasmatic nuclei of the hypothalamus, but also with many other brain areas that are known to be involved in the regulation of several functions [80]. In studies with people who conventionally were considered to be completely blind (they did not have active retinal rods and cones, but active ipRGCs) it has been shown [133] that this non-image forming occular sense can affect several aspects of conscious awareness, subconscious awareness and health independently from the circadian system. It can be concluded that it is essential that

- complex fenestration systems should not block the blue area of the solar spectrum in order to allow the people in the room to correctly synchronize their internal clock with the environmental cycles of light and probably also because of other health aspects. Venetian blinds with colored slats (especially with red slats) or colored roller blinds (especially with red fabrics) are examples of systems that should be avoided or at least used carefully.

- artificial lighting designers should be careful with blue light, especially with wavelengths around 480 nm, in order to minimize unwanted impact on the synchronization of the internal clock of the people in the room. It is clear that the now almost obsolete incandescent lights had poor color rendering properties and very low energy efficiency but a small portion of blue light. It can be very useful to adapt the spectrum of the artificial lights depending on the daytime.

4.6 Criteria for outdoor color specifications and color uniformity

In construction projects it is very important that no unexpected differences in the perceived color of the building skin are noticed by observers. First of all the term 'perceived color' of the facade has to be defined. The color impression can be expressed as a point in one of the three-dimensional color vector spaces (e.g. RGB, XYZ, L*a*b*, ...). Since perceived color differences are to be evaluated, it is important that equal Euclidean distances in the color vector space correlate with equal visually perceived color differences, which means that the color vector space should be 'perceptually uniform'. None of the color vector spaces is perfect with respect to this issue [132] and color perception has individual variations but the L*a*b*-system (CIELAB, either for 2° small-field foveal view or 10° large-field view) was specially designed with the goal of being 'perceptually uniform'. The dimensions in the L*a*b* vector-space are the lightness of the color (the L*-value), the contribution in the red-green dimension (a*-value) and contribution from the yellow-blue dimension (b*-value). Within the color vector space it is therefore possible to evaluate also the chromaticity (or color saturation, or colorfulness) and hue in addition to the color distance. The hue is related to the relative portion from the red/green dimension and the relative portion from the blue/yellow dimension. This means that hue is determined by the fraction a*/b*. Normally, there will be no dispute about construction work, if the subjective color impression is acceptable. The problem of individual human color difference evaluation is that impressions of color differences are highly

subjective since

- the perception of color can differ strongly from person to person.

- human vision is not objective and sometimes recognizes color differences between completely identical colors if there is a non-uniform borderzone between them. For example, if there is a large gray area, a black stripe, a white stripe and another large gray area with exactly the same gray as the first gray zone, then the second gray area appears to be brighter than the first one.

- color differences can be recognized much more easily, if the colored areas are adjacent to each other without any border line between them.

- color differences can be recognized much more easily, if the colored areas are on a background with a uniform color.

Since the subjective impression is not a reliable criterion, objective criteria have to be used in order to evaluate color differences. First of all, the term 'perceived color' of the facade has to be defined. in order to decide if the differences are within the tolerances or if they are bigger than permitted. In general, color differences can be considered to be insignificant when $\Delta a^* \ll 1$, $\Delta b^* \ll 1$ and $\Delta E = \sqrt{(\Delta L^*)^2 + (\Delta a^*)^2 + (\Delta b^*)^2} \ll 1$ when surfaces are illuminated by the unpolarized reference illuminant D65 and evaluated with the sensitivity of the CIE1931 colorimetric 2° or 10° standard observer within the CIE1964 L*a*b* color vector space. But for other boundary conditions, color differences can appear:

- Metamerism: Colors with the same reflectance spectrum have the same apparent color under all illumination conditions. By contrast, metameric colors with different reflectance spectra can have the same apparent color when they are illuminated with one specific illuminant and a different apparent color when they are illuminated with another illuminant.

- Polarization: Sometimes the polarization of the illuminant can have a strong impact on the perceived color. A strongly polarized illuminant, for example, is the blue skylight which is polarized by Rayleigh scattering at air-particles. This can have a strong effect on the polarization dependent color of some types of toughened (tempered) glass panes with solar-control coatings consisting of thin films. Because of practical relevance, it should be noted here that obviously people should not wear polarizing sunglasses when evaluating color differences under daylight conditions.

- Influence of the viewing angle and the angle of incidence: The reflectance spectrum (and therefore the color) of many surfaces strongly depends on the angle of incidence and the angle of the reflected light that is reaching the eye of the observer. Color can be a bi-directional property. Color differences can therefore appear when identical surfaces are viewed under different viewing angles and/or with different angles of incidence of the illuminant. Non-identical colored surfaces can e.g. have the same color when they are viewed under normal incidence, but they can have different colors when they are viewed under oblique angles of incidence.

It can be concluded, that it is definitely not easy to define generally valid criteria for outside color specifications and color uniformity in construction projects. One important aspect is, that manufacturers want to have well defined tolerances for lab-measurements, which can be used for the quality management in the production. But building owners and architects expect color uniformity under real illumination conditions, which also includes for example polarized blue skylight or red-shifted sunlight in the evening. It can be concluded that it is neither appropriate nor advisable to use a small number of human observers as the basis for color difference evaluations because of the subjective color perception of the human eye. Instead of this, all involved parties should agree on measurable criteria in an early stage of the planning process and the criteria should take into account all the above mentioned aspects. It also seems to be clear, that the frequently used criterion $\Delta E \leq 1$, with diffuse illumination with a spectral distribution corresponding to D65, is too simple in many cases.

4.7 Color rendering of objects in a daylit room viewed from outdoors

The color rendering index Ra, as specified in EN410 [58] cannot be used to characterize the color rendering quality when objects in a room are viewed by an observer standing outside the room when the source of illumination is also outside the room. Therefore a new index $Ra_{\text{out-in}}$ has been defined. It would be advantageous if the color of human skin were to be rendered with high quality when people are looking indoors from outdoors, so that the users in a room do not look pale or ill. Color rendering of objects in a room viewed by an observer who is outdoors is also relevant for the case of internal "white venetian blinds" which are white for observers in a room and which also should appear white when the observer is outside. Instead, "white venetian blinds" often look greenish from the outside when they are mounted behind spectrally selective solar-control glazing. When outdoor observers are viewing objects through glazing, they normally see an image of the objects plus a superimposed reflected image of the outdoor surroundings of the building. For product characterization of complex fenestration systems that is independent of location and specific buildings, it is essential to exclude the context-dependent, superimposed reflected image from the color rendering properties.

As depicted in Figure 13, one can see that the case of the exterior observer can be treated with a similar methodology as the case of the internal observer. The only difference is that the transmittance of the glazing τ has to be replaced by τ^2 in all equations needed to calculate Ra in EN410 [58] since the incident light has to pass the glazing before it reaches the colored surface and the reflected light has to pass the glazing again, before it reaches the eye of the observer. The huge difference between the spectral distribution of τ_λ and τ_λ^2 is the reason for the poor color rendering properties of many solar-control glazing for outdoor observers viewing objects in a room. It is important to note also the difference between eq. (29) for the outdoor observer observing indoor objects that are illuminated by transmitted daylight and eq. (11) for visual contact of an indoor observer with the exterior. The color tristimulus for an external observer, looking through the facade/glazing toward a colored surface in a room
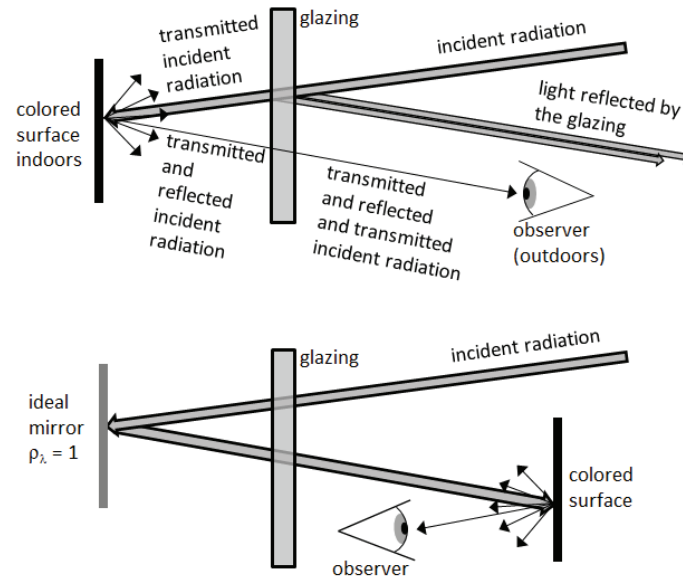
Figure 13: The observer recognizes the same apparent color for the upper and the lower configuration, as long as angle-dependent effects, specular reflections from the glazing and multiple reflections between the colored surface and the glazing can be neglected and with the assumptions of clear (non-scattering) glazing and the source of illumination also being located outdoors. For the lower configuration, it is clear that the formulae for Ra, given in EN410, can be used by simply replacing the transmittance of the glazing τ by τ^2 [15].

under daylight conditions is

$$
\begin{aligned}
X_{\text{out-in}} &:= \frac{\int_{380 \text{ nm}}^{780 \text{ nm}} S_\lambda \, \tau_\lambda^2 \, \rho_\lambda \, \overline{x}_\lambda \, d\lambda}{\int_{380 \text{ nm}}^{780 \text{ nm}} S_\lambda \, d\lambda} \\
Y_{\text{out-in}} &:= \frac{\int_{380 \text{ nm}}^{780 \text{ nm}} S_\lambda \, \tau_\lambda^2 \, \rho_\lambda \, \overline{y}_\lambda \, d\lambda}{\int_{380 \text{ nm}}^{780 \text{ nm}} S_\lambda \, d\lambda} \\
Z_{\text{out-in}} &:= \frac{\int_{380 \text{ nm}}^{780 \text{ nm}} S_\lambda \, \tau_\lambda^2 \, \rho_\lambda \, \overline{z}_\lambda \, d\lambda}{\int_{380 \text{ nm}}^{780 \text{ nm}} S_\lambda \, d\lambda}
\end{aligned}
\tag{12}
$$

where S_λ is the spectrum of the incident daylight, $\overline{x}_\lambda, \overline{y}_\lambda$ and $\overline{z}_\lambda$ are the spectral tristimulus values for the observer (e.g. for the CIE 1931 colorimetric standard 2° observer [59]), τ_λ is the spectral transmittance of the facade element and ρ_λ is the spectral reflectance of the colored surface.

Following EN410 [58], the tristimulus value of the light transmitted by the glazing and reflected

by each of the eight test colors i is

$$X_{\text{i, out-in}} := \frac{\int_{380\text{ nm}}^{780\text{ nm}} S_\lambda \, \tau_\lambda^2 \, \beta_{i,\lambda} \, \overline{x}_\lambda \, d\lambda}{\int_{380\text{ nm}}^{780\text{ nm}} S_\lambda \, d\lambda}$$

$$Y_{\text{i, out-in}} := \frac{\int_{380\text{ nm}}^{780\text{ nm}} S_\lambda \, \tau_\lambda^2 \, \beta_{i,\lambda} \, \overline{y}_\lambda \, d\lambda}{\int_{380\text{ nm}}^{780\text{ nm}} S_\lambda \, d\lambda} \tag{13}$$

$$Z_{\text{i, out-in}} := \frac{\int_{380\text{ nm}}^{780\text{ nm}} S_\lambda \, \tau_\lambda^2 \, \beta_{i,\lambda} \, \overline{z}_\lambda \, d\lambda}{\int_{380\text{ nm}}^{780\text{ nm}} S_\lambda \, d\lambda}$$

where $\beta_{i,\lambda}$ is the spectral reflectance of each test color $i \in [1,8]$. The trichromatic coordinates in the CIE 1960 uniform chromaticity diagram are

$$u_{\text{out-in}} = \frac{4\,X_{\text{out-in}}}{X_{\text{out-in}} + 15Y_{\text{out-in}} + 3Z_{\text{out-in}}} \tag{14}$$

$$v_{\text{out-in}} = \frac{6_{\text{ out-in}}}{X_{\text{out-in}} + 15Y_{\text{out-in}} + 3Z_{\text{out-in}}} \tag{15}$$

$$u_{\text{i, out-in}} = \frac{4\,X_{\text{i, out-in}}}{X_{\text{i, out-in}} + 15Y_{\text{i, out-in}} + 3Z_{\text{i, out-in}}} \tag{16}$$

$$v_{\text{i, out-in}} = \frac{6_{\text{ i, out-in}}}{X_{\text{i, out-in}} + 15Y_{\text{i, out-in}} + 3Z_{\text{i, out-in}}} \tag{17}$$

where $u_{\text{out-in}}$ and $v_{\text{out-in}}$ are for the incident light and $u_{\text{i, out-in}}$ and $v_{\text{i out-in}}$ are for the eight test colors i. With the following equations (18) to (23)

$$u'_{\text{i, out-in}} = \frac{10.872 + 0.8802\frac{c_{\text{i, out-in}}}{c_{\text{out-in}}} - 8.2544\frac{d_{\text{i, out-in}}}{d_{\text{out-in}}}}{16.518 + 3.2267\frac{c_{\text{i, out-in}}}{c_{\text{out-in}}} - 2.0636\frac{d_{\text{i, out-in}}}{d_{\text{out-in}}}} \tag{18}$$

$$v'_{\text{i, out-in}} = \frac{5.520}{16.518 + 3.2267\frac{c_{\text{i, out-in}}}{c_{\text{out-in}}} - 2.0636\frac{d_{\text{i, out-in}}}{d_{\text{out-in}}}} \tag{19}$$

$$c_{\text{out-in}} = \frac{1}{v_{\text{out-in}}}\left(4 - u_{\text{out-in}} - 10\,v_{\text{out-in}}\right) \tag{20}$$

$$d_{\text{out-in}} = \frac{1}{v_{\text{out-in}}}\left(1.708\,v_{\text{out-in}} + 0.404 - 1.48\,u_{\text{out-in}}\right) \tag{21}$$

$$c_{\text{i, out-in}} = \frac{1}{v_{\text{i, out-in}}}\left(4 - u_{\text{i, out-in}} - 10\,v_{\text{i, out-in}}\right) \tag{22}$$

$$d_{\text{i, out-in}} = \frac{1}{v_{\text{i, out-in}}}\left(1.708\,v_{\text{i, out-in}} + 0.404 - 1.48\,u_{\text{i, out-in}}\right) \tag{23}$$

it is possible to calculate the co-ordinates in the CIE1964 ($U^\star$,$V^\star$,$W^\star$) color space:

$$W^\star_{\text{i, out-in}} = 25 \left(\frac{100 \, Y_{\text{i, out-in}}}{Y_{\text{out-in}}} \right)^{\frac{1}{3}} - 17 \tag{24}$$

$$U^\star_{\text{i, out-in}} = 13 \, W^\star_{\text{i, out-in}} \left(u'_{\text{i, out-in}} - 0.1978 \right) \tag{25}$$

$$V^\star_{\text{i, out-in}} = 13 \, W^\star_{\text{i, out-in}} \left(v'_{\text{i, out-in}} - 0.3122 \right) \tag{26}$$

Following EN410 [58], the total distortion ΔE of each color i in the CIE1964 (U*, V*, W*) color vector space can be determined with

$$\Delta E_{\text{i, out-in}} = \sqrt{ \left(U^\star_{\text{i, out-in}} - U^\star_{\text{r, i}} \right)^2 + \left(V^\star_{\text{i, out-in}} - V^\star_{\text{r, i}} \right)^2 + \left(W^\star_{\text{i, out-in}} - W^\star_{\text{r, i}} \right)^2 } \tag{27}$$

where $U^\star_{\text{r, i}}$, $V^\star_{\text{r, i}}$ and $W^\star_{\text{r, i}}$ are taken from table 7 in EN410 [58]. This allows the specific color rendering index $Ri_{\text{out-in}}$ to be calculated for each test color i when the observer and the source of illumination are outdoors:

$$Ri_{\text{out-in}} := 100 - 4.6 \, \Delta E_{\text{i, out-in}} \tag{28}$$

and finally the general color rendering index $Ra_{\text{out-in}}$ for observers looking into the room from outdoors (see also [15]):

$$Ra_{\text{out-in}} := \frac{1}{8} \sum_{i=1}^{8} Ri_{\text{out-in}} \tag{29}$$

Equation 28 can be applied to the supplementary test colors with the numbers 9-14 as discussed in Chapter 4.4.5. Colors 9 to 12 are saturated red, yellow, green and blue. Color 13 is close to the color of Caucasian human skin and color 14 is a saturated green that is similar to the leaves of trees. As people tend to react sensitively to the appearance of other people, it may be appropriate to give high priority to color 13, so that outdoor observers do not misinterpret the room occupants to be pale or unwell. In analogy to Chapter 4.4.5 and [58], it can be noted that or $Ra_{\text{out-in}} > 90$ corresponds to very good color rendering. $Ra_{\text{out-in}} > 80$ corresponds to good color rendering. Similar thresholds apply for the $Ri_{\text{out-in}}$ for individual colors [15].

The comparison of Ra and $Ra_{\text{out-in}}$ for some solar-control systems is shown in Figure 14. It can be concluded that the quality of the color rendering is lower in almost all cases, when the observer is looking from outdoors to the room [15]. The difference is often so large that the quality of the color rendering changes from "very good" to "good" or it loses the attribute "good" [15]. The difference is significant in many cases and can be much larger than 25% [15]. The evaluation of test color 9 (saturated red) is particularly interesting since the solar control glazing are performing not good with respect of color rendering of red with $R9$ and $R9_{\text{out-in}}$ being significantly smaller than 80 and since there is a very big difference between $R9$ and $R9_{\text{out-in}}$ [15]. Ra is well defined only for approximately white light, $R9$ is therefore not defined for the roller blind made from a coated, thin polymer film, which shows interference patterns in the red spectral range [15]. It should be noted, that the color rendering of the Caucasian

Conventional color rendering evaluation of different products (when the observer is in the room)

Test sample description	τ_e	τ_v	Ra	R1	R2	R3	R4	R5	R6	R7	R8	R9	R10	R11	R12	R13	R14	mean value of R1-R14
Green glass from Annex D of EN410	-	0.77	98	99	98	96	98	98	96	97	98	98	93	97	93	99	98	97
roller blind of coated, thin polymer film in gap between glass panes	-	0.08	74	91	84	57	72	94	79	65	46	n.a.	71	55	79	92	75	74
solar control DGU Nr. 1	0.26	0.52	91	89	95	95	88	90	94	95	85	56	87	86	85	88	98	88
solar control DGU Nr. 2	0.33	0.67	94	92	95	99	92	92	93	98	91	68	86	93	84	90	99	91
clear DGU	0.95	0.96	99	99	100	100	100	99	99	98	98	99	99	99	99	100	100	99

New color rendering evaluation of different products (when the observer is outdors)

Test sample description	τ'_e	τ'_v	Ra$_\text{out-in}$	R1$_\text{out-in}$	R2$_\text{out-in}$	R3$_\text{out-in}$	R4$_\text{out-in}$	R5$_\text{out-in}$	R6$_\text{out-in}$	R7$_\text{out-in}$	R8$_\text{out-in}$	R9$_\text{out-in}$	R10$_\text{out-in}$	R11$_\text{out-in}$	R12$_\text{out-in}$	R13$_\text{out-in}$	R14$_\text{out-in}$	mean value of R1$_\text{out-in}$ - R14$_\text{out-in}$
Green glass from Annex D of EN410	-	0.77	95	98	96	92	97	97	93	95	97	96	87	94	87	97	95	94
roller blind of coated, thin polymer film in gap between glass panes	-	0.08	50	92	60	10	52	94	48	34	11	n.a.	18	15	46	98	49	48
solar control DGU Nr. 1	0.26	0.52	84	79	91	91	77	81	89	90	71	19	76	74	71	77	97	77
solar control DGU Nr. 2	0.33	0.67	88	85	90	98	84	85	88	95	81	40	74	86	70	82	99	83
clear DGU	0.95	0.96	99	99	99	99	99	99	98	98	98	98	98	98	98	100	99	99

Relative Difference between Rx$_\text{out-in}$ and Rx for x $\in$ [1,14] or x = a

Test sample description		a	1	2	3	4	5	6	7	8	9	10	11	12	13	14	mean value of 1-14
Green glass from Annex D of EN410		-2%	-1%	-2%	-4%	-2%	-2%	-3%	-2%	-1%	-2%	-7%	-3%	-7%	-1%	-2%	-3%
roller blind of coated, thin polymer film in gap between glass panes		-32%	2%	-29%	-82%	-28%	0%	-39%	-49%	-77%	n.a.	-75%	-73%	-41%	7%	-35%	-40%
solar control DGU Nr. 1		-8%	-11%	-5%	-4%	-12%	-10%	-5%	-5%	-17%	-67%	-13%	-14%	-16%	-12%	-1%	-14%
solar control DGU Nr. 2		-6%	-8%	-5%	-1%	-8%	-8%	-5%	-3%	-10%	-41%	-14%	-7%	-17%	-10%	-1%	-10%
clear DGU		0%	0%	0%	-1%	-1%	0%	0%	-1%	-1%	-1%	-1%	-1%	-1%	0%	0%	-1%

Figure 14: Comparison of Ra and $Ra_\text{out-in}$ for some solar-control systems and double glazing units (DGU). Ra and $Ra_\text{out-in}$ are based on the color rendering properties of the moderately saturated test colors 1-8 according to EN410 [58]. Ri and $Ri_\text{out-in}$ for the supplementary test colors 9-14 have been calculated with the methods specified in CIE 13.3 [42]. These test colors are excluded from Ra by definition in EN410. They are also excluded from $Ra_\text{out-in}$ in order to guarantee a valid comparability between the new criterion and Ra. τ_e and τ_v are the solar and light transmittance respectively. τ'_e and τ'_v are the solar and light transmittance from indoors to outdoors. $\tau = \tau'$ because the test samples are non-scattering [15] (see also Figure 23 on page 61).

human skin (color 13) is not good for solar control DGU No. 1, when the observer is outdoors [15].

In the set-up shown in Figure 15, human observers can experience the color rendering quality when objects in a room are viewed from outdoors and the source of illumination is also outdoors. It could be a topic of future research to assess whether the set-up proposed in Figure 15 can be used for direct measurements of $Ra_\text{out-in}$. In this case, the observer could be replaced by a luminance camera with a color filter wheel which is designed and calibrated for color measurements [114]. The colored surface should be replaced by the 8 or 14 reference colors plus a well-defined white reference to set the white balance of the detection system [15]. With such a set-up, it is probably possible to measure directly the color tristimulus with and without glazing ($X_\text{out-in}, Y_\text{out-in}, Z_\text{out-in}$ and $X_\text{i, out-in}, Y_\text{i, out-in}, Z_\text{i, out-in}$ respectively) instead of using equations 12 and 13. In the case of measurements, it would be advisable to change the "gray room" on the right side of Figure 15 into a dark room since no base illuminance is necessary to ensure that the detector sensitivity corresponds to photopic vision.
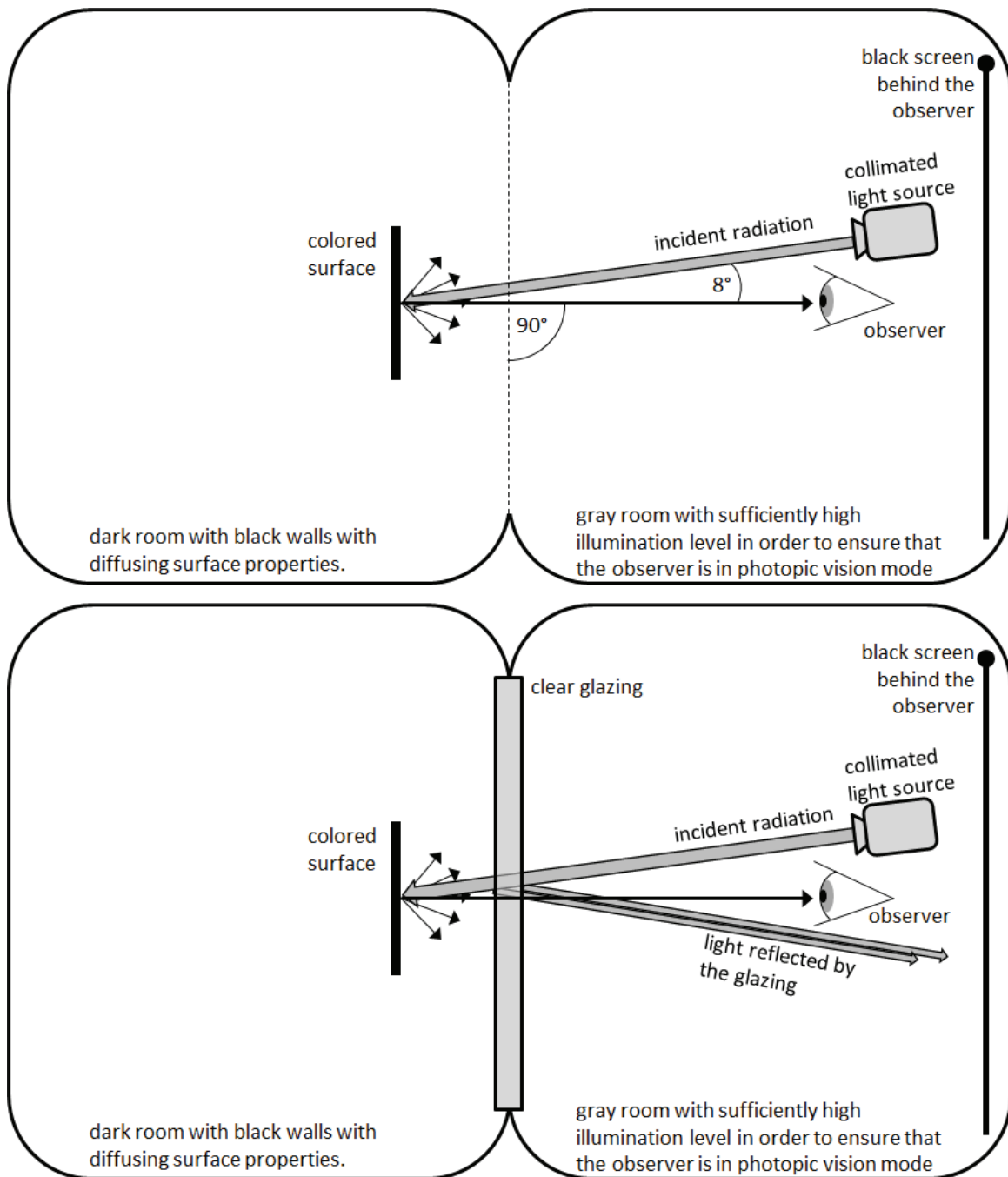
Figure 15: A possible set-up for observation of color rendering properties in the case of clear glazing and outdoor observers. It is important that the observer does not see the directly reflected image of the light source. Reflected images on the glazing do have an influence on the color impression in real situations but they should be excluded from the product characteristic $Ra_{\text{out-in}}$ which should be independent of the individual location and luminance of the surroundings of a certain building [15].

4.8 Influence of building envelope materials on the increased temperature of urban agglomerations relative to the surrounding rural areas (urban heat island effect)

It is well-known that the operative temperature in urban agglomerations can differ significantly from the temperature of the nearby rural areas. The difference has a typical diurnal pattern with increased temperatures, especially in the late afternoon and the night, known as the urban heat island (UHI) effect and with sometimes negative temperature differences in the morning which is called the urban cool island (UCI) effect [92], [40]. The UHI effect typically leads to 4 K higher temperatures compared to the surrounding rural areas which aggravates problems during heat waves, especially in warm climates, by increasing sickness and mortality rates. The UHI effect also leads to higher energy consumption for cooling and to overheating of buildings. An analysis of the interaction between "energy and climate in the built environment" was published by M. Santamouris et. al. in 2001 [108]. In general the following reasons are known for the UHI

- lower albedo due to darker surfaces (e.g. asphalt streets) and increased multiple reflections in urban canyons.

- higher density of local (waste) heat generation

- lower heat loss due to convection because of reduced wind speed caused by greater roughness in the urban environment

- increased surface area because of the morphology/roughness of the urban environment

- lower evaporation due to the reduction of vegetated areas

- increased radiative temperature because of buildings with warm surfaces in the surrounding environment.

The building skin (the facades and especially the roof) can help to minimize this effect by lowering the absorption of solar radiation (increased solar reflectance) and by increasing the infrared (IR) heat exchange with the clear sky, which is especially relevant in the case of warm climates with clear sky conditions in summer. The effects of this approach have been the subject of thorough research since the 1990s. An overview of the topic is provided by the Cool Pavements Compendium distributed by the U.S. Environmental Protection Agency and the references there-in [119].

The solar reflectance index (SRI) was introduced by the ASTM task group to promote the development and exploitation of cool construction materials by combining both effects, the solar reflectance properties and the emissivity into a single number. The SRI is therefore a measure of the effectiveness of a horizontal or low-sloped opaque surface in mitigating UHI overheating effects [22]. It is currently defined by the ASTM 1980-11 standard as the relative temperature of a surface (T_s) with respect to the temperature of a standard white surface (T_w) and the temperature of a standard black surface (T_b) under reference solar and ambient conditions. The definitions of the standard white surface (SRI = 100, solar reflectance= 0.80,

thermal emissivity = 0.90) and the standard black surface (SRI = 0, solar reflectance = 0.05, thermal emissivity =0.90) are such that SRI values greater than 100 and less than 0 are possible [22]. ASTM 1980-11 also specifies standard solar irradiation conditions and an ambient air temperature of 310 K, a sky temperature of 300 K and convective coefficients corresponding to low, medium and high wind speeds. Using these parameters, a heat-balance equation is solved iteratively to determine the steady-state temperature of the surface in question. Alternatively, the SRI for surfaces with a solar reflectance between 0.2 and 0.9 can be determined using an approximate equation with an average error of 0.9 and a maxi-mum error of 2, which is also cited in ASTM 1980-11. The SRI is therefore a measure for the daily peak temperature but it does not evaluate the effectiveness of radiative cooling during the night. On commission to the Betonverband Strasse, Landschaft, Garten e.V (German Concrete Association), Fraunhofer ISE measured the spectral reflectance properties of 16 different concrete pavers, calculated the resulting SRI values and correlated these to other optical properties. Eight of the pavers were chosen to represent neutral colours between black and white, while the other eight represented yellow, red and brown colours. The results can be found in [22].

It is clear, that the SRI is not meaningful, if the actual conditions are not similar to the reference conditions. In addition to that, the SRI is a simplified static measure for the daily peak temperature, as already mentioned above. If the impact of specific materials for building envelopes on the diurnal pattern of the UHI effect is to be evaluated, more sophisticated dynamic models (like e.g. [40]) have to be used.

4.9 Special aspects of transparent building-integrated PV (BIPV) envelope components

Multifunctional transparent building-integrated PV (BIPV) envelope components include the additional function to convert solar energy into solar electricity. The passive solar gains and the impact on thermal comfort are not independent from the solar electricity yield, because the passive solar gains and the temperature of the inner surface of the facade are affected by the portion of the absorbed solar energy that is converted into electricity and which is therefore no longer available to heat the facade components. All other (visual and optical) criteria are not affected by the additional PV function, since the PV-cells have the same visual and optical effect as e.g. screen-printed patterns with the same reflectance and transmittance. A methodology to simulate the electricity yield with special focus on the simulation of complex BIPV systems and the determination of the cell temperature has been developed under the guidance of the author of this document [115], [20]. Details are given in chapter 6.4.

4.10 Special aspects of building-integrated transparent solar thermal (BIST) collectors

Glazing-integrated solar thermal collectors present a particularly effective way to extract absorbed energy from the facade. The inlet temperature of the absorber and the flow rate have a very large influence on the passive solar gains and the temperature of the inner surface of the building envelope. Maximum solar gains and temperatures occur under stagnation conditions with a negligible flow rate. It is therefore impossible to decouple the active and passive solar gain evaluation for such systems and the g-value is not a constant any more, it becomes a function of the inlet temperature T_{in} and the fluid flow $\dot{q}$; g-value $= f(T_{in}, \dot{q})$. All other (visual and solar) parameters are not affected by the additional solar thermal function. A methodology for the evaluation of transparent solar thermal collectors and the integration of the model into the building simulation program TRNSYS has been developed under the guidance of the author of the present thesis [86], [17]. The model is described in chapter 6.5.

5 Measurement of the fundamental characteristics of solar-control systems

5.1 Calorimetric g-value measurements

Several different test facilities have been built around the world. They can be subdivided into indoor and outdoor test facilities. Outdoor test facilities have been built for example in several European countries within the European project "PASsive Solar Components and SYStems testing" (PASSYS) [97], in the U.S. [81], in Brazil [85] and recently in Holzkirchen, Germany [113] and Freiburg, Germany [87]. Indoor test facilities have been built for example in Freiburg, Germany [100], Rosenheim, Germany [18], Japan [82], Canada [39], Singapore [41], [43], South Corea [78] and a test facility is currently beeing build up at the China Academy of Building Research in Bejing.

This chapter specifies methods for the calorimetric measurement of g under stationary/steady-state laboratory conditions. It especially does not deal with transient conditions which frequently occur in outdoor test-facilities due to the changing sun-position and outdoor temperature. It also describes the corresponding error analysis [14]. The method is based on more than 25 years of experience with g-value testing at Fraunhofer ISE, Freiburg, Germany. Werner J. Platzer started the activities with the goal of characterizing transparent insulating materials [99]. They were continued to characterize many other transparent and translucent facade components with a focus on solar-control systems [8]. Recently, the activities have been extended to facade components that include active solar energy converters like building-integrated PV (BIPV) or building-integrated solar thermal collectors (BIST). Chapter 5.1 is the basis for the contributions of the author to the development of the new standard ISO/CD 19467 [5] to which the author of this document contributed as a member of the committee ISO/TC163/SC1/WG17.

In the case of *facades with dynamically adaptable properties*, g strongly depends on the actual setting. For the case of venetian blinds with rotatable slats this means, for example, that the g-value strongly depends on the actual tilt angle β_k of the slats [8], [10], [11]. In this document, β_k is used to describe the switching state of a dynamic facade in general, not only to specify the tilt angle of venetian blinds. Another example of dynamic facade properties results from the building integration of solar thermal collectors. In this case, g can vary by approximately a factor of 2, depending on the operation mode of the collector [17]. In general, it can be stated, that calorimetric measurements under steady-state laboratory conditions determine $g(\beta_k)$ for one specific setting of the parameter β_k. In most cases, several individual measurements with different settings of β_k are necessary in order to characterize a building skin component with sufficient accuracy.

The *direction of the incident radiation* has a strong impact on g [104], [105], [8]. In some cases, the component properties are rotationally symmetric and depend only on the angle of incidence α_i, which is especially true for insulating glazing units. Venetian blinds and other slatted or louvered devices with horizontal slats are sufficiently well approximated by symmetric properties with respect to the profile-angle α_p [8], [10]. However, no simple sym-

metry can be found in many other cases. A major advantage of indoor calorimetric g-value measurements with light coming from one well-defined direction is that they allow complex building components or complex fenestration systems to be characterized by increasing the number of measurements with different directions of the incident radiation step by step until a sufficiently accurate characterization is achieved.

During the measurements, the laboratory conditions should be close to the reference conditions, but it is never possible to reproduce the reference conditions exactly. The result of the measurements is therefore the solar heat gain coefficient under experimental laboratory conditions g_{exp}. It is then necessary either to prove that the difference between laboratory and reference conditions is negligible or to correct g_{exp} to reference conditions. This chapter describes also methods to correct experimentally determined values g_{exp} to reference conditions.

See also chapter 4.1.1 for the definition of g.

5.1.1 basic principles of steady-state lab measurements

In all cases, the test sample is irradiated with a solar simulator. The external environment in front of the sample is temperature-controlled and the outer surface of the test sample is exposed to artificial wind conditions. Two different approaches for calorimetric measurement of g are discussed.

- "cooled plate method": The test sample is mounted in front of a cooled flat-plate absorber (fig. 17) with an air gap between the inner surface of the sample and the cooled plate. The purpose of the absorber is to remove the energy that passes through the test sample. The convective-radiative heat transfer coefficient between the absorber and the indoor surface of the sample is set by choosing the width of this air gap. The evaluation of the measurement is based on a local energy balance at the center of the sample, directly resulting in the center of glazing value. For very small samples there can be an influence of the edges also at the center of the sample. Test samples therefore have to be sufficiently large when a generally valid center of glazing value g is to be determined. Edge effects can be analyzed with the heat flux sensors no. 1,3,7,10 and 11 (see figure 18)

- "cooled box method": The test sample is mounted in front of a cooled box. The evaluation is based on an energy balance for a model room behind the test sample (fig. 19). The set-up is in some ways similar to the set-up for U-value hot box measurements. A detailed description of such a method (without error analysis) is also given in [90]. The present document describes the method that has been implemented at Fraunhofer ISE, Freiburg, Germany, in detail. Cooled box methods always determine the overall g-value including potential edge effects. The center of glazing value can be determined with this method when the influence of edges and lateral losses can be neglected. This means that these parts of the test sample must be covered with insulation material to a sufficient extent.
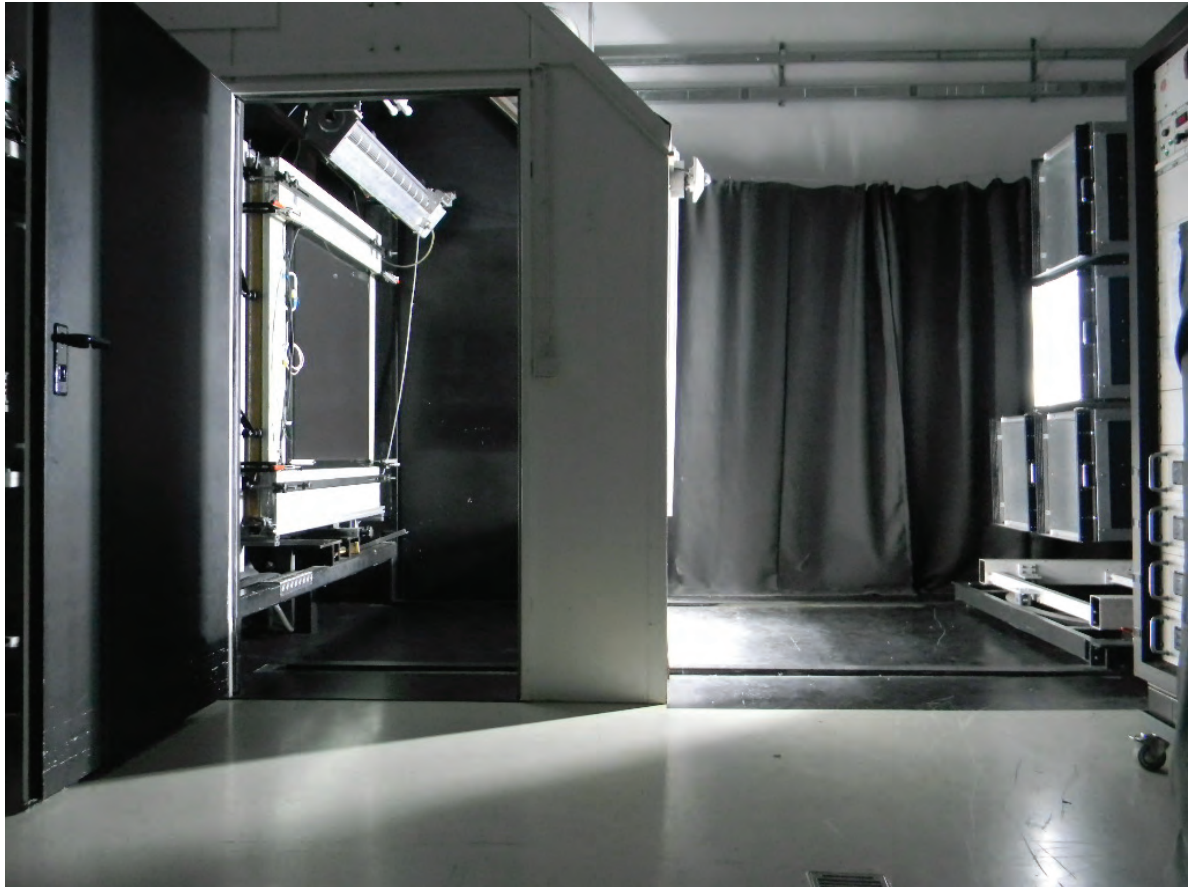
Figure 16: Picture of the device for calorimetric g-value testing at Fraunhofer ISE, Freiburg, Germany.
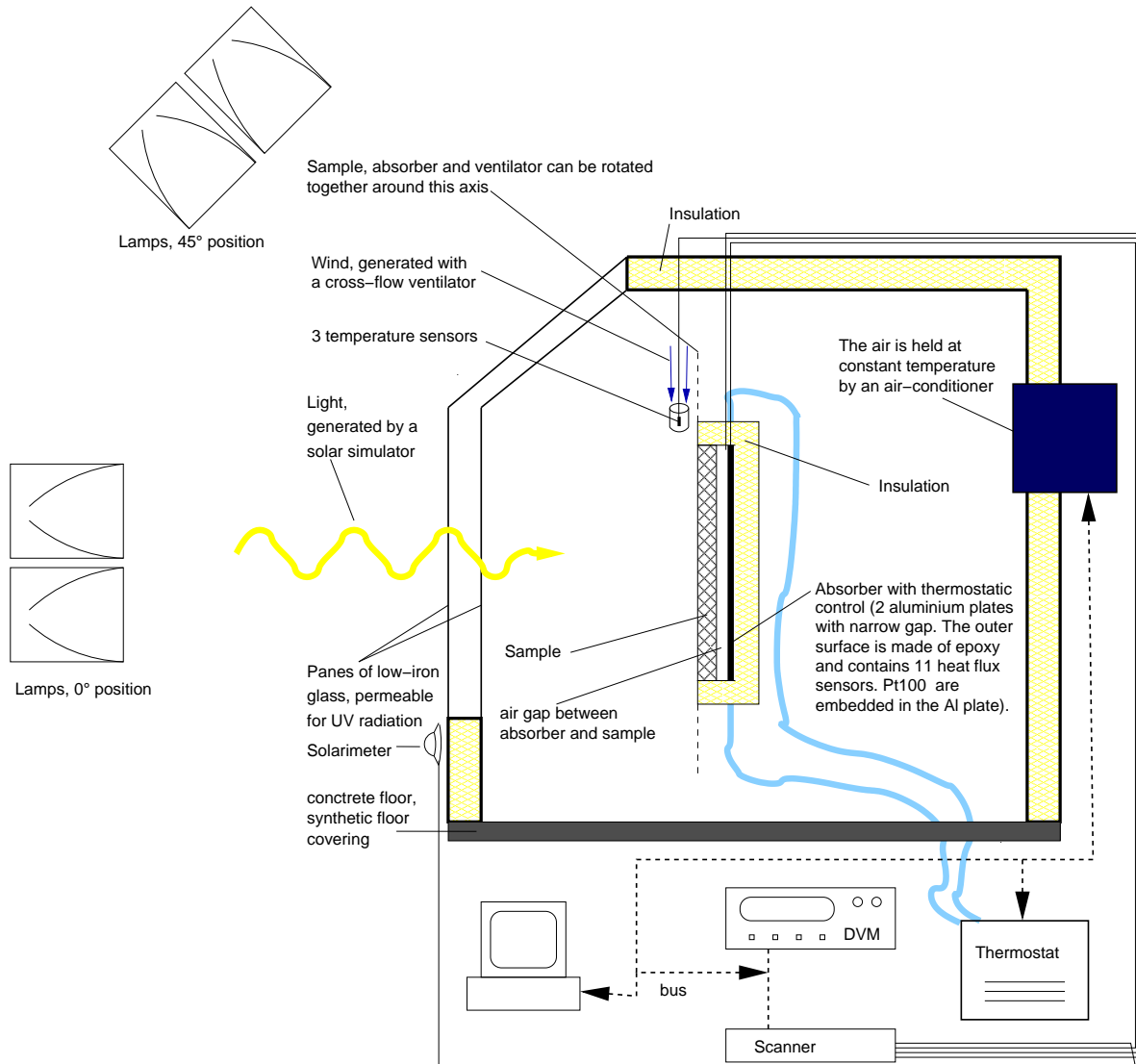
Figure 17: Schematic drawing of the device for calorimetric g-value testing. The modification of the angle of incidence can be realized in two different ways: Either the lamps remain in 0°-position and the sample is rotated around a vertical axes. Or the solar height angle α_s is changed by moving the lamps. The combination of both movements is necessary to realize combined non-zero facade azimuth angle γ_f and non-zero α_s. This set-up is called the "cooled-plate" method.
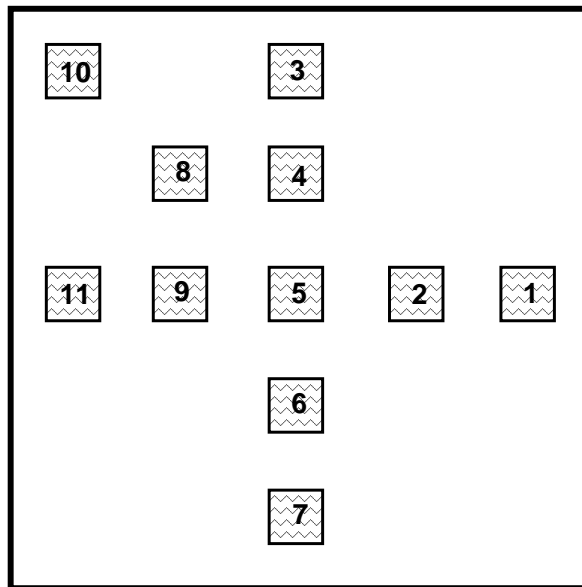
Figure 18: Positioning of the 11 heat-flux sensors for the detection of the heat flux q_{abs} $[W/m^2]$ into the absorber. The central heat flux sensor no. 5 is used for the evaluation of the "center of glazing"-value.
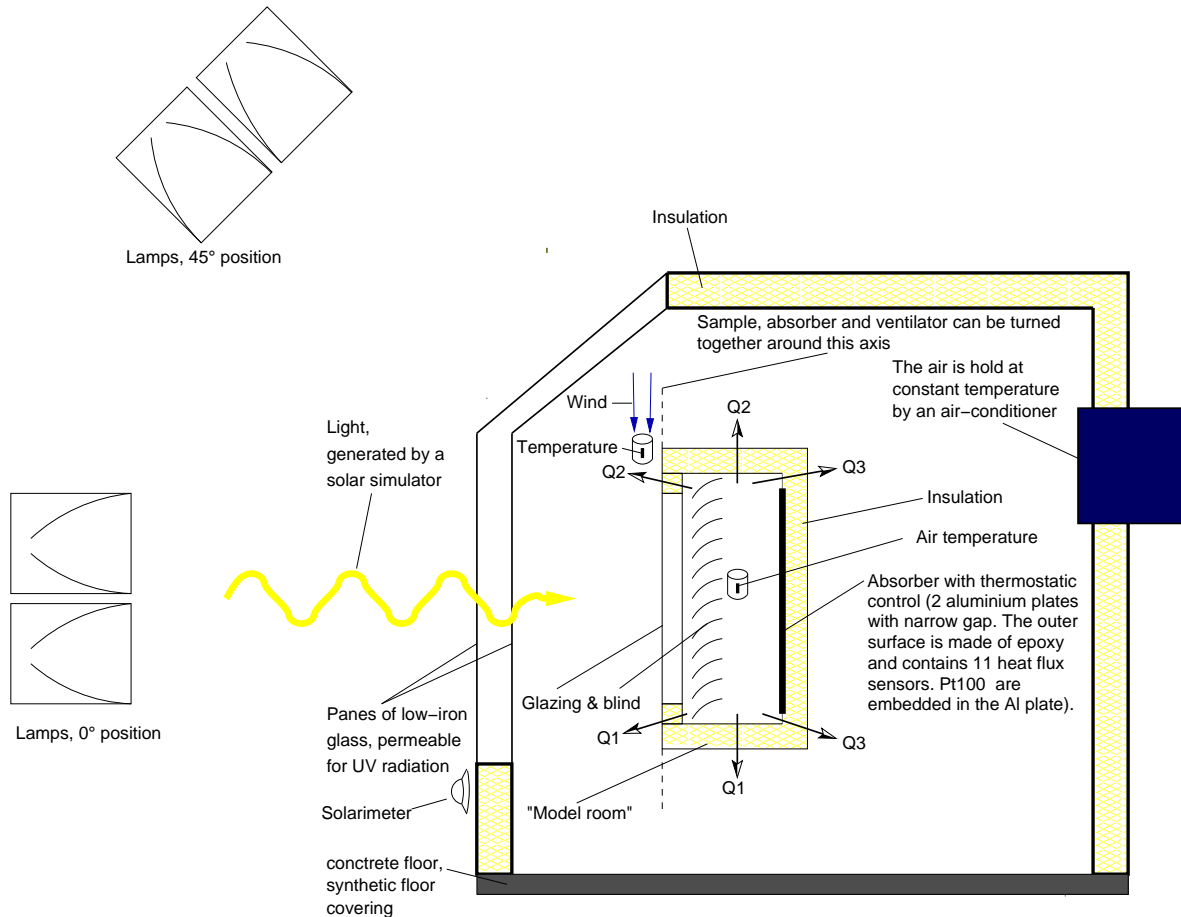
Figure 19: Schematic drawing of the set-up for the calorimetric g-value testing of combinations of glazing and internal venetian blind. This set-up is called the "cooled-box" method. A model room is mounted in front of the absorber. Q1 - Q3 are additional loss heat flow rates due to the non-local evaluation and the increased size of the loss area compared to fig. 17. In the following Q1 is denoted with $Q_{\mathrm{additional,bottom}}$ Q2 with $Q_{\mathrm{additional,top}}$ and Q3 is denoted with $Q_{\mathrm{additional,back}}$. In the case of the "cooled-box" method, the internal temperature is treated differently compared to the "cooled-plate" method. In case of the "cooled-plate", the internal temperature is the temperature of the surface of the absorber. In the case of the "cooled-box method", it depends on the air temperature behind the test sample and the radiative temperature of the absorber (see chapter 5.1.2).

5.1.2   Procedure to determine the g-value under laboratory conditions (g_{exp})

Fundamental evaluation equation

The experimentally determined total solar energy transmittance g_{exp} is defined as:

$$g_{\text{exp}} := \frac{Q_{\text{abs}} + Q_{\text{loss}}}{A_{\text{ref}} \, E_{\text{ref}}} \tag{30}$$

Q_{abs} is the heat flow rate [W] into the absorber. A_{ref} is the clear area of the irradiated surface. E_{ref} is the irradiance in the reference plane. Q_{loss} is the loss heat flow rate resulting from a possible temperature difference between the interior space ("indoors") and the exterior space ("outdoors"). During the g-value measurement, efforts are made to keep Q_{loss} small compared to Q_{abs} by maintaining the smallest possible temperature difference between the interior space and the surroundings, so that the g value is only weakly sensitive to errors in the loss heat flow rate. This becomes evident when looking at the error amplification factor or sensitivity coefficient $\frac{\Delta g_{\text{exp}}}{g_{\text{exp}}}$ for the loss heat transfer rate, which is given to a first approximation by:

;

$$\frac{\Delta g_{\text{exp}}}{g_{\text{exp}}} \doteq \frac{Q_{\text{loss}}}{g_{\text{exp}}} \cdot \frac{\partial g_{\text{exp}}}{\partial Q_{\text{loss}}} \cdot \frac{\Delta Q_{\text{loss}}}{Q_{\text{loss}}} = \underbrace{\frac{Q_{\text{loss}}}{Q_{\text{abs}} + Q_{\text{loss}}}}_{\ll 1, \text{ if } (Q_{\text{loss}} \ll Q_{\text{abs}})} \cdot \frac{\Delta Q_{\text{loss}}}{Q_{\text{loss}}} \tag{31}$$

Relative errors in Q_{abs}, A_{ref} or E_{ref} influence the final result with a sensitivity coefficient of around 1. Thus, there is no significant error amplification in the definition of the problem. The fundamental evaluation equation (30) is therefore non-problematic with respect to error amplification. In general it is possible that special details have to be considered during the evaluation. But a fixed procedure can be defined for two cases, which comprise a large fraction of all measurements made:

- **Samples with a flat glass pane as the indoor-facing surface:** Test samples, in which a flat glass pane forms the indoor-facing surface and which should be tested with standard heat transfer coefficients applying to the indoor-facing surface. This category includes all multiple-pane glazing units, all glazing units with a venetian blind or other light-redirecting structure mounted between adjacent panes, and all combinations of exterior sun-shading devices and glazing units. The test sample is mounted such that there is an air gap between the indoor pane and the absorber (see fig. 17). These samples can be tested with both methods, the cooled plate method and the cooled box method.

- **Internal venetian blinds:** Internal (indoor) venetian blinds are mounted indoors in a room behind a glazing unit (viewed from outdoors). For this case, the glazing unit and venetian blind to be tested are mounted in a special model room which is mounted in front of the absorber (see fig. 19).

The scientific validation of this procedures has been done in the EU project ALTSET [100], [106] and the national German project REGES [18].

Please note: Our definition in eq. (30) implies that the losses or gains Q_{loss} due to a temperature difference are added or subtracted from the heat flow rate Q_{abs} that has been collected by the calorimeter during the measurement with sun. Our definition is in line with the implementation of the g-value in building simulation programs. It is therefore in line with the possible usage of the measured value. But there is also another possiblity to define the g-value. This second possibility (also used in ISO15099 [74]) is to define that Q_{abs} is the heat flow rate collected by the calorimeter "with sun" and that Q_{loss} is the heat flow rate collected "without sun" but with exactly the same temperature difference between inside and outside. Eq. (30) would then turn into:

$$\text{Alternative definition (ISO15099): } g_{\text{exp}} = \frac{Q_{\text{with sun}} - Q_{\text{without sun}}}{A_{\text{ref}} \, E_{\text{ref}}} \tag{32}$$

where

$$\text{Alternative definition (ISO15099): } Q_{\text{without sun}} = U_{\text{without sun}}^{\text{ISO15099}} \quad \Delta T_{\text{without sun}} \tag{33}$$

$U_{\text{without sun}}^{\text{ISO15099}}$ is the U-value of the test sample in the dark measurement. For the second definition it is essential to ensure that $T_{\text{without sun}} = T_{\text{with sun}}$ for the internal and external environment in the dark measurement. But this is never possible exactly in an experimental (non-theoretical) situation. This especially means that dark measurements with very little temperature difference have to be performed in case of measurements with $\Delta T \approx 0$. We therefore use

$$Q_{\text{loss}} = U_{\text{without sun}} \quad \Delta T_{\text{with sun}} \tag{34}$$

In our case $U_{\text{without sun}}$ is the U-value of the test sample in the dark measurement where

$$\frac{T_{\text{internal without sun}} + T_{\text{external without sun}}}{2} = \frac{T_{\text{internal with sun}} + T_{\text{external with sun}}}{2} \tag{35}$$

For more details and an error analysis see chapter 5.1.2. It is important to note that the two definitions (30) and (32) only lead to significantly different g-value results when $\Delta T \gg 0$.

Fundamental equation for the "cooled plate" method

For spatially localised evaluation eq. (30) simplifies to

$$g_{\text{exp}} = \frac{q_{\text{abs}} + q_{\text{loss}}}{E_{\text{ref}}} \tag{36}$$

q_{abs} is the measured value from the central heat flux sensor 5, corresponding to the heat flux $[W/m^2]$ into the absorber. E_{ref} is the irradiance in the reference plane. q_{loss} is the loss heat flux which results due to a possible temperature difference between the interior space and the exterior space.

The overall measurement uncertainty of the center of glazing value of g_{exp} is given by:

$$
\begin{aligned}
\Delta g_{\text{exp}} &= \sqrt{\left(\frac{\partial g_{\text{exp}}}{\partial q_{\text{abs}}} \Delta q_{\text{abs}}\right)^2 + \left(\frac{\partial g_{\text{exp}}}{\partial q_{\text{loss}}} \Delta q_{\text{loss}}\right)^2 + \left(\frac{\partial g_{\text{exp}}}{\partial E_{\text{ref}}} \Delta E_{\text{ref}}\right)^2 + (\Delta_{\text{imperfect test sample}})^2} \\
&= \sqrt{\left(\frac{\Delta q_{\text{abs}}}{E_{\text{ref}}}\right)^2 + \left(\frac{\Delta q_{\text{loss}}}{E_{\text{ref}}}\right)^2 + \left(\frac{(q_{\text{abs}} + q_{\text{loss}})}{E_{\text{ref}}^2} \Delta E_{\text{ref}}\right)^2 + (\Delta_{\text{imperfect test sample}})^2} \tag{37}
\end{aligned}
$$

The expanded measurement uncertainty values according to GUM [71] are used for the measurement uncertainties ΔX_i of the individual measured quantities X_i. As all of the measured quantities have the same extension factor, $k_i = 2$, it is not necessary to divide by individual k_i values before the sum of the squared quantities is calculated.

Fundamental equation for the "cooled box" method

The cooled box method is inevitable for indoor-mounted solar-control systems (e.g. internal venetian blinds or roller blinds) and other building components with non-flat indoor surface. In this case, the application of eq. (30) results in

$$
g_{\text{exp}} = \frac{A_{\text{abs}}\,\overline{q_{\text{abs}}} + Q_{\text{additional, bottom}} + Q_{\text{additional, top}} + Q_{\text{loss}}}{A_{\text{ref}}\,E_{\text{ref}}}
\tag{38}
$$

$\overline{q_{\text{abs}}}$ is the average heat flux $[W/m^2]$ into the absorber (see section 5.1.2). E_{ref} is the irradiance in the plane of the outdoor pane and A_{ref} is the clear area of the irradiated surface (outdoor pane area excluding the insulated spacers). $Q_{\text{additional, bottom}}$ and $Q_{\text{additional, top}}$ are small additional heat flow rates through the opaque, insulated walls of the model room. Q_{loss} $[W]$ is the loss heat flow rate which results due to a possible temperature difference between the interior space and the exterior space.
The resulting measurement uncertainty is:

$$
\Delta g_{\text{exp}} = \left[\left(\frac{A_{\text{abs}}\Delta \overline{q_{\text{abs}}}}{A_{\text{ref}}E_{\text{ref}}} \right)^2 + \left(\frac{\overline{q_{\text{abs}}}\Delta A_{\text{abs}}}{A_{\text{ref}}E_{\text{ref}}} \right)^2 + \left(\frac{\Delta Q_{\text{additional, top}}}{A_{\text{ref}}E_{\text{ref}}} \right)^2 + \left(\frac{\Delta Q_{\text{additional, bottom}}}{A_{\text{ref}}E_{\text{ref}}} \right)^2 \right.
$$
$$
\left. + \left(\frac{\Delta Q_{\text{loss}}}{A_{\text{ref}}E_{\text{ref}}} \right)^2 + \left(\frac{(A_{\text{abs}}\,\overline{q_{\text{abs}}} + Q_{\text{loss}})}{(A_{\text{ref}}E_{\text{ref}})^2} \right)^2 \left(A_{\text{ref}}^2\Delta E_{\text{ref}}^2 + E_{\text{ref}}^2\Delta A_{\text{ref}}^2 \right) + \Delta_{\text{UPr}}^2 \right]^{(1/2)}
\tag{39}
$$

whereby $\Delta_{\text{UPr}} = \Delta_{\text{imperfect test sample}}$.

The measurement uncertainties Δq_{abs}, Δq_{loss} und ΔE_{ref} und $\Delta_{\text{imperfect test sample}}$ are explained and defined in the following sections.

Measurement of the heat flux into the absorber q_{abs} or $\overline{q_{\text{abs}}}$

The heat flux into the absorber is measured with eleven heat flux sensors which are permanently installed in the absorber. The calibration of the heat flux sensors is done with opaque calibration panels with thermal conductivity λ specifications that are traceable to national standards and with an additional temperature controlled plate. Both, the calibration panel and the temperature controlled plate are put in front of the absorber in order to generate

a well-known heat flux which is then compared with the signal of the heat flux sensors using the evaluation procedures defined in [71]. In the following, it is thus assumed that the measurement uncertainty for each of the eleven heat flux sensors is known.

In case of quasi-homogeneous samples, the spatially localised "center of glazing" evaluation is based on the signal q_{abs} of heat flux sensor no. 5 in the centre of the absorber (see fig. 18). In case of inhomogeneous samples the average $\overline{q_{\text{abs}}}$ of heat flux sensors no. 3-7 is taken or an additional metal plate is mounted in front of sensors no. 4-6 in order to average the heat flux between the areas with and without heat flux sensors.

q_{abs} for the cooled plate method (evaluation with one heat flux sensor)

When samples with flat indoor-surface are measured with the cooled plate method, the absorber represents the "indoor space". In this case, the heat flux q_{abs} to be entered into eq. (30) is the measured value from the heat flux sensor no. 5 in the centre of the absorber. The measurement uncertainty $\Delta q_{\text{abs, i}}$ of sensor i can thus be obtained from

$$\Delta q_{\text{abs, i}} = 2 \sqrt{\left(\frac{\Delta q_{\text{abs, i, calibration tolerance}}}{2}\right)^2 + \left(\frac{\sigma_{q_{\text{abs}}}}{\sqrt{n}}\right)^2} \tag{40}$$

Here, $\Delta q_{\text{abs, i, calibration tolerance}}$ is the expanded measurement uncertainty resulting from the calibration of the heat flux sensor. $\Delta q_{\text{abs, i, calibration tolerance}}$ is divided by 2, because expanded uncertainty values have already been multiplied by a factor of 2 according to [71].

$\overline{q_{\text{abs}}}$ for the cooled-box method (evaluation with the average of several heat flux sensors)

The set-up for the measurement with the cooled box (with model room behind the sample) is shown in fig. 19. It is especially useful for the measurement of internal solar-control systems (sun-shading devices that are mounted indoors). In this case, the "indoor room" is represented by an enclosed air space ("model room") and the average value $\overline{q_{\text{abs}}}$ from several heat flux sensors must be entered into eq. (38). The average is taken, because the depth of the model room means that it can no longer be assumed that the heat flow rate into the absorber can be evaluated locally. In this case, the value measured in the centre of the absorber (heat flux sensor no. 5 in fig. 18) is not necessarily representative for the average over the complete height of the sample. Therefore, the average of the values from the heat flux sensors 3 to 7 is used, applying the assumption that the heat transport occurs essentially two-dimensionally, because a convection roll forms that causes only very slight lateral heat transport. In general, the following equation applies for the average over n heat flux sensors:

$$\overline{q_{\text{abs}}} = 1/n \sum_{i=1}^{n} q_{\text{abs, i}} \tag{41}$$

The resulting measurement uncertainty Δq_{abs} for any arbitrary selection of n heat flux sensors with individual measured values $q_{\text{abs,i}}$ is given by:

$$\Delta \overline{q_{\text{abs}}} \quad = \quad 1/n \sum_{i=1}^{n} \Delta q_{\text{abs, i}} \quad \left(> 1/n \sqrt{\sum_{i=1}^{n} \Delta q_{\text{abs, i}}^2} = \sqrt{\sum_{i=1}^{n} \left(\frac{\Delta q_{\text{abs, i}}}{n} \right)^2} \right) \tag{42}$$

$$\Delta q_{\text{abs, i}} \quad = \quad 2 \sqrt{\left(\frac{\Delta q_{\text{abs, i, calibration tolerance}}}{2} \right)^2 + \left(\frac{\sigma_{q_{\text{abs, i}}}}{\sqrt{n}} \right)^2} \tag{43}$$

The uncertainties for the different heat flux sensors $\Delta q_{\text{abs, i}}$ are added linearly, because the considered case does not involve several measured values which are expected to be equal and where the measured values are distributed normally around a (correct) average value. In other words: If we assume for the moment, that all heat flux sensors have exactly the same relative error. Then the relative error for $\overline{q_{\text{abs}}}$ is equal to the relative error for $q_{\text{abs,i}}$ only for the case of linear addition. In the case of quadratic addition, identical relative errors for the different heat flux sensors $\frac{\Delta q_{\text{abs,i}}}{q_{\text{abs,i}}} = \frac{\Delta q_{\text{abs,j}}}{q_{\text{abs,j}}}$ always result in $\frac{\Delta \overline{q_{\text{abs}}}}{\overline{q_{\text{abs}}}} < \frac{\Delta q_{\text{abs,i}}}{q_{\text{abs,i}}}$, which would be a contradiction, as the relative systematic uncertainty cannot be reduced by averaging over several *different* heat flux values. The error could only be reduced by multiple measurements when the *same* heat flux at the *same* position would be measured with different sensors.

Additional heat transfer rate $Q_{\text{additional, back}}$ towards space behind the model room above the absorber: The small additional heat transfer rate $Q_{\text{additional, back}}$ $[W]$, which occurs above and below the absorber through the back surface of the model room, is generally of the magnitude of 3 % of the heat transfer rate through the absorber itself. It is thus treated with the following simplified approach:

$$Q_{\text{additional}} \quad = \quad A_{\text{additional, bottom}} \, q_{\text{additional, bottom}} + A_{\text{additional, top}} \, q_{\text{additional, top}} \tag{44}$$
$$\Delta Q_{\text{additional}} \quad \leq \quad 0.20 \, Q_{\text{additional}} \tag{45}$$

Determination of E_{ref} and the measurement uncertainty ΔE_{ref}

As solar simulators do not provide ideally parallel radiation, the irradiance depends on the distance from the solar simulator (see also fig. 20). The individual layers of the test sample and the absorber are thus irradiated with slightly different irradiance values. For the case of the calorimeter at Fraunhofer ISE, a typical value for the relative change in the irradiance at the position of the sample is $f = 0.7\%/cm$, where f is defined as

$$f := \frac{E_{\text{s, out}}/E_{\text{abs}} - 1}{x_{\text{abs}} - x_{\text{s, out}}} \tag{46}$$

$x_{\text{s, out}}$ or $E_{\text{s, out}}$ is the position or the irradadiance on the outdoor sample surface respectively. x_{abs} or E_{abs} is the position or the irradadiance on the absorber respectively. It is clear that
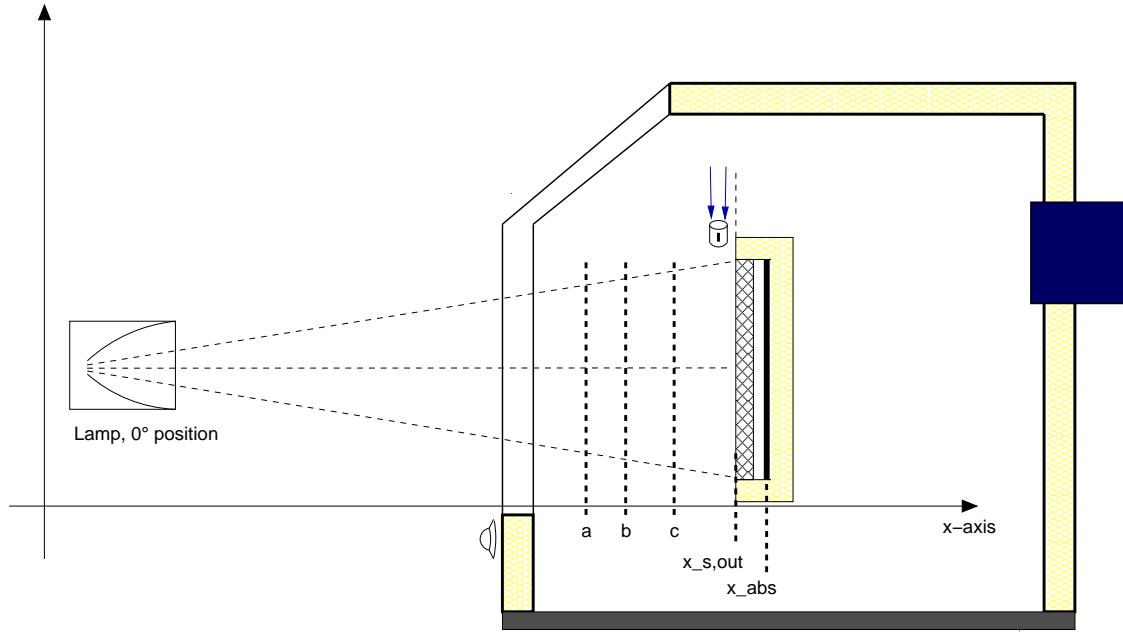
Figure 20: Description of the influence of divergent (non-parallel) incident irradiation. The irradiance E is reduced from $x = a$ to $x = c$ due to the divergency of the light. There is also a difference between the irradiance at the absorber E_{abs} and e. g. the irradiance $E_{\text{s, out}}$ at the outer surface of the test sample.

the reference irradiance E_{ref}, which is used for the evaluation of the g measurements, is to be determined in the proper plane. How the x-position dependence of the irradiance value needs to be taken into account during the evaluation depends on whether the evaluation is done with the cooled plate method (section 5.1.2) or with the cooled box method (section 5.1.2).

The non-parallel irradiation also means that the direction of the incident direction is not perfectly well-defined. The sample receives radiation from $[\alpha_{\text{s}} \pm \Delta\alpha_{\text{s}}, \gamma_{\text{f}} \pm \Delta\gamma_{\text{f}}]$. $\Delta\alpha_{\text{s}}$ and $\Delta\gamma_{\text{f}}$ depend on the distance between the lamp and the sample, the size of the lamp, the reflector geometry and the arrangement of the different lamps of the simulator (see also figure 16). The effect of the variation of the direction of the incident radiation can be considerable in case of samples with strongly angular selective properties like venetian blinds with dark colored slats. We always aim to minimize the divergency in the direction in which the sample is most sensitive to non-parallel irradiation. In the case of venetian blinds with horizontal slats this means that the divergency in the vertical direction has to be minimized.

Another question is how to practically measure the irradiance E_{ref} in the desired plane x_{ref}. For the measurement of the irradiance on the outdoor sample surface, the sample has to be moved backwards (or even removed) since it is otherwise not possible to position the sensor surface of the pyranometer in the plane $x = x_{\text{s, out}}$ because of the thickness of the pyranometer. The irradiance distribution in the plane $x = x_{\text{s, out}}$ is therefore determined before the actual measurement of g and the values are being compared with an additional monitor pyranometer. The monitor pyranometer is also used when the test sample is in place.

It allows to control that the overall irradiance level of the lamps is equal to the level during the scanning of the irradiance distribution. The monitor pyranometer is not used to normalize the irradiance distribution continuously, as the fluctuation of the irradiance from the solar simulator is much smaller than the accuracy of the monitor pyranometer. The fluctuation of the monitor pyranometer is taken into account only in determining the value of the error bar of E_{ref}. Another possibility is to measure the irradiance in a plane in front of the sample at the position $x_{\mathrm{scan}} \neq x_{\mathrm{ref}}$. In this case

$$E_{\mathrm{ref}} = E_{\mathrm{scan}} \left(1 + f\left(x_{\mathrm{scan}} - x_{\mathrm{ref}}\right)\right) \tag{47}$$

where f is defined according to eg. (46)

$E_{\mathbf{ref}}$ for the cooled box method

For the cooled box method, an energy balance has to be made on the enclosing boundaries of the model room behind the sample (fig. 19). E_{ref} is therefore the average irradiance at the balance boundary plane at position x_{ref}. This is the outdoor surface of the glazing unit $x_{\mathrm{ref}} = x_{\mathrm{s, out}}$ for the case of the method developed at Fraunhofer ISE.

$$E_{\mathrm{ref}} = 1/n \sum_{i=1}^{n} E_{\mathrm{scan, i}} \tag{48}$$

whereby the measured values $E_{\mathrm{scan, i}}$ are the measurement positions i along a vertical line in the centre of the sample.

If the irradiance scan was made in the desired plane x_{ref}, then the values measured during the scan can be used directly for the evaluation of g. However, the fluctuation of the simulator $\Delta E_{\mathrm{fluctuation}} = \frac{\sigma_{\mathrm{MonPyr}}}{\sqrt{n}}$ must be added to the uncertainty which results from the calibration of $E_{\mathrm{scan, i}}$.

The resulting measurement uncertainty ΔE_{ref} for any arbitrary selection of n measurement points with individual values $E_{\mathrm{ref,i}}$ is then

$$\Delta E_{\mathrm{ref}} = 1/n \sum_{i=1}^{n} \Delta E_{\mathrm{ref, i}} \tag{49}$$

$$\Delta E_{\mathrm{ref, i}} = 2\sqrt{\left(\frac{\Delta E_{\mathrm{scan,i}}}{2}\right)^2 + \left(\frac{\sigma_{\mathrm{MonPyr}}}{\sqrt{n}}\right)^2 + \left(\frac{\overline{E_{\mathrm{MonPyr, g\text{-}mess}}} - \overline{E_{\mathrm{MonPyr, scan\text{-}mess}}}}{\sqrt{3}}\right)^2}$$

The $\Delta E_{\mathrm{ref, i}}$ errorbars are added linearly, because the considered case does *not* involve several measured values which are expected to be equal. See also the analogous determination of the average heat flux (Section 5.1.2). $\left(\overline{E_{\mathrm{MonPyr, g\text{-}mess}}} - \overline{E_{\mathrm{MonPyr, scan\text{-}mess}}}\right)$ is the difference between the averages of the monitor pyranometer during the actual g value measurement and during the irradiance scan.
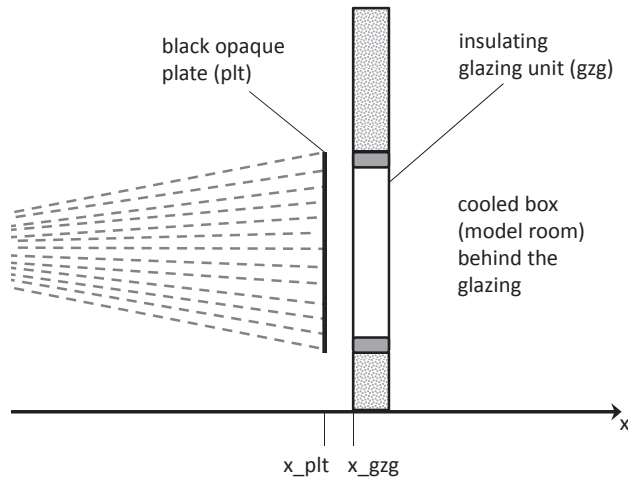
Figure 21: Description of the influence of divergent (non-parallel) incident irradiation in case of a black plate which is mounted outdoors in front of an insulating glazing unit. Without the black plate or a shading system, the irradiance is higher at x_{plt} than at x_{gzg} due to the divergency of the light. In this case, the reference irradiation for the evaluation of the g-value measurement is $E_{\mathrm{ref}} = E_{\mathrm{plt}}$.

Special care has to be taken in case of test samples with additional externally mounted devices (like e.g. venetian blinds) and when these layers absorb, scatter or re-direct the irradiation. As an example, the theoretical case of a black opaque plate which is mounted in in front of the outdoor-side of an insulating glazing panel (fig. 21) is considered. Since all radiation is absorbed or reflected at the plane of the black plate at $x = x_{\mathrm{plt}}$ it is clear that q_i is determined by E_{plt}. In case of such an external device on the outdoor side, the reference irradiation for the evaluation of the g-value measurement is therefore $E_{\mathrm{ref}} = E_{\mathrm{plt}} > E_{\mathrm{gzg}}$. Please see also chapter 5.1.2 for a detailed discussion of E_{ref}.

E_{ref} for the cooled plate method

For cooled plate method there is no unique position of the reference plane for E_{ref} which is valid for all types of samples. Nevertheless it is possible in most cases to use one general reference plane x_{ref} when the sample specific effects are included in the errorbar ΔE_{ref}. The following examples are intended to explain the influence of the sample on the reference plane:

- For clear non-scattering and non-absorbing samples g is equal to the solar transmittance τ_e of the test sample. There is no secondary inward flowing fraction in this case ($q_i = 0$ In this case the equation $E_{ref} = E_{abs}$ applies because the irradiance incident on the absorber is reduced by τ_e. The measured heat flux q_{abs} at the absorber is therefore independent from the position x_s of the sample (see also fig. 20).

- If the outer pane of a multiple-pane glazing unit consists of an opaque black panel, the equation $E_{ref} = E_{s, out}$ applies. q_{abs} is independent from x_{abs} (the distance between solar simulator and absorber) in this case.

- For a non-absorbing sample, for which the outdoor pane is ideally diffusely and isotropically scattering, the equation $E_{ref} = E_{s, out}$ also applies.

- A non-absorbing, multiple-pane glazing unit with ideal clear panes except the outdoor pane has no secondary inward flowing fraction q_i and $g = \tau_e$. The solar transmittance consists of two parts, direct-direct transmittance $\tau_{e,d-d}$ and the direct diffuse transmittance $\tau_{e,d-dif}$

$$\tau_e = \tau_{e,d-d} + \tau_{e,d-dif} \tag{50}$$

Only the outdoor pane has a non-negligible direct-diffuse transmittance $\tau_{e,d-dif} \neq 0$. If the irradiance was measured by scanning in the x_{scan} plane and the irradiance distribution E_{scan} was determined there, then the following equation applies:

$$E_{ref} = E_{scan} \left(1 + f \left(\frac{\tau_{e,d-dif}}{\tau_e} \left(x_{s, out} - x_{scan} \right) + \frac{\tau_{e,d-d}}{\tau_e} \left(x_{abs} - x_{scan} \right) \right) \right) \tag{51}$$

where f has been defined in eq. (46).

In real samples, absorption always occurs in various layers, often combined with scattering. Werner J. Platzer developed the general formula eq. (52) for E_{ref} in the ALTSET project (report ALTSET-ISE-1-1997):

$$E_{ref} = \tag{52}$$
$$E_{scan} \left[1 + f \left(\frac{q_i}{g} \left(x_{q_i} - x_{scan} \right) + \frac{\tau_{e,d-dif}}{g} \left(x_{diff} - x_{scan} \right) + \frac{\tau_{e,d-d}}{g} \left(x_{abs} - x_{scan} \right) \right) \right]$$

$(x_{dif} - x_{scan})$:   distance of the plane relevant for $\tau_{e,d-dif}$ from the scanning plane
$(x_{q_i} - x_{scan})$:   distance of the plane relevant for q_i from the scanning plane

Practical approach: If particularly stringent requirements on the accuracy of g apply, the evaluation is made on the basis of eq. (52). However, this is generally not the case. Normally, experienced laboratory personnel estimate the position of the relevant plane and evaluate the

resulting additional uncertainty ΔE_{Div} with the help of eq. (52). For examples on how to do such an estimation see [106]. The following equation then applies for ΔE_{ref}:

$$\Delta E_{\text{ref}} = 2\sqrt{\left(\frac{\Delta E_{\text{scan}}}{2}\right)^2 + \left(\frac{\Delta E_{\text{Div}}}{\sqrt{3}}\right)^2 + \left(\frac{\sigma_{\text{MonPyr}}}{\sqrt{n}}\right)^2 + \left(\frac{\overline{E_{\text{MonPyr, g-mess}}} - \overline{E_{\text{MonPyr, scan-mess}}}}{\sqrt{3}}\right)^2}$$

(53)

where $\left(\overline{E_{\text{MonPyr, g-mess}}} - \overline{E_{\text{MonPyr, scan-mess}}}\right)$ is the difference between the averages of the monitor pyranometer during the actual g value measurement and during the irradiance scan.

Determination of the loss heat flux q_{loss}

The loss heat flux q_{loss} arises due to a difference between the interior temperature T_{int} and the exterior temperature T_{ext}. In order to minimize the error bar of g, temperatures are chosen with the aim of minimizing q_{loss}.

Determination of q_{loss} and Δq_{loss} for the cooled plate method

When the absorber represents the interior space, the loss heat flux is given by

$$q_{\text{loss}} = U^* \left(T_{\text{abs}} - T_{\text{ext}}\right)$$

(54)

U^* is determined from a dark measurement (solar simulator off) with a non-negligible temperature difference. The average sample temperature is chosen to be similar to that during the actual g value measurement, because the conductivity of samples generally depends on the temperature, particularly due to heat transport by infrared radiation. Non-linear effects due to the changed temperature difference are neglected as being effects of higher order.

$$U^* = \frac{q_{\text{abs, dark}}}{\left(T_{\text{abs, dark}} - T_{\text{ext, dark}}\right)}$$

(55)

Thus, the following equations apply:

$$\Delta q_{\text{loss}} = \sqrt{\left(\left(T_{\text{abs}} - T_{\text{ext}}\right)\Delta U^*\right)^2 + \left(U^* \Delta T_{\text{abs}}\right)^2 + \left(U^* \Delta T_{\text{ext}}\right)^2}$$

(56)

$$\Delta U^* = \sqrt{\left(\frac{\Delta q_{\text{abs, dark}}}{\left(T_{\text{abs, dark}} - T_{\text{ext, dark}}\right)}\right)^2 + \left(\frac{\Delta T_{\text{abs, dark}}}{\left(T_{\text{abs, dark}} - T_{\text{ext, dark}}\right)^2}\right)^2 + \left(\frac{\Delta T_{\text{ext, dark}}}{\left(T_{\text{abs, dark}} - T_{\text{ext, dark}}\right)^2}\right)^2}$$

The expanded uncertainty should be entered for the uncertainty $\Delta X_{i,\text{calibration}}$ of the measured quantity X_i, which results from the calibration uncertainty and statistical fluctuation.

$$\Delta X_i = 2\sqrt{\left(\frac{\Delta X_{i,\text{calibration}}}{2}\right)^2 + \left(\frac{\sigma_{X_i}}{\sqrt{n}}\right)^2}$$

(57)

Determination of q_{loss} and Δq_{loss} for the cooled box method

$$Q_{\mathrm{loss}} = Q_{\mathrm{loss,walls}} + Q_{\mathrm{loss,sample}} \tag{58}$$

The loss heat flow rate Q_{loss} is the sum of the loss heat flow rate for the insulating walls of the model room $Q_{\mathrm{loss,walls}}$ and the loss heat flow rate for the sample itself, $Q_{\mathrm{loss,sample}}$. The two heat flow rates are similar and small, being typically 1% to 4% of the heat flow rate into the absorber. In case of the measurement of an internal venetian-blind (see fig. 19) it applies:

$$
\begin{aligned}
Q_{\mathrm{loss,walls}} &= (U \cdot A)_{\mathrm{walls,back}} \left(T_{\mathrm{eff,i,back}} - T_{\mathrm{ext}} \right) \\
&\quad + (U \cdot A)_{\mathrm{walls,front}} \left(T_{\mathrm{eff,i,front}} - T_{\mathrm{ext}} \right)
\end{aligned}
\tag{59}
$$

$$Q_{\mathrm{loss,sample}} = U \, A_{\mathrm{sample}} \left(T_{\mathrm{eff,i,back}} - T_{\mathrm{ext}} \right) \tag{60}$$

The loss coefficients $(U \cdot A)_{\mathrm{walls,back}} \, [W/K]$ and $(U \cdot A)_{\mathrm{walls,front}} \, [W/K]$ were determined by a 2-dimensional thermal simulation with the THERM program [121]. The validity of these loss coefficients was proven within the REGES project [18] by measuring a well-known sample with an extremely high secondary heat transfer factor.

$T_{\mathrm{eff,i,front}}$ is the effective internal temperature for the front walls (on the outdoor side of the venetian blind (fig. 19)). $T_{\mathrm{eff,i,back}}$ is the effective internal temperature for the back walls (on the indoor side of the venetian blind). $T_{\mathrm{eff,i,back}}$ depends on the emissivity ϵ of the venetian blind. An ideally infrared-reflective sample would "sense" only the air temperature and not the radiative temperature of the absorber, such that

$$T_{\mathrm{eff,i,back}} = T_{\mathrm{eff,i,front}} = T_{\mathrm{air}} \quad \bigg| \text{whereby}\, \epsilon = 0 \tag{61}$$

For a venetian blind with $\epsilon \approx 1$, the effective interior temperature

$$T_{\mathrm{eff,i,back}} \approx 1/8 \Big(5\,T_{\mathrm{absorber}} + 3\,T_{\mathrm{air}} \Big) \quad \bigg| \text{whereby}\, \epsilon = 1 \tag{62}$$

$$T_{\mathrm{eff,i,front}} \approx 1/8 \Big(5\,T_{\mathrm{glazing}} + 3\,T_{\mathrm{air}} \Big) \quad \bigg| \text{whereby}\, \epsilon = 1 \tag{63}$$

Because the emissivity of the sample is generally not known, it is recommended that the evaluation be made twice, once assuming $\epsilon = 0$ and once assuming $\epsilon = 1$, and that the average of both results be used when determining the g.

Error treatment: Q_{loss} is small compared to Q_{abs} because we try to measure with equal temperatures on the indoor and outdoor side of the sample. It is thus sufficient to estimate the error as follows:

$$\Delta Q_{\mathrm{loss}} \leq 0.25 \; Q_{\mathrm{loss}} \tag{64}$$

Determination of the absorber temperature T_{absorber} and $\Delta T_{\text{absorber}}$

All evaluation approaches require the temperature of the absorber surface T_{absorber}, which is not measured directly. The measured quantity is the temperature in the underlying aluminium plate T_{Al}. The absorber temperature T_{absorber} must be calculated from the measured temperature, T_{Al}, and the thickness and conductivity of the polymer layers and aluminium layers between the absorber surface and the measurement sensor. The surface temperature can be calculated from the temperature T_{Al} measured by the sensor as follows:

$$T_{\text{absorber}} = T_{\text{Al}} + q \cdot \left(\frac{\delta_{\text{K}}}{\lambda_{\text{K}}} + \frac{\delta_{\text{Al}}}{\lambda_{\text{Al}}} \right)$$

$$\Delta T_{\text{abs}} = \left[\Delta T_{\text{Me"s}}^2 + \left(\left(\frac{\delta_{\text{K}}}{\lambda_{\text{K}}} + \frac{\delta_{\text{Al}}}{\lambda_{\text{Al}}} \right) \Delta q_{\text{abs}} \right)^2 + \right. \tag{65}$$

$$\left. + q_{\text{abs}}^2 \cdot \left[\left(\frac{1}{\lambda_{\text{K}}} \Delta \delta_{\text{K}} \right)^2 + \left(\frac{\delta_{\text{K}}}{\lambda_{\text{K}}^2} \Delta \lambda_{\text{K}} \right)^2 + \left(\frac{1}{\lambda_{\text{Al}}} \Delta \delta_{\text{Al}} \right)^2 + \left(\frac{\delta_{\text{Al}}}{\lambda_{\text{Al}}^2} \Delta \lambda_{\text{Al}} \right)^2 \right] \right]^{\frac{1}{2}}$$

whereby δ_{Al} and δ_{K} are the thicknesses of the undisturbed aluminium and polymer layers respectively which are located between the free absorber surface and the material layer which has the temperature measured by the sensor. Of course, the measured temperature cannot be allocated exactly to a certain layer of the aluminium plate. Thus, this error should be taken into account as an additional uncertainty in the layer thickness. The magnitude of this additional uncertainty factor was estimated with the help of a thermal simulation. The result of the thermal simulation of the absorber plate indicates that the additional uncertainty in the thickness of the aluminium layer can be estimated to be the diameter of the sensor (2.6 mm).

Determination of the exterior temperature T_{ext} and ΔT_{ext}

The exterior temperature is determined by the radiative temperature and the air temperature in the space in front of the sample surface. The weighting of the air and radiative temperatures is defined by the ratio of the heat transfer coefficients, $h_{\text{e,conv}}$ and $h_{\text{e,rad}}$. The radiative heat transfer $h_{\text{e,rad}}$ is described by a linear approximation:

$$h_{\text{e,rad}} := \frac{\sigma \left(T_{\text{sample}}^4 - T_{\text{measurement cabin}}^4 \right)}{\left(\frac{1}{\epsilon_{\text{sample}}} + \frac{1}{\epsilon_{\text{measurement cabin}}} - 1 \right) \left(T_{\text{Probe}} - T_{\text{measurement cabin}} \right)} \tag{66}$$

The radiative temperature of the measurement cabin is determined by the temperature of the inner pane of the measurement cabin and the temperature of the internal wall surfaces. The weighting results from the solid angles S_{pane} and S_{wall} of the pane and the walls respectively

[111]. The effective exterior temperature is thus:

$$T_{\text{ext}} := \frac{T_{\text{air}}\, h_{\text{e, conv}} + \left(T_{\text{wall}} \overbrace{0.7\, \cos(\gamma)}^{S_{\text{wall}}} + T_{\text{pane}} \overbrace{0.3\, \cos(\gamma)}^{S_{\text{pane}}} \right) h_{\text{e,rad}}}{h_{\text{e,conv}} + h_{\text{e,rad}}} \tag{67}$$

whereby γ is the azimuth angle, by which the sample is rotated around the vertical axis toward the pane of the measurement cabin (see also 17).

Radiative temperature: The average temperature of the internal wall surfaces of the measurement cabin T_{wall} and the average temperature of the inner pane T_{glass} are estimated on the basis of measurements which were carried out once.

$$T_{\text{glass}} \approx T_{\text{wall}} \approx T_{\text{air}} + (4\,K \pm 2\,K)\, \frac{E_{\text{ref}}}{550\,W/m^2} \tag{68}$$

These values do not have a large effect on the g value, firstly because the loss heat flow rate is small ($T_{\text{int}} \approx T_{\text{ext}}$) and secondly because the exterior temperature T_{ext} is determined much more strongly by the air temperature than by the radiative temperature, because the convective heat transfer is larger than the radiative heat transfer.

The error is determined according to:

$$
\begin{aligned}
\Delta T_{\text{ext}} = 2 \Bigg[& \left(\frac{h_{\text{e,conv}}\, \Delta T_{\text{air}}}{h_{\text{e,conv}} + h_{\text{e, rad}}} \right)^2 + \left(\frac{0.7\, \cos(\gamma)\, h_{\text{e,rad}} \Delta T_{\text{wall}}}{h_{\text{e,conv}} + h_{\text{e,rad}}} \right)^2 + \left(\frac{0.3\, \cos(\gamma)\, h_{\text{e,rad}}\, \Delta T_{\text{glass}}}{h_{\text{e,conv}} + h_{\text{e,rad}}} \right)^2 \\
& + \left(\left(\frac{T_{\text{air}}}{h_{\text{e,conv}} + h_{\text{e,rad}}} + \frac{T_{\text{air}}\, h_{\text{e,conv}} + (T_{\text{wall}}\, 0.7 + T_{\text{glass}}\, 0.3)\, \cos(\gamma)\, h_{\text{e, rad}}}{(h_{\text{e,conv}} + h_{\text{e,rad}})^2} \right) \Delta h_{\text{e,conv}} \right)^2 \\
& + \left(\left(\frac{T_{\text{air}}\, h_{\text{e,conv}} + (T_{\text{wall}}\, 0.7 + T_{\text{glass}}\, 0.3)\, \cos(\gamma)\, h_{\text{e,rad}}}{(h_{\text{e,conv}} + h_{\text{e,rad}})^2} \right. \right. \\
& \left. \left. + \frac{(T_{\text{wall}}\, 0.7 + T_{\text{glass}}\, 0.3)\, \cos(\gamma)}{h_{\text{e,conv}} + h_{\text{e,rad}}} \right) \Delta h_{\text{e,rad}} \right)^2 \Bigg]^{(1/2)} \tag{69}
\end{aligned}
$$

Determination of h_e and Δh_e and the subdivision into $h_{\text{e, rad}}$ and $h_{\text{e, konv}}$

The local exterior heat transfer coefficient is determined from a dark measurement (solar simulator off) without a sample at each location of a heat flux plate (see figure 18).

$$h_e := \frac{q_{\text{abs}}}{T_{\text{ext}} - T_{\text{abs}}} \tag{70}$$

The absorber can be either heated or cooled, but normally we measure with a hot absorber. The external wind conditions are created with a cross-flow ventilator located above the outdoor surface of the test sample (see fig. 16). The wind direction and the wind speed are adjusted

such that both, the heat transfer coefficient in the middle of the test sample (plate no. 5) and the average heat transfer coefficient in front of the plates no. 3-7 agree with the reference heat transfer coefficient. The error is determined according to:

$$\Delta h_e = 2\sqrt{\left(\frac{\Delta q_{\text{abs}}}{T_{\text{ext}} - T_{\text{abs}}}\right)^2 + \left(\frac{q_{\text{abs}} \Delta T_{\text{abs}}}{(T_{\text{ext}} - T_{\text{abs}})^2}\right)^2 + \left(\frac{q_{\text{abs}} \Delta T_{\text{ext}}}{(T_{\text{ext}} - T_{\text{abs}})^2}\right)^2} \tag{71}$$

ΔT_{ext} is determined according to (69). The errors for T_{air} and q_{abs} are determined according to (57). $h_{\text{e,rad}}$ is determined according to eq. (66). In mosts cases $h_{\text{e,rad}} = 5 \pm 1\, W/(m^2 K)$. The following equations then apply for $h_{\text{e,conv}}$ and $\Delta h_{\text{e,conv}}$:

$$h_{\text{e,conv}} = h_e - h_{\text{e,rad}} \tag{72}$$

$$\Delta h_{\text{e,conv}} = 2\sqrt{\Delta h_e^2 + \Delta h_{\text{e, rad}}^2} \tag{73}$$

Special care has to be taken in case of test samples that influence the external heat transfer coefficients $h_{\text{e,conv}}$ or $h_{\text{e,rad}}$ by themselves.
The external heat transfer coefficient on the outdoor side of the test sample is the weighted sum of the radiative and the convective heat transfer coefficient (see eq. (67)). In case of test samples with a flat surface and with an emittance of $\epsilon \geq 0.84$ on the outdoor side, the outdoor surface complies with the reference surface. Test samples with non flat outdoor surfaces that enhance or reduce the convective heat transfer - like e.g. venetian blinds - change the boundary conditions by themselves and the changed convective heat transfer coefficient is an intrinsic property of the test sample. The situation is similar in case of test samples with a significantly different emissivity ϵ than the reference surface (floatglass) like e.g. "position one low-emissivity coatings" on the outdoor surface. **In all these cases it is essential that the external air temperature $T_{\text{ext,air}}$ and the external radiative temperature $T_{\text{ext,rad}}$ are identical** since the external temperature T_{ext} depends on the external convective and radiative heat transfer coefficient (see eq. (67)), which means that T_{ext} would not be well-defined any more because of the unknown heat transfer coefficients $h_{\text{e,conv}}$ and/or $h_{\text{e,rad}}$ in case of such special samples.

Determination of h_i and Δh_i

Determination of h_i and Δh_i for the cooled plate method

For the case of spatially localised evaluation with the cooled plate method (fig. 17), the test sample is mounted such that there is an air gap of 10 mm between the indoor pane and the absorber. The convective-radiative heat transfer coefficient between the absorber and the indoor surface of the sample is then $h_i = 8 \pm 1\ W/(m^2 K)$ and thus agrees with the standard conditions of $7.7 W/(m^2 K)$ according to DIN EN 410 and $8 W/(m^2 K)$ ISO 9050. In such a

narrow gap, the convective heat transfer coefficient is clearly defined, because the air flow is laminar for the prevailing temperatures. The radiative heat transfer coefficient is obtained from the well-known analytical solution for infrared heat transport between flat, parallel plates. The emissivity of glass is known and the emissivity of the absorber ϵ_{abs} was measured

$$\epsilon_{\mathrm{abs}} = 0.98 \pm 0.03 \tag{74}$$

This approach was validated in the ALTSET [100] and REGES [18] research projects.

Determination of h_i for the cooled box method

In case of the set-up with the cooled box, we aim to reach realistic internal heat transfer conditions by using a model room behind the sample. We normally do not use the set-up with the cooled box to measure samples with flat internal surfaces. It is in most cases used to measure facades with internal venetian blinds, where the slatted solar-control system is mounted indoors. The internal temperature is in this case a mixture of the air-temperature and the radiative temperature of the absorber (see also chapter 5.1.2). In order to check the internal heat transfer coefficients, it has been proven by measurements with a copper plate with flat surfaces with a known (small) thermal resistance. This calibration panel was mounted in the sample holder of the model room instead of a test sample. The external heat transfer coefficient was determined in this case with an independent dark measurement without the model room and without a test sample according to chapter 5.1.2. We did two measurements, one with an uncoated copper plate with almost negligible emissivity and one with a black coated copper plate with an emissivity of 0.98 ± 0.04. For the uncoated copper plate we determined

$$h_{\mathrm{i,\ uncoated\ copper}} = 3.92 \pm 0.3\ W/(m^2 K) \approx h_{\mathrm{i,\ convective}} \tag{75}$$

and for the coated copper plate we determined

$$h_{\mathrm{i,\ copper,\ coated\ with}\ \varepsilon\ =\ 0.98} = 8.05 \pm 0.5\ W/(m^2 K) \tag{76}$$

This means that the internal heat transfer coefficient matches with the reference condition of $h_{\mathrm{i,\ ref}} = 8\ W/(m^2 K)$ in case of samples with a high emissivity: .

Determination of $\Delta_{\mathbf{imperfect\ test\ sample}}$

In general, only one sample of an entire facade construction is provided for measurement, and the measurement laboratory does not have any influence on the sample production or selection. The measurement laboratory is thus unable to gather any statistics to determine reproducibility among samples. Also, this is not the task of the measurement laboratory, as changes in production at a later date can also cause variation. Nevertheless, it is recommended that an additional uncertainty factor for the test sample be introduced for the case of test samples with intrinsically variable properties (e.g. venetian blinds). For instance, this is

justified by the fact that the configuration of the slats of a venetian blind is never defined perfectly, as the slats in general have slightly different tilt angles in the upper and lower part of the blind. For this reason, we add a further measurement uncertainty $\Delta_{\text{imperfect test sample}}$, which can be estimated on the basis of relevant experience. For venetian blinds, for which g is relatively insensitive to changes in the slat tilt angle, $\Delta_{\text{imperfect test sample}}$ can be chosen to be smaller than for samples for which g depends sensitively on the slat tilt angle.

5.1.3   Correction of g_{exp} to reference conditions

g is influenced by the following boundary conditions:

- a room which is not perfectly black on the indoor side of the sample has the effect that some of the transmitted radiation is reflected back to the outdoor environment.

- external and internal convective heat transfer conditions affect the fraction of the absorbed radiation that is transferred to the internal environment.

- the spectrum of the incident radiation affects both, the absorbed and the transmitted radiation in the case of spectrally selective samples.

- non-equal radiative and air temperatures on the outdoor surface of the sample are especially relevant when the outdoor side of the sample is not flat or has a significantly different emissivity ϵ than float glass.

The goal of laboratory measurements is to determine g for a certain set of reference boundary conditions. These reference boundary conditions can correspond to national or international reference conditions for product comparisons or product ratings. However, the reference conditions can also be specific conditions valid for a certain building and location under consideration. An example are very windy conditions in higher storeys of some high-rise buildings. During the measurements, the laboratory conditions should be close to the reference conditions, but it is never possible to reproduce the reference conditions exactly. The result of the measurements is therefore the solar heat gain coefficient under experimental laboratory conditions g_{exp}. It is then necessary to either prove that the difference between laboratory and reference conditions is negligible or to correct g_{exp} to reference conditions.

Correction of the effect of the non-ideal black absorber

$g_{\text{exp}} \neq g$ if some of the transmitted radiation is reflected back to the outdoor environment and is therefore not absorbed by the cooled plate or in the cooled box behind the sample. The absorptance of the absorber of the calorimeter at Fraunhofer ISE is high over the complete solar spectral range: $\alpha_{\lambda,\text{abs}} = 0.98 \pm 0.02$ fÃ$\frac{1}{4}$r $\lambda \in [300\,\text{nm}, 2500\,\text{nm}]$. If only the absorptance of the absorber is not equal to reference conditions, the following relationship between g and

g_{exp} can be established (see also fig. 22):

$$
\begin{aligned}
g &= \tau_{\text{e}} + q_{\text{i}} \\
g_{\text{exp}} &= \tau_{\text{e}} \underbrace{\frac{\alpha_{\text{abs,exp}}}{1 - \rho_{\text{abs}}\,\rho'_{\text{s}}}}_{\text{a}} + q_{\text{i}} \underbrace{\frac{\alpha_{\text{s,exp}}}{\alpha_{\text{s}}}}_{\text{b}} \quad \Big| \text{ whereby } 0.98 \leq a \leq 1 \text{ and } 1 \leq b \leq 1.02 \quad (77) \\
\alpha_{\text{s,exp}} &= \alpha_{\text{s}} \bigg(1 + \overbrace{\frac{\alpha'_{\text{s}}}{\alpha_{\text{s}}}\,\tau_{\text{e}}\,\rho_{\text{abs}}\,\frac{1}{1 - \rho_{\text{abs}}\,\rho'_{\text{s}}}}^{\text{b}} \bigg)
\end{aligned}
$$

α_{s} and α'_{s} are the solar absorptance values for radiation from the outdoor and the indoor side of the test sample respectively. They can be determined by

$$
\alpha_{\text{s}} := \frac{\int \alpha_{\lambda,\text{s}}\,S_\lambda\,d\lambda}{\int S_\lambda\,d\lambda} \quad \Big| \text{ where } S_\lambda \text{ is the spectral distribution of the solar simulator.} \quad (78)
$$

$\alpha_{\lambda,\text{s}}$ is the spectral absorptance of the sample for radiation coming from the outdoor side and can be determined according to

$$
\alpha_{\lambda,\text{s}} = 1 - \rho_{\lambda,\text{s}} - \tau_{\lambda,\text{s}} - \eta \tag{79}
$$

η is only necessary in the case of active renewable energy harvesting components - such as building-integrated PV (BIPV) or solar thermal collectors (BIST) - integrated into the test sample. η then denotes the efficiency of solar energy conversion for the test conditions in order to take into account that some of the incident radiation is converted into useful energy forms and extracted from the test sample. This specifically means that η has to be set to zero when collectors are not operated (stagnation condition) or when a PV system is in the open circuit state.

The test sample absorptance for radiation coming from the indoor side α'_{s} can be determined analogously whereby it is clear that $\rho_{\lambda,\text{s}} \neq \rho'_{\lambda,\text{s}}$ in general. It should be noted that in general also $\tau_{\lambda,\text{s}} \neq \tau'_{\lambda,\text{s}}$ in the case of complex fenestration systems as can be seen for the example given in figure 23. Only in the case of clear samples it is generally true that $\tau_{\lambda,\text{s}}$ and $\tau'_{\lambda,\text{s}}$ are equal because of the reversibility principle for light rays.

Practical line of action: In most cases we measure only g_{exp}. The next step is to estimate all the properties needed in eq. (77) such as τ_{e}, α_{s} etc. to correct g_{exp} to g. We then vary these estimated values within the physically meaningful limits. The maximum variation of g resulting from this variation gives the uncertainty $\Delta g_{\alpha_{\text{abs}} \neq 0}$ of the correction for the non-ideal black absorber. $\Delta g_{\alpha_{\text{abs}} \neq 0}$ is then added linearly to the error bar of g.

Correction for a non-reference spectrum of the solar simulator

The spectrum of the incident radiation affects both, the absorbed and the transmitted radiation in the case of spectrally selective samples. In the case of natural illumination conditions, the spectrum of the incident radiation is influenced by
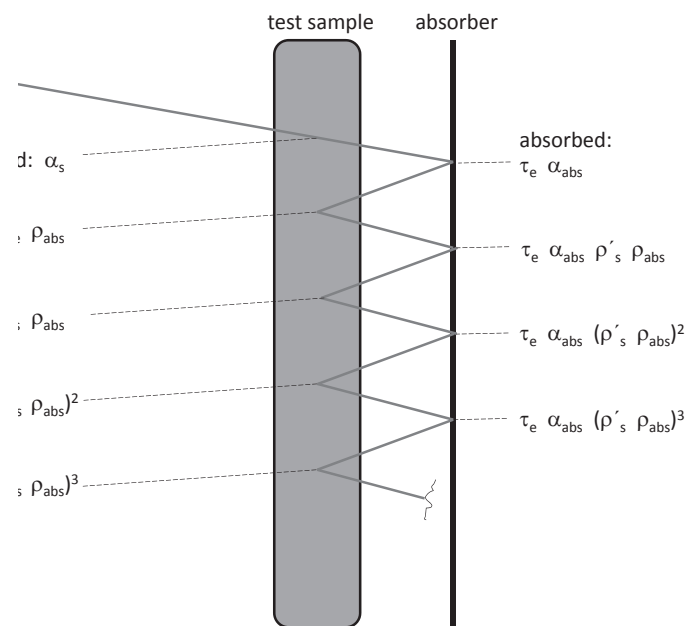
Figure 22: Description of the influence of a not ideally black absorber ($\alpha_{\mathrm{abs}} > 1$). The contributions of the absorption due to multiple reflection constitute a geometric series and can therefore be summed up in the expression given in eq. (77).

stack of black hollow tubes   light scattering glass
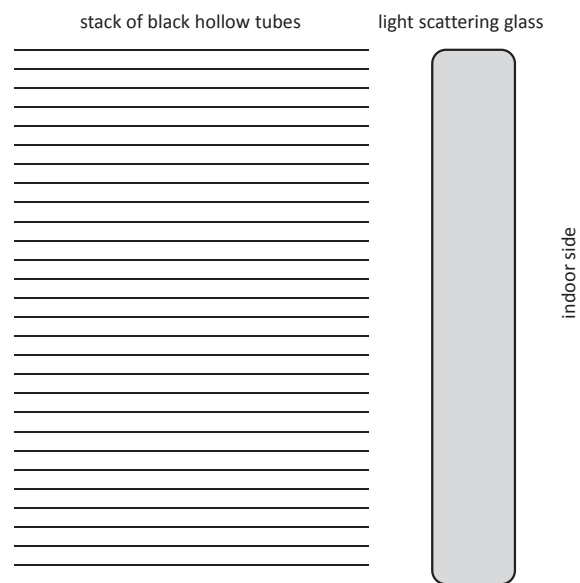
indoor side

Figure 23: For the case of complex fenestration systems it can not be assumed that the directional-hemispherical transmittance from the outdoor side $\tau_{\lambda,\text{s}}$ is equal to the directional-hemispherical transmittance from the indoor side $\tau'_{\lambda,\text{s}}$ as can be seen for the case of the example given here. At normal incidence, a large portion of the light coming from the outdoor side is transmitted which is not the case for light coming from the indoor side since it is scattered first at the diffusing pane. In this case therefore $\tau'_{\lambda,\text{s}} \ll \tau_{\lambda,\text{s}}$ for normal incidence.

- the sky conditions (e.g. blue or overcast sky)

- the spectrum of the direct part of the irradiation varies during the day and is affected by the path length of the sun ray through the atmosphere (air mass) and the conditions of the penetrated atmosphere (turbidity, ...).

- the spectral reflectance of the surrounding surfaces (e.g. green grass) determines the spectrum of the radiation due to the ground albedo and neighboring surfaces.

It is therefore essential to agree on a reference spectrum for product comparisons and product rating. In Europe the reference spectrum is defined in [58], which differs slightly from the ISO reference spectrum in [73]. The spectrum of a solar simulator depends mainly on the type of the illuminant and the age of the illuminant. At Fraunhofer ISE we use HMI lamps which have too much blue light during the first hours of operation. We therefore run them for several hours before the first measurement. After their rated service lifetime, they do not have enough blue light so that they have to be exchanged before they actually fail. All the walls and the floor are covered with a low-reflectance coating with $\rho_\lambda \leq 0.04$ for $\lambda \in [300\text{nm}, 2500\text{nm}]$ in order to avoid stray light. With this procedure we can avoid spectral corrections of g_{exp} in most cases. Spectral corrections are nevertheless necessary in some cases, such as transparent and translucent extruded polycarbonate multi-wall panels with a co-extruded UV-protection layer on the outdoor surface that also blocks some of the blue light (see table 2). All this has been assessed in detail in the research projects ALTSET [100] and REGES [18]. If necessary, a spectral correction can be applied with the following formula:

$$
\begin{aligned}
g_{\text{exp}} \ &= \ \tau_{\text{e,solsim}} + q_{\text{i,solsim}} \\
&\doteq \ g + (\tau_{\text{e,solsim}} - \tau_{\text{e}}) \ + \ q_{\text{i,solsim}} \ \left(1 - \frac{\alpha_{\text{s}}}{\alpha_{\text{s,solsim}}}\right) \ \bigg| \text{and therefore} \tag{80}
\end{aligned}
$$

$$
g \ \doteq \ g_{\text{exp}} - (\tau_{\text{e,solsim}} - \tau_{\text{e}}) \ \underbrace{- \ q_{\text{i,solsim}} \ \left(1 - \frac{\alpha_{\text{s}}}{\alpha_{\text{s,solsim}}}\right)}_{\text{can be neglected very often if } q_i \ll \tau_e} \tag{81}
$$

whereby the subscript "$_{\text{solsim}}$" denotes properties which are valid for the solar simulator spectrum. For the spectral correction in the case of samples with $q_i \ll \tau_e$, only the spectral transmittance τ_λ is needed in addition to the solar heat gain coefficient g_{exp}. $\tau_{\text{e,solsim}}$ can then be determined by

$$
\tau_{\text{e,solsim}} := \frac{\int \tau_\lambda \, S_{\lambda,\text{solsim}} \, d\lambda}{\int S_{\lambda,\text{solsim}} \, d\lambda} \tag{82}
$$

where $S_{\lambda,\text{solsim}}$ is the spectrum of the solar simulator. If also q_i is to be corrected, the sample absorptance $\alpha_{\text{s,solsim}}$ is needed which can be determined according to

$$
\alpha_{\text{s,solsim}} := \frac{\int \alpha_\lambda \, S_{\lambda,\text{solsim}} \, d\lambda}{\int S_{\lambda,\text{solsim}} \, d\lambda} \tag{83}
$$

and where $\alpha_\lambda \, S_{\lambda,\text{solsim}}$ can be determined according to eq. (79).

Table 2: Comparison of $\tau_{e,solsim}$ for different illuminants. Only three digits are valid, four digits are given in order to facilitate a relative comparison of the different values. The result for the Xe-lamp is given only for information, it is not used for g-value testing.

$\tau_{e,solsim}$ for different lamp types and reference spectra for a PC multi-wall panel with co-extruded UV-protection layer [21]				
illuminant:	EN410 standard	ISO9050 standard	HMI-lamp (Osram, 4000W)	Xenon-lamp (not used for SHGC testing)
$\tau_{e,solsim}$:	0.5437	0.5543	0.5388	0.5738

Correction for non-reference external and internal convective heat transfer conditions

Convective and radiative heat transfer conditions on the indoor and outdoor sides of the test sample affect only q_i. Both, the assessment of the impact of non-reference heat transfer conditions and the correction to reference conditions can be done using the γ-formalism developed by Jean Rosenfeld [107],[106]. First of all the parameter $\gamma \in [0,1]$ is determined according to

$$q_{i,exp} = \frac{(R_{e,exp} + \gamma \, R_s) \, \alpha_s}{R_{e,exp} + R_s + R_{i,exp}} \tag{84}$$

where R is always a thermal resistance $[m^2 K/W]$. $R_{e,exp}$ and $R_{i,exp}$ are the surface thermal resistances at the outdoor (external) and indoor surfaces respectively. R_s is the thermal resistance of the test sample. The term "$\gamma \, R_s$" can be interpreted as a sliding variable resistor where γ determines the location of the absorptance in the test sample [106]. q_i can then be corrected to reference heat transfer conditions R_e and R_i according to

$$q_i = \frac{(R_e + \gamma \, R_s) \, \alpha_s}{R_e + R_s + R_i} \quad \Big| \quad \text{whereby } \gamma \text{ is determined from eq. (84)} \tag{85}$$

5.2 Remarks on Transmittance measurements

The transmittance specifies the fraction of electromagnetic radiation that is transmitted through materials or building envelope components. The solar transmittance τ_e together with the secondary inward flowing fraction fraction q_i constitutes the total solar energy transmittance g. The set-up for transmittance measurements consists of a light source and a detection system. The sample is mounted in front of the detection system. The detection system is a radiation detector with or without ulbricht sphere. The detector and the light source have to be chosen according to the wavelength of the incident radiation and the transmitted radiation. In the construction sector, the following wavelength ranges are relevant:

- **terrestrial UV radiation**, $\lambda \in [300 \text{ nm}, 400 \text{ nm}]$, consists of UVA radiation, $\lambda \in [315 \text{ nm}, 400 \text{ nm}]$, and UVB radiation , $\lambda \in [300 \text{ nm}, 315 \text{ nm}]$. UVB and UVC radiation with wavelengths smaller than 300 nm is blocked by the atmospheric ozone layer when the ozone layer is not damaged. The UV radiation is responsible for many degradation/aging processes of materials, especially when combined with humidity. It also has an impact on the human skin. It is therefore relevant, if the UV radiation is blocked by the building skin. Conventional floatglass blocks UVB radiation almost completely. Highly transmissive low-iron floatglass does not block the UVB radiation completely.

- **light**, $\lambda \in [380 \text{ nm}, 780 \text{ nm}]$, is detected by the human eye. The sensitivity of the human eye strongly depends on the wavelength of the radiation (V_λ-curve [58]). V_λ is different for scotopic vision during the night and photopic vision during daytime.

- **solar radiation**, $\lambda \in [300 \text{ nm}, 2.500 \text{ nm}]$, contains UV, light and NIR radiation.

- **thermal radiation (FIR)**, $\lambda \in [5.000 \text{ nm}, 50.000 \text{ nm}]$, emitted by objects with temperatures in $[-20°\text{C}, 80°\text{C}]$, is transmitted by many construction materials such as polymeric materials which strongly affects the heat insulation properties of envelope components. Floatglass is almost opaque for thermal radiation with a small "window" around 12.000 nm.

Transmittance measurements of clear, non-scattering materials at normal incidence are state of the art. But transmittance measurements for oblique angles of incidence or measurements of light scattering or light re-directing components are in many cases beyond state of the art, as has been shown by a round-robin intercomparison study of transmittance and reflectance measurements of light-scattering and patterned glass with spectrophotometers and integrating spheres by the international commission on glass, technical committee 10 [130]. Figure 24 shows some of the effects, that have to be considered, when light-scattering, light re-directing and/or inhomogeneous test samples are to be measured. The measured transmittance can only be correct, if the sensitivity of the detection system is identical for all kinds of transmitted rays and if there is no escape-light that does not reach the detector.

Some of the most common effects, which can distort the results of transmittance measurements, are:

reflective screen printed pattern

incident light

width of the
spot of the
transmitted
radiation on
the rear side
of the test
sample

width of the
spot of the
incident
light on the
outer
surface of
the test
sample

glass

width of the
incident
beam

the transmitted radiation
consits of several beams
due to multiple reflections

incident light with
an oblique angle of
incidence

clear
glass

incident
beam

the transmitted radiation contains
rays of re-directed light caused by
the patterned surface of the sample

clear
glass

Figure 24: Schematic representation of some of the effects that can occur, when measuring light scattering or light re-directing test samples

- in many cases, the size of the spot of the incident light is much bigger than the size of the spot of the transmitted light. There are two principally different possibilities to overcome this problem:

  - A small incident beam together with an ulbricht sphere with a sufficiently big sample port can be used, but the sample port has to be big enough to capture all the transmitted light. The disadvantage of this method is, that the signal is often very low due to the necessary reduction of the size of the beam of the incident light.
  - If both, the size of the sample and the size of the beam are much bigger than the sample port of the ulbricht sphere, lateral losses within the test sample can be compensated in many cases with lateral gains.

- Problems occur, when the sensitivity of the detection system depends on the direction of the light that enters the ulbricht sphere. Possible reasons for such problems are detector ports without baffles or other inhomogeneities on the inner surface of the ulbricht sphere. Other possible reasons are the influence of a relatively big sample port relative to the inner surface of the sphere or an inner surface of the sphere which is not diffusely reflecting (with non-lambertian reflectance).

- Another reason can be light which is absorbed at non-perfectly sharp edges of the sample port of the ulbricht sphere. The border of the sample port of an ulbricht sphere must be very thin (sharp edge). Otherwise unwanted losses occur due to light which is absorbed by this surface or light which is reflected back to the outside by this surface.

- The polarization state of the incident radiation has to be either unpolarized or polarized in a well defined direction. Otherwise errors can occur, especially when measuring under oblique angles of incidence.

- Inhomogeneous test samples can be considered to be "quasi-homogeneous" when the size of the beam of the incident light is much bigger than the size of the typical dimension of the inhomogeneity of the sample. An example of a quasi-homogeneous test sample is a woven fabric with holes and uniform color, when the size and the distribution of the holes is such, that there are many holes within the spot of the incident light. Color patterns on fabrics are often bigger than the size of the beam of the incident light, so that they cannot be considered to be quasi-homogeneous. In such cases each colored area should be measured separately and the different results should be averaged according to the area percentage of the different colors.

- Special care has to be taken in case of samples with luminescence effect (e.g. with flourescent or phosphorescent pigments), which change the wavelength of the radiation or which add light with a different wavelength to the regularly transmitted light.

The specification of requirements for transmittance measurements is an ongoing research topic. Currently there are efforts within the European standardization group CEN/TC333/WG3/TG5 to improve the standard EN14500 [1] in order to improve the measurement procedures for $\tau_{\text{n-n}}$ and $\tau_{\text{n-h}}$ with contributions from the author of this document. There are also ongoing efforts to replace both, the transmittance and the reflectance by the property bi-directional scattering distribution function ($BSDF$), for example in the US complex glazing database managed by LBL [52].

6 Modeling of passive solar gains

6.1 Principles for the modeling of convection, conduction and thermal radiation heat transfer

6.1.1 Modeling of heat conduction

It is well-known that the temperature distribution T in homogenous and isotrop and IR-opaque solids which are opaque for IR and solar radiation can be described with the differential equation (86) using the thermal conductivity λ^2 as scalar parameter:

$$\nabla(\lambda\nabla T) = \rho\, c_p\, \frac{\partial T}{\partial t} \tag{86}$$

Equation (86) can be deduced from the relation $\mathbf{q} = -\lambda\nabla T$ for the vector $\mathbf{q}$ of the heat flux density (established by Fourier und Biot) and from the *continuity equation* $\nabla\mathbf{q} = -\rho\, c_p\, \frac{\partial T}{\partial t}$. Here c_p denotes the specific heat capacity and t denotes the time. Under stationary conditions this leads to

$$\nabla(\lambda\nabla T) = 0 \ \mid \text{for stationary conditions} \tag{87}$$

(87) is an elliptical differential equation which evolves into the Laplace-Equation (88) for all cases with constant λ.

$$\lambda\, \Delta T = 0 \ \mid \text{for constant } \lambda \tag{88}$$

In chapter 3 it has been explained, that heat conduction in building materials is caused by co-action of several fundamental effects and that the concept of a temperature and spacial constant thermal conductivity λ is not justified in strict mathematical terms in most cases. On the other hand it is extremely helpful for the intuitive or approximative physical understanding of heat transport phenomena, when the problem can be approximatively described by the Laplace-equation (88). The reason is that the Laplace-equation is a potential equation and that all the powerful results and methods of potential theory can be used to simplify the modeling of heat transfer problems when the approximation of a constant effective thermal conductivity λ_{eff} is made. For the numerical modeling of heat transfer problems the variable properties of λ can then be taken into account iteratively. The big advantage of this approximation is that the first order description can be understood analytically in many cases. In addition to that all the rules and equations developed in electrodynamics like Krichhoff-laws for resistances etc. can be used.

In chapter 3 it has been mentioned that the effective thermal conductivity λ_{eff} becomes direction dependent in case of anisotropic solids. In this case the Fourier relation can be written in the form:

$$\mathbf{q} = -\lambda_{\text{eff}}\, \nabla T = - \begin{pmatrix} \lambda_{\text{eff } 1,1} & \lambda_{\text{eff } 1,2} & \lambda_{\text{eff } 1,3} \\ \lambda_{\text{eff } 2,1} & ... & ... \\ ... & ... & \lambda_{\text{eff } 3,3} \end{pmatrix} \nabla T \ \mid \text{in case of anisotropic solids} \tag{89}$$

---

[2]the same greek letter λ is used for *wavelength* and *thermal conductivity* since this corresponds with the conventions in international standards and since it is improbable that they are mixed up with each other

$\lambda \approx 0.034$ W/(m * K) $\lambda \approx 0.030$ W/(m * K)
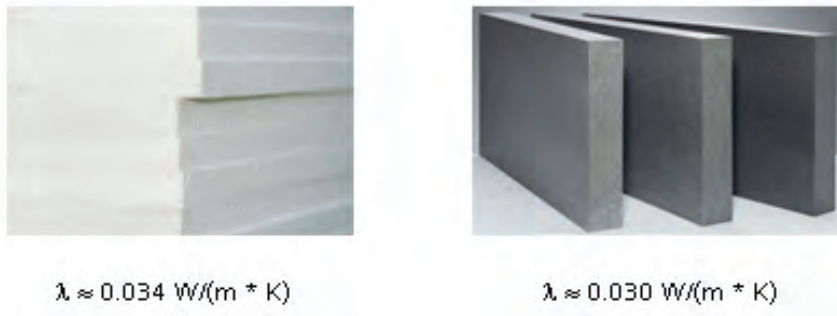
Figure 25: Comparison of the effective thermal conductivity λ_{eff} of two insulation materials with different IR-transmittance of the base material. Both materials are principally identical, the only difference is that the dark grey material contains additional graphite particles in order to lower the IR-transparency of the thin walls of the pores.

In case of layered (anisotropic) solids with plain layers it can be of great help to transform the co-ordinate system in the way that one of the axis of the co-ordinate system (e.g. the z-axis) is perpendicular to the layers. The thermal conductivity parallel to the layers can then be denoted with $\lambda_{\text{eff}\|}$ and with $\lambda_{\text{eff}\perp}$ for the heat flux perpendicular to the layers. Equation (89) then transforms into

$$\mathbf{q} = -\lambda_{\text{eff}} \, \nabla T = - \begin{pmatrix} \lambda_{\text{eff}\|} & 0 & 0 \\ 0 & \lambda_{\text{eff}\|} & 0 \\ 0 & 0 & \lambda_{\text{eff}\perp} \end{pmatrix} \nabla T \mid \text{in case of solids with plane layers} \quad (90)$$

6.1.2 Modeling of convective heat transfer

Convection describes heat and/or mass transport in fluids and gases. Convective heat transfer means, that thermal energy is transferred from one point to another by means of diffusion (brownian motion of individual particles in fluids or gases with preferential direction) or by advection (where groups of particles with a certain temperature are moved to another place). Convection phenomena can occur because of

- fluid or gas movements caused by local density differences (free convection)

- fluid or gas motion generated mechanically by an external source, like e.g. a fan (forced convection)

- combined forced and free convection (mixed convection)

Convective heat transfer from a surface to a gas is the most important convection mode in facades or other parts of the building skin. The heat flux $\dot{q}_w$ from the wall to the fluid is typically described with Newton's cooling law, which is at the same time the equation that is used to define the surface heat transfer coefficient or film coefficient h:

$$\dot{q}_w = h \, (T_w - T_{\text{Fluid}}) \quad (91)$$

where T_w is the local or average wall temperature. T_{Fluid} is the local or average fluid temperature. h is the local or average surface heat transfer coefficient respectively. h is influenced by the wall properties (e.g. roughness and shape of the surface) and by the flow properties (e.g. velocity and laminar or turbulent flow patterns). It is well known, that the influencing factors can be summarized in dimensionless characteristics in order to be able to apply known solutions to similar problems (theory of similarity developed by Nusselt). The background is, that the governing differential equations can be made dimensionless leading to dimensionless characteristic numbers in front of the different terms in the equations. Different flow phenomena are *similar* when they have the same characteristic numbers. Similar heat transfer conditions exist, when both, the flow phenomena and the boundary conditions are similar.

Characteristic numbers for free convection are

- the Nusselt-number Nu

$$Nu = \frac{h_{konv}\, d}{\lambda} \tag{92}$$

with the characteristic dimension d and the thermal conductivity λ of the fluid.

- the Prandtl-number Pr

$$Pr = \frac{\nu}{a} \tag{93}$$

with the kinematic viscosity ν and the temperature conductivity a of the fluid.

- the Grashof-number Gr for isothermal $Gr_{\text{isothermal}}$

$$Gr_{\text{isothermal}} = \frac{g\,\beta\,\Delta T\, l^3}{\nu^2} \tag{94}$$

or isoflux boundary conditions Gr_{isoflux} [110]

$$Gr_{\text{isoflux}} = \frac{g\,\beta\,q\, l^4}{\bar{\lambda}\,\nu^2} \tag{95}$$

with the gravitational constant g, the isobaric thermal volume expansion coefficient β, the temperature difference ΔT and the thermal conductivity $\bar{\lambda}$ of the fluid at the average fluid temperature.

The characteristic numbers can be transformed into other characteristic numbers by multiplication. Sometimes, the Rayleigh-number Ra[3] is used instead of Gr.

$$Ra = Gr\,Pr \tag{96}$$

In summary, it can therefore be said, that convective heat transfer phenomena can be described as a relation

$$Nu = f\left(Gr,\ Pr,\ \text{boundary conditions}\right) \tag{97}$$

---

[3]The Rayleigh-number Ra should not be confused with the general color rendering index Ra

in case of free convection.

Characteristic numbers for forced convection are Nu, Pr and the Reynolds-number Re

$$Re = \frac{v\,d}{\nu} \tag{98}$$

with the average velocity v of the fluid. Heat transfer by forced convection can therefore be described as a relation

$$Nu = f\left(Re,\ Pr,\ \text{boundary conditions}\right). \tag{99}$$

It is very important to note that the boundary conditions are often neither isoflux nor isothermal within facade components and at the surfaces of the facade components. It is therefore essential to be very careful when relations for Nu are generalized and used for other situations. This is only possible when both, the flow pattern and the boundary conditions are similar.

6.1.3 Modeling of radiative heat transfer

Radiative heat transfer within construction elements can be described in most cases as radiative heat transfer between grey-diffuse surfaces in good approximation. This means, that it is assumed, that the spectral emissivities of the surfaces are independent from the wavelength and the direction of the reflected or emitted radiation. In some cases average or effective emissivities are used in order to take into account moderate direction dependencies (see. e.g. EN12898 [61] for the calculation of the "corrected" emissivity of coated glass based on the measurement of the normal emissivity).

In general, the heat transfer within a "grey-diffuse enclosure" with N isothermal surfaces A_x with $x \in [1, N]$ can be described according to Siegel et.al. [111] by N different equations for the net energy density $\dot{q}_k$ $[W/m^2]$ transferred from surface k to all other surfaces

$$\dot{q}_k = \sum_{j=1}^{N} q_j \left(\frac{\delta_{kj}}{\varepsilon_j} - F_{k \to j} \frac{1 - \varepsilon_j}{\varepsilon_j} \right) = \sum_{j=1}^{N} F_{k \to j}\, \sigma\, \left(T_k^4 - T_j^4 \right) \tag{100}$$

with $k \in [1, N]$, with the Kronecker-Delta δ_{kj}, the temperature T_x of surface x and with the geometry factors for thermal radiation $F_{i \to j}$. The following equations define or explain δ_{kj} and $F_{i \to j}$:

$$\delta_{kj} = \begin{cases} 1, \text{when } k = j \\ 0, \text{when } k \neq j \end{cases} \tag{101}$$

$$A_i\, F_{i \to j} = A_j F_{j \to i} \quad \text{(reciprocity principle)} \tag{102}$$

$$\sum_{j=1}^{N} F_{k \to j} = 1,\ \forall\, k. \quad \text{and} \quad F_{j \to j} \neq 0,\ \text{if } A_j \text{ is concave} \tag{103}$$

The set of N non-linear equations (100) can be solved iteratively, but it would be much easier, when the radiative heat transport can be linearized so that the radiative heat transfer can be described with thermal resistances. The next paragraph analyzes this possibility.

Equation (100) can be transformed into

$$\dot{q}_k = \sum_{j=1}^{N} q_j \left(\frac{\delta_{kj}}{\varepsilon_j} - F_{k \rightarrow j} \frac{1 - \varepsilon_j}{\varepsilon_j} \right) = \sum_{j=1}^{N} \underbrace{F_{k \rightarrow j} \, \sigma \, \frac{\left(T_k^4 - T_j^4 \right)}{\left(T_k - T_j \right)}}_{h_{k \rightarrow j}} \, (T_k - T_j) \tag{104}$$

with the radiative heat transfer coefficient $h_{k \rightarrow j}$

$$h_{k \rightarrow j} := \frac{\sigma \left(T_k^4 - T_j^4 \right) F_{k \rightarrow j}}{T_k - T_j} \approx 4 \, F_{k \rightarrow j} \, \sigma \, \overline{T}_{kj}^3 \tag{105}$$

where

$$\overline{T}_{kj} \quad := \quad 0.5 \, (T_k + T_j) \quad \text{and} \tag{106}$$

$$h_{k \rightarrow j} \quad = \quad h_{j \rightarrow k}, \quad \text{if} \quad A_j = A_k \text{ according to eq. (102)} \tag{107}$$

The accuracy of the approximation in eq. (105) can be evaluated by inserting ζ so that $T_k = \overline{T}_{kj} - \zeta$ and $T_j = \overline{T}_{kj} + \zeta$. This means that

$$T_k^4 - T_j^4 = \left(4 \overline{T}_{kj}^2 - 2 \left(\overline{T}_{kj}^2 - \zeta^2 \right) \right) 2 \overline{T}_{kj} \, (T_k - T_j) \,. \tag{108}$$

The approximation is therefore accurate, when the following condition is fulfilled:

$$\zeta^2 << \overline{T}_{kj}^2 \,.$$

It is obvious, that this is true at $\overline{T}_{kj} = 293K$ even for $\zeta = 50K$, so that $(T_k - T_j) = 100K$, since

$$\zeta^2 < 0.03 \, \overline{T}_{kj}^2 \tag{109}$$

Typical temperature differences between components of facade elements are in most cases smaller than $50K$, (105) is therefore a good approximation and eq. (100) can be simplified considerably:

$$\dot{q}_k = \sum_{j=1}^{N} q_j \left(\frac{\delta_{kj}}{\varepsilon_j} - F_{k \rightarrow j} \frac{1 - \varepsilon_j}{\varepsilon_j} \right) = \sum_{j=1}^{N} h_{k \rightarrow j} \, (T_k - T_j) \tag{110}$$

This set of N linear equations can be solved and the temperature dependence of $h_{k \rightarrow j}$ can be taken into account iteratively.

6.2 On the modeling of the effective Solar Heat Gain Coefficient g_{eff}

In this chapter a general method for the determination of g_{eff} as basis for a realistic performance evaluation of solar control properties of facades is described. It is particularly designed to be used for venetian blinds. The new method has proven to be of great practical value to planning teams of huge office buildings in Germany, Austria and Switzerland. It can be used either 'stand-alone' (without building simulation) for comparisons of different facade variants or within building simulation programs. Some parts of the proposed methodology could be used in standards (e.g. EN13363) or to improve the accuracy of building simulation programs which are currently on the market. Practical experience with the new methodology led to insights which are the basis for the design of two new products. These new products are compared with state of the art products in chapter 6.2.4 on the basis of the new methodology.

6.2.1 Description of the basic approach

The fundamental idea of the proposed methodology is the following (see also figure 27):

´stand-alone´ version: Hourly solar irradiation (direct and diffuse) is determined with the Perez-Model [94] [95] from typical meteorological data (e. g. [50]). For every hour with direct irradiation, the hourly average total solar energy transmittance $g_{\text{eff-h}}$ and the monthly average total solar energy transmittance $g_{\text{eff-m}}$ are then calculated, taking into account direct *and* diffuse irradiation into account [8]. This is done for every relevant facade orientation. The frequency of the occurrence of $g_{\text{eff-h}}$ and the values of $g_{\text{eff-m}}$ are then proposed as the basis for product comparisons. Since it is too expensive and too time-consuming to perform calorimetric measurements of g_{tot} for many different directions of the incident radiation and many different tilt angles of the slats of blinds, g_{tot} is calculated with a thermal-optical model which is able to take these measurements into account as supporting points for the model. There is one parameter $\varkappa$ in the model which can be used to tune the model for compliance with the measurements. A similar methodology can also be applied for glare protection analysis and daylight supply [9]. The approach has proven to be of great practical value to many planning teams of huge office buildings in Germany, Austria and Switzerland. For examples see figure 26. Results of the new methodolgy have also been presented in [9].

Use within building simulation programs: The model described above for g_{tot} can be used in building simulation programs also. It can be used to incorporate the complex angular dependency of g_{tot} into these software programs. In addition to that, it provides a method to generalize calorimetric measurements to arbitrary boundary conditions and to make them usable for building simulation programs. Examples of boundary conditions in this context include arbitrary directions of the incident irradiation and arbitrary tilt angles of the slats of blinds.

Figure 26: Left: GALLILEO, new high-rise building for the Dresdner Bank in Frankfurt (Main), Germany. Centre: GALAXY, new building for the Commerzbank in Wien, Austria. Right: Basel Messeturm, Basel, Switzerland. We were involved in the development and planning of the facades by order of Bug AluTechnic, Kennelbach, Austria. For this task we used the new methodology which is presented in this paper.

Building performance analysis - general

Physical models for $g_{\text{tot}}(\alpha_s, \gamma_{\text{f}})$, luminance on the facade and illuminance in the room. All models are validated by measurements

Typical meteorological data for the location and facade orientation

Determination of control strategies for shading systems

Calculation of average values
($g_{\text{eff-h}}$, $g_{\text{eff-m}}$, average luminance, average illuminance)

Analysis of frequency distribution (product comparisons, standards)

Thermal building simulation (room temperatures, energy consumption)
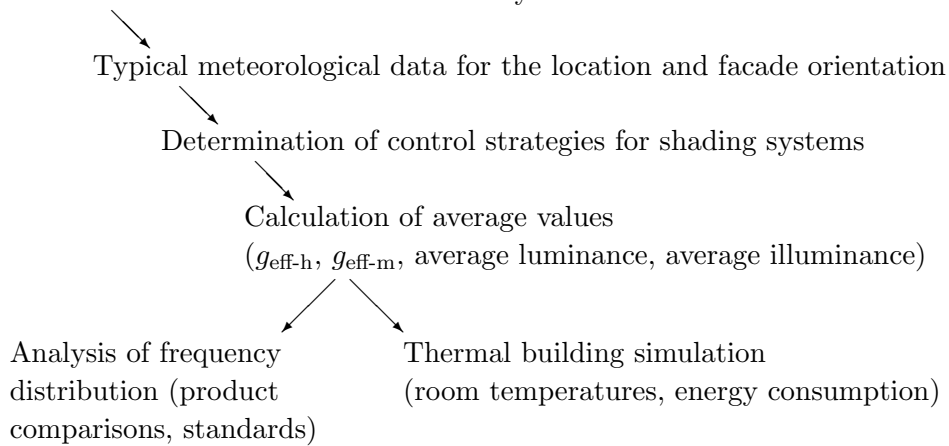
Figure 27: Based on validated model calculations for $g_{\text{tot}}(\alpha_s, \gamma_{\text{f}})$, luminance on the facade (in case of glare protection analysis) and illuminance in the room (analysis of daylight supply), average hourly values (effective values) are calculated for a specific location and a specific facade orientation. The efficiency of the facade is then evaluated either on the basis of the frequency distribution of the effective values or by dynamic thermal building simulation, which then provides information on energy consumption and the frequency distribution of room temperatures.

6.2.2 Determination of $g_{\mathbf{tot}}(\alpha_s, \gamma_{\mathbf{f}})$

Principles The proposed model does not treat the facade on the level of its individual constituents. This would mean that the model would start from the Maxwell Equations using rigorous coupled wave analysis (rcwa), for example. Such a sophisticated approach can be necessary, e.g. when someone wants to model the properties of microstructured thin films on glass panes providing stationary solar protection and light redirection [51]. There are many possible levels of simplification. The next level of simplification would be to use complex refractive indices for glass panes and individual layers of coatings and calculate the properties of the facade with ray-tracing or iterative procedures. This is helpful for understanding the angle-dependent colour rendering properties of the double silver coatings which are commonly used for low-e solar-control glazing. Many approaches use the next step of simplification and treat the complete shading device and each glass pane, coated or uncoated, as separate layers. With this simplification, the modelling has already completely lost all the information about the angular behaviour of the constituents of the facade, it cannot be predicted physically by the model. The simplification of the model has to be compensated with additional angular characterisation, which is not easy because polarisation effects can be significant. For normal incidence only, this method is used in ISO9050 [73], EN410 [58], ISO15099 [74] and many other standards. The computer programs WIS [129] and WINDOW [131] use an angle-dependent variant of this approach.

The proposed model for g_{tot} introduces an additional simplification level and treats the whole glazing unit as one layer and the shading device as another. One advantage is that the angluar dependence of the glazing and shading device can be characterised externally with the method that best meets the requirements for the system under consideration. Another advantage is that manufacturers of glazing and shading devices have to guarantee only for the properties of their product, not for the combination. A similar approach is used for the case of normal incidence in EN13363-1 [62]. The different steps which are proposed to be used for the determination of g_{tot} are displayed in figure 28.

Angle-dependent characterisation of the glazing The angle-dependent characterisation of the glazing (g-value g_{gzg}, solar transmittance $\tau_{e,\text{gzg}}$, the light transmittance $\tau_{v,\text{gzg}}$ and the diffuse light and solar reflectance of the inner surface) consists of four main steps:

- Experimental determination of the properties for $\alpha_{\text{in}} = 0°$. This can be done by spectral measurements and calculations according to EN410 [58] or ISO9050 [73]. Another possibility is to measure the properties of the glazing unit directly as a ´black box´.

- Experimental determination of the properties for $\alpha_{\text{in}} > 0°$. Since glazing properties are almost constant for small α_{in}, α_{in} has to be significantly larger than $0°$. We normally use $\alpha_{\text{in}} = 60°$ for our characterisation. The glazing properties are normally determined from on individual panes. If these measurements are not available/possible, the properties can be estimated using knowledge from other measurements. In the next paragraphs of this chapter, methods for this estimation will be given.

- Determination of the glazing properties for arbitrary incidence angles.

- Determination of the properties for diffuse irradiation.

Analysis of *thermal* building performance

Physical model for g_{tot}
$\begin{cases} \bullet \text{ glazing properties } g_{\text{gzg}}(\alpha_{in}),\ \tau_{e,\text{gzg}}(\alpha_{in}) \text{ and } \tau_{v,\text{gzg}}(\alpha_{in}) \\ \bullet \text{ properties of shading system: } \tau_{\text{bld}}(\alpha_s, \gamma_{\text{f}}, \beta_k) \text{ and } \rho_{\text{bld}}(\alpha_s, \gamma_{\text{f}}, \beta_k) \\ \bullet\ n \text{ optional calorimetric measurements: } g_{\text{tot}}(\alpha_{s,n}, \gamma_{\text{f, n}}, \beta_{k,n}) \\ \Rightarrow \text{ properties of combination: } g_{\text{tot}}(\alpha_s, \gamma_{\text{f}}, \beta_k) \end{cases}$

Typical meteorological data for the location and facade orientation

Determination of control strategies for shading systems

Calculation of average values $g_{\text{eff-h}}$, $g_{\text{eff-m}}$

Analysis of frequency distribution (product comparisons, standards)

Thermal building simulation (room temperatures, energy consumption)

Figure 28: The proposed steps for the determination of $g_{\text{tot}}(\alpha_s, \gamma_{\text{f}}, \beta_k)$ are added to the principle steps of figure 27. In case of venetian blinds β_k is the tilt angle of the slats. In general β_k can be interpreted as a parameter that defines a particular switching state of a shading system with switchable properties.

Glazing characterisation for $\alpha_{\text{in}} = 0°$ is state of the art. Characterisation for oblique angles of incidence is more difficult, since polarisation effects can be significant [104]. Because of that we used polarised spectral measurements at $\alpha_{\text{in}} = 60°$. The spectral properties of the individual coated or uncoated panes were measured at $\alpha_{\text{in}} = 0°$ and $\alpha_{\text{in}} = 60°$. For $\alpha_{\text{in}} = 60°$ we measured s- and p-polarisation separately. $\alpha_{\text{in}} = 60\circ$ properties of individual uncoated glass panes can also be calculated with the Fresnel-Equations from $\alpha_{\text{in}} = 0\circ$ spectral properties. The solar and light properties of the glazing unit where calculated for each polaristion first. We then averaged the results at the end assuming unpolarised light. The calculations for $\alpha_{\text{in}} = 0°$ were done according to [58].

The results were generalised to arbitrary α_{in} with an empirical model that was developed by Arne Roos et al. in the European research project ADOPT [79] [104]. The model parameter p_{roos} is equal to the number of panes in the glazing unit $\big(p_{\text{roos}} = 1$, 2 or 3$\big)$. $q_{\text{roos}} \in [1, 10]$ represents the 'material' category of the coating. If the angle-dependent glazing properties are not available, one can try to estimate the value of the glazing category parameter q_{roos} using table 3 taken from [104]. Formula (118) was originally designed to fit angle-dependent g-values. Strictly speaking, other parameters a_{roos}, b_{roos}, c_{roos}, and α_{roos}, β_{roos}, γ_{roos} are needed when the solar and light transmittance are to be predicted with this model on the basis of the category parameter q_{roos}. Our results for g_{gzg} - shown in table 4 - confirm in many cases the values for the category parameter given in table 3, but there are exceptions. We found that q_{roos} does not only depend on the coating category but also on the type of glass substrate. Glazing C is a double-silver coating on glass with a low iron content. It has a considerably higher q_{roos} value than other double-silver coatings. In our assessment of different solar control glazings we found a range of $q_{\text{roos}} \in [0.7, 3.2]$ for different solar control glazings which corresponds to a 5% relative difference in g_{gzg} (see figure 29).

For the determination of the angle-dependent solar and light transmittance, the parameter q_{roos} was obtained by fitting (118) to the values of $g_{\text{gzg}}(\alpha_{\text{in}} = 60°)$ and $g_{\text{gzg}}(\alpha_{\text{in}} = 0°)$. We then used the same value of q_{roos} for light and solar transmittance. This means that we assumed that

$$q_{\text{roos},\tau_e} \approx q_{\text{roos},\tau_v} \approx q_{\text{roos}} \tag{111}$$

Table 4 shows that $q_{\text{roos}} \geq q_{\text{roos},\tau_e}$ and $q_{\text{roos}} \leq q_{\text{roos},\tau_v}$ in reality. The uncertainty which is caused by this assumption can be determined from figure 3 and table 4. For most glazing listed in table 4, the difference between q_{roos} and q_{roos,τ_e} is less than 0.5, which means that the relative error is less than 3% for incidence angles between $0°$ and $60°$. For most glazing listed in table 4, the difference between q_{roos} and q_{roos,τ_e} or q_{roos,τ_v} is less than 0.5, which means that the relative error in τ_e or τ_v is less than 2% for incidence angles between $0°$ and $60°$. We found the biggest error in the case of a glazing with low iron content (glazing C) caused by the difference of 1.5 between q_{roos,τ_e}, and q_{roos}, which leads to a relative error of less than 8% in τ_e for incidence angles between $0°$ and $60°$. The errors in τ_v are generally smaller than the errors in τ_e for the measured solar control glazings. For the heat mirror glazing (glazing R) we found relative errors of less than 2% for τ_e and relative errors of less than 7% for τ_v for incidence angles between $0°$ and $60°$. The assumption in equation (111) therefore leads to a small or moderate overestimation of τ_e and a small or moderate underestimation of τ_v, which both lead to a small or moderate overestimation of g_{tot} when the glazing is combined with an internal solar protection device (see equation (131)).

The model is summarised by the following set of equations [104]:

$$
\begin{aligned}
a_{\text{roos}} &= 8 & (112)\\
b_{\text{roos}} &= 0.25/q_{\text{roos}} & (113)\\
c_{\text{roos}} &= 1 - a_{\text{roos}} - b_{\text{roos}} & (114)\\
\alpha_{\text{roos}} &= 5.2 + 0.7\,q_{\text{roos}} & (115)\\
\beta_{\text{roos}} &= 2 & (116)\\
\gamma_{\text{roos}} &= \big(5.26 + 0.06\,p_{\text{roos}}\big) + \big(0.73 + 0.04\,p_{\text{roos}}\big)\,q_{\text{roos}} & (117)\\
g_{\text{gzg}}[\alpha_{in}] &= g_{\text{gzg}}[0°]\left(1 - a_{\text{roos}}\left(\tfrac{\alpha_{in}}{90°}\right)^{\alpha_{\text{roos}}} - b_{\text{roos}}\left(\tfrac{\alpha_{in}}{90°}\right)^{\beta_{\text{roos}}} - c_{\text{roos}}\left(\tfrac{\alpha_{in}}{90°}\right)^{\gamma_{\text{roos}}}\right) & (118)
\end{aligned}
$$

we added the following formulas

$$
\begin{aligned}
\tau_{\text{e, gzg}}[\alpha_{in}] &\approx \tau_{\text{e, gzg}}[0°]\left(1 - a_{\text{roos}}\left(\tfrac{\alpha_{in}}{90°}\right)^{\alpha_{\text{roos}}} - b_{\text{roos}}\left(\tfrac{\alpha_{in}}{90°}\right)^{\beta_{\text{roos}}} - c_{\text{roos}}\left(\tfrac{\alpha_{in}}{90°}\right)^{\gamma_{\text{roos}}}\right) & (119)\\[2mm]
\tau_{\text{v, gzg}}[\alpha_{in}] &\approx \tau_{\text{v, gzg}}[0°]\left(1 - a_{\text{roos}}\left(\tfrac{\alpha_{in}}{90°}\right)^{\alpha_{\text{roos}}} - b_{\text{roos}}\left(\tfrac{\alpha_{in}}{90°}\right)^{\beta_{\text{roos}}} - c_{\text{roos}}\left(\tfrac{\alpha_{in}}{90°}\right)^{\gamma_{\text{roos}}}\right) & (120)\\[2mm]
q_{\text{i, gzg}}[\alpha_{in}] &:= g_{\text{gzg}}[\alpha_{in}] - \tau_{\text{e, gzg}}[\alpha_{in}] & (121)
\end{aligned}
$$

The main advantage of the empirical formula (118) is that the specific angular dependence of the properties of different coating types can be taken into account accurately and easily.

Table 3: Typical values of the glazing category parameter q_{roos}, obtained by fitting (119) to the corresponding experimental functions, taken from [104]

glazing (coating) type	q_{roos}
Absorbing electrochromic	1
Double silver	1
Absorbing, "grey" or "green" glass	2
Single silver (thick or thin)	2.5
Tin oxide, "K-glass"	3.5
Antireflection glass (SiO)	3.5
Float glass	4
$a - Si/SiO_2$	4.5
Titanium oxide	6
Titanium nitride, TiN	10
Stainless steel, SS	10
TiN/SS	10
$a - Si$	10

Table 4: g-value, solar transmittance and light transmittance for different solar control double glazed units (DGU), one heat mirror DGU ($\mathcal{R}$) and one clear glass DGU ($\mathcal{S}$). The results are based on polarised spectral measurements. The parameter q_{roos,τ_e} was determined by fitting (119) to the values of $\tau_{e,\mathrm{gzg}}(\alpha_{\mathrm{in}} = 60°)$ and $\tau_{e,\mathrm{gzg}}(\alpha_{\mathrm{in}} = 0°)$. q_{roos,τ_v} has been determined by fitting (120) to the measured values of $\tau_{v,\mathrm{gzg}}$.

glazing	$g_{\mathrm{gzg}}(0°)$	$g_{\mathrm{gzg}}(60°)$	q_{roos}	$\tau_e(0°)$	$\tau_e(60°)$	q_{roos,τ_e}	$\tau_v(0°)$	$\tau_v(60°)$	q_{roos,τ_v}
A	0.361	0.278	1.3	0.328	0.240	0.9	0.654	0.506	1.3
B	0.280	0.211	1.0	0.234	0.177	1.1	0.485	0.392	1.9
C	0.342	0.293	3.2	0.327	0.261	1.7	0.572	0.482	2.9
D	0.346	0.281	2.0	0.258	0.188	0.8	0.424	0.345	2.1
E	0.306	0.227	1.0	0.260	0.183	0.7	0.528	0.401	1.2
F	0.318	0.243	1.2	0.286	0.209	0.9	0.552	0.428	1.3
G	0.375	0.296	1.6	0.341	0.262	1.2	0.642	0.526	2.2
H	0.371	0.279	1.0	0.322	0.232	0.8	0.625	0.494	1.6
I	0.272	0.205	1.1	0.242	0.175	0.8	0.500	0.372	1.0
K	0.340	0.263	1.3	0.309	0.232	1.0	0.635	0.500	1.5
L	0.253	0.187	0.9	0.212	0.146	0.6	0.449	0.334	1.0
M	0.300	0.230	1.2	0.252	0.193	1.2	0.594	0.423	0.7
O	0.328	0.247	1.0	0.297	0.214	0.8	0.607	0.463	1.2
P	0.286	0.203	0.7	0.236	0.164	0.7	0.502	0.373	1.0
$\mathcal{R}$	0.563	0.438	1.4	0.446	0.343	1.2	0.711	0.587	2.4
$\mathcal{S}$	0.749	0.660	4.3	0.690	0.596	3.6	0.805	0.717	4.7

The reflectance of the glazing can be generalized to arbitrary angles of incidence with (122), which was proposed by Alessandro Dama during his research semester at Fraunhofer ISE [48].

$$\rho^x_{y,\text{gzg}}(\alpha_{\text{in}}) \approx \begin{cases} 1 - \tau_{y,\text{gzg}}(\alpha_{\text{in}}) - \underbrace{[1 - \rho^x_{y,\text{gzg}}(\alpha_{\text{in}} = 0°) - \tau_{y,\text{gzg}}(\alpha_{\text{in}} = 0°)]}_{\text{absorptance for normal incidence } \alpha^x(\alpha_{\text{in}} = 0°)} & \Big| \; \alpha_{\text{in}} \leq 75° \\ 1 - \tau_{y,\text{gzg}}(\alpha_{\text{in}}) - \alpha^x(\alpha_{\text{in}} = 0°) \frac{\alpha_{\text{in}} - 90°}{15°} & \Big| \; \alpha_{\text{in}} > 75° \end{cases} \tag{122}$$

The subscript $_y$ can be either $_v$ or $_e$, the superscript ^{x} can be either $'$ or nothing. The approximation ensures that $\tau + \rho \leq 1$.

The diffuse properties were determined with (123) [98]. $\mathcal{A}$ can either be g, τ, ρ' or ρ. The subscript $_y$ can be either $_v$, $_e$ or nothing (in case of g). This formula is only valid for rotationally symmetric properties. The diffuse irradiation is assumed to be isotropic.

$$\mathcal{A}_{y,\text{dif}} = \sum_{k=0}^{6} a_k \, \mathcal{A}_y(15 \, k) \tag{123}$$

$$\begin{aligned} a_0 &= 0.0170 & a_4 &= 0.2241 \\ a_1 &= 0.1294 & a_5 &= 0.1294 \\ a_2 &= 0.2241 & a_6 &= 0.0170 \\ a_3 &= 0.2588 \end{aligned}$$

Characterisation of angle-dependent blind properties Characterisation of venetian blinds with ray-tracing methods has been validated and demonstrated [8]. We have not changed the methodology since then. For roller blinds, we use the angle-dependent solar and light properties which have been measured on a sample of the fabric.

Diffuse properties of venetian blinds and vertical blinds

Diffuse properties of venetian blinds with horizontal slats have been determined with (124) under the assumption that the properties of the blinds depend only on the profile angle. This assumption neglects the fact that the reflectance of the surface of one slat also depends on the angle of incidence. $\mathcal{A}(\alpha_p)$ can be either τ, ρ' or ρ. The subscript $_y$ can be either $_v$ or $_e$. (124) is only valid for properties with azimuthal or profile angle symetry. The diffuse irradiation is assumed to be isotropic. Figure 29 shows the diffuse reflectance for two different venetian blinds.

It is common practice in building simulation to model external blinds as an extra glass pane. This means that the properties of the blind are assumed to have rotationally symmetric reflectance and transmittance instead of profile angle symmetry. Figure 4 on page 5 illustrates the difference between profile angle and incidence angle symmetry. Figures 30, 31 and 32 demonstrate that the difference in symmetry is relevant for the energy performance of venetian blinds. The transmittance of blinds with opened slats is in most cases significantly underestimated, when the profile angle symmetry is not taken into account. In the case of external venetian blinds, the total solar energy transmittance is therefore underestimated in

general when the profile angle symmetry is not taken into account. The opposite effect occurs for the reflectance when profile angle symmetry is not taken into account: The general overestimation of the reflectance of venetian blinds leads to an underestimation of the total solar energy transmittance in the case of internal venetian blinds. The relevance for building simulation is discussed in detail in [11].

In the case of vertical blinds (with vertical slats made of fabric) (124) can be used, when the facade azimuth angle γ_f is used instead of the profile angle α_p. This means that $\mathcal{A}(\gamma_f)$ has to be considered instead of $\mathcal{A}(\alpha_p)$.

$$\mathcal{A}_{y,\mathrm{dif}} \approx b_0 \mathcal{A}_y(0) + \sum_{k=1}^{6} b_k\big(\mathcal{A}_y(15\,k) + \mathcal{A}_y(-15\,k)\big) \tag{124}$$

$$
\begin{aligned}
b_0 &= 0.1304 & b_4 &= 0.0653 \\
b_1 &= 0.1261 & b_5 &= 0.0338 \\
b_2 &= 0.1130 & b_6 &= 0.0043 \\
b_3 &= 0.0923
\end{aligned}
$$

Equation (124) is an approximation for the diffuse-hemispherical property $\mathcal{A}_{y,\mathrm{dif}}$ which is defined in (125) for the case of polar coordinates $[\theta, \phi]$.

$$\mathcal{A}_{y,\mathrm{dif}} := \frac{1}{\pi} \int_{-\pi}^{\pi} \int_{0}^{\frac{\pi}{2}} \mathcal{A}_y\big(\alpha_s(\theta,\phi), \gamma_f(\theta,\phi)\big)\ \cos\big(\alpha_{\mathrm{in}}(\theta,\phi)\big)\ \sin(\theta)\ d\theta\, d\phi \tag{125}$$

$$= \frac{1}{\pi} \int_{-\frac{\pi}{2}}^{\frac{\pi}{2}} \int_{-\frac{\pi}{2}}^{\frac{\pi}{2}} \mathcal{A}_y(\alpha_s, \gamma_f)\ \cos(\alpha_s)^2\, \cos(\gamma_f)\ d\alpha_s\, d\gamma_f \tag{126}$$

$$= \frac{1}{\pi} \int_{-\frac{\pi}{2}}^{\frac{\pi}{2}} \int_{-\frac{\pi}{2}}^{\frac{\pi}{2}} \mathcal{A}_y(\alpha_p)\ \frac{\cos(\gamma_f)}{(\cos(\alpha_p)^2\ \sec(\gamma_f) + \cos(\gamma_f)\ \sin(\alpha_p)^2)\,(1 + \cos(\gamma_f)^2\ \tan(\alpha_p)^2)}\ d\alpha_p\, d\gamma_f \tag{127}$$

$$\approx: b_0 \mathcal{A}_y(0) + \sum_{k=1}^{6} b_k\big(\mathcal{A}_y(15\,k) + \mathcal{A}_y(-15\,k)\big)\ \Big|\ \text{which is equivalent to (124)}$$

b_k is defined for k = 0, …, 5 by

$$b_k := \frac{1}{\pi} \int_{-\frac{\pi}{2}}^{\frac{\pi}{2}} \int_{(15\,k-7.5)\,\frac{\pi}{180}}^{(15\,k+7.5)\,\frac{\pi}{180}} \frac{\cos(\gamma_f)}{(\cos(\alpha_p)^2\ \sec[\gamma_f] + \cos(\gamma_f)\ \sin(\alpha_p)^2)\,(1 + \cos(\gamma_f)^2\ \tan(\alpha_p)^2)}\ d\alpha_p\, d\gamma_f \tag{128}$$

b_6 is defined by

$$b_6 := \frac{1}{\pi} \int_{-\frac{\pi}{2}}^{\frac{\pi}{2}} \int_{82.5\,\frac{\pi}{180}}^{\frac{\pi}{2}} \frac{\cos(\gamma_f)}{(\cos(\alpha_p)^2\ \sec[\gamma_f] + \cos(\gamma_f)\ \sin(\alpha_p)^2)\,(1 + \cos(\gamma_f)^2\ \tan(\alpha_p)^2)}\ d\alpha_p\, d\gamma_f \tag{129}$$
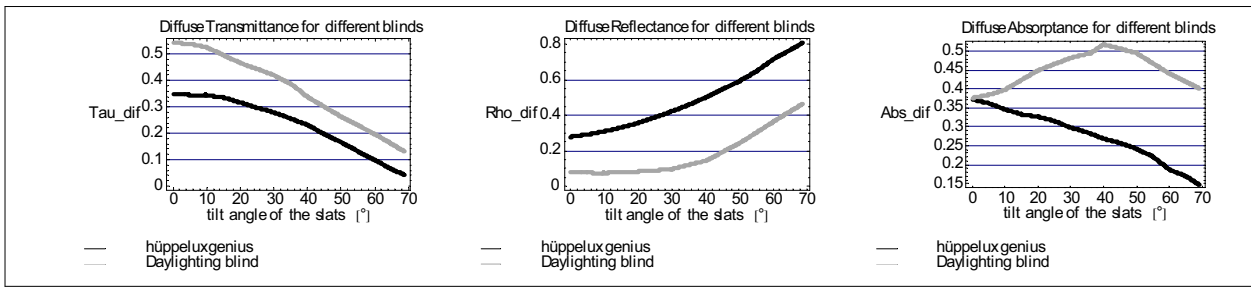
Figure 29: Diffuse transmittance, reflectance and absorptance for two different venetian blinds. The daylighting-venetian blind has slats with a mirror-finished top-surface. The 'Genius slats' are presented in figure 62

.
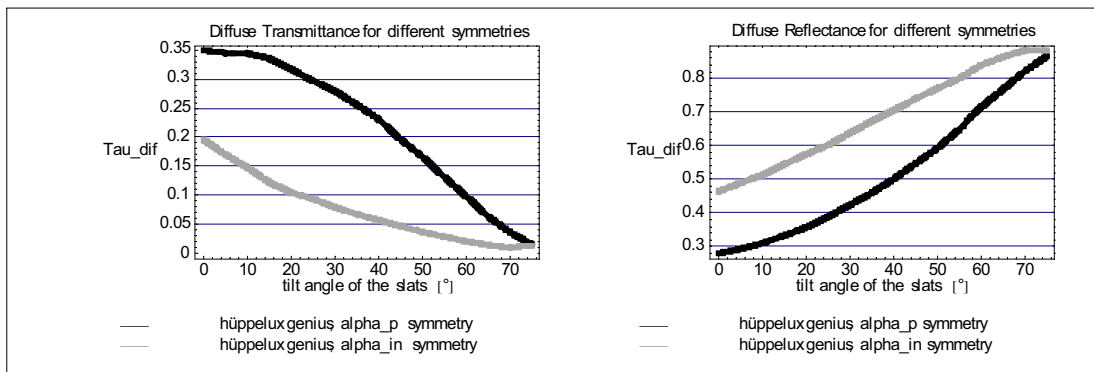
Figure 30: Diffuse transmittance and reflectance for a venetian blind with 'Genius slats'. 'alpha_in symmetry' means the inaccurate assumption that $\mathcal{A}(\alpha_{in}) \approx \mathcal{A}(\alpha_s = \alpha_{in}, \gamma_f = 0°)$. 'alpha_p symmetry' means the assumption that $\mathcal{A}(\alpha_s, \gamma_f) \doteq \mathcal{A}(\alpha_p(\alpha_s, \gamma_f), \gamma_f = 0°)$. $\mathcal{A}$ can either be τ_{bld} or ρ_{bld}.
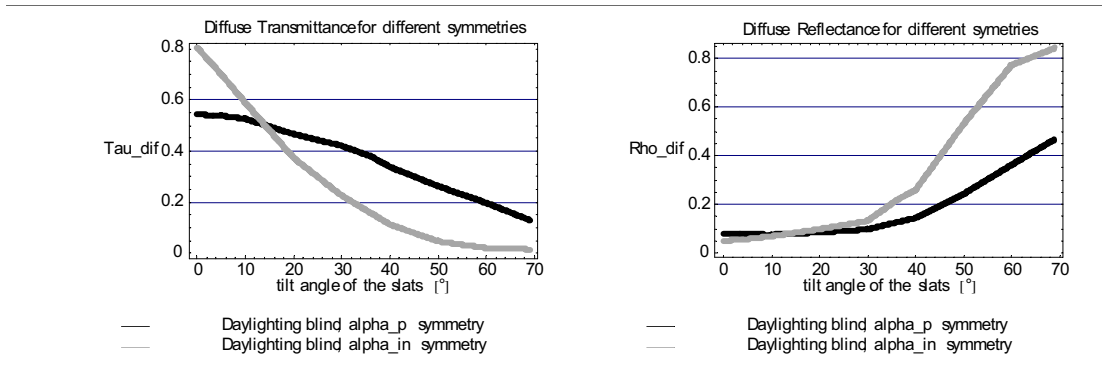
Figure 31: Diffuse transmittance and reflectance for a daylighting venetian blind. 'alpha_in symmetry' means the inaccurate assumption that $\mathcal{A}(\alpha_{in}) \approx \mathcal{A}(\alpha_s = \alpha_{in}, \gamma_f = 0°)$. 'alpha_p symmetry' means the assumption that $\mathcal{A}(\alpha_s, \gamma_f) \doteq \mathcal{A}(\alpha_p(\alpha_s, \gamma_f), \gamma_f = 0°)$. $\mathcal{A}$ can either be τ_{bld} or ρ_{bld}.
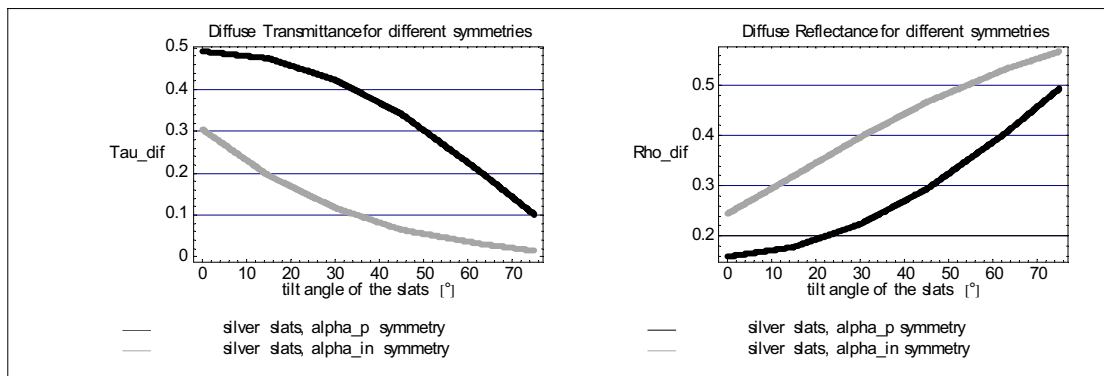
Figure 32: Diffuse transmittance and reflectance for a venetian blind with convex (conventionally shaped) slats. The top surface of the slats is matt silver ($\rho_{e,tot} = 0.59$), the bottom is light grey ($\rho_{e,tot} = 0.58$). 'alpha_in symmetry' means the inaccurate assumption that $\mathcal{A}(\alpha_{in}) \approx \mathcal{A}(\alpha_s = \alpha_{in}, \gamma_f = 0°)$. 'alpha_p symmetry' means the assumption that $\mathcal{A}(\alpha_s, \gamma_f) \doteq \mathcal{A}(\alpha_p(\alpha_s, \gamma_f), \gamma_f = 0°)$. $\mathcal{A}$ can either be τ_{bld} or ρ_{bld}.

Determination of $g_{\text{tot}}(\alpha_s, \gamma_{\mathbf{f}})$ for the combination of glazing and blind The goal of the whole assessment is to be able to calculate the hourly or monthly effective total solar energy transmittance $g_{\text{eff-h}}$ or $g_{\text{eff-m}}$ respectively for a given irradiance situation with direct and diffuse solar radiation and to assess the impact of these 'average' properties (see again figure 28). The diffuse sky is subdivided into $n = 145$ patches according to [120] in order to be able to take the diffuse radiation into account [8]. Each patch irradiates the facade under consideration from a different direction $[\alpha_{s,n}, \gamma_{f,n}]$. The ground was assumed to be an isotropic diffuse reflector with an albedo of 0.2. The ground surface was divided into $m = 90$ discrete patches. Therefore the properties of the facade have to be known for all $m + n$ directions and all the possible directions of the direct solar radiation. In the case of switchable facade properties (tiltable slats, retractable roller blind or switchable glazing) the different states of the system have to be taken into account additionally. It is obviously much too costly to measure $g_{\text{tot}}(\alpha_s, \gamma_f, \text{switching condition})$ for all these cases directly with a calorimeter. On the other hand, direct calorimetric measurements are very important since they are able to quantify the effects of imperfect product attributes. Imperfect product attributes are for example unevenly tilted slats or imperfectly shaped slats. The proposed method uses in case of internal shading systems some calorimetric measurements as supporting points for a general model of $g_{\text{tot}}(\alpha_s, \gamma_f, \text{switching condition})$. The measurements are taken into account via one parameter $\varkappa$ which has a physical meaning, as will be discussed later. Because of the physical meaning of the parameter, the model can also be used fully predictively when the possible extreme values of $\varkappa$ are used to generate error bars.

Internal blinds / Internal venetian blinds: For internal venetian blinds which are mounted in the room behind the glazing, the first step was equation (130), an empirical approach which is a generalised and improved version of the formula given in EN13363-1 [62]. It is generalised, because it can take into account arbitrary angles of incidence. It is improved because it treats internal blinds in combination with solar control glazings much more accurately than the original formula. It has been used successfully in the planning teams for several high-rise office buildings in the last few years. The next step is equation (131) which is a further development of equation (130) that is physically more meaningful. The two principle ideas of all the formulas are to mix α_{in}-dependent glazing properties with α_p-dependent properties of blinds with translation invariant properties (e.g. venetian blinds) and to use solar and light properties at the same time in order to take into account the change of the spectrum of the radiation after being transmitted through spectrally selective layers.

The first approach for g_{tot} was

$$\widetilde{g_{\text{tot}}}[\alpha_s, \gamma_{\text{f}}, \beta_{\text{k}}] = \underbrace{g_{\text{gzg}}[\alpha_{in}[\alpha_s, \gamma_{\text{f}}]]}_{\text{enters the room}}$$

$$- \underbrace{\frac{\tau_{\text{e, gzg}}[\alpha_{in}[\alpha_s, \gamma_{\text{f}}]] \quad \tau_{x^\star,\text{ dif, gzg}} \quad \rho_{x^\star,\text{ bld}}[\alpha_p[\alpha_s, \gamma_{\text{f}}], \beta_{\text{k}}]}{1 - \rho_{x^\star,\text{ dif, bld}}[\beta_{\text{k}}] \quad \rho'_{x^\star,\text{ dif, gzg}}}}_{\text{reflected back to the exterior}}$$

$$- \quad \varkappa \; \underbrace{\frac{\tau_{\text{e, gzg}}[\alpha_{in}[\alpha_s, \gamma_{\text{f}}]] \quad \alpha'_{x^\star,\text{ dif, gzg}} \quad \rho_{x^\star,\text{ bld}}[\alpha_p[\alpha_s, \gamma_{\text{f}}], \beta_{\text{k}}]}{1 - \rho_{x^\star,\text{ dif, bld}}[\beta_{\text{k}}] \quad \rho'_{x^\star,\text{ dif, gzg}}}}_{\text{outward flowing fraction of energy that is reflected by the blind and then absorbed in the glazing}}$$

$$- \underbrace{g_{\text{gzg}}[\alpha_{in}[\alpha_s, \gamma_{\text{f}}]] \quad \alpha_{x^\star,\text{ bld}}[\alpha_p[\alpha_s, \gamma_{\text{f}}], \beta_{\text{k}}] \quad \frac{\Lambda_{\text{internal}}}{\Lambda_2}}_{\text{extra heat losses due to solar heating of the blind}}$$

$$(130)$$

where

- $\alpha'_{x^\star,\text{ dif, gzg}} = (1 - \rho'_{x^\star,\text{ dif, gzg}} - \tau_{x^\star,\text{ dif, gzg}})$ and
  $\alpha_{x^\star,\text{ bld}}[\alpha_p[\alpha_s, \gamma_{\text{f}}], \beta_{\text{k}}] = (1 - \rho_{x^\star,\text{ bld}}[\alpha_p[\alpha_s, \gamma_{\text{f}}], \beta_{\text{k}}] - \tau_{x^\star,\text{ bld}}[\alpha_p[\alpha_s, \gamma_{\text{f}}], \beta_{\text{k}}])$

- $\rho_{x^\star,\text{ bld}} = \begin{cases} \rho_{v,\text{ bld}} \text{ in the case of solar-control glazing with a selectivity } \mathcal{S} := \frac{\tau_{\text{v, gzg}}}{\tau_{\text{e, gzg}}} \approx 2.0 \\ \min(\rho_{\text{e, bld}}, \rho_{\text{v, bld}}) \text{ in the case of heat-mirror glazing with a selectivity } \mathcal{S} \approx 1.5 \\ \rho_{e,\text{ bld}} \text{ in the case of a glazing unit made of clear glass with a selectivity } \mathcal{S} \approx 1.2 \end{cases}$

  For the corresponding quantities $\tau_{x^\star,\text{ bld}}$, $\rho_{x^\star,\text{ dif, bld}}$, $\tau_{x^\star,\text{ dif, gzg}}$ and $\rho'_{x^\star,\text{ dif, gzg}}$, the subscript $_{x^\star}$ has to be replaced by $_e$ or $_v$ accordingly.

- The angle-dependent reflectance and transmittance of the blind can be either measured or calculated with OPTICAD [93] ray-tracing [8]. The diffuse properties $\rho_{x^\star,\text{ dif, bld}}[\beta_{\text{k}}]$ and $\tau_{x^\star,\text{ dif, bld}}[\beta_{\text{k}}]$ are calculated with (124).

- The angle-dependent transmittance of the glazing is calculated with (119). Parameter q_{roos} of (119) is determined from measurements at normal incidence and $\alpha_{in} = 60°$. The angle dependent reflectance of the glazing is calculated using (122) and (119). The diffuse properties $\rho'_{x^\star,\text{ dif, gzg}}$ and $\tau_{x^\star,\text{ dif, gzg}}$ are calculated with (123).

- $\varkappa$ adjusts the outward-flowing fraction of the energy that is reflected by the blind and then absorbed by the glazing. $\varkappa \in [0, 1]$ is the parameter which can be used to fit the model to the results of calorimetric measurements in order to generalise calorimetric measurements of g_{tot} to arbitrary directions of the incident solar radiation $[\alpha_s, \gamma_{\text{f}}]$ and arbitrary tilt angles of the slats β_{k}. If one does not know the angular properties of the glazing, then $\varkappa$ and q_{roos} (in (119)) can both be considered as parameters. $\varkappa$ has a limited range of values because of its physical meaning, the range for q_{roos} can be restricted to $[1, 10]$ according to table 3. Parameter variations can therefore be used to derive the range between the possible extreme values of g_{tot}.

- $\Lambda_2 := 18 \; \frac{W}{m^2 K}$ (similar to EN13363-1 [62])

- $\Lambda_{\text{internal}} := \left(\frac{1}{U_{\text{gzg}}} + \frac{1}{\Lambda_2}\right)^{-1}$ (similar to EN13363-1 [62])

A disadvantage of model (130) is the last term which characterises the 'extra heat losses due to solar heating of the blind'. The use of g_{gzg} in that formula lowers the precision, but it would be worse to replace g_{gzg} with $\tau_{\text{e,gzg}}$ because this would not take into account multiple reflections between glazing and blind. $\frac{\tau_{\text{e,gzg}}}{1-\rho_{x^\star,\,\text{dif, bld}}[\beta_{\text{k}}]\,\rho'_{x^\star,\,\text{dif, gzg}}}$ should therefore be used instead of g_{gzg}. In case of glazing made from glass with low iron content and therefore very small $q_{\text{i,gzg}}$, it is possible that $g_{\text{gzg}} < \frac{\tau_{\text{e,gzg}}}{1-\rho_{x^\star,\,\text{dif, bld}}[\beta_{\text{k}}]\,\rho'_{x^\star,\,\text{dif, gzg}}}$. It is therefore possible that (130) does not overestimate g_{tot} in every case. A more accurate formulation is (131):

$$g_{\text{tot}}[\alpha_s, \gamma_{\text{f}}, \beta_{\text{k}}] := \tau_{\text{e,tot}}[\alpha_s, \gamma_{\text{f}}, \beta_{\text{k}}] + q_{\text{i,tot}}[\alpha_s, \gamma_{\text{f}}, \beta_{\text{k}}] \tag{131}$$

where

$$\tau_{\text{e,tot}}[\alpha_s, \gamma_{\text{f}}, \beta_{\text{k}}] = \tau_{\text{e,gzg}}[\alpha_{in}[\alpha_s, \gamma_{\text{f}}]]\ \tau_{x^\star,\text{bld}}[\alpha_p[\alpha_s, \gamma_{\text{f}}], \beta_{\text{k}}]$$
$$+ \frac{\tau_{\text{e,gzg}}[\alpha_{in}[\alpha_s, \gamma_{\text{f}}]]\ \rho_{x^\star,\text{bld}}[\alpha_p[\alpha_s, \gamma_{\text{f}}], \beta_{\text{k}}]\ \rho'_{x^\star,\text{dif,gzg}}\ \tau_{x^\star,\text{dif,bld}}[\beta_{\text{k}}]}{1 - \rho_{x^\star,\text{dif,bld}}[\beta_{\text{k}}]\ \rho'_{x^\star,\text{dif,gzg}}} \tag{132}$$

and

$$q_{\text{i,tot}}[\alpha_s, \gamma_{\text{f}}, \beta_{\text{k}}] = \underbrace{g_{\text{gzg}}[\alpha_{in}[\alpha_s, \gamma_{\text{f}}]] - \tau_{\text{e, gzg}}[\alpha_{in}[\alpha_s, \gamma_{\text{f}}]]}_{q_{\text{i, gzg}}}$$
$$+ \quad \underbrace{(1 - \varkappa)\frac{\tau_{\text{e,gzg}}[\alpha_{in}[\alpha_s, \gamma_{\text{f}}]]\ \alpha'_{x^\star,\text{ dif, gzg}}\ \rho_{x^\star,\text{bld}}[\alpha_p[\alpha_s, \gamma_{\text{f}}], \beta_{\text{k}}]}{1 - \rho_{x^\star,\text{dif,bld}}[\beta_{\text{k}}]\ \rho'_{x^\star,\text{dif,gzg}}}}_{\text{inward flowing fraction of energy that is reflected by the blind and then absorbed in the glazing}}$$
$$+ \quad \underbrace{\tau_{\text{e,gzg}}[\alpha_{in}[\alpha_s, \gamma_{\text{f}}]]\ \frac{\alpha_{x^\star,\text{bld}}[\alpha_p[\alpha_s, \gamma_{\text{f}}], \beta_{\text{k}}]}{1 - \rho_{x^\star,\text{dif,bld}}[\beta_{\text{k}}]\ \rho'_{x^\star,\text{dif,gzg}}}\left(1 - \frac{\Lambda_{\text{internal}}}{\Lambda_2}\right)}_{\text{extra heat gains due to solar absorption in the blind}}$$
$$\tag{133}$$

(132) leads directly to the equation for the light transmittance:

$$\tau_{\text{v,tot}}[\alpha_s, \gamma_{\text{f}}, \beta_{\text{k}}] = \tau_{\text{v,gzg}}[\alpha_{in}[\alpha_s, \gamma_{\text{f}}]]\ \tau_{\text{v,bld}}[\alpha_p[\alpha_s, \gamma_{\text{f}}], \beta_{\text{k}}]$$
$$+ \frac{\tau_{\text{v,gzg}}[\alpha_{in}[\alpha_s, \gamma_{\text{f}}]]\ \rho_{\text{v,bld}}[\alpha_p[\alpha_s, \gamma_{\text{f}}], \beta_{\text{k}}]\ \rho'_{\text{v,dif,gzg}}\ \tau_{\text{v,dif,bld}}[\beta_{\text{k}}]}{1 - \rho_{\text{v,dif,bld}}[\beta_{\text{k}}]\ \rho'_{\text{v,dif,gzg}}} \tag{134}$$

Internal roller blinds: The model has been used and validated also for roller blinds. In this case the properties of the blind do not depend on α_p. In most cases they are rotationally symmetric to a good approximation. This means that the profile angle α_p has to be replaced by the angle of incidence α_{in} in equations (131), (132), (133) and (134).

Internal vertical blinds
In the case of internal vertical blinds (made from vertical fabric slats) α_s has to be projected

Table 5: g_{tot} for a white venetian blind with 80 mm slat width and partly perforated concave slats. This internal blind is combined with a solar control glazing with $g_{\text{gzg}}(0°) = 0.25$. The results of the models are given with three digits for comparison. $g_{\text{tot,calorimeter}}$ was measured directly with our calorimeter. $g_{\text{tot,eq.(131)}}$ was determined with (131). $g_{\text{tot,eq.(130)}}$ was determined with (130). F_c is defined by $F_c := \frac{g_{\text{tot,eq.(131)}}}{g_{\text{gzg}}(\alpha_{in})}$. The model parameter was set to $\varkappa = 0.4$.

α_s [°]	γ_{f} [°]	tilt-angle [°]	$g_{\text{tot,calorimeter}}$	$g_{\text{tot,eq.(131)}}$	$g_{\text{tot,eq.(130)}}$	$g_{\text{tot,EN13363-1}}$	F_c
0	0	72 ± 3	0.16 ± 0.03	0.166	0.163	0.207	0.65
0	0	50 ± 2	0.18 ± 0.03	0.190	0.188	0.217	0.75
60	0	0 ± 2	0.15 ± 0.03	0.148	0.148	0.171	0.78

Table 6: g_{tot} for a daylighting venetian blind with 80 mm slat width and partly perforated concave slats. This internal blind is combined with a solar control glazing with $g_{\text{gzg}}(0°) = 0.25$. The results of the models are given with three digits for comparison. $g_{\text{tot,calorimeter}}$ was measured directly with our calorimeter. $g_{\text{tot,eq.(131)}}$ was determined with (131). $g_{\text{tot,eq.(130)}}$ was determined with (130). F_c is defined by $F_c := \frac{g_{\text{tot,eq.(131)}}}{g_{\text{gzg}}(\alpha_{in})}$. The model parameter was set to $\varkappa = 0.4$.

α_s [°]	γ_{f} [°]	tilt-angle [°]	$g_{\text{tot,calorimeter}}$	$g_{\text{tot,eq.(131)}}$	$g_{\text{tot,eq.(130)}}$	$g_{\text{tot,EN13363-1}}$	F_c
0	0	68 ± 2	0.21 ± 0.03	0.203	0.198	0.221	0.8
0	0	50 ± 2	0.23 ± 0.03	0.238	0.232	0.238	0.9
60	0	0 ± 3	0.17 ± 0.03	0.186	0.186	0.185	1.0

onto a horizontal surface which is perpendicular to the facade. Therefore the profile angle α_p has to be replaced by the facade azimuth γ_{f} in equations (131), (132), (133) and (134).

Other internal blinds
In the case of other special blinds with less symmetry in the optical properties, α_p has to be replaced by $[\alpha_s, \gamma_{\text{f}}]$ in equations (131), (132), (133) and (134).

Validation

Tables 5, 6 and 7 reveal the very good agreement between measurements and model calculations with (130) and (131). The slats of the venetian blinds in tables 5 and 6 are partly perforated in order to improve the visual contact with the exterior. The formula given in EN13363-1 [62] shows good accuracy in the case of low reflectance of the blind when it is generalised to profile angle symmetry. In the case of higher reflectance EN13363-1 [62] significantly overestimates the total solar energy transmittance of the combination of glazing and blind, especially for solar control glazing. The reason for the overestimation is that EN13363-1 [62] uses $g_{\text{gzg}}^2 \rho_{\text{e, bld}}$ for the radiation that is reflected out of the room instead of the formula on the right hand side of (135)

$$g_{\text{gzg}}^2 \, \rho_{\text{e,bld}} \quad \Rightarrow \quad \tau_{\text{e,gzg}} \, \rho_{\text{v,bld}} \, \tau_{\text{v,gzg}} \quad | \quad \text{for spectrally selective glazings with S} \approx 2 \quad (135)$$

The formula in EN13363-1 [62] could be replaced by (131) in order to improve this standard wich is part of the German building code.

Table 7: g_{tot} for a daylighting venetian blind with 50 mm slat width and concave slats. The top surface is mirror-finished, the bottom surface is stone grey. This internal blind is combined with a solar control glazing with $g_{\text{gzg}}(0°) = 0.31$. The results of the models are given with three digits for comparison. $g_{\text{tot,calorimeter}}$ was measured directly with our calorimeter. $g_{\text{tot,eq.(131)}}$ was determined with (131). $g_{\text{tot,eq.(130)}}$ was determined with (130). F_c is defined by $F_c := \frac{g_{\text{tot,eq.(131)}}}{g_{\text{gzg}}(\alpha_{in})}$. The model parameter was set to $\varkappa = 0.4$.

α_s [°]	γ_{f} [°]	tilt-angle [°]	$g_{\text{tot,calorimeter}}$	$g_{\text{tot,eq.(131)}}$	$g_{\text{tot,eq.(130)}}$	$g_{\text{tot,EN13363-1}}$	F_c
45	0	-1 ± 3	0.25 ± 0.03	0.272	0.272	0.273	0.99
60	0	-1 ± 3	0.21 ± 0.03	0.223	0.222	0.223	0.98
60	0	28 ± 4	0.19 ± 0.03	0.206	0.203	0.211	0.90
30	45	28 ± 4	0.23 ± 0.03	0.237	0.233	0.239	0.92
45	45	28 ± 4	0.21 ± 0.03	0.206	0.204	0.212	0.90
60	0	45 ± 3	0.13 ± 0.03	0.108	0.111	0.183	0.47
30	45	45 ± 3	0.21 ± 0.03	0.231	0.225	0.235	0.90
0	0	65 ± 4	0.25 ± 0.03	0.257	0.247	0.266	0.84
45	0	65 ± 4	0.14 ± 0.03	0.130	0.136	0.211	0.47

Spectral modelling

Equation (132) can also be used for spectral modelling. In case of venetian blinds this leads to:

$$\tau_{\text{tot},\lambda}[\alpha_s, \gamma_{\text{f}}, \beta_{\text{k}}] = \tau_{\text{gzg},\lambda}[\alpha_{in}] \ \tau_{\text{bld},\lambda}[\alpha_p, \ \beta_{\text{k}}]$$
$$+ \ \frac{\tau_{\text{gzg},\lambda}[\alpha_{in}] \ \rho_{\text{bld},\lambda}[\alpha_p, \beta_{\text{k}}] \ \rho'_{\text{dif,gzg},\lambda} \ \tau_{\text{dif,bld},\lambda}[\beta_{\text{k}}]}{1 - \rho_{\text{dif,bld},\lambda}[\beta_{\text{k}}] \ \rho'_{\text{dif,gzg},\lambda}} \qquad (136)$$

and

$$q_{\text{i,tot},\lambda}[\alpha_s, \gamma_{\text{f}}, \beta_{\text{k}}] := g_{\text{gzg},\lambda}[\alpha_{in}] - \tau_{\text{gzg},\lambda}[\alpha_{in}]$$
$$+ \ (1 - \varkappa)\frac{\tau_{\text{gzg},\lambda}[\alpha_{in}] \ \alpha'_{\text{dif,gzg},\lambda} \ \rho_{\text{bld},\lambda}[\alpha_p, \beta_{\text{k}}]}{1 - \rho_{\text{dif,bld},\lambda}[\beta_{\text{k}}] \ \rho'_{\text{dif,gzg},\lambda}}$$
$$+ \ \tau_{\text{gzg},\lambda}[\alpha_{in}] \ \frac{\alpha_{\text{bld},\lambda} \ [\alpha_p, \beta_{\text{k}}]}{1 - \rho_{\text{dif,bld},\lambda}[\beta_{\text{k}}] \ \rho'_{\text{dif,gzg},\lambda}} \left(1 - \frac{\Lambda_{\text{internal}}}{\Lambda_2}\right) \qquad (137)$$

$g_{\text{gzg},\lambda}[\alpha_{in}]$ can be calculated with the formulas given in EN410 or ISO9050 for $\alpha_{in} = 0°$ since these models do not consider non-linear convection effects which would depend on the temperature of the panes. Therefore the overall absorptance is not relevant in these formulas. In the case of $\alpha_{in} \neq 0°$, $g_{\text{gzg},\lambda}$ should be calculated separately for s- and p-polarisation first. Then the results for s- and p-polarisation should be averaged assuming unpolarised irradiation. Equations (136) and (137) are more accurate than equations (132) and (133). The main reason is, that (133) uses terms such as $[\tau_{\text{e, gzg}} \times \alpha'_{x^\star, \text{dif, gzg}}]$ instead of $[\tau_{\text{gzg},\lambda} \times \alpha'_{\text{dif, gzg},\lambda}]$. Nevertheless we normally did not use the spectral equations since the non-spectral equations are sufficiently accurate in most cases and since the necessary input for the spectral model is much more complex. Another advantage of the non-spectral equations is, that the solar and light transmittance and reflectance for different slat tilt-angles are product characteristics which can be also used for other purposes (e.g. assessment of the supply with daylight or glare protection).

External blinds   External venetian blinds

In the case of external venetian blinds with horizontal slats which are mounted outside the room in front of the glazing, we used an improved and generalised version of the model given in EN13363-1 [62]:

$$
\begin{aligned}
g_{\text{tot}}[\alpha_s, \gamma_{\text{f}}, \beta_k] = {} & \tau_{\text{e, bld}}\big[\alpha_p[\alpha_s, \gamma_{\text{f}}], \beta_{\text{k}}\big] \quad g_{\text{gzg}}\big[\alpha_{in}[\alpha_s, \gamma_{\text{f}}]\big] \\
& + \left(1 - \rho_{\text{e, bld}}\big[\alpha_p[\alpha_s, \gamma_{\text{f}}], \beta_{\text{k}}\big] - \tau_{\text{e, bld}}\big[\alpha_p[\alpha_s, \gamma_{\text{f}}], \beta_{\text{k}}\big] \right) \frac{\Lambda_{\text{external}}}{\Lambda_2} \\
& + \tau_{\text{e, bld}}\big[\alpha_p[\alpha_s, \gamma_{\text{f}}], \beta_{\text{k}}\big] \left(1 - g_{\text{gzg}}\big[\alpha_{in}[\alpha_s, \gamma_{\text{f}}]\big] \right) \frac{\Lambda_{\text{external}}}{\Lambda_1}
\end{aligned}
\tag{138}
$$

$$
\tau_{\text{e, tot}}[\alpha_s, \gamma_{\text{f}}, \beta_k] = \frac{\tau_{\text{e, gzg}}\big[\alpha_{in}[\alpha_s, \gamma_{\text{f}}]\big] \quad \tau_{\text{e, bld}}\big[\alpha_p[\alpha_s, \gamma_{\text{f}}], \beta_{\text{k}}\big]}{1 - \rho'_{\text{e, dif, bld}}[\beta_{\text{k}}] \ \rho_{\text{e, dif, gzg}}}
\tag{139}
$$

$$
q_{\text{i, tot}}[\alpha_s, \gamma_{\text{f}}, \beta_k] = g_{\text{tot}}[\alpha_s, \gamma_{\text{f}}, \beta_k] - \tau_{\text{e, tot}}[\alpha_s, \gamma_{\text{f}}, \beta_k]
\tag{140}
$$

therefore

$$
\tau_{\text{v, tot}}[\alpha_s, \gamma_{\text{f}}, \beta_{\text{k}}] = \frac{\tau_{\text{v, gzg}}\big[\alpha_{in}[\alpha_s, \gamma_{\text{f}}]\big] \quad \tau_{\text{v, bld}}\big[\alpha_p[\alpha_s, \gamma_{\text{f}}], \beta_{\text{k}}\big]}{1 - \rho'_{\text{v, dif, bld}}[\beta_{\text{k}}] \ \rho_{\text{v, dif, gzg}}}
\tag{141}
$$

where

- The angle-dependent reflectance and transmittance of the blind can be either measured or calculated with OPTICAD® [93] ray-tracing [8]. The diffuse properties $\rho_{x^\star, \text{ dif, bld}}[\beta_{\text{k}}]$ and $\tau_{x^\star, \text{ dif, bld}}[\beta_{\text{k}}]$ are calculated with (124).

- The angle-dependent transmittance of the glazing is calculated with (119). Parameter q_{roos} of (119) is determined from measurements at normal incidence and $\alpha_{in} = 60°$. The angle-dependent reflectance of the glazing is calculated using (122) and (119). The diffuse properties $\rho'_{x^\star, \text{ dif, gzg}}$ and $\tau_{x^\star, \text{ dif, gzg}}$ are calculated with (123).

- $\Lambda_1 := 6 \ \frac{W}{m^2 K}$ (similar to EN13363-1)

- $\Lambda_2 := 18 \ \frac{W}{m^2 K}$ (similar to EN13363-1)

- $\Lambda_{\text{external}} := \left(\frac{1}{U_{\text{gzg}}} + \frac{1}{\Lambda_1} + \frac{1}{\Lambda_2} \right)^{-1}$ (similar to EN13363-1)

External roller blinds

The model has also been used for external roller blinds. In this case, the properties of the blind do not depend on α_p. In most cases, they are rotationally symmetric, to a good approximation. This means that the profile angle α_p has to be replaced by the angle of incidence α_{in} in (138).

Other External blinds

In the case of other special blinds with less symmetry in the optical properties, α_p has to be replaced by $[\alpha_s, \gamma_{\text{f}}]$ in (138).

Validation

We validated (138) for every new facade with calorimetric measurements before we used this

Table 8: g_{tot} for s_enn$^{®}$ mounted externally in front of two different glazings. $g_{\text{gzg}} = 0.57$ for the g-value of the reversed heat-mirror glazing with low-e coating on position 2 (inner surface of outer pane). $g_{\text{gzg}} = 0.36$ for the solar control glazing. $g_{\text{tot,eq.(138)}}$ has been calculated with (138).

glazing type	α_s [°]	γ_{f} [°]	$g_{\text{tot,calorimeter}}$	$g_{\text{tot,eq.(138)}}$
heat mirror	0	0	0.16 ± 0.02	0.16
heat mirror	45	0	0.02 ± 0.02	0.04
solar control	0	0	0.10 ± 0.02	0.12
solar control	45	0	0.01 ± 0.01	0.04

formula to calculate effective g-values. The validation for s_enn is shown in table 8. In this case we measured the angular dependent transmittance and we calculated the reflectance with our raytracing-tool. The agreement between measurements and calculations is good. Further validation experiments are given in [8].

6.2.3 Determination of the hourly and monthly effective g-values $g_{\text{eff-h}}$ and $g_{\text{eff-m}}$

The principles of the methodology to determine the effective (average) monthly or hourly g-values, $g_{\text{eff-m}}$ or $g_{\text{eff-h}}$ respectively, have been published in [8]. The different steps are displayed in figure 28.

Typical radiance distributions of the sky and corresponding radiances for the direct solar radiation are calculated for every hour in the relevant time period for the location and facade orientation under consideration. In our calculations, this was done on the basis of hourly direct horizontal and diffuse horizontal irradiance data taken from the appropriate Test Reference Years [50]. The sky radiance distribution was calculated using the Perez model [94] [95]. The continuous radiance distribution of the diffuse sky was discretized by splitting it into 145 circular angular patches with cone openings of 11.15° according to Tregenza [120]. The ground was assumed to be an isotropic diffuse reflector with an albedo of 0.2. The ground surface was divided into 90 discrete patches. Direct irradiation was treated as a parallel beam. The direction of the beam was calculated from the geographical position, date and time. A modified version of the program gendaylit [101] was used for the calculation of the direct solar and sky radiance distribution.

The control strategy for the blind determined by the thermal and visual requirements of the user defines the setting of the facade system in each hour i of the specified period with I hours in total. The setting is characterised by the tilt angle of the slats (in the case of venetian blinds) and/or the position of the lower end of a venetian/roller blind or refers to the state of switchable glazing.

$g_{\text{eff-m}}$ or $g_{\text{eff-h}}$: $g_{\text{eff-h},i}$ for the specified hour i is determined with

$$g_{\text{eff-h},\,i} := \frac{\sum_{n \in N} \ g_{\text{tot}}\big(\alpha_{s,n}, \gamma_{\text{f,n}}, \beta_{k,i}\big) \ \mathcal{L}_{n,i} \ \Delta\Omega_n \ \cos\big(\alpha_{in,n}\big)}{\sum_{n \in N} \ \mathcal{L}_{n,i} \ \Delta\Omega_n \ \cos\big(\alpha_{in,n}\big)} \tag{142}$$

N is the number of patches for the diffuse sky and ground, plus one patch for the direct sun. $\Delta\Omega_n$ is the solid angle of patch n. $\mathcal{L}_{n,i}$ is the radiance of patch n in hour i. $\beta_{k,i}$ means the setting of the facade in hour i. $\alpha_{in,n}$ is the angle of incidence for radiation coming from patch n. $g_{\text{eff-m},j}$ for month j is determined with

$$g_{\text{eff-m},\,j} \quad := \quad \frac{\sum_{i \in I}\sum_{n \in N} \ g_{\text{tot}}\big(\alpha_{s,n}, \gamma_{\text{f,n}}, \beta_{k,i}\big) \ \mathcal{L}_{n,i} \ \Delta\Omega_n \ \cos\big(\alpha_{in,n}\big)}{\sum_{i \in I}\sum_{n \in N} \ \mathcal{L}_{n,i} \ \Delta\Omega_n \ \cos\big(\alpha_{in,n}\big)} \tag{143}$$

$$\neq \quad \frac{1}{I}\sum_{i \in I} \ g_{\text{eff-h},\,i} \tag{144}$$

where I is the number of hours in the specified period.

6.2.4 Comparsion of two new systems with the state of the art on the basis of g_{eff}

Abstract The author has developed two new sun-shading systems together with two different companies. These systems are compared with state of the art products on the basis of the new general evaluation method for facades with venetian blinds or other solar control systems that has been prestented in detail in [10]. The main advantage is that the method can take into account realistic user behaviour (different utilisation modes). Without the new methodology, it would not have been possible to *recognise* the weaknesses of products which are currently on the market. This *recognition* was the basis for the design of the two new products:

- The new stainless steel blind s_enn$^{\circledR}$ selectively shields certain regions of the sky. This leads to a transparent appearance while direct insolation of the room and the associated glare is prevented in most cases.

- The special shape of the 'Genius slats' of a new venetian blind ensures good sun-shading properties which are relatively independent of the actual setting of the slats over broad ranges, which ensures robust performance despite so-called 'faulty operation'. In other words: The performance of the new venetian blind is relatively insensitive to different utilisation modes.
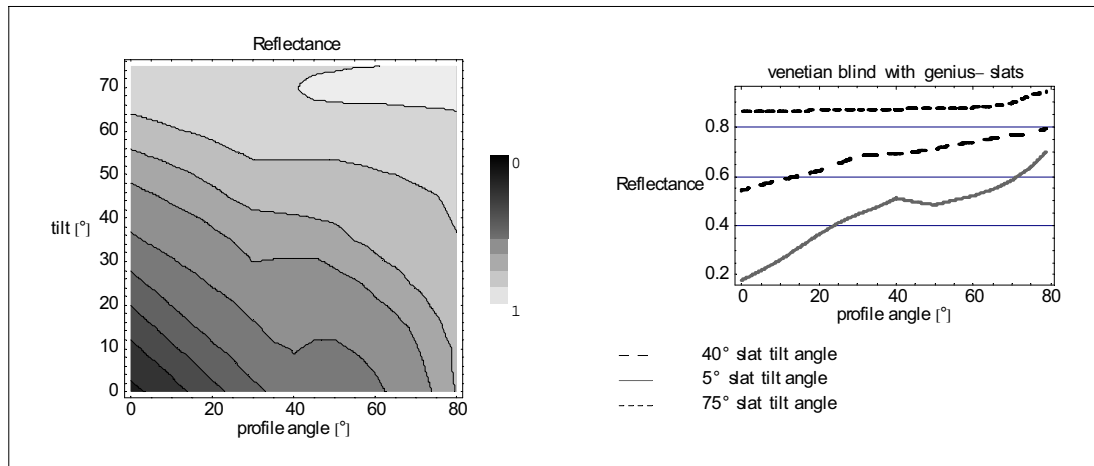
Figure 33: Reflectance of a venetian blind with 'Genius slats'.

Angle-dependent reflectance and transmittance of the new products The transmittance and the reflectance of the new 'Genius slats' from Hüppelux, Oldenburg, Germany are shown in figure (62) on page 137. The geometry of the slats was designed by Hans-Peter Baumann (from the company Baumann-Hüppe) together with the author of this paper. A patent claim has been filed for this blind. The distance between the slats is smaller than usual. The distance between the slats, the height of the ridge in the slat and the position of the ridge is optimised such that the direct sun hits only the outer flank of the ridge in most cases, which leads to a high reflectance also in the case of partly opened slats (figure 33). This is essential in order to ensure that the performance of the venetian blind is robust against so-called 'faulty operation'. The reflectance of a daylighting venetian blind - with concave slats with a mirror-finished top surface - depends strongly on the tilt angle of the slats (see figure 34) which leads to a very different performance. This state of the art product is the classic example for a blind with performance that is *not* robust against faulty operation. It requires automatic control, when good solar protection has to be ensured.

The other new system is the new stainless steel blind s_enn®. (see figure 37). I designed the key element - the profile of the section - for the company clauss markisen, Bissingen-Ochsenwang, Germany. The lower end of the outer surface is a sharp edge which cuts out the direct sun without generating possibly glary bright stripes on the inner surface of the blind. In this way,
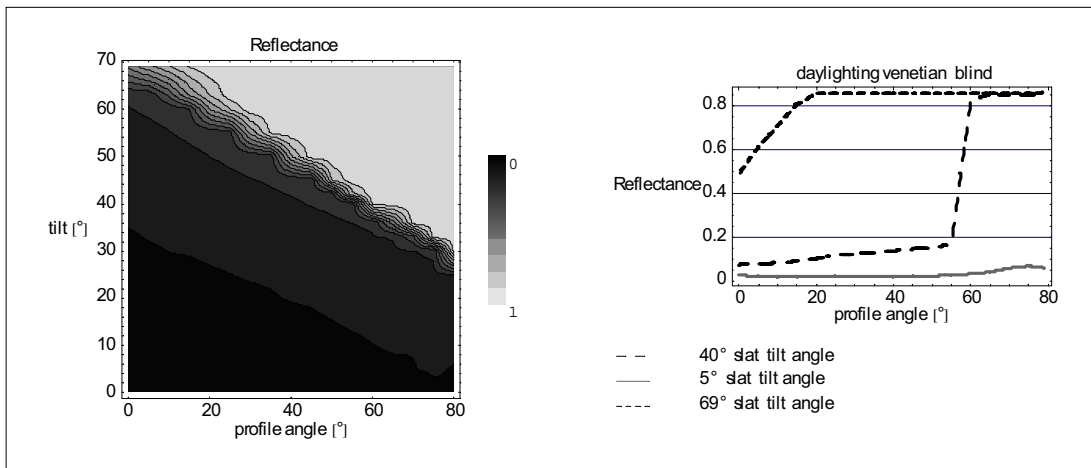
Figure 34: Reflectance of a daylighting venetian blind. The reflectance depends strongly on the tilt angle of the slats.
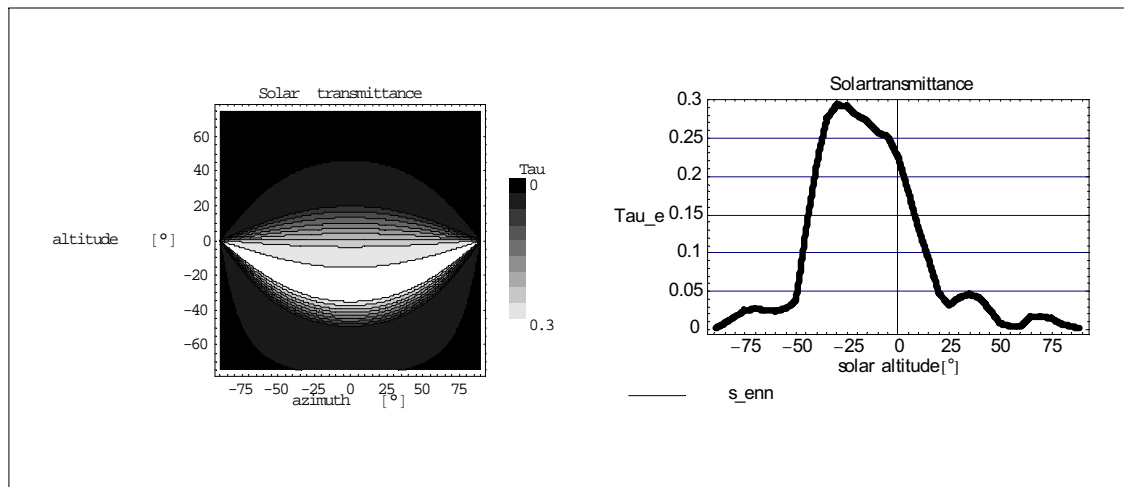
Figure 35: Solar transmittance of the stainless steel blind s_enn®. $\gamma_\mathrm{f} = 0°$ in the figure on the right hand side.

the profile selectively shields certain areas of the sky which leads to a transparent appearance while direct irradiation of the room is prevented in most cases. The compact profile with its many edges can withstand significantly higher wind loads than conventional venetian blinds or roller blinds. A test in the wind channel of the I.F.I. Institute for Industrial Aerodynamics in Aachen, Germany demonstrated this: A conventional external roller blind could be used without problems up to a wind speed of 29 km/h and an external venetian blind up to 40 km/h. s_enn® could still be used without problems at the speed of 65 km/h which is the maximum wind speed of this wind channel. A patent claim has been filed for this blind. Figure 35 shows the angle-dependent transmittance of s_enn®. s_enn® was awarded an innovation prize at the 2003 R+T Trade fair in Stuttgart, Germany which is the most important international trade fair for sun-shading systems. In March 2004 s_enn® was awarded the Bavarian State Prize at the 56th International Handicraft Fair in Munich, Germany. In November 2004 s_enn® was awarded the Innovationprice for small and medium-sized enterprises of the banks "Volksbanken" and "Raiffeisenbanken".

Determination of control strategies as a basis for performance assessment   Before the performance of a facade can be assessed, the probable usage of the facade has to be

Figure 36: The new stainless steel blind s_enn®. The man is outside, behind the blind. Picture: ©Clauss Markisen.

defined. It is very important to have realistic ideas about the requirements of the users that affect the desired setting [8]. One cannot avoid the discussion about a realistic setting, although nobody is able to predict the behaviour and the preferences of the future users. Since we need to minimise planning risks and since we do not know *exactly* how the facade will be used, the only possibility is to make sure that the facade together with the building provides good thermal and visual comfort for different utilisation modes. This seems to be an obvious statement which can be taken into account easily. However, this leads directly to the very difficult definition of a borderline between 'correct' and 'faulty' operation. Different opinions about the position of this borderline are very often the reason for legal disputes between a building owner/user and the planning team. A good system has to provide good thermal and visual comfort when it is 'used correctly' and it must not create severe problems when it is 'mis-used'. In this context 'used correctly' means 'used as planned'. 'Mis-used' means 'used outside the planning specifications'.

From our experience at Fraunhofer ISE, we conclude that view retention and protection against direct irradiation are both very important and that most people are not willing to close roller blinds completely, and that people also do not like to fully extend and close venetian blinds. Many people do not accept venetian blinds with completely closed slats, because the partly closed position provides better contact with the exterior and higher indoor illuminance levels. We were involved in the planning of several high-rise office buildings where we used the following control strategies for venetian blinds as the basis for the performance assessment [kuhn,2000]:

- Strategy 'closed' (best case): The facade is in the mode which provides the best possible solar protection. In the case of venetian or roller blinds, this means that the blind is fully
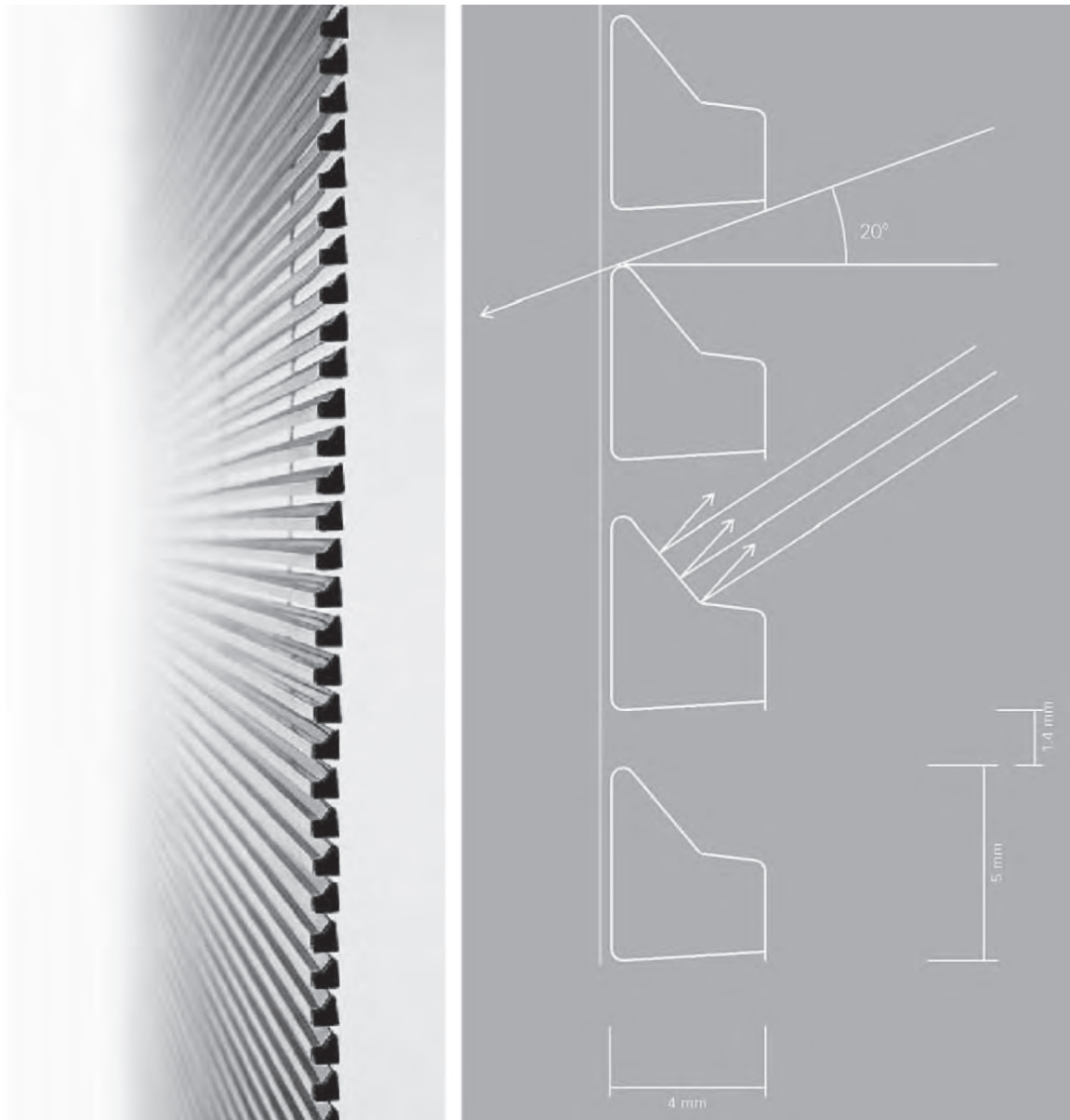
Figure 37: The key element of the new stainless steel blind s_enn® - the profile of the section - was designed by the author for the company clauss markisen, Bissingen-Ochsenwang, Germany. Picture ©Clauss Markisen.

extended and the slats of venetian blinds are completely closed, whenever the facade is irradiated directly by the sun. The blind is fully retracted, when the facade is in the shade or when there is no direct illumination. For a given combination of blind and glazing, this control strategy maximises the overheating protection and glare protection when the sun hits the facade directly. In the case of opaque systems, this control strategy ignores the need for visual contact to the exterior. The dimensions of the room and the windows will determine whether the supply of daylight is sufficient or not.

- Strategy 'cut-off' (worst case without faulty operation): This is the borderline between correct operation and faulty operation.
  In the case of internal or external venetian blinds and internal vertical blinds, the blind is fully retracted when the facade is in the shade or when there is no direct illumination. When the sun is shining directly on the facade, the blind is fully extended but the the slats are tilted into the cut-off-position. The 'cut-off' slat position depends on the actual position of the sun. In this position, the slats are opened as far as possible without letting the sun shine directly through the blind. For the cut-off strategy, the tilt angle of the slats is determined by the profile angle of the sun. This control strategy ensures at least some overheating protection. The visual contact to the exterior between the opened slats is an advantage, at least for higher positions of the sun. Because the room is protected against direct irradiation, the strategy ensures that there are not any disturbingly bright, directly lit stripes on desks or workbenches. The dimensions of the room and the windows will determine whether the supply of daylight is sufficient or not. This does not imply at all that an automatic adjustment of the slats is necessary. The user is free to close the slats more than cut-off, but overheating protection is not guaranteed, if the slats are opened further than cut-off. Especially in the case of tall buildings with fully glazed facades it can be questioned whether people will really accept complete extension of the blind. In such cases automatic control can help to minimise planning risks. An idea is to control the extension of the blind automatically and to allow the user to set any desired tilt angle of the slats.

In the case of roller blinds, we did not find a general equivalent to the cut-off position of the slats of a venetian blind. One important difficulty that complicates the definition of a generally accepted border line between correct and faulty operation is the fact, that the transparency (or view retention) can be very different for different types of roller blinds. A basic approach could be to define that the roller blind only has to be extended to the position where the horizontal line of sight of a person sitting at a workplace is not obstructed. This control strategie could be a realistic choice, especially for roller blinds made from opaqe or translucent fabrics.
In the case of roller blinds made from mirror foils or switchable glazing, the visual contact with the exterior is probably sufficient for most people even in the state where the system provides maximum solar protection. For these systems, a realistic control strategy probably has to take into account whether the daylight supply in the room is sufficient or not.
Roller blinds made of translucent fabrics with holes are also transparent in principle, but the scattering properties of the fabric determine whether the view retention is sufficient or not when the sun is shining directly on the facade. The visual performance of these devices is therefore in between the extremes of non-transparent fabrics and non-diffusing mirror-foils or switchable glazing.

Assessment of the solar control performance - Analysis of the frequency distribution of $g_{\text{eff-h}}$ or $g_{\text{eff-m}}$ The large difference in the robustness of the performance of different internal venetian blinds is shown in chapter 6.2.4.

Chapter 6.2.4 contains an analysis of the monthly effective g-values for the example of the new external stainless steel blind s_enn®.

The relevance of the new method for building simulation is assessed in chapter 6.2.5.

Comparative analysis of the performance of different internal venetian blinds   The performance of a venetian blind with 80 mm wide 'Genius slats' and a gap of 43 mm between the slats was analysed on a summer day on the basis of equations (21) and (32) of [10]. Figure 38 shows g_{tot} and the solar irradiance on a day with high irradiation (June 21, in Freiburg, Germany, data from Test Reference Year 7 [50]). The black line shows $g_{\text{eff-h}}$ for the glazing without the blind. The medium grey line shows $g_{\text{eff-h}}$ for the cut-off control strategy. The light grey line shows $g_{\text{eff-h}}$ for closed slats. The bars indicate the irradiation that impinges on the outer surface of the facade. Solid black bars indicate direct irradiation, light grey bars show the corresponding global irradiation. The diffuse irradiation is the difference between global and direct irradiation. The figure illustrates the influence of the high solar altitude and diffuse irradiation on the effective g-value. Before 8:30 and after 17:30 there is no direct irradiation, the blind is retracted and $g_{\text{eff-h}}$ is almost constant for the diffusely irradiated glazing. When the direct irradiation hits the facade $g_{\text{eff-h}}$ is lowered because of the high angle of incidence of the direct irradiation. If, as discussed above, the cut-off position of the slats is taken as the design limit for the building, a g-value between 0.14 and 0.17 can be assumed for the time with direct irradiation at this day, a figure which is well below the glazing g-value of 0.31 for normally incident light. Of course it is impossible to analyse the actual design of a building over a period of just one day. The assessment is restricted to this one day for the sake of clarity. The figure also shows the strong dependence of the effective g-value on the control strategy.

Table 9 shows the frequency distribution of the number of hours with a certain hourly effective g-value $g_{\text{eff-h}}$ for a venetian blind with 'Genius slats' and a daylighting blind, mounted on the indoor side of a solar control glazing (g-value of the solar control glazing: $g_{\text{gzg}} = 0.31$, according to EN410). The analysed time span is June 21 - September 21. $g_{\text{eff-h}}$ has been calculated with equations (21) and (32) of [10]. We analysed only hours with direct irradiation and fully extended blinds. One can see from figure 39 and table 9, that internal venetian blinds can provide significant solar protection, when they are combined with solar control glazing. From the tabular representation, one can easily determine the maximum $g_{\text{eff-h}}$ for a certain combination of blind, glazing and facade orientation. The number of hours corresponding to this maximum $g_{\text{eff-h}}$ is directly linked to the importance of this value.

For the daylighting venetian blind with closed slats on a south oriented facade, for example, the maximum value of $g_{\text{eff-h}} = 0.17$ appears probably only during 1 hour within the time span [June 21 - September 21]. $g_{\text{eff-h}} = 0.16$ appears only during 7 hours. Both values are not very important for building planning, whereas $g_{\text{eff-h}} = 0.15$ is a very important performance criterion because it appears probably during 316 hours within the time span under consideration. Table 9 also shows that the performance of the daylighting venetian blind changes dramatically, when the slats are tilted into cut-off postion: Now the maximum effective g-value $g_{\text{eff-h}} = 0.27$ and there are more than 100 hours with $g_{\text{eff-h}} > 0.24$. For the new blind
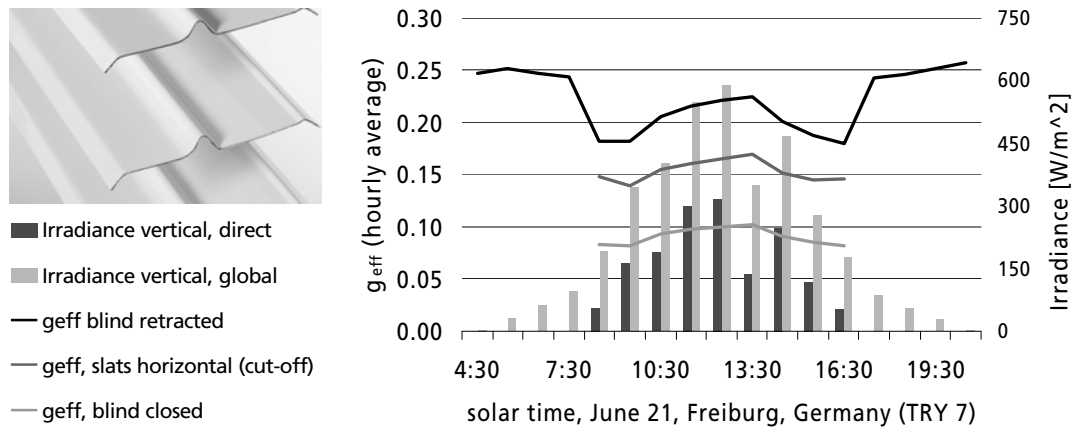
Figure 38: Hourly effective g-values $g_{\text{eff-h}}$ for an internal venetian blind with 'Genius slats' in combination with a solar control glazing ($g_{\text{gzg}} = 0.31$) on a south-oriented facade in Freiburg, Germany for a summer day. Solar irradiaton data where taken from the german test reference year 7 [50].

with genius-slats, the maximum effective g-value $g_{\text{eff-h}} = 0.21$ and the most probable effective g-value (390 h) is $g_{\text{eff-h}} = 0.20$.

The ability to protect the building from excessive solar gains depends strongly on the setting of the tilt angle of the slats for both blinds. Nevertheless, there is a large difference in the performance of these blinds: The effective g-value of the 'Genius slats' $g_{\text{eff-h}}$ changes continously and smoothly with variation of the tilt angle of the slats (see figure 40 and figure 42). $g_{\text{eff-h}}$ of the daylighting venetian blind is quite high for many tilt angles of the slats (see figure 41). Only when the slats are closed almost completely does the daylighting blind provide good solar protection. This behaviour had to be expected also from figure 34. In summary, one can say that figures 40 and 41 show the very different robustness of the blinds against different utilisation modes or so-called 'faulty operation'. It would be very risky in any case to plan a building on the assumption that the blinds are always closed. The risk would be much greater in the case of daylighting venetian blinds.

Performance analysis for the external stainless steel blind s_enn® The very good solar protection functionality of s_enn® is shown in the tables 10 and 11. In both cases, s_enn® is mounted outside of the double glazed unit. Meteorological data has been taken from test reference year 5 for Würzburg, Germany [50]. $g_{\text{eff-m}}$ has been calculated with equations (28) and (33). We analysed only hours with direct irradiation and fully extended blind. The effective g-values range from $g_{\text{eff-m}} = 0.05$ to $g_{\text{eff-m}} = 0.08$, whereas the g-value for direct

Comparison between internal blinds with mirror-finished and genius-slats
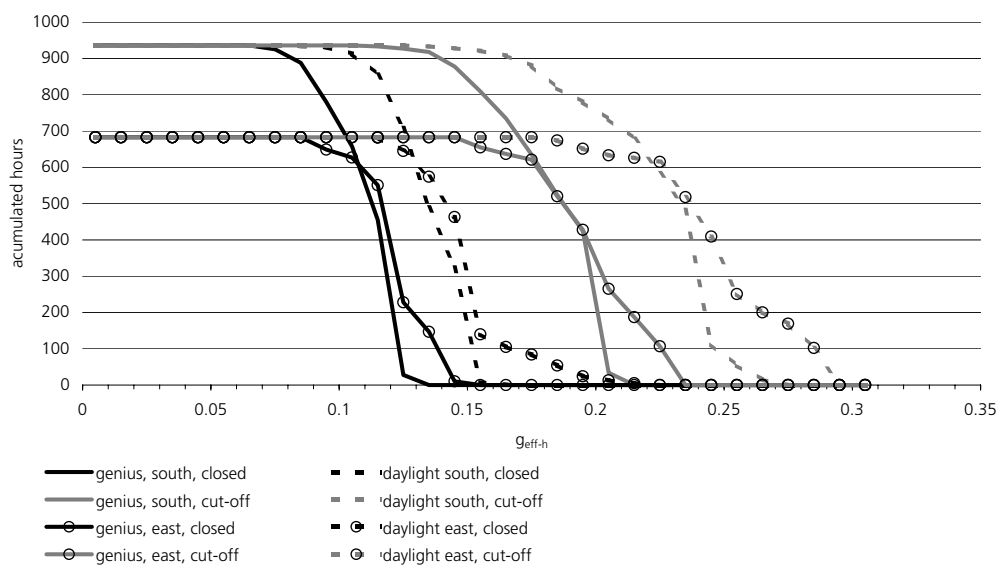
Figure 39: Cumulative number of hours with a certain hourly effective g-value $g_{\text{eff-h}}$ and above for two different internal blinds, combined with a solar-control glazing ($g_{\text{gzg}} = 0.31$). The analysed time span is June 21 - September 21. Solar irradiation data were taken from the German Test Reference Year 7 [50]. We analysed only hours with direct irradiation and fully extended blinds.

Table 9: Frequency distribution of the number of hours with a certain hourly effective g-value $g_{\text{eff-h}}$ for a venetian blind with 'Genius slats' and a daylighting blind, mounted on the indoor side of a solar-control glazing ($g_{\text{gzg}} = 0.31$ (according to EN410)). The analysed time span is June 21 - September 21. We analysed only hours with direct irradiation and fully extended blinds. In the first column of the table the *mean* values of $g_{\text{eff-h}}$ are given for each class.

$g_{\text{eff-h}}$	genius, south, closed	genius, south, cut-off	genius, east, closed	genius, east, cut-off	daylighting, south, closed	daylighting, south cut-off	daylighting, east, closed	daylighting, east, cut-off
0.055	0	0	0	0	0	0	0	0
0.065	11	0	0	0	0	0	0	0
0.075	37	0	0	0	2	0	0	0
0.085	108	0	34	0	3	0	0	0
0.095	122	0	22	0	18	0	0	0
0.105	203	3	76	0	57	0	1	0
0.115	427	6	323	0	147	0	37	0
0.125	28	9	81	0	219	3	71	0
0.135	0	40	137	0	166	5	111	0
0.145	0	69	10	28	316	7	323	0
0.155	0	74	0	18	7	13	35	0
0.165	0	100	0	16	1	28	21	0
0.175	0	111	0	101	0	62	30	9
0.185	0	100	0	92	0	38	30	23
0.195	0	390	0	163	0	47	11	18
0.205	0	34	0	78	0	54	8	7
0.215	0	0	0	80	0	95	5	11
0.225	0	0	0	107	0	101	0	97
0.235	0	0	0	0	0	371	0	109
0.245	0	0	0	0	0	58	0	158
0.255	0	0	0	0	0	39	0	51
0.265	0	0	0	0	0	15	0	31
0.275	0	0	0	0	0	0	0	67
0.285	0	0	0	0	0	0	0	102
0.295	0	0	0	0	0	0	0	0

Performance analysis of an internal venetian blind with ´Genius´ slats
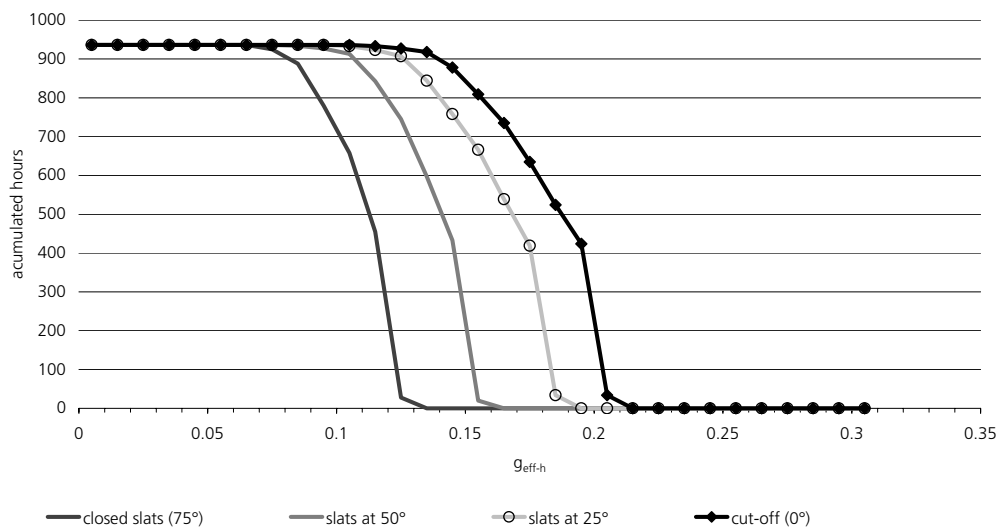
Figure 40: Cumulative number of hours with a certain hourly effective g-value $g_{\text{eff-h}}$ and above for an internal venetian blind with 'Genius slats', combined with a solar-control glazing ($g_{\text{gzg}} = 0.31$). The analysed time span is June 21 - September 21. Solar irradiation data were taken from the German Test Reference Year 7 [50]. We analysed only hours with direct irradiation and fully extended blinds.

Figure 41: Cumulative number of hours with a certain hourly effective g-value $g_{\text{eff-h}}$ and above for an internal daylighting blind, combined with a solar-control glazing ($g_{\text{gzg}} = 0.31$). The analysed time span is June 21 - September 21. Solar irradiaton data where taken from the german test reference year 7 [50]. We analysed only hours with direct irradiation and fully extended blind.
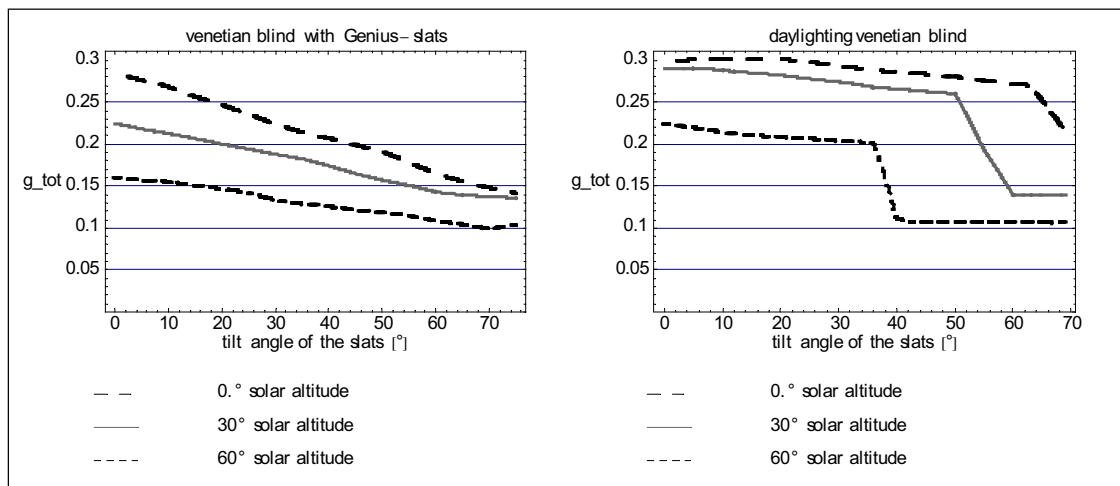
Figure 42: Comparison of the tilt-angle dependent total solar energy transmittance g_{tot} for two different internal blinds, combined with a solar-control glazing ($g_{\text{gzg}} = 0.31$). g_{tot} has been calculated with (21) of [10]. It can be seen, that small tilt-angle changes never cause drastic changes in g_{tot} in the case of the 'Genius slats'.

Table 10: Monthly effective g-values $g_{\text{eff-m}}$ for s_enn®, mounted outside a heat-mirror glazing ($g_{\text{gzg}} = 0.60$). We analysed only hours with direct irradiation and fully extended blinds. The direct sun does not hit the north oriented facade in winter, so no $g_{\text{eff-m}}$ has been caculated for these months.

	Jan	Feb	Mar	Apr	May	Jun	Jul	Aug	Sep	Oct	Nov	Dec	total
south	0.08	0.06	0.06	0.05	0.06	0.06	0.06	0.06	0.06	0.06	0.07	0.09	0.06
west	0.08	0.07	0.07	0.07	0.07	0.06	0.07	0.07	0.07	0.07	0.08	0.07	0.07
north	-	-	-	0.06	0.07	0.07	0.07	0.07	0.07	-	-	-	0.07

Table 11: Monthly effective g-values $g_{\text{eff-m}}$ for s_enn®, mounted outside a solar-control glazing ($g_{\text{gzg}} = 0.36$ (according to EN410)). We analysed only hours with direct irradiation and fully extended blinds. The direct sun does not hit the north oriented facade in winter, so no $g_{\text{eff-m}}$ has been caculated for these months.

	Jan	Feb	Mar	Apr	May	Jun	Jul	Aug	Sep	Oct	Nov	Dec	total
south	0.06	0.05	0.05	0.05	0.05	0.05	0.05	0.05	0.05	0.05	0.06	0.07	0.05
west	0.06	0.06	0.06	0.06	0.05	0.05	0.05	0.06	0.06	0.06	0.06	0.06	0.06
north	-	-	-	0.05	0.05	0.05	0.05	0.05	0.06	-	-	-	0.05

irradiation with normal incidence $g_{\text{tot}}(0°, 0°) = 0.17$. Only the more realistic effective g-values - that take into account realistic sun positions and diffuse irradiation - demonstrate the very good performance of s_enn®.

6.2.5 Relevance for thermal building simulation

Real angular dependence or symmetry with respect to α_{in}? It is common practice for building energy simulations with TRNSYS [117], ESP-r [53], DOE-2 [56] or TAS [118] to model external blinds by globally reducing the irradiation or to model them as additional glass panes and to make the assumption that $\mathcal{A}(\alpha_{in}) \approx \mathcal{A}(\alpha_s = \alpha_{in}, \gamma_f = 0°)$, where $\mathcal{A}$ stands for τ_{bld} or ρ_{bld}. This means, that the angle-dependent properties are treated, as if they where rotationally symmetric. This approach will be called α_{in}-symmetry in the following text. Currently there are efforts made to use bi-directional (BSDF) data as input for the LBNL-WINDOWS program [131] and also the building simulation programm EnergyPlus [57]. BSDF data helps to overcome the issues of angular dependency but huge datasets are needed and most of the Goniometers are not able to measure spectral polarised BSDF-data. The present approach is an intermediate way which is very accurate and does not need huge input data sets. It is based on the assumption that $\mathcal{A}(\alpha_s, \gamma_f) \doteq \mathcal{A}(\alpha_p(\alpha_s, \gamma_f), \gamma_f = 0°)$ [10]. This approach will be called 'α_p-symmetry' in the following text. The difference between α_p- and α_{in}-symmetry is shown in figure 4 on page 5. The first order approximation in the more realistic α_p-symmetry approach is to neglect that the reflectance on the surface of one individual slat depends on the angle of incidence, but to take into account the real geometry of the slats. It is shown in [10] that only α_p-symmetry leads to suffiently accurate results for the angle-dependent g_{tot}-values. It was shown that the assumption of rotationally symmetric proterties is very inaccurate in the case of venetian blinds or vertical blinds, it might be sufficiently accurate for roller blinds. External venetian blinds are frequently used in Germany, Switzerland and
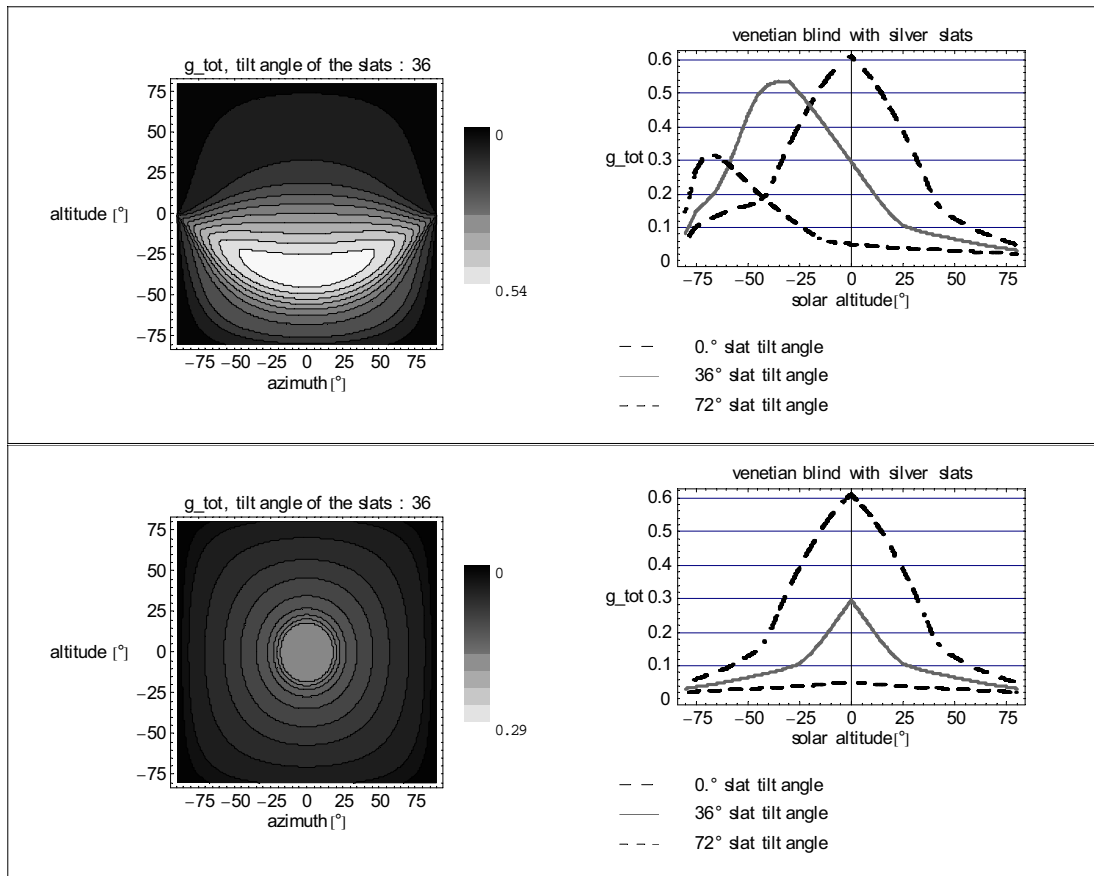
Figure 43: Total solar energy transmittance g_{tot} for an external venetian blind with slver/grey slats, combined with a heat-mirror glazing ($g_{gzg} = 0.60$). The lower graphs show g_{tot} under the inaccurate assumption of α_{in}-symmetry, the upper graphs are valid for α_p-symmetry. The graphs on the right hand side provide a cross section with an azimuth $\gamma_f = 0°$.

Austria. The different g_{tot} for α_{in}-symmetry and for real angular dependence (α_p-symmetry) are illustrated in figure 43 for the case of a venetian blind, mounted externally in front of a heat-mirror glazing with $g_{gzg} = 0.60$. The top surface of the convex (conventionally shaped) slats is matt silver ($\rho_{e,tot} = 0.59$), the bottom is light grey ($\rho_{e,tot} = 0.58$). g_{tot} has been calculated with formula (28) of [10]. For the accuracy of g_{tot} see table 6 of [10]. The diffuse properties of this blind without glazing are shown in figure 10 in [10].

The effect of the different symmetry assumptions on the solar gains of buildings has been quantified with the calculation of the monthly effective g-values g_{eff-m}.

External blinds

g_{eff-m} has been calculated with formula (33) for the above mentioned external venetian blind with silver/grey slats in combination with the heat-mirror glazing with $g_{gzg} = 0.60$. We analysed only hours with direct irradiation and fully extended blinds. The results are given in table 12. The relative difference between the results for real angular dependence (α_p-symmetry) and for incorrect rotationally symmetric blind properties (α_{in}-symmetry) is, in case of south

oriented facades, between 35% and 104%! For east oriented facades, the relative difference is between 21% and 52%. This means that the inaccurate α_{in}-symmetry approach significantly underestimates the solar gains for external blinds. This can certainly be significant for the thermal building performance - especially if there are large glazed areas - and should therefore be taken into account in thermal building simulations. This could be done by incorporating equations (28), (29) and (30) of [10] into the thermal building simulation programs.

Table 12: Monthly effective g-values $g_{\text{eff-m}}$ for an external sliver/light grey venetian blind in combination with a heat-mirror glazing with $g_{\text{gzg}} = 0.60$. We analysed only hours with direct irradiation and fully extended blinds. g-values are given with three digits in order to allow a relative comparison. The absolute value of the third digit is not significant.

slats	orientation	symmetry	June	July	Aug.	Sept.
0°	south	α_{in}	0.148	0.147	0.154	0.155
0°	south	α_p	0.206	0.202	0.209	0.209
		rel. difference:	40%	38%	36%	35%
20°	south	α_{in}	0.093	0.093	0.098	0.099
20°	south	α_p	0.162	0.157	0.157	0.150
		rel. difference:	74%	69%	61%	52%
45°	south	α_{in}	0.050	0.050	0.053	0.054
45°	south	α_p	0.102	0.098	0.095	0.089
		rel. difference:	104%	95%	80%	63%
cut-off	south	α_{in}	0.148	0.147	0.154	0.155
cut-off	south	α_p	0.206	0.202	0.209	0.209
		rel. difference:	40%	38%	36%	35%
0°	east	α_{in}	0.253	0.244	0.266	0.258
0°	east	α_p	0.307	0.300	0.318	0.323
		rel. difference:	21%	23%	19%	25%
45°	east	α_{in}	0.067	0.066	0.070	0.071
45°	east	α_p	0.098	0.100	0.103	0.104
		rel. difference:	45%	52%	48%	47%
cut-off	east	α_{in}	0.144	0.145	0.138	0.130
cut-off	east	α_p	0.182	0.188	0.181	0.180
		rel. difference:	26%	29%	31%	38%

Internal blinds

In the different building simulation programs there are different methods for the treatment of internal shading devices. It is *not* common practice to treat internal shading devices as extra internal glass layer. But it was not clear, how to to provide a general expression for $g_{\text{tot}}[\alpha_s, \gamma_f, \beta_k]$ for arbitrary α_s, γ_f and β_k within the building simulation programm. This could be solved by by incorporating equations (21), (22) and (23) of [10] into the thermal building simulation programs. For the accuracy of these equations see table 3-5 of [10]. The effect of the different symmetries has been quantified for a venetian blind with 'Genius slats' mounted internally behind a solar-control glazing ($g_{\text{gzg}} = 0.31$). We analysed only hours with direct irradiation and fully extended blind. The results are given in table 13. The relative difference

between the results of $g_{\text{eff-m}}$ for α_p- and α_{in}-sxmmetry is, in the case of south oriented facades, between 5% and 9%. For east oriented facades, the relative difference is between 4% and 6%. This can also be significant for the thermal building performance in the case of large glazed areas.

Table 13: Monthly effective g-values $g_{\text{eff-m}}$ for an internal venetian blind with 'Genius slats' in combination with a solar-control glazing with $g_{\text{gzg}} = 0.31$. We analysed only hours with direct irradiation and fully extended blind. g-values are given with three digits in order to allow a relative comparison. The absolute value of the third digit is not significant. The slats are either in fixed position (0° (horizontal) or 20°) or in the cut-off position.

slats	orientation	symmetry	June	July	Aug.	Sept.
0°	south	α_{in}	0.152	0.156	0.167	0.176
0°	south	α_p	0.164	0.167	0.178	0.185
		rel. difference:	8%	7%	7%	5%
20°	south	α_{in}	0.139	0.143	0.154	0.163
20°	south	α_p	0.152	0.155	0.165	0.172
		rel. difference:	9%	8%	7%	6%
cut-off	south	α_{in}	0.152	0.156	0.167	0.176
cut-off	south	α_p	0.164	0.167	0.178	0.185
		rel. difference:	8%	7%	7%	5%
0°	east	α_{in}	0.204	0.198	0.203	0.200
0°	east	α_p	0.213	0.208	0.212	0.211
		rel. difference:	4%	5%	4%	5%
20°	east	α_{in}	0.185	0.180	0.183	0.182
20°	east	α_p	0.193	0.188	0.191	0.19
		rel. difference:	4%	4%	4%	4%
cut-off	east	α_{in}	0.197	0.192	0.193	0.191
cut-off	east	α_p	0.206	0.202	0.203	0.202
		rel. difference:	5%	5%	5%	6%

These results for the effective g-values $g_{\text{eff-m}}$ give the same order of magnitude for the difference between α_{in}- and α_p-symmetry as to be expected from the assessment of the difference for the diffuse-hemispherical transmittance in section 3.3 of [10]. We found therefore two proofs for the same fact. The calculation of g_{tot} is independent from the calculation of the diffuse properties in the case of external systems. In case of internal systems The influence of the diffuse properties of the blind on g_{tot} is only a second order effect. The results presented in tables 13 and 12 are therefore an independent second proof that correct treatment of the angular dependence of the g-value in building simulation is relevant and necessary.

Importance of different control strategies   It has been shown in chapter 6.2.4 that different control strategies for the tilt angle of the slats can cause large differences in g_{eff} in the case of internal venetian blinds. The relative difference between the control strategies 'cut-off' and 'closed' is approximately 60% for the 'Genius slats' and 70% for an internal

daylighting blind. This is a significant difference that has to be taken into account during building planning. Figure 42 also explaines this fact. We know from our work as expert witness in court cases that there are buildings with severe overheating problems, which are caused by building planners´ assumption that the slats of venetian blinds are always closed, which was not the case. It has been shown in [8] that the influence of the control strategy is even greater in the case of external venetian blinds. The relative difference can be much larger than 100%! For planning safety and reliability it is therefore essential to take realistic control strategies for solar control systems into account.

6.2.6   Conclusions on the use and modelling of g_{eff}

A new approach for the modelling of solar gains through facades has been presented. It is based on the modelling of g_{eff} and consists of two main parts:

- Determination of the angular dependent total solar energy transmittance (g-value) g_{tot}. The calculation of g_{tot} for arbitrary directions of the incident radiation $[\alpha_s, \gamma_f]$ and arbitrary switching conditions of the facade system can be based on a limited number of calorimetric measurements of g_{tot}. In the case of slatted blinds, the necessary input can be minimized by assuming that the optical properties of the blind (*not the properties of the facade*) follow α_p-symmetry.

- Calculation of effective monthly or hourly g-values $g_{\text{eff-m}}$ or $g_{\text{eff-h}}$. The solar-control performance of facades can be compared realistically on the basis of effective g-values ($g_{\text{eff-m}}$ or $g_{\text{eff-h}}$) and therefore independently from a specific building or a specific facade. $g_{\text{eff-m}}$ and $g_{\text{eff-h}}$ only depend on the location and the facade orientation. They take into account diffuse irradiation and can be used to evaluate different utilisation modes/user perferences. The values are therefore a reliable basis for product comparisons. They are especially designed for building owners that want to compare different products before a contract is awarded.

It has been shown that the new model is more accurate than other methods and that it is able to provide a general expression for $g_{\text{tot}}[\alpha_s, \gamma_f, \beta_k]$ for arbitrary α_s, γ_f and slat tilt angles β_k. The new formula for g_{tot} could be used to improve the formulas given in the European Standard EN13363 [62]. The new model could also be implemented in building simulation programs in order to improve the accuracy without the necessity of the determination of huge datasets of polarized angle dependent or BSDF data for the individual layers. It has been shown that the new model is more accurate than other methods and that it is able to provide a general expression for $g_{\text{tot}}[\alpha_s, \gamma_f, \beta_k]$ for arbitrary α_s, γ_f and β_k. One important conclusion from the comparison of different methods is, that the relative error in the solar thermal gains, calculated with building simulation programs, can be very large (up to 100%), especially for external venetian blinds. The new model could be implemented in building simulation programs in order to improve the accuracy and it could be used in product standards.

The effective - monthly average - g-values $g_{\text{eff-m}}$ and $g_{\text{eff-h}}$ can be calculated on the basis of the angle-dependent g_{tot} for different control strategies for the solar protection devices. The solar-control performance of different facades can be compared realistically on the basis of these

effective g-values. The analysis of the sensitivity of $g_{\text{eff-m}}$ or the frequency of the occurrence of $g_{\text{eff-h}}$ towards different control strategies can significantly improve planning safety, although the real behaviour of the future users is not known. This new approach has been used sucessfully for the planning of several high-rise office buildings in Germany, Switzerland and Austria. It would be of great help for building planning, when the acceptance of different control strategies would be assessed on a sound scientific basis in future work.

The practical experience with the approach led to insights which are the basis for the design of two new products. The performance of these new products has been evaluated with the new method and compared with state of the art products.

6.3   "Black-box model" as interface between calorimetric measurements and dynamic whole-building simulation models

General   The general idea is to create an interface for building simulation programs (e.g. [53], [56], [57] or [117]) which allows the properties of complex fenestration systems to be integrated without any modelling of the details within the building simulation program itself. The method has already been published in [13]. The reasons for the development of the "black-box model" was the following:

- There are always new facades which are too complex for the internal models which are included in the building simulation program itself. It is important for the success of new developments that the advantages of innovations can be demonstrated by building designers. The lack of an interface for these new products often slows down the market penetration of new daylighting and solar-control systems.

- In some cases, the thermal and optical properties of facades can not be described by models with sufficient accuracy. This is especially the case when the real component deviates significantly from the ideal design. An example could be a glazing unit with multiple integrated prismatic or light re-directing layers with imperfect edges and imperfect surface flatness of the light re-directing surfaces.

- Semi-empirical models have been developed for facades with venetian blinds which are able to describe the angle-dependent properties of the facade accurately, without needing too many (expensive) measurements [10]. However, to study the impact of such complex fenestration systems on overall building performance, it is necessary to integrate these models into a building simulation program.

Therefore a method was implemented in a whole building simulation program which requires only data which is measurable on the complete glazing unit. As input, the new method needs only the angle-dependent g-value/solar factor and solar transmittance of the total facade unit. If available, the solar reflectance ρ_e (for solar radiation incident on the outer surface of the facade unit) can also be used as input, which improves the accuracy of modelling the external surface temperature. It is important to notice that it is not always necessary to measure g, τ_e and ρ_e: in some cases these properties can be calculated with mathematical models, (for example, with the models given in [10] for the case of facades with venetian blinds).

The general idea of the model is to describe every complex fenestration system with a two-layer model. Each of the two virtual layers has an effective solar absorptance with the desired angular dependence. Between the two layers, there is a temperature-dependent thermal resistance. This idea is quite similar to the ideas behind the γ-model which was developed by Rosenfeld [107] for the correction of non-standard boundary conditions during calorimetric g-value measurements.

Description of the model

Input data The starting point of the model is a set of measured or externally calculated values. Each data set i is valid for different directions of the incident light and different settings of the control parameter β_k. The model needs the following input:

- g-value $g_\mathrm{tot}[\alpha_{s,\mathrm{i}}, \gamma_{\mathrm{f},\mathrm{i}}, \beta_{\mathrm{k},\mathrm{i}}]$ (mandatory). In addition to the g-value, it is necessary to specify the thermal boundary conditions (surface resistances R_e and R_i) which have been used for the determination of g_tot.

- U_tot-value (mandatory). The centre-of-glazing U-value of the total facade (i.e. glazing + blind) is required for the same thermal boundary conditions as the g-value.

- Solar transmittance $\tau_{\mathrm{e, tot}}[\alpha_{s,\mathrm{i}}, \gamma_{\mathrm{f},\mathrm{i}}, \beta_{\mathrm{k},\mathrm{i}}]$ (mandatory).

- Solar reflectance $\rho_{\mathrm{e, tot}}[\alpha_{s,\mathrm{i}}, \gamma_{\mathrm{f},\mathrm{i}}, \beta_{\mathrm{k},\mathrm{i}}]$. (Optional. Needed only for accurate modelling of the temperature of the external surface, not needed for the correct modelling of the solar gains and the internal surface temperature.)

Instructions for using the new interface in ESP-r and a description of the data format for the new interface can be found in [3].

The black-box model has also been implemented in the whole building simulation software TRNSYS by [86] in his PHD under the supervision of the author of this thesis.

Modelling of the centre-of-glazing U-value In general, the U-value of a facade depends on the difference between the exterior and the interior temperature and on the temperatures of the surfaces which exchange heat via thermal radiation heat transfer. The temperature difference is mainly responsible for the convection patterns. The radiative heat transfer can be approximated to be proportional to T_mean^3, where T_mean is the mean temperature of the facade component in K [55]. In most cases, the influence of the temperature difference is much smaller than the influence of the mean temperature of the sample. The influence of the temperature *difference* on the U-value is therefore neglected. The U-value of glazing typically increases with raising T_mean. It typically increases with rates between 0.3%/K and 1%/K. We therefore approximate the sample U-value with

$$U[T_\mathrm{mean}] = U[283\,K]\ \left(a_0 + a_1\,T_\mathrm{mean} + a_2\,T_\mathrm{mean}^2 + a_3\,T_\mathrm{mean}^3\right) \tag{145}$$

Therefore

$$R_{\mathrm{s}}[T_{\mathrm{mean}}] = U[T_{\mathrm{mean}}]^{-1} - R_{\mathrm{e}} - R_{\mathrm{i}} \tag{146}$$

Special case: Unknown temperature dependence of centre-of-glazing U-value

If the temperature dependence of the U-value for the centre of glazing is unknown, we use the following coefficients as an approximation (these are typical values for insulating glazing units with U-values around 1.2 $W/(m^2 K)$):

$$
\begin{aligned}
a_0 &= -0.8395 \\
a_1 &= 0.0065 \\
a_2 &= 0 \\
a_3 &= 0
\end{aligned}
\tag{147}
$$

Determination of the total solar absorptance $\alpha_{\mathbf{e,tot}}$ The total solar absorptance $\alpha_{\mathrm{e,tot}}$ is

$$\alpha_{\mathrm{e,tot}}[\alpha_{s,\mathrm{i}}, \gamma_{\mathrm{f,i}}, \beta_{\mathrm{k,i}}] = 1 - \tau_{\mathrm{e,tot}}[\alpha_{s,\mathrm{i}}, \gamma_{\mathrm{f,i}}, \beta_{\mathrm{k,i}}] - \rho_{\mathrm{e,tot}}[\alpha_{s,\mathrm{i}}, \gamma_{\mathrm{f,i}}, \beta_{\mathrm{k,i}}] \tag{148}$$

Special case: Unknown total reflectance

In many cases, the total solar reflectance $\rho_{\mathrm{e,tot}}$ for radiation coming from outside is not known (no calculated or measured values available). In these cases, the total reflectance $\rho_{\mathrm{e,tot}}$ is estimated to be the mean value between the maximum possible physically meaningful value and the minimum possible physically meaningful value (which is zero):

$$\rho_{\mathrm{e,tot}}[\alpha_{s,\mathrm{i}}, \gamma_{\mathrm{f,i}}, \beta_{\mathrm{k,i}}] \approx 0.5 \left(1 - \tau_{\mathrm{e,\ tot}}[\alpha_{s,\mathrm{i}}, \gamma_{\mathrm{f,i}}, \beta_{\mathrm{k,i}}]\right) \tag{149}$$

which means that in this case

$$\alpha_{\mathrm{e,tot}}[\alpha_{s,\mathrm{i}}, \gamma_{\mathrm{f,i}}, \beta_{\mathrm{k,i}}] \approx 0.5 \left(1 - \tau_{\mathrm{e,\ tot}}[\alpha_{s,\mathrm{i}}, \gamma_{\mathrm{f,i}}, \beta_{\mathrm{k,i}}]\right) \tag{150}$$

Calculation of the absorptance in the two virtual layers   The next step is the calculation of the absorptance in the two virtual layers. It is known (see e.g. [58]) that

$$
\begin{aligned}
q_{\mathrm{i,tot}}[\alpha_{s,\mathrm{i}}, \gamma_{\mathrm{f,i}}, \beta_{\mathrm{k,i}}] &:= g_{\mathrm{tot}}[\alpha_{s,\mathrm{i}}, \gamma_{\mathrm{f,i}}, \beta_{\mathrm{k,i}}] - \tau_{\mathrm{e,tot}}[\alpha_{s,\mathrm{i}}, \gamma_{\mathrm{f,i}}, \beta_{\mathrm{k,i}}] \\
&= \frac{R_{\mathrm{e}}^{\star}\, \alpha_{\mathrm{outer\ layer}} + \left(R_{\mathrm{e}}^{\star} + R_{\mathrm{s}}^{\star}[T_{\mathrm{mean}}^{\star}]\right)\, \alpha_{\mathrm{inner\ layer}}}{R_{\mathrm{e}}^{\star} + R_{\mathrm{s}}^{\star}[T_{\mathrm{mean}}^{\star}] + R_{\mathrm{i}}^{\star}}
\end{aligned}
\tag{151}
$$

where $T_{\mathrm{mean}}^{\star}$ is the mean sample temperature during the determination of the g-value. $R_{\mathrm{x}}^{\star}$ are the specific surface thermal resistance values which have been used for the g-value and

U-value determination. $\alpha_{\text{inner layer}}$ and $\alpha_{\text{outer layer}}$ are the virtual solar absorptance values in the inner and outer layer of the black box model. With

$$\alpha_{\text{e,tot}}[\alpha_{s,\text{i}}, \gamma_{\text{f,i}}, \beta_{\text{k,i}}] = \alpha_{\text{inner layer}}[\alpha_{s,\text{i}}, \gamma_{\text{f,i}}, \beta_{\text{k,i}}] + \alpha_{\text{outer layer}}[\alpha_{s,\text{i}}, \gamma_{\text{f,i}}, \beta_{\text{k,i}}] \tag{152}$$

we find

$$\alpha_{\text{inner layer}}[\alpha_{s,\text{i}}, \gamma_{\text{f,i}}, \beta_{\text{k,i}}] = \frac{q_{\text{i,tot}}[\alpha_{s,\text{i}}, \gamma_{\text{f,i}}, \beta_{\text{k,i}}]\left(R_{\text{e}}^{\star} + R_{\text{s}}^{\star}[T_{\text{mean}}^{\star}] + R_{\text{i}}^{\star}\right) - \alpha_{\text{e,tot}}[\alpha_{s,\text{i}}, \gamma_{\text{f,i}}, \beta_{\text{k,i}}]\, R_{\text{e}}^{\star}}{R_{\text{s}}^{\star}[T_{\text{mean}}^{\star}]}$$

$$\tag{153}$$

and

$$\alpha_{\text{outer layer}}[\alpha_{s,\text{i}}, \gamma_{\text{f,i}}, \beta_{\text{k,i}}] \quad =$$

$$\frac{\alpha_{\text{e,tot}}[\alpha_{s,\text{i}}, \gamma_{\text{f,i}}, \beta_{\text{k,i}}]\left(R_{\text{e}}^{\star} + R_{\text{s}}^{\star}[T_{\text{mean}}^{\star}]\right) - q_{\text{i,tot}}[\alpha_{s,\text{i}}, \gamma_{\text{f,i}}, \beta_{\text{k,i}}]\left(R_{\text{e}}^{\star} + R_{\text{s}}^{\star}[T_{\text{mean}}^{\star}] + R_{\text{i}}^{\star}\right)}{R_{\text{s}}^{\star}[T_{\text{mean}}^{\star}]} \tag{154}$$

Treatment of diffuse irradiation It is well known that the diffuse irradiation is very significant for the solar gains and that the angular dependence has to be considered for the calculation of the solar gains caused by diffuse irradiation [8]. In [8] and [10], the diffuse sky is divided into 145 discrete sky patches according to [120] and the ground is divided into 5 different rings with constant radiance. This procedure leads to very accurate modelling of the solar gains. This procedure could also be implemented in building simulation programs.

A simpler approach is to divide the diffuse irradiation into two components, one coming from the upper half of the hemisphere (in most cases above the horizon), the other being reflected from the ground (the lower half of the hemisphere). It is shown in section 6.3.2, for the case of venetian blinds, that it is necessary to treat these two components of the diffuse irradiation seperately, rather than assuming isotropic diffuse irradiation. This statement can also be proven heuristically for the case of an external venetian blind with matt silver slats without glazing: from the formulae given in [10], the solar transmittance for the upper half of the hemisphere can be deduced to be:

$$\mathcal{A}_{y,\text{dif upper hem.}} \quad \approx \quad b_0 \mathcal{A}_y[0] + 2 \sum_{k=1}^{6} b_k \mathcal{A}_y[15\,k] \tag{155}$$

$$
\begin{array}{llll}
b_0 & = & 0.1304 & \qquad b_4 = 0.0653 \\
b_1 & = & 0.1261 & \qquad b_5 = 0.0338 \\
b_2 & = & 0.1130 & \qquad b_6 = 0.0043 \\
b_3 & = & 0.0923 &
\end{array}
$$

where $\mathcal{A}_y[\alpha_p]$ is the solar transmittance $\tau_e[\alpha_p]$ as a function of the profile angle in this case. The formula is valid for all facade systems with properties which are symmetric with respect

Diffuse Transmittance for silver painted slats

Tau_dif

tilt angle of the slats [°]

— for upper hemisphere only
for lower hemisphere only
-- Total diffuse transmittance
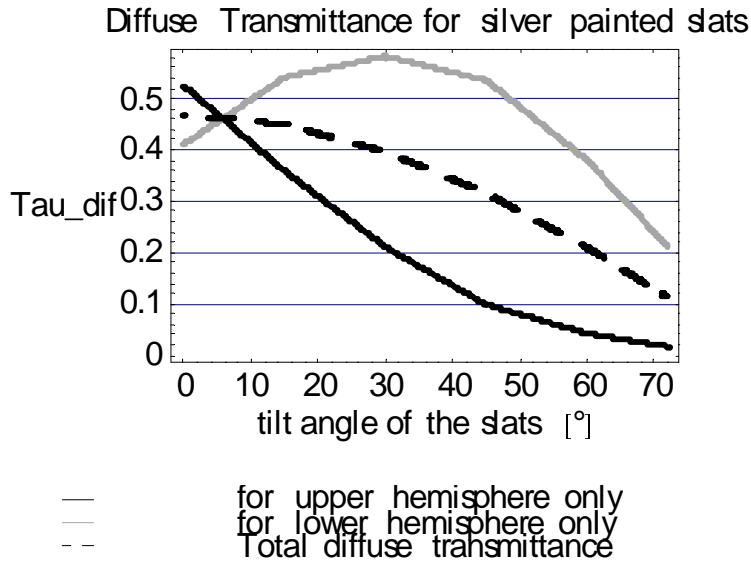
Figure 44: Diffuse transmittance for an external venetian blind with convex (conventionally shaped) slats without glazing. The top surface of the slats is matt silver ($\rho_{e,tot} = 0.59$), the bottom is light grey ($\rho_{e,tot} = 0.58$).

to profile angle. The diffuse properties for the lower half of the hemisphere can be calculated analogously:

$$\mathcal{A}_{y,\text{dif lower hem.}} \approx b_0 \mathcal{A}_y[0] + 2 \sum_{k=1}^{6} b_k \mathcal{A}_y[-15\ k] \tag{156}$$

In figure 44, the solar transmittance values for the upper and the lower halves of the hemisphere are shown for different tilt angles of the slats together with the total diffuse-hemispherical solar transmittance. It can be seen that the values for the upper half of the hemisphere are significantly lower than the values for the lower half of the hemisphere and the total values when the slats are tilted more than $10°$ against a horizontal plane.

General rules for the calculation of diffuse properties

In general, the diffuse-hemispherical properties of facade systems $\mathcal{A}_{y,\text{dif}}$ can be calculated in the co-ordinate system $[\alpha_s, \gamma_f]$ with equation (16) given in [10]:

$$\mathcal{A}_{y,\text{dif}} := \frac{1}{\pi} \int_{-\frac{\pi}{2}}^{\frac{\pi}{2}} \int_{-\frac{\pi}{2}}^{\frac{\pi}{2}} \mathcal{A}_y[\alpha_s \frac{\pi}{180}, \gamma_f \frac{\pi}{180}] \cos(\alpha_s)^2 \cos(\gamma_f)\ d\gamma_f\ d\alpha_s \tag{157}$$

where α_s and γ_f are expressed in degrees. Therefore

$$\mathcal{A}_{y,\text{dif lower hem.}} \quad := \quad \frac{2}{\pi} \int_{-\frac{\pi}{2}}^{0} \int_{-\frac{\pi}{2}}^{\frac{\pi}{2}} \mathcal{A}_y[\alpha_s \frac{\pi}{180}, \gamma_f \frac{\pi}{180}[\ \cos(\alpha_s)^2 \cos(\gamma_f) \ d\gamma_f \ d\alpha_s \tag{158}$$

and

$$\mathcal{A}_{y,\text{dif upper hem.}} \quad := \quad \frac{2}{\pi} \int_{0}^{\frac{\pi}{2}} \int_{-\frac{\pi}{2}}^{\frac{\pi}{2}} \mathcal{A}_y[\alpha_s \frac{\pi}{180}, \gamma_f \frac{\pi}{180}] \ \cos(\alpha_s)^2 \cos(\gamma_f) \ d\gamma_f \ d\alpha_s \tag{159}$$

Treatment of variable internal and external heat transfer coefficients The g-value varies according to the thermal boundary conditions, especially according to the heat transfer coefficients h_e and h_i. For example: the higher the wind speed, the higher is the external heat transfer coefficient h_e. This leads to more effective transfer of the absorbed energy $\alpha_{e,\text{tot}}$ to the outside and therefore results in a lower g-value.

This effect is taken into account in the new black box model since the values for the solar absorptances $\alpha_{\text{inner layer}}$ and $\alpha_{\text{outer layer}}$ in the virtual layers are fixed and since the building simulation program calculates R_e and R_i for every time-step according to the meteorological input data for the location under examination.

Treatment of thermal mass Two aspects of the thermal mass have to be taken into account in the black-box model:

- The total thermal mass

- The distribution of the thermal mass between the two virtual layers.

To assess the effect, the following cases have been compared:

- equal distribution of the typical thermal mass of a double-glazed unit ($6mm$ glass panes) between the two virtual layers in the black-box model.

- 96 % of the total mass of case 1 concentrated in the outer virtual layer.

- 96 % of the total mass of case 1 concentrated in the inner virtual layer.

The details of this evaluation are described in [68]. The results are the following: The average difference between the first case and last two cases was less than $0.05\,K$. It is therefore assumed that we can neglect this effect.

Treatment of back reflectance from the room   Since the black-box model uses effective absorptance values for each virtual layer, there is no change necessary in the building simulation programs for the internal treatment of back reflectance from the room. For the case of ESP-r, this means that the reflections from the room are correctly taken into account according to the descriptions in [116].

Examples   The angle-dependent properties of facades are the starting point for the calculation of the facade properties which are used as input for the black-box model (see section 6.3). The angle-dependent properties of facades can be either measured or calculated. For facades with venetian blinds, they can be calculated with the equations given in [10].

Examples: External blinds   As an example for external blinds, a venetian blind with convex matt silver slats is used. The near-normal-hemispherical solar reflectance of the surfaces of the slats is $\rho_{\text{e,n-h}} = 0.51$. The near-normal-diffuse solar reflectance of the surfaces of the slats is $\rho_{\text{e,n-dif}} = 0.47$. For the definition of the surface properties of the slats and the conditions for the reflectance measurements, see the European Standard EN14500 [1], to which the first author has contributed. The slats have additional small curved rims at the edges of the slats in order to increase their mechanical stability. Therefore the thickness of the slats is not negligible. This venetian blind (with small variations in the type of the matt silver colour of the slats) is the most common venetian blind in Germany, Switzerland and Austria. It has also been used for the assessments in [68]. In this example, the venetian blind has been combined with low-e glazing with $g_{\text{gzg}} = 0.58$, $\tau_{\text{e,gzg}} = 0.51$ and $\tau_{\text{v,gzg}} = 0.75$. The angle-dependent g-value and solar transmittance τ_e of this facade are shown in figures 45 and 46. They have been calculated with the equations given in [10]. The angle-dependent total solar absorptance has been calculated for the special case of unknown reflectance. The results are shown in figure 47. From the total absorptance, the solar absorptances in the two virtual layers have been calculated for the boundary conditions of $R_e = (23W/(m^2K))^{-1}$, $R_i = (8W/(m^2K))^{-1}$ and a U-value for the centre of glazing of $1.2\ W/(m^2K)$. $\alpha_{\text{inner layer}}$ and $\alpha_{\text{outer layer}}$ for the two virtual layers are shown in figures 48 and 49.

Figures 49 should be inserted here.

Examples: Internal blinds   The characterisation of facades with internal blinds has been discussed extensively in section 2.5.1. of [10] and in [11]. In this section, an internal Genius blind (for details see [11]) in combination with solar-control glazing with $g_{\text{gzg}}[0°] = 0.31$ is used as an example. The same combination has also been used in [11] and [68] as an example. Equations (21)-(24) from [10] were used for the calculation of the facade properties. The validation of these formulae is documented in table 4 and table 5 in [10]. The g-value g_{tot} and the solar transmittance $\tau_{\text{e,tot}}$ are shown in figures 51 and 50.

In addition to the formulae given in [10], a new formula for the calculation of the solar
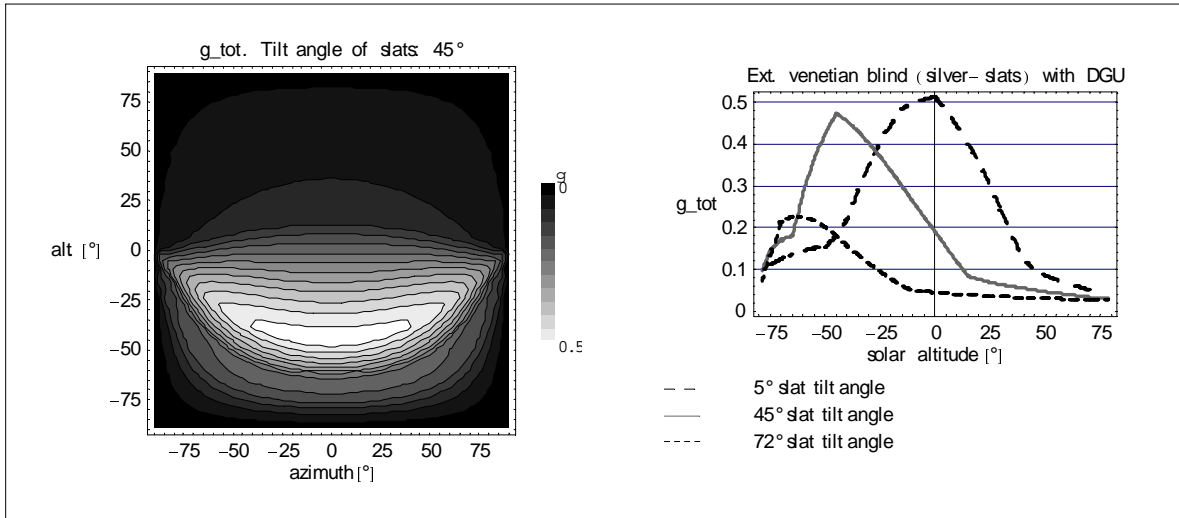
Figure 45: g-value for an external, matt silver venetian blind with convex (conventionally shaped) slats in combination with glazing with $g_{\mathrm{gzg}} = 0.58$. The line graphs on the right hand side are valid for $\gamma_f = 0$
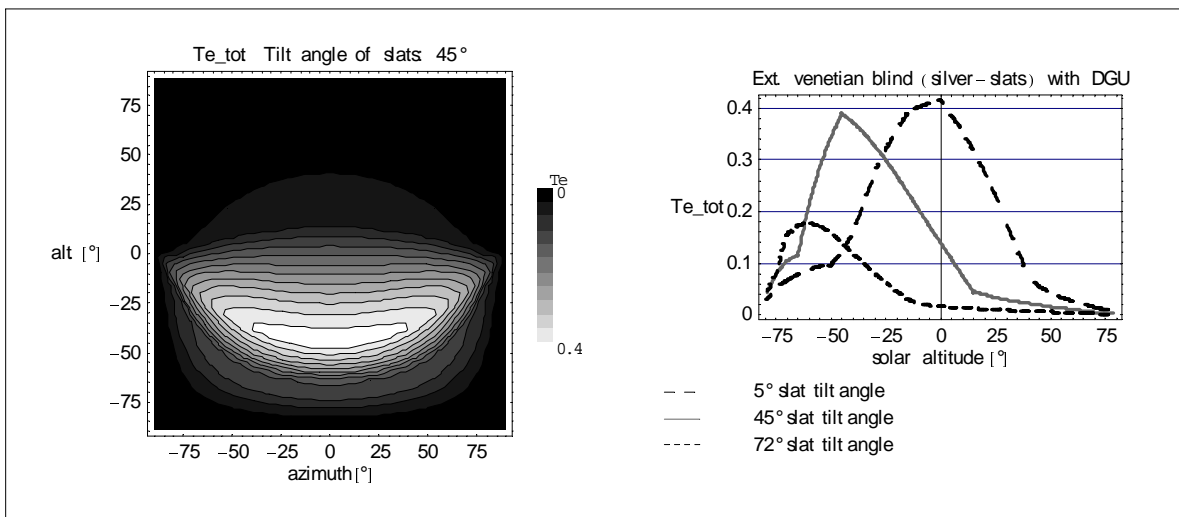

Figure 46: Solar transmittance τ_e for an external, matt silver venetian blind with convex (conventionally shaped) slats in combination with a glazing with $g_{\mathrm{gzg}} = 0.58$. The line graphs on the right hand side are valid for $\gamma_{\mathrm{f}} = 0$.
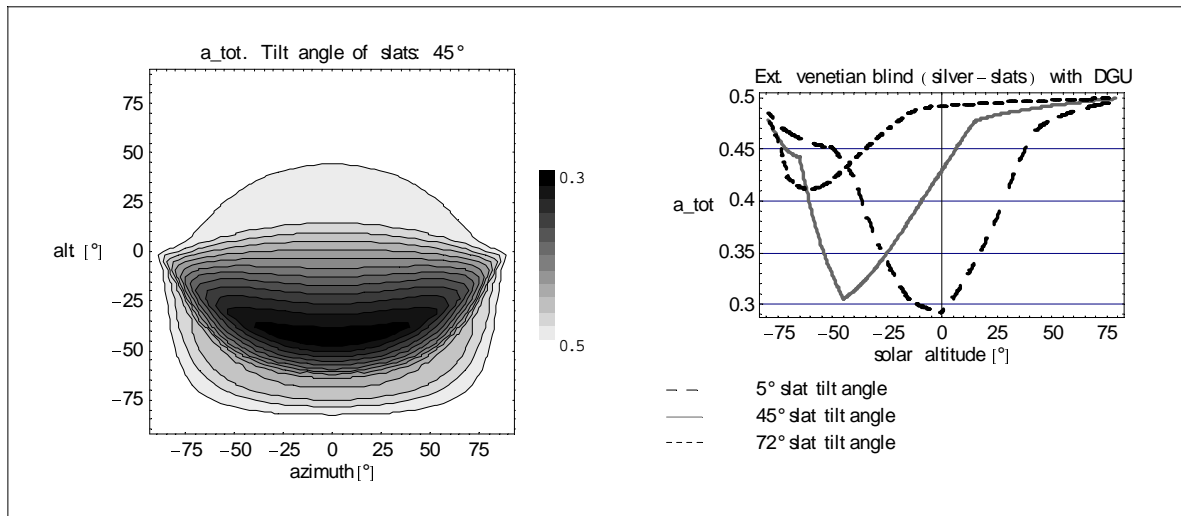
Figure 47: Angle-dependent total solar absorptance $\alpha_{e,tot}$ in the facade for an external, matt silver venetian blind with convex (conventionally shaped) slats in combination with glazing with $g_{gzg} = 0.58$. $\alpha_{e,tot}$ has been calculated for the special case of unknown reflectance $\rho_{e,tot}$. The line graphs on the right hand side are valid for $\gamma_f = 0$.
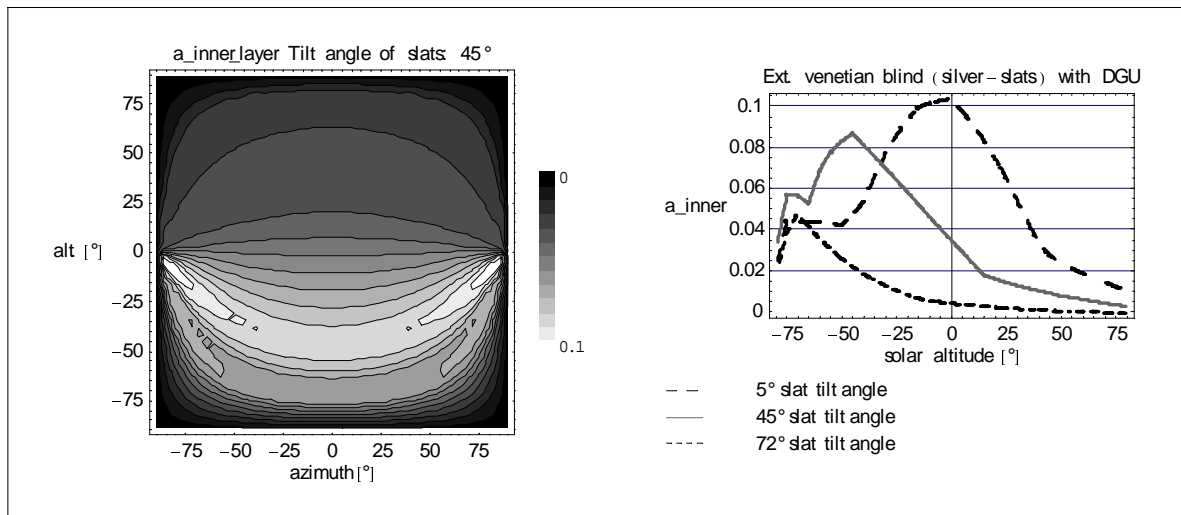
Figure 48: Angle-dependent solar absorptance $\alpha_{inner\ layer}$ in the facade for an external, matt silver venetian blind with convex (conventionally shaped) slats in combination with glazing with $g_{gzg} = 0.58$. $\alpha_{inner\ layer}$ has been calculated for the special case of unknown reflectance $\rho_{e,tot}$. The line graphs on the right hand side are valid for $\gamma_f = 0$.
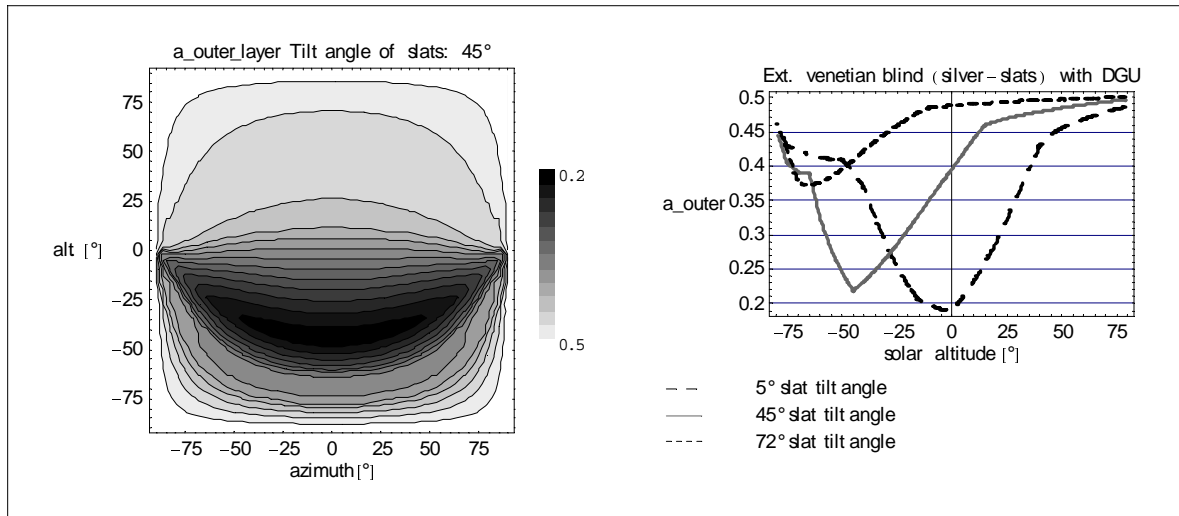
Figure 49: Angle-dependent solar absorptance $\alpha_{\text{outer layer}}$ in the facade for an external, matt silver venetian blind with convex (conventionally shaped) slats in combination with glazing with $g_{\text{gzg}} = 0.58$. $\alpha_{\text{outer layer}}$ has been calculated for the special case of unknown reflectance $\rho_{\text{e,tot}}$. The line graphs on the right hand side are valid for $\gamma_{\text{f}} = 0$.
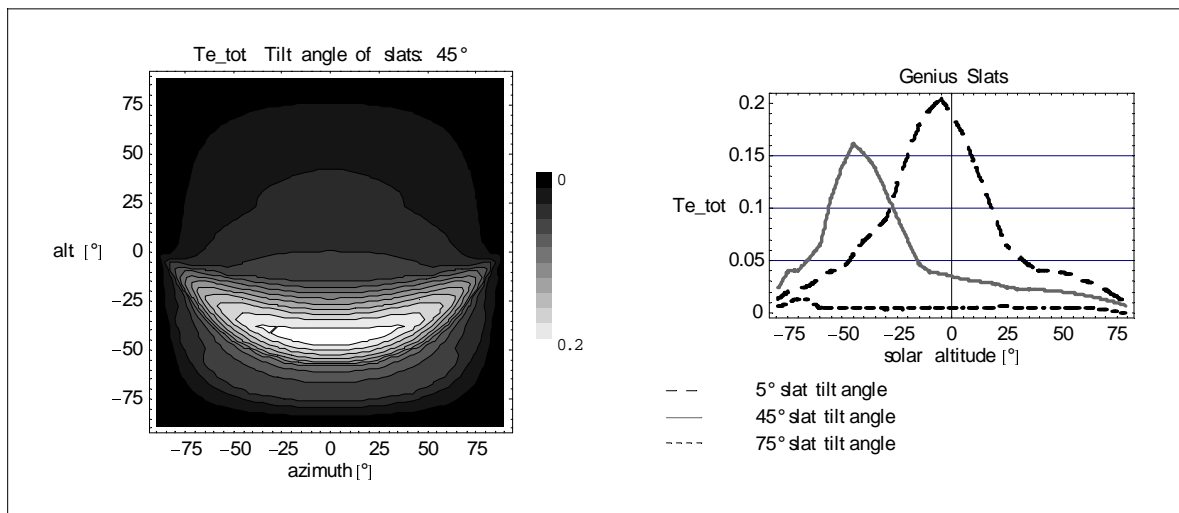

Figure 50: Solar transmittance τ_e for an internal venetian blind with Genius slats in combination with glazing with $g_{\text{gzg}} = 0.31$. The line graphs on the right hand side are valid for $\gamma_{\text{f}} = 0$.
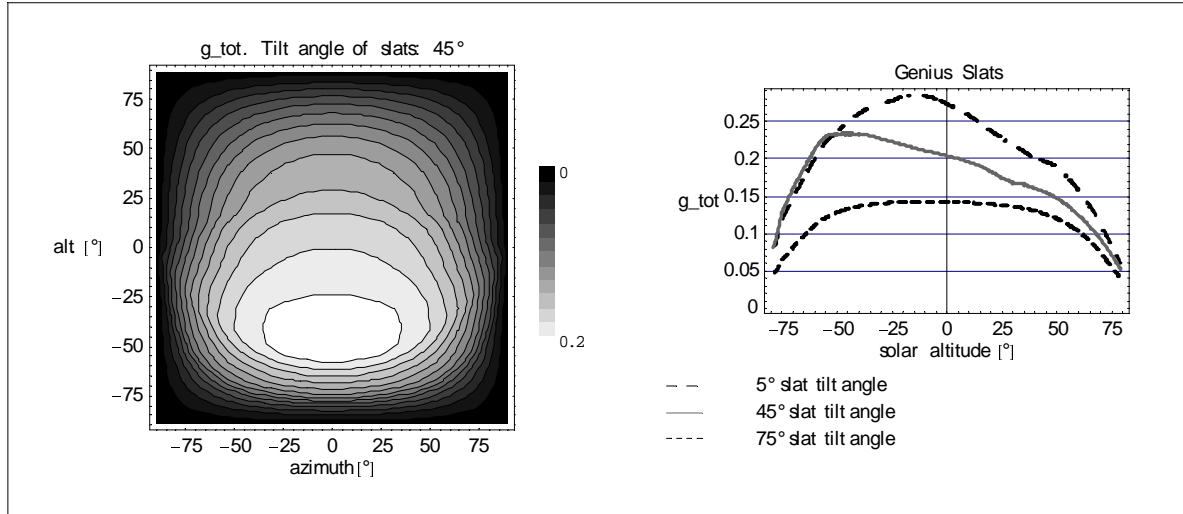
Figure 51: *g*-value for an internal venetian blind with Genius slats in combination with glazing with $g_{\mathrm{gzg}} = 0.31$. The line graphs on the right hand side are valid for $\gamma_f = 0$.

reflectance $\rho_{\mathrm{e,tot}}$ was used:

$$
\begin{aligned}
\rho_{\mathrm{e,tot}}[\alpha_s, \gamma_{\mathrm{f}}, \beta_{\mathrm{k}}] &= \rho_{\mathrm{e,gzg}}[\alpha_{in}[\alpha_s, \gamma_{\mathrm{f}}]] \\
&+ \tau_{\mathrm{e,gzg}}[\alpha_{in}[\alpha_s, \gamma_{\mathrm{f}}]] \ \tau_{x^\star,\mathrm{dif,gzg}} \ \frac{\rho_{x^\star,\mathrm{bld}}[\alpha_p[\alpha_s, \gamma_{\mathrm{f}}], \beta_{\mathrm{k}}]}{1 - \rho_{x^\star,\mathrm{dif,bld}}[\beta_{\mathrm{k}}] \ \rho'_{x^\star,\mathrm{dif,gzg}}}
\end{aligned}
\tag{160}
$$

The angle-dependent total solar absorptance was calculated for the case of known reflectance with equation 148. The results are shown in figure 52. It should be noted that the total solar absorptance decreases for the situations where the venetian blind has a high transmittance. This means that more light is being transmitted directly instead of being absorbed in the blind. The solar absorptance in the two virtual layers has been calculated from the total absorptance for the boundary conditions of $R_e = (23W/(m^2K))^{-1}$, $R_i = (8W/(m^2K))^{-1}$ and a U-value of the centre of glazing of the facade of 1.1 $W/(m^2K)$. $\alpha_{\mathrm{inner\ layer}}$ and $\alpha_{\mathrm{outer\ layer}}$ for the two virtual layers are shown in figure 53 and 54.

Figures 51 - 54 should be inserted here.

6.3.1   Implementation of the black-box model in ESP-r

Description of the implementation   The implementation is described in detail in [3].

Validation of the implementation   The correct implementation in ESP-r has been checked with a simple case that can be calculated correctly also with the existing models in ESP-r [68]. For this purpose, a double-glazed unit(DGU) with a low-e coating on the outer surface of the inner pane was chosen. Glazing properties: $g_{\mathrm{gzg}} = 0.58$, $\tau_{\mathrm{v,gzg}} = 0.75$ and
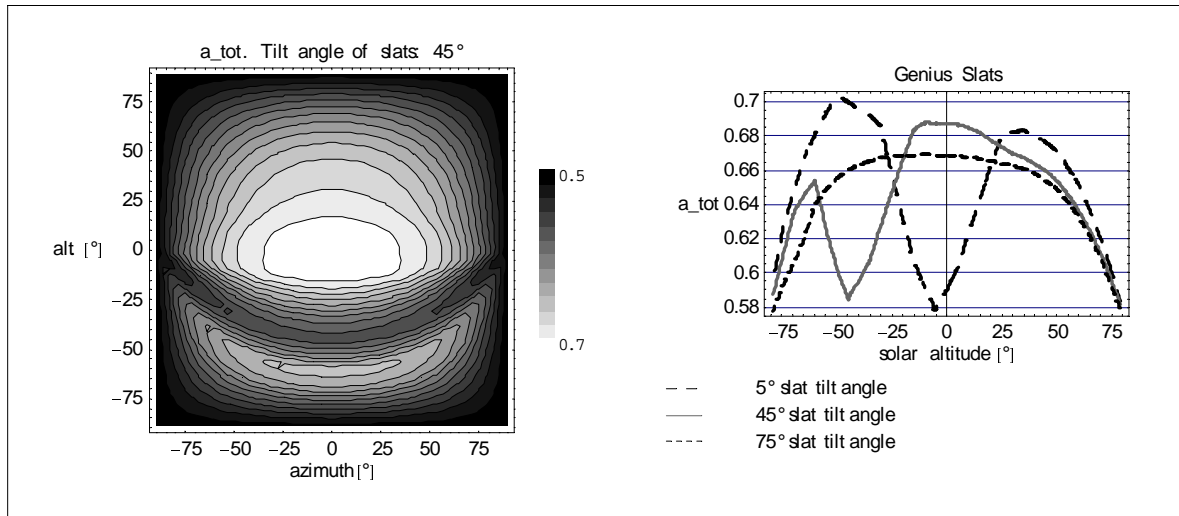
Figure 52: Angle-dependent total solar absorptance $\alpha_{\mathrm{e,tot}}$ in the facade for an internal venetian blind with Genius slats in combination with glazing with $g_{\mathrm{gzg}} = 0.31$. $\alpha_{\mathrm{e,tot}}$ has been calculated for the case of known reflectance $\rho_{\mathrm{e,tot}}$. The line graphs on the right hand side are valid for $\gamma_{\mathrm{f}} = 0$.
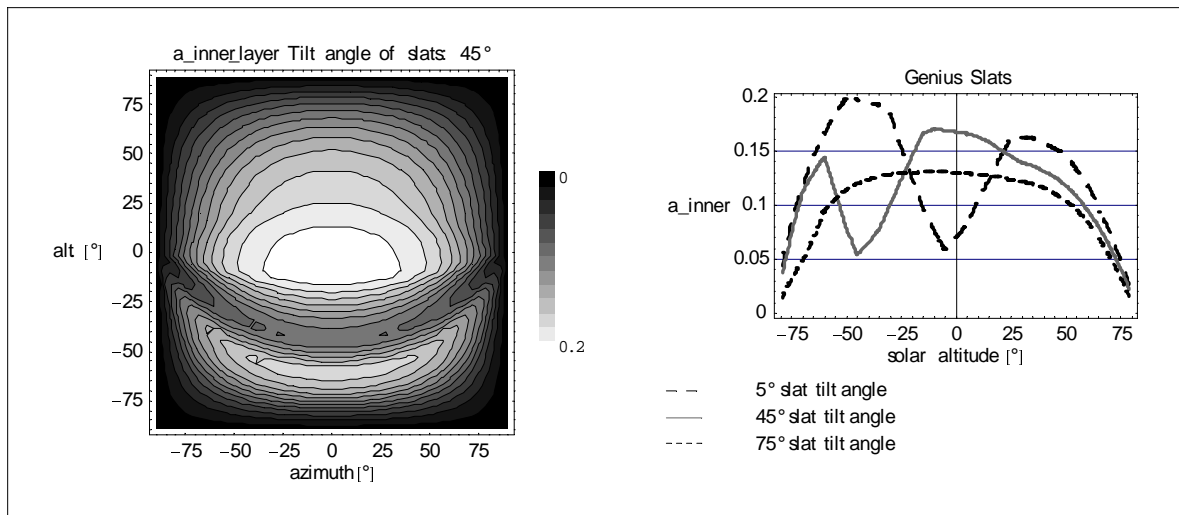

Figure 53: Angle-dependent solar absorptance $\alpha_{\mathrm{inner\ layer}}$ in the facade for an internal venetian blind with Genius slats in combination with glazing with $g_{\mathrm{gzg}} = 0.31$. $\alpha_{\mathrm{inner\ layer}}$ has been calculated for the case of known reflectance $\rho_{\mathrm{e,tot}}$. The line graphs on the right hand side are valid for $\gamma_{\mathrm{f}} = 0$.
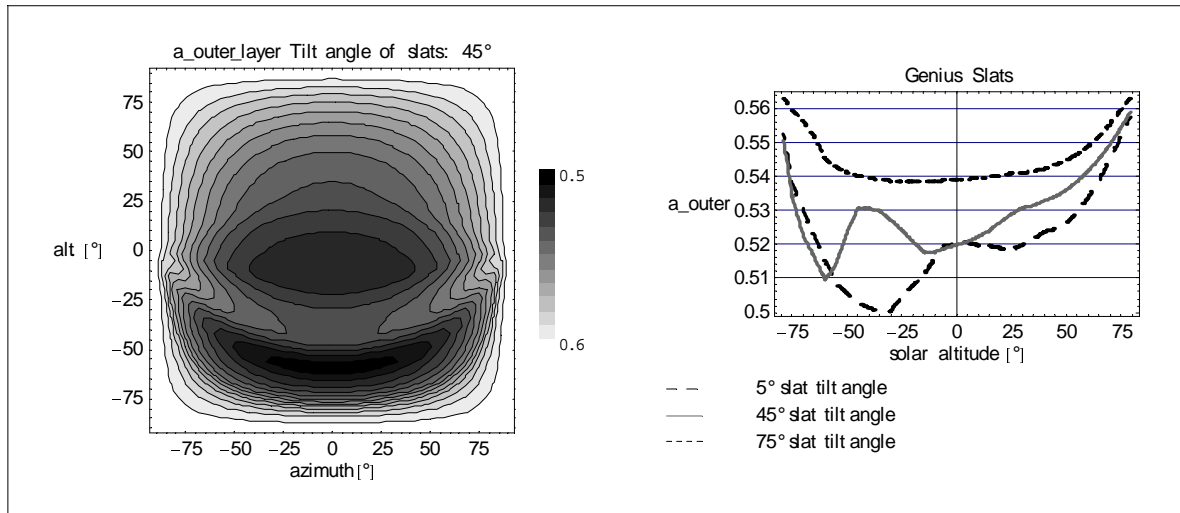
Figure 54: Angle-dependent solar absorptance $\alpha_{\text{outer layer}}$ in the facade for an internal venetian blind with Genius slats in combination with glazing with $g_{\text{gzg}} = 0.31$. $\alpha_{\text{outer layer}}$ has been calculated for the case of known reflectance $\rho_{\text{e,tot}}$. The line graphs on the right hand side are valid for $\gamma_f = 0$.

U-value $= 1.0 \ W/(m^2\,K)$. The results for the new black-box model and the existing model were practically identical: the average difference between the results for the operative temperatures of the two models was $0.09\,K$, the maximum difference was always less than $0.2\,K$ (for details see [68]). Other checks, for both isotropic and non-isotropic glazing, were also carried out to ensure that the calculations of the virtual layer absorptances and the sky and ground reflected diffuse transmittances and absorptances were calculated correctly. It was concluded that the model has been implemented correctly.

6.3.2   Assessment of the impact of the new model implemented in ESP-r

In [10] it was shown that the solar gains through facades can be incorrect when the wrong angular dependence of the g-value is used. In [10], the author specifically assessed the difference between the assumption of properties with profile angle symmetry and rotationally symmetric properties. However, the effect on the results of building simulations were not assessed in [10]. This has now been done using the new black-box model implemented in ESP-r. The details are given in [68]. In [68], the operative temperature, the heating loads and the cooling loads of an office-room were analysed for the two different cases of angular dependence. The different angular symmetries for g_{tot} are illustrated in detail in figure 12 of [10]. In [68] these effects were analysed for four different blinds (matt silver venetian blind, venetian blind with Genius slats, stainless steel blind and 'daylighting' venetian blind with mirror-finished top surface of the slats). We combined these venetian blinds with three different facade types (completely glazed (transparent area 90 %), large horizontal window (transparent area 35 %) and single window (transparent area 22 %). For the room model, a typical office configuration in the main building of Fraunhofer ISE was used. It has a medium-heavy construction consisting of light-weight internal walls but concrete floor, ceiling and external walls. The external walls

have a U-value of $U = 0.18\ W/(m^2 K)$. The real building uses passive cooling techniques: a special night-ventilation system without any mechanical cooling is used in this building. For the sake of simplicity and easy comparison with other buildings, the passive cooling was not taken into account. Only the cases with and without a mechanical cooling system were assessed. An evaluation of the real Fraunhofer ISE building can be found in [96]. An analysis was carried out with the building located in Freiburg (Germany), Stockholm (Sweden) and Milan (Italy) with facade orientations of south, south-west, and west. The intention was to quantify the impact of the black-box model and the use of the correct angular dependent facade properties for the case of a realistic building. More details are given in [68]. Only the main conclusions and results are given here. The main result is that **it is very important to use the correct angular dependence in building simulations:**

- For a fully glazed, south-facing facade in Freiburg, Germany with an external venetian blind with matt-silver slats, it was found that the wrong assumption of rotationally symmetric angular dependence leads to an **underestimation of the total summer cooling load by** 47% in the case of a mechanically cooled building. The underestimations of the total cooling load for the same building at the locations Milan and Stockholm are -55% and -99% respectively [68].

- For the same cases (but without a cooling system and with a west-facing instead of a south-facing facade), the assumption of the wrong rotationally symmetric properties leads to an **underestimation of the average temperature by more than** $2.5\ K$ **and an underestimation of the maximum temperature by up to** $5.2\ K$ [68].

- The heating energy demand is generally overestimated when the incorrect rotationally symmetric angular dependence is used. The relative overestimation of the heating demand for Freiburg, Milan and Stockholm is 17%, 23% and 20% respectively [68].

These results highlight the improvements that can be achieved with the new interface for ESP-r. The application of the new black-box model is by no means limited to venetian blinds. There are many other types of complex glazing on the market which can now be modelled accurately in ESP-r. The roof glazing of the German Museum ´Haus der Geschichte´ (which contains metallic light-redirecting structures in order to transmit only the diffuse irradiation from the northern part of the sky) can be considered as an example for this type. For other examples see section 6.3.

6.3.3   Summary - black box model

A new method for integrating complex fenestration systems in building simulation programs has been described in detail. The method is designed to be used for complex fenestration system components with non-trivial angular dependence. All these complex components can be treated in the same simple way:

- Measure $g_{\text{tot}}, \tau_{\text{e,tot}}$ and preferably also $\rho_{\text{e,tot}}$ for different directions of the incident radiation. If possible/applicable, the number of necessary measurements can be reduced

when the data points can be interpolated with a sufficiently accurate physical model.

- Create an input file with these data for ESP-r.

- Run the building simulations.

The method has been implemented in ESP-r and the implementation has been validated. It should be easy to implement the method in other detailed simulation programs such as [57], [56], [117] or [118]. It was shown that there are practically relevant cases in which the new method can help to significantly increase the accuracy of determining the heating and cooling loads and the room temperatures. It was shown that the error of conventional simulation techniques can be quite large (55 % underestimation of the cooling load in Milan is possible when the wrong angular dependence is used).

6.4 On the modelling of g and thermal comfort for transparent BIPV systems

Multifunctional transparent building integrated PV (BIPV) envelope components include the additional function to convert solar energy into solar electricity. The passive solar gains and the impact on the thermal comfort are not independent from the solar electricity yield. The passive solar gains and the temperature of the inner surface of the facade depend on the portion of the absorbed solar energy that is converted into electricity and which is therefore no longer available for the warming of the facade components. The efficiency of the PV-cells, the modules that consist of the PV-cells and the whole system strongly depends on the function of the inverter. The inverter not only converts the DC solar electricity into AC and feeds the electricity to the grid. The inverter also tries to select the maximum power point on the current-voltage-characteristic (I-V characteristic) for each module-string in order to maximize the output power. Each module string consists of serially connected PV modules plus optional bypass diodes for the minimization of the negative effects of partial shading, such as reduced electricity yield and overheating of shaded pv-cells (hot spots). Each module consists of one or more serially connected strings of PV-cells plus optional bypass diodes. In most cases there is only one string of PV-cells per module in order to increase the output voltage and to decrease the output current in order to minimize the resistive (ohmic) losses. The efficiency of the PV-cells is also depending on the temperature of the PV-cells which is determined by the irradiation conditions, the outside temperature, the wind conditions and in case of glazing integrated PV-cells also on the room temperature. This means that the boundary conditions, the individual irradiation condition on each PV-cell and the electrical set-up of the complete BIPV system including the inverter are determinant for the fraction of the absorbed radiation which is converted into electricity. A methodology for the electricity yield simulation with special focus on the simulation of complex BIPV systems has been developed under the guidance of the author of this document [115], [20]. An overview on the simulation methodology is given in figure 55. It is therefore now possible to evaluate the combined effects of passive solar gains and BIPV electricity yield generation dynamically, also in situations with complex partial shading patterns on the modules. Active facade system pay at least parts of the investment costs by themselves within the service lifetime or earlier.

It is therefore essential to refer to life cycle costs LCC (or total cost of ownership) [€/m^2] when comparing the costs of facade systems. The evaluation and modeling of LCC for BIPV systems is currently developed within the PHD thesis of K. Fath under the guidance of the author of this document. Firs results are published in [4].

typical weather data, including global direct and diffuse
irradiation, temperature and wind conditions

geometrical and optical
properties of the building
skin and the sourroundings

calculation of the sky radiance distribution

calculation of the absorbed radiation in each individual cell
by ray-tracing including shading and reflected radiation
from the surroundings and the ground

calculation of the temperature of the PV cells

electrical set-up of the complete
System including cells, modules,
bypass diodes and inverter

calculation of the cell I-V characteristics including
dark-current properties

calculation of the system I-V characteristics
including dark-current properties

MPP tracking and inverter modelling

cell operation points

electricity yield for the time step under consideration

Figure 55: Overview on the iterative calculation procedure for each time step within the model for electricity yield simulation of complex BIPV systems developed by Sprenger et. al. [115], [20] under the guidance of the author of this document.

6.5 On the modelling of g and thermal comfort for transparent building integrated solar thermal collector systems

Solar thermal collectors can extract heat efficiently from the building skin. They therefore have a significant impact on both, the temperature of the facade element and the energy balance of the room with such facade elements. It is therefore essential to further develop building simulation programs to create tools for the modeling of the secondary heat gains of facades with integrated solar collectors in addition to methods for the building independent product characterization. The secondary inward flowing fraction strongly depends on the temperature of the absorber of the collector. The temperature of the absorber is determined by the inlet temperature T_{in} and the flow rate $\dot{q}$ in addition to the boundary temperatures and
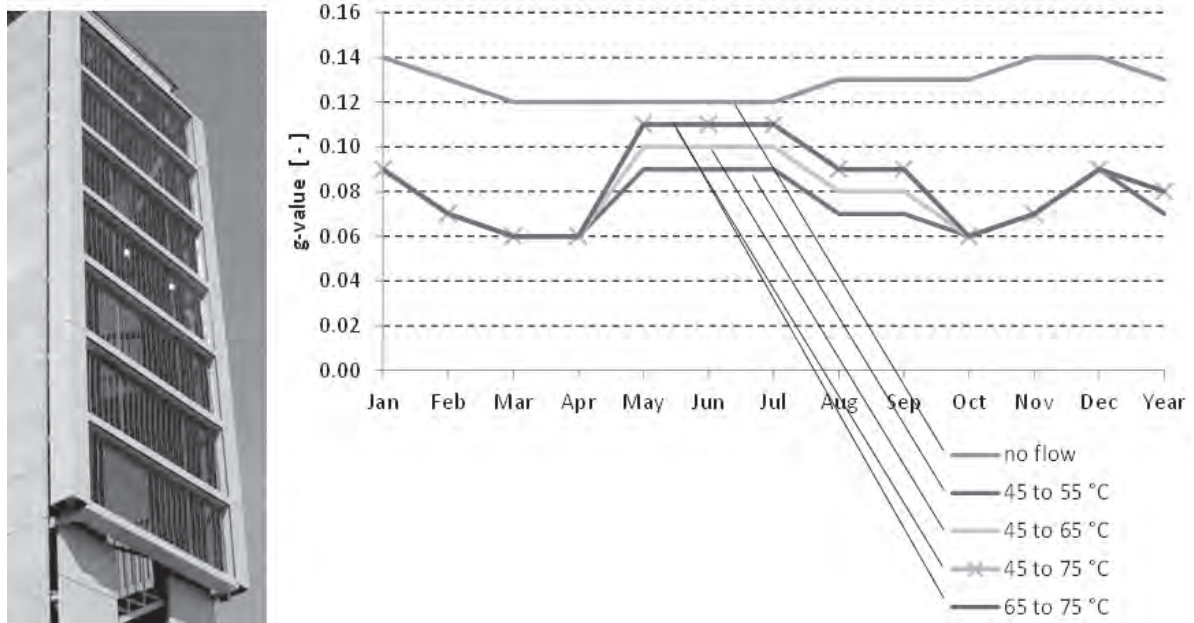
Figure 56: Monthly average g-value of the transparent solar thermal collectors shown in figures 69 and 68. The g-value of the facade collectors depends on the operation mode of the collectors. The maximum solar gains (no flow) are achieved when no heat is extracted from the absorber (stagnation conditions). The minimum solar gains are achieved when the collector is used for low-temperature solar heating (45°) in winter and desiccant de-humidification (55°) in summer [17].

the irradiation-level. g therefore becomes a function of these two parameters $g = f(T_{in}, \dot{q})$. Ch. Maurer has developed such methodologies within the framework of his Ph.D. thesis [86] in the European research project Cost-Effective under the guidance of the author of this thesis. The theoretical analysis of the implementation of the collectors in a 40-storey high-rise building is documented in [16]. The influence of T_{in} and $\dot{q}$ on the g-value is demonstrated in [17] and in figure 56.
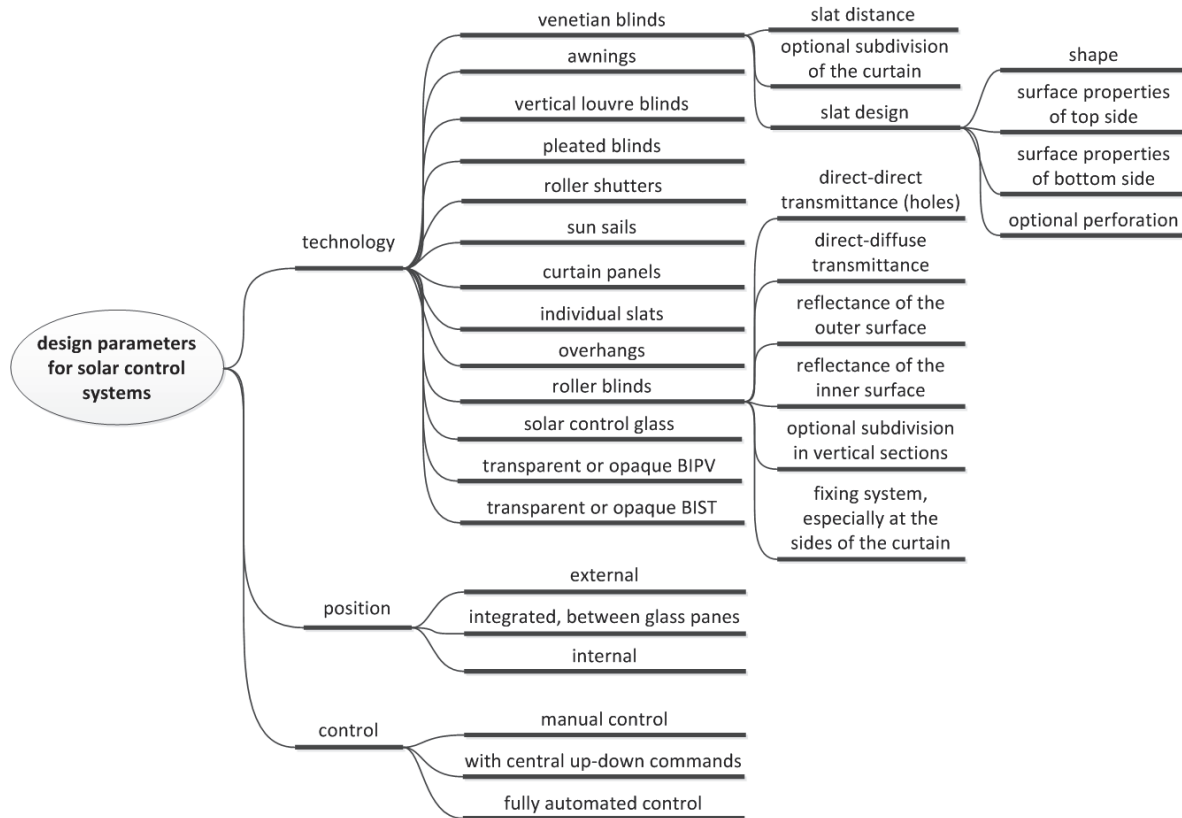
Figure 57: Design parameters for solar-control systems

7 New facade systems for solar-control

This section presents some solar-control systems which have been developed by the author together with scientific or industrial partners. The patent list in the bibliography (with numbers [23] - [30]) provides an overview on concepts for solar-control systems that have been invented or co-invented by the author of this document. Chapter 7.1 provides an overview on the state of the art and chapters 7.2 - 7.7 describe new developments with contributions from the author of this thesis.

7.1 State of the art

Figure 57 provides an overview of the design parameters that have to be specified when solar-control systems are to be chosen for a certain construction project or when new systems are to be developed. The evaluation criteria have been discussed in detail in chapter 4. Figure 9 on page 10 provides an overview of the evaluation criteria. This chapter therefore focuses on discussion of the design parameters. Different technologies are available:

- **Venetian blinds** are defined by the slat design, the slat distance and the optional subdivision of the curtain into two or more separately controllable sections (see also figure 57). An optional vertical subdivision of the curtain into a separately controlled upper section and a lower section would be very good for the performance, but it is omitted in most cases for financial reasons. The upper section is very important for daylighting and the lower-section could be controlled separately according to the visual comfort requirements. Many different slat shapes are available ranging from simple c-shaped slats to sawtooth-shaped retroreflecting slats (e.g. from Retrosolar). The surface properties of the top-side of the slats determine not only the reflectance of the blind, they also have a strong influence on the light transmittance when the slats are not closed. Glossy or mirror-finished surface properties should be used very carefully because of possible glare due to light reflections and possibly non-robust performance (see chapter 6.2.4). However, completely matt surfaces are also not advisable because of possible aesthetic problems with fingerprints. The surface properties of the bottom side of the slats are very important for the brightness (luminance) on the indoor-facing surface of the blind. This brightness in turn, is not only significant with respect to glare protection but also affects visual contact to the outside, since visual contact can be disturbed considerably if the individual slats are too bright. It is possible to use spectrally selective surface properties for the slats of venetian blinds (see figure 58). The selective slats with high light reflectance and low NIR-reflectance within the solar spectral range transmit light much better than the radiation with longer wavelengths than within the visual range (≥ 780 nm). This means that external venetian blinds with these slats provide the same daylighting and better overheating protection than conventional blinds with slats with similar reflectance values for both solar NIR radiation and light.

- The performance of **roller blinds** is determined by both the properties of the curtain and the light-tightness of the mounting system (in some cases with vertical guide rails at the sides of the curtain). The reflectance of the outer surface of the curtain determines the solar-control performance. Another important aspect of the curtain is its direct-direct transmittance, which determines both the ability of the system to block direct vision of the very bright solar disc (with luminances of $\approx 10^9$ cd) and the possibility for visual contact to the exterior. It is clear that both criteria cannot be fulfilled perfectly at the same time and that a compromise has to be found. An extreme case is presented by completely non-diffusing and very transparent coated thin polymer films which can be used instead of fabrics. These foils provide very good visual contact but only limited glare protection and often poor color rendering. The direct-diffuse transmittance determines the brightness of the inner surface of the curtain and therefore has a major influence on glare protection and visual contact to the exterior, since visual contact is not possible in the case of very bright curtains. It is clear that a visual inspection of the properties of a curtain should therefore include situations with direct illumination of the system. The light-exclusion properties of the mounting system are relevant in bedrooms, for glare protection in offices and for the darkening performance in the case of laboratories etc. The requirements are very different for the different types of use (chapter 4). Roller blinds can be mounted internally or between the panes of an insulating glazing unit, a closed cavity facade or a double-facade. "External roller blinds" are often called "window facade awnings".

- **Vertical louvre blinds** consist of vertical strips of fabrics that can be rotated around
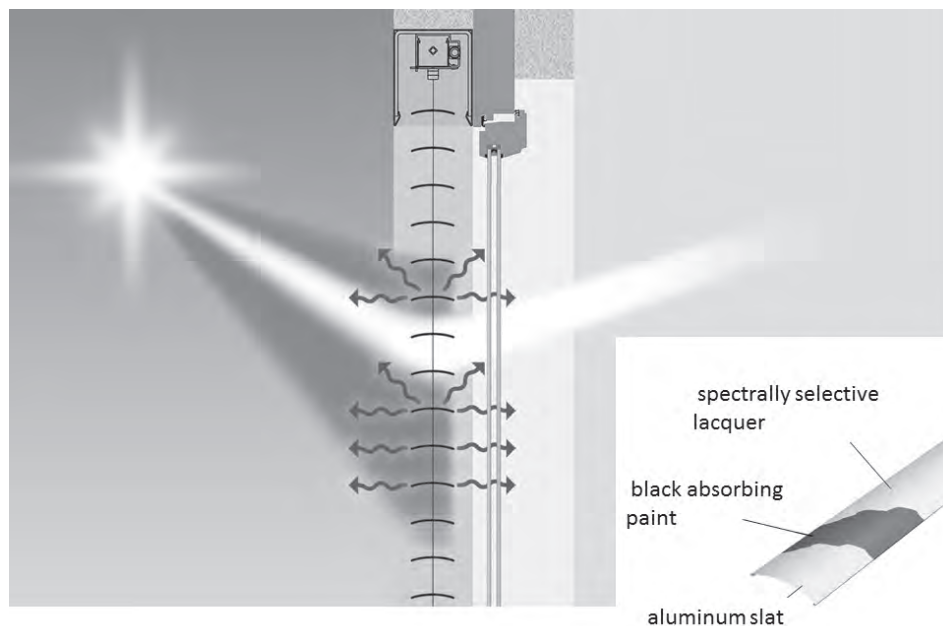
Figure 58: Venetian blind with spectrally selective slats with high light reflectance and high absorptance in the solar NIR spectral range. A large portion of the solar NIR radiation is transmitted through the cover lacquer and absorbed in the black paint below. Most of the incident visible light is reflected by the slats and can therefore - depending on the tilt angle of the slats - contribute to the daylight supply of the room. picture ©Warema.

vertical axes. The requirements on the curtain material are similar to the requirements for roller blinds with the difference that it is not important to provide visual contact through the curtain since visual contact is possible between the slats. The slats can be retracted horizontally.

- **Awnings** can be mounted internally or externally. Internal awnings are mounted horizontally below roof windows, often in big entrance halls etc. External awnings are used to shade conservatories/winter gardens or patios. The solar-control performance of patio awnings is determined by the solar transmittance and the solar absorptance of the curtain, since the device should reduce the direct insolation but should not become too hot in order to avoid uncomfortably high radiative temperatures.

- **Pleated blinds** can consist of a pleated fabrics. They are folded when they are retracted. The design parameters for fabrics of pleated blinds are similar to those of roller blinds. However, there are no light-tight mounting systems for pleated blinds.

- External or internal **curtain panels** consist of a fabric and upper and lower fixings. They can be moved horizontally, but they cannot be retracted. The design parameters for the fabric are similar to the parameters for roller blinds. Since the blinds cannot be retracted, they are always visible and consume space. External curtain panels are often metal fabrics with horizontal sliding fixings at the top and at the bottom. Sometimes perforated metal plates are used instead of fabrics.

- **Roller shutters** are external devices which in most cases, are designed to provide shelter

during the night and during absence of the occupants (burglary protection). However, in many cases, especially in private homes, they are also used for solar-control in summer. They consist of horizontal laths that are hinged together and can be retracted by a roll at the top. The laths can be made of polymer material or metal. The laths can be filled with insulation material. A new daylighting and solar-control roller shutter with translucent rods has been developed by the author (see chapter 7.4).

- **Externally mounted fixed or rotatable individual slats** are typically much larger than the slats of a venetian blind. They can be made of metal, glass or polymer material. There are a lot of similarities between glass slats (with or without screen printed patterns) and fabrics of roller blinds, therefore a similar reasoning applies for the discussion of the design parameters. In many cases glass slats with a high direct transmittance are used, which means that the glare protection performance of such systems is limited. The individual slats can be mounted horizontally or vertically. New slats have been developed by the author (see chapter 7.5).

- **Overhangs** are static cantilever extensions of a building, formed by the roof overhang, integrated into the facade or especially designed to provide shelter for an entrance or a patio. They effectively provide solar protection in summer, especially in the case of southern orientation because of the high profile angle of the sun in summer. They are much less effective in western or eastern orientation.

- **Sun sails** consist of a piece of fabric and a fixing system, forming something like a freestanding roof. They can be rigid and not retractable or retractable. Rigid sun sails also provide rain protection for outdoor areas. The discussion about the design parameters of fabrics of sun sails is very similar to the discussion for awnings. Rigid sun sails have to be windproof.

- **solar-control glass panes** can have switchable or constant properties. They can be used in glazing units, glass slats or as ventilated glass panes in double-skin facades.

  Classic solar-control glass panes with constant properties have spectrally selective transmittance. The spectral selectivity of single, double or triple glazing can be characterized by the ratio S between the light transmittance and the g-value $S = \tau_v/g$. Typical values for double glazing are S $\approx$ 2, e.g. $S = 66/34$ or $S = 50/25$. Higher values of S are difficult to achieve under the boundary condition of high values of the general color rendering index Ra. The spectrally selective glass panes are normally nano-coated with interference coatings. The nano-coating consists in most cases of two or three silver layers which provide low-emissivity at the same time. Triple-silver coatings normally provide better color rendering properties than double-silver coatings. Most high-performance coatings are not stable under normal atmospheric conditions and therefore have to be integrated into sealed glazing units or laminated safety glass.

  Switchable layers on glass panes can change their visual and solar-control properties because of intrinsic or extrinsic triggers. The switching mechanism can be based on the following principles:

  - The transmittance of **electrochromic** layers can be switched externally by applying a certain voltage to the glazing. The optical properties are influenced by changing the oxidation state of tungsten oxide electrically. Different darkening

levels are possible depending on the voltage. Color rendering properties are challenging in many cases because of the deep blue color of the tungsten oxide. Different measures are taken to compensate this effect. Electrochromic glazing provide good visual contact with the exterior but limited glare protection because of the non-scattering properties and because it does not block visual contact with the solar disc. Electrochromic layers on glass are available on the market and used in the construction industry and the automotive industry.

– **Gaschromic** glazing can be switched by inserting a chemically oxidizing or reducing gas into the glazing cavity adjacent to the switchable coating. In most cases, the optical properties are influenced by changing the oxidation state of tungsten oxide with the oxidizing or reductive gas. The optical properties are similar to the properties of electrochromic layers. No energy is required to maintain the switching state. Large areas can be switched more evenly than with electrochromic glazing.

– The transmittance of **photoelectrochromic** layers can be switched similarly to electrochromic glazing with the difference that the coating itself generates the voltage which is needed for the switching of the optical properties. Opening or closing the electric circuit externally darkens or bleaches the device respectively. The device can only be switched into the dark state when it is irradiated by the sun.

– No external trigger is possible in case of **photochromic** layers which always switch into the dark mode when they are irradiated by the sun. The main challenge of most photochromic glass panes is the strong temperature dependence of the switching mechanism. Photochromic layers are mainly used in sunglasses and not in facade systems.

– **Thermochromic** layers change their color depending on the temperature of the layer. No application in construction products is known, since most of the layers have little influence on the light transmittance.

– **Thermotropic** layers [128] change their scattering properties depending on the temperature of the thermotropic layer. The basic physical mechanism is good mixing of two different phases at low temperatures and segregation of the two phases at higher temperatures. The scattering above the phase change temperature is often caused by multiple Mie-scattering by domains with dimensions similar to the wavelength of the incident radiation [91]. Thermotropic layers are e.g. polymer blends, hydrogels or lyotropic liquid-crystal polymers LCP, which have to be encapsulated between two glass panes. Polymer blends consist of two or more polymers which are blended together, switching from a homogeneous miscible phase at lower temperatures to a heterogeneous immiscible phase at higher temperatures. Hydrogels are networks of polymer chains dispersed in water, being evenly distributed or forming discrete domains depending on the temperature. Lyotropic liquid-crystal polymers LCP consist of dissolved polymers in a solvent, forming different liquid crystal phases depending on the temperature. In all cases the differences in the refractive index of the segregated phases at higher temperature create scattering similar to the fat droplets in milk. There have been several research projects in the construction sector dealing e.g. with the application of thermotropic layers in facade elements or as overheating protection for solar thermal collectors in stagnation conditions. Thermotropic layers are not completely clear and non-scattering in the "clear state" in most cases. It is therefore difficult to use these materials in the

vision area, where visual contact with the exterior has to be provided. The most difficult situation is when people are viewing a dark scene in the shadow, while the glazing is directly irradiated by the sun (haze).

– **Polymer-dispersed liquid-crystal layers PDLC** have properties similar to thermotropic LCP-layers with the difference that the switching is activated by an electric field. They therefore can be switched externally. They also have some residual haze in the "clear-state", especially under oblique angles of incidence. Glass panes with PDLC-layers are available on the market. Because of the small influence on the g-value and the possibility of haze they are normally used only for internal applications such as privacy screens, e.g. in some of the German ICE-trains behind the train driver's cabin.

More details on switchable layers can be found e.g. in [37].

- **Transparent building-integrated PV-elements (BIPV)** can be used as a substitute for transparent fabrics, screen-printed glazing or static blinds. The efficiency is higher than the efficiency of conventional solar-control systems, since parts of the absorbed radiation is converted into useful electricity. Several systems are available on the market. They can be integrated into sealed glazing units (warm facade) or mounted externally as ventilated glass panels.

- **Transparent building-integrated solar thermal (BIST) collector elements** can be used instead of static blind systems or fabrics to reduce the transmitted solar energy. They can be integrated into glazing units (warm facades). At least one system with glazing-integrated collector was available on the market (Robin Sun, www.robinsun.com). Alternatively, they can be installed additionally in front of the facade like e.g. a balcony parapet. An example of this is given by vacuum tube collectors which provide similar aesthetics to conventional protection systems, that prevent people from falling off balconies, floor-to-ceiling windows or fully glazed facades (see figure 69). In the case of additionally mounted systems, care has to be taken to prevent glass pieces from falling down if one of the tubes break. The collectors therefore should be protected with an additional laminated glass pane or other measures. When collectors are mounted on tilted cantilever extensions of facades, the additional glass pane (with its additional reflectance losses) can be omitted by using other protective systems (see e.g. figure 59)

The control of sun-shading systems is very important for their real performance, since solar-control systems are only effective when they are in operation and not retracted. External devices are motorized in most cases with different priority levels in the control algorithm. The highest priority level is normally assigned to firefighter and wind-protection triggers. The performance can be enhanced greatly by using presence detection and by closing the blinds completely when nobody is in the room during the cooling season. If no presence detection is available, it helps to pre-set the blinds at night in order to ensure that the blinds are completely closed in the early morning during the cooling season and that they are completely retracted during the heating season. More advanced control modes are sometimes used (e.g. cut-off control, where the slats are tilted dynamically in order to maximize visual contact and at the same time blocking the direct irradiation). Silent motors enhance greatly the acceptance of all control algorithms that change the blind position when someone is in the room.
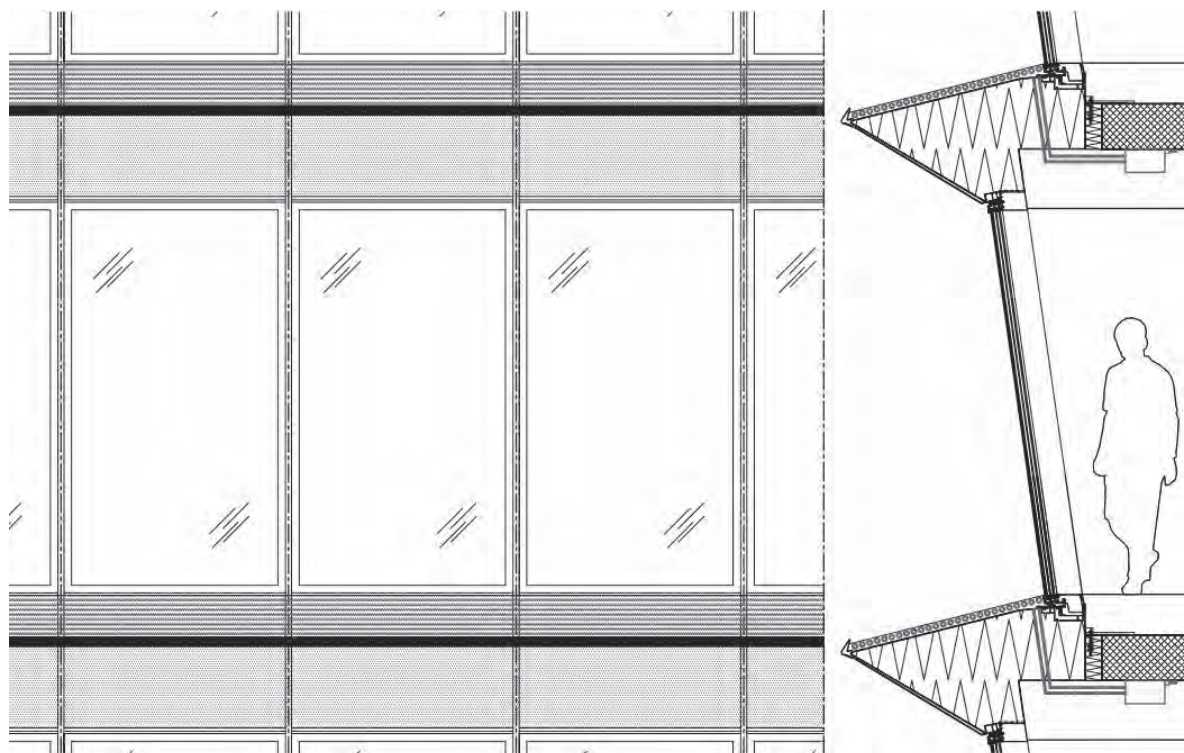
Figure 59: A concept for the integration of solar thermal vacuum tube collectors in facades. The collectors are mounted on top of an overhang which provides static solar-control, especially on south-facing facades. With this concept no additional glass pane is needed for protection in case of breakage of one of the vacuum tubes. The concept is part of a catalogue of facade concepts. The aim of the catalogue is to assist building design teams to integrate solar thermal or BIPV components into the construction of the external building envelope [47]. The catalogue has been developed by the project partner Emmer Pfenninger and Partner AG, Switzerland within the EU-funded 'Cost-Effective' research project under the co-ordination of the author of this thesis.
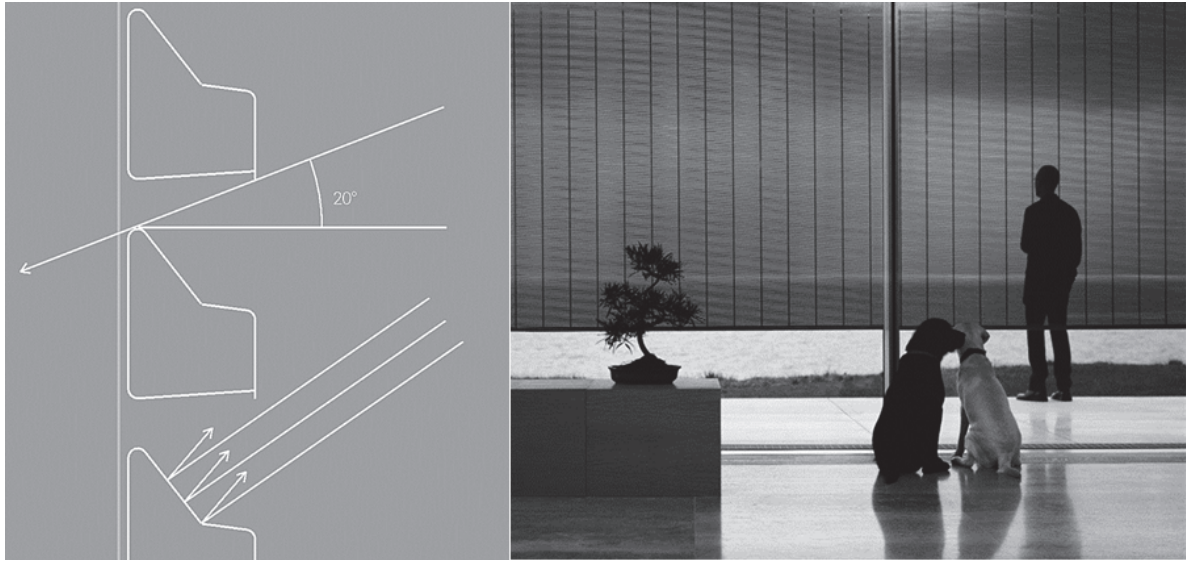
Figure 60: New stainless steel blind s_enn®. The person on the photo at the right-hand side is standing outdoors. The shape of the rods of the new stainless steel blind s_enn® was developed by the author of this thesis. The blind can be retracted by a roller at the top of the blind, similar to a conventional roller blind. The wind resistance of this blind is much higher than for conventional venetian blinds or roller blinds due to the shape of the rods. Pictures ©clauss-markisen [44].

7.2 New stainless steel blind

The shape of the rods of the new stainless steel blind s_enn® (see figure 60), was developed by the author of this thesis, who is a co-inventor of this system [23]. The system selectively shields certain regions of the sky. This leads to very good solar protection (see chapter 6.2.4) and a transparent appearance, while direct insolation of the room and the associated glare is prevented in most cases. s_enn® was awarded an innovation prize at the 2003 R+T Trade fair in Stuttgart, Germany which is the most important international trade fair for sun-shading systems. In March 2004 s_enn® was awarded the Bavarian State Prize at the 56th International Handicraft Fair in Munich, Germany. In November 2004 s_enn® was awarded the Innovation Price for small and medium-sized enterprises by 'Volksbanken and Raiffeisenbanken' banks. This solar-control system has been used by several famous architects, e.g. by Murphy/Jahn (Chicago) for the "Horizon Serono" building in Geneva, where 6.500 m^2 of this blind were installed in 2004.

7.3 Venetian blind with new slat shape

The special shape of the 'Genius slats' (see figure 62 and 61) of a new venetian blind ensures good sun-shading properties which are relatively independent of the actual setting of the slat angle over broad ranges, which ensures robust performance despite so-called 'faulty operation'

Figure 61: Internal venetian blind with 'Genius slats' in the 56-storey building Main-Tower in Frankfurt(Main), Germany. The original internal venetian blinds with mirror finished surface have been replaced since 2008 step by step by venetian blinds with genius slats in order to avoid overheating [124].

(see chapter 6.2.4). The top side is white with high solar and light reflectance for good solar-control and light re-directing properties. The bottom side is light gray in order to reduce the luminance on the inner side of the blind for improved glare protection. Both sides are matt, with little gloss, in order to minimize irritating and glaring light reflections. The special shape prevents people from looking onto the directly irradiated bright area on the top side of the slat, since this area is shielded in many cases by the "ridge" in the middle of the slat. Venetian blinds with these slats have been installed e.g. in the Roche-Tower, Basel, Switzerland, or in the Main-Tower in Frankfurt(Main), Germany (see figure 61). The Roche-Tower is one of the largest buildings of Switzerland with 41 floors above the ground, 178 m height and a total floor area of approx. 83.000 m^2. The Roche-Tower was designed by the architects Herzog & de Meuron in 2015. The Main-Tower is one of the highest buildings in Germany with with 56 floors above the ground, 200 m height (without antenna) and a total floor area of approx. 101.705 m^2. The Main-Tower was designed by the architects Schweger + Partner in 2000. The original internal venetian blinds with mirror-finished top surface have been replaced successively since 2008 by venetian blinds with 'Genius slats' in order to avoid overheating [124]. For a comparison of the performance of the 'Genius slats' with mirror-finished slats see chapter 6.2.4 and especially figure 42 on page 105 .

Figure 62: Internal venetian blind with the trade name 'Genius slats'. The 'Genius slats' were invented by Hans-Peter Baumann, Rolf Brunkhorst and the author [24].

7.4 Roller shutter with daylighting functionality

A daylighting roller shutter (see figures 63 and 64) was developed by the author. It consists of translucent horizontal laths that are connected by hinges and can be retracted by a roll at the top. The laths are made of extruded polycarbonate. The inner and outer surfaces are transparent while the internal bars are translucent white. The translucent bars block the direct irradiation. The new roller shutter is intended to be used in all offices or rooms, except bedrooms, instead of conventional roller shutters. The idea behind the development is that the darkening function of conventional roller shutters is not needed in these cases and that the daylighting function of conventional roller shutters is very poor.

Figure 63: Daylighting roller shutter, viewed from outdoors. A cross-section of the translucent lath can be seen in the upper illustration. The new laths were developed by the author. Photos ©Prokuwa Kunststoff GmbH, Dortmund

Figure 64: Daylighting roller shutter, seen from indoors. On the top, a cross-section of the translucent lath can be seen. Photos ©Prokuwa Kunststoff GmbH, Dortmund

Figure 65: External blind consisting of large-scale slats, each with an ellipsoidal cover mounted for measurement in the calorimeter in the TestLab Solar Facades at the Fraunhofer Institute for Solar Energy Systems ISE in Freiburg, Germany. The slats have integrated translucent and opaque sections in order to enhance the daylighting and glare protection functionality. Pictures ©Fraunhofer ISE.

7.5 Large-scale slats with transparent ellipsoidal covers

Translucent slats for large-scale external solar-control systems were invented by the author, Peter Nitz and Christof Meyer in 2007 [28] (see figure 65). Each slat has a transparent ellipsoidal cover and integrated translucent and opaque sections to enhance the daylighting and glare protection functionality. The slats have similar performance to the laths of the daylighting roller shutter. They are also made of extruded polycarbonate. The idea is to mount them externally on the facade of a building in front of and/or above the windows, preferably on south-oriented facades. They then provide solar-control and in some cases also glare protection. The advantage of the slats in comparison to conventional aluminum slats is their transmission of diffuse daylight and the drastically reduced weight.
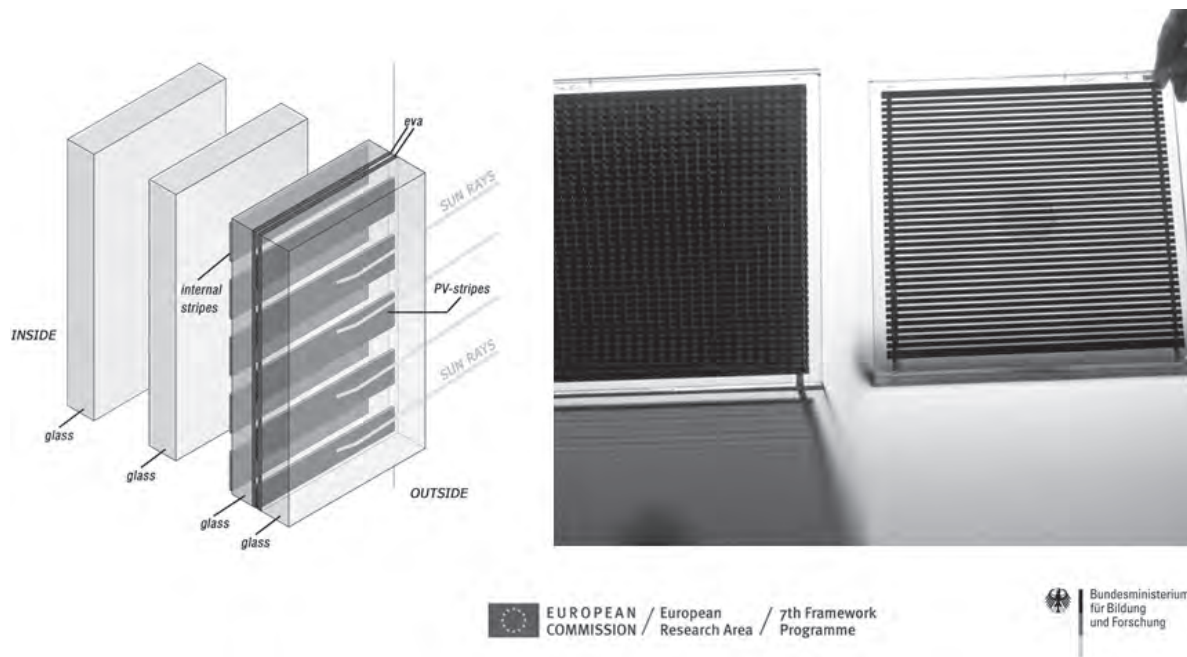
Figure 66: The angle-selective transparent BIPV-system PVShade® contains two layers of thin-film PV-strips in the outermost glass panes of a triple glazing. The arrangement of the PV-stripes is the origin for the angle-selective transmittance.

7.6 Angle-selective transparent BIPV-system

The angle-selective transparent BIPV-system PVShade® is shown in figures 66 and 67. The system was invented by the author of this thesis in 2006 [25]. It was optimized and further developed by F. Frontini in his Ph.D. thesis under the supervision of the author of the present thesis [69]. This multifunctional facade system generates photovoltaic electricity and simultaneously provides solar control and glare protection. It is especially designed to be used in the sill area of completely glazed facades as shown in figure 67. This area has very little effect on the daylighting conditions in the room. It therefore can be equipped with a static solar-control system in order to reduce the cooling load of the building. The angle-selective transmittance originates from the arrangement of the two layers of PV-strips. It selectively shields higher sun positions and allows visual contact in horizontal and downward directions. A methodology for the optical and electricity yield simulation of this complex fenestration system (CFS) with BIPV-functionality has been developed under the guidance of the author of the present thesis by W. Sprenger in his Ph.D. thesis (see chapter 2.4.4 and chapter 4.4.2 in [115]).
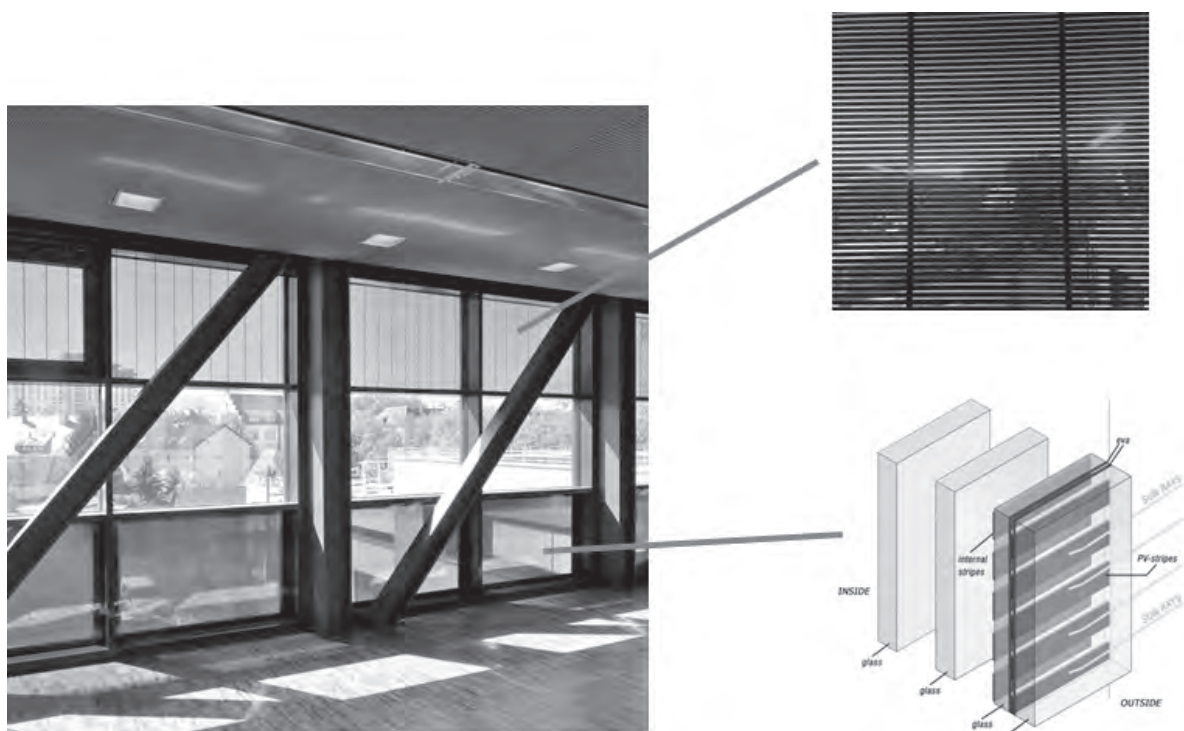
Figure 67: The angle-selective BIPV system installed in the sill area of a seminar room of Fraunhofer ISE in Freiburg, Germany. The solar-control system in the upper facade segment is the stainless steel blind, as described in chapter 7.2.

Figure 68: New transparent solar thermal collector. The left-hand photo demonstrates the possibility of visual contact from indoors to outdoors. The photo on the right-hand side shows the new facade element mounted in the Testlab Solar Facades at Fraunhofer ISE in Freiburg, Germany. Pictures © ZAG, Ljubljana, Slovenia and Fraunhofer ISE, Freiburg, Germany.

7.7 Angle-selective transparent solar thermal facade collectors

Figure 68 shows prototypes of a new type of building-integrated transparent solar thermal collector (TSTC). These angle-selective solar thermal collectors were invented by Michael Hermann and the author, in 2006 [27, 26]. The basic idea is to integrate openings with angle-selective transmittance into an absorber and to integrate the absorber within a sealed glazing unit or a closed cavity facade. The facade cavity with the absorber is continuously flushed with a very low flux of dry air in the case of closed cavity facades. The multifunctional facade elements allow visual contact to the exterior, provide solar and glare control and generate useful solar thermal heat gains. In summer, during the cooling season, the collector is intended to be used as heat source for thermally driven cooling systems or desiccant de-humidification systems. Desiccant de-humidification systems are particularly interesting since market available systems can already be operated at relatively low temperatures of e.g. $55°C$. The importance of de-humidification will increase, since energy efficient cooling systems like thermally activated building systems (TABS) usually lower the temperature of the ceiling and since condensation has to be avoided under all circumstances. During the heating season the collector is intended to be used as a renewable heat source for low-temperature heating systems, like floor-heating systems. The solar radiation coming from directions with high solar profile angles is selectively shielded by the external surface of the absorber, while visibility through the collector is retained in the horizontal or downward directions for people inside the building. The integration of the new transparent solar thermal facade collectors into a 40-storey high-rise building with desiccant de-humidification and thermally driven cooling systems has been assessed theoretically in [16] with co-authorship of the author of this thesis. The new multifunctional TSTC systems were installed in a pilot building as part of the Eu-

ropean research project Cost-Effective [46], together with a thermally driven cooling system for the offices in the uppermost story of this building (see figure 69). The semi-transparent collectors were installed together with air-heating vacuum facade collectors. The pilot building is the building of the Slovenian National Building and Civil Engineering Institute ZAG, in Ljubljana, Slovenia. The energy consumption and the thermal comfort of the offices in this building has been monitored. The results and a comparison with simulations are described in [6] and [7] with co-authorship of the author of this document. A detailed physical model for this multifunctional facade component was developed by C. Maurer within his Ph.D. thesis [86, 17] under the guidance of the author of this thesis. More details about this tool can be found in chapter 6.5.

air heating vacuum tube collectors (Kollektorfabrik)

transparent solar thermal collectors (Permasteelisa)

www.cost-effective-renewables.eu

EUROPEAN / European / 7th Framework
COMMISSION / Research Area / Programme

Figure 69: Installation of the angular selective solar thermal facade collectors in a pilot building of the European research project Cost-Effective www.cost-effective-renewables.eu which has been co-ordinated by the author. The angular selective solar thermal collectors have been invented by Michael Hermann and the author, in 2006 [27, 26]. The semi-transparent collectors are installed together with air-heating vacuum collectors. The pilot building is the building of the Slovenian National Building and Civil Engineering Institute ZAG in Ljubljana, Slovenia. photos ©ZAG.

8   Conclusion and outlook

8.1   Summary of the results

The document summarizes the results achieved within last 16 years by the author.

It comprises the **further development of performance criteria** for solar-control systems. The main contribution is the introduction of the "effective g-value g_{eff}", which is the first product characteristic that includes not only the static properties of the solar-control system but also the control, which is essential for a realistic performance evaluation. It is important to note that the "center-of-glazing" property g_{eff} is independent from the specific building. It only depends on the orientation and location and can therefore be used for a general performance characterization within a climatic zone. Another contribution is the new criterion for the color rendering of objects in the room, seen from an observer outside the building $Ra_{\text{out-in}}$. This performance aspect was not considered quantitatively until now. Contributions to performance criteria for BIPV or BIST solar-control systems with active photovoltaic or solar thermal energy conversion have been made, which also includes life-cycle-cost aspects. The chapter on performance criteria represents the background of the author for his contributions to the European Standards EN14500 (*Blinds and shutters - Thermal and visual comfort - Test and calculation methods*), and EN14501 (*Blinds and shutters - Thermal and visual comfort - Performance characteristics and classification*) as a member of the committee CEN/TC33/WG3/TG5.

A methodology for calorimetric g-value measurements has been developed. The detailed documentation of this methodology together with the analysis of the measurement uncertainty was a major contribution the international standard ISO/CD 19467 (*Thermal performance of windows and doors - Determination of solar heat gain coefficient using solar simulator*). The author has contributed to the content of this standard with these results as a member of the committee ISO/TC163/SC1/WG17. The error analysis takes into account error contributions from differences between lab conditions and reference conditions, systematic biases due to imperfect sensor calibration and statistical errors. It also includes methods for the correction of significant differences between reference conditions and lab conditions.

The mathematical-physical modeling of the interaction of the solar radiation with the building skin is another major part. It ranges from the modeling of the transmission of daylight and the modeling of secondary heat gains to the modeling of photovoltaic or solar thermal energy conversion. This includes the modeling of the performance of the facade component itself (modeling of g_{eff}) and the modeling of the performance of the facade component in the building context (black-box model and virtual transparent solar thermal collector as component for dynamic building simulation programs).

Evaluation criteria for solar control systems have been further developed by introducing the **new criterion $Ra_{\text{out-in}}$** for color rendering of objects in the room, illuminated by daylight and viewed by an observer outside the building. The background for this new criterion is that it would be advantageous if the color of human skin were to be rendered with high quality

when people are looking indoors from outdoors, so that occupants of a room do not look pale or ill. Color rendering of objects in the room viewed by an observer who is outdoors is also relevant for other cases such as internal "white venetian blinds" which are white for observers in the room and which should also appear white when the observer is outside. Instead, white venetian blinds often look greenish from the outside when they are mounted behind spectrally selective solar-control glazing and they are therefore sometimes rejected and replaced by less efficient blinds with gray slats. Application of the new criterion for several solar control systems showed that the quality of color rendering is lower in almost all cases, when the observer is looking from outdoors into the room. The difference is significant in many cases and can be much larger than 25%, with the effect that the quality of the color rendering changes from "very good" to "good" or it loses the attribute "good". The new criterion can therefore help to optimize the facade with respect to both, the solar-control performance and user acceptance.

Chapter 7.1 provides a detailed **overview on the state of the art of solar-control systems** together with a general analysis of the **design parameters for solar control systems** (see Figure 57 on page 128). The state of the art analysis includes multifunctional solar control systems which include active solar energy conversion with PV-cells or solar thermal collectors. Chapters 7.2 - 7.7 present **6 new solar-control systems** which have been invented and further developed with strong contributions of the author. Some of them received national and international innovation prices and/or have been installed by famous architects in very large buildings.

8.2   Recommendations for future research

Strongly improved calculation capacities of desktop computers allow much higher complexity in the modelling of complex fenestration systems. One approach for further development is based on goniometric measurements of the bi-directional scattering distribution function BSDF. The exploitation of such complex characteristics together with a strongly improved management of the information flow within the semantic web (internet of things) seems to be very promising in order to enhance accuracy and increase the reliability on the construction site. There are several activities concerning building information modelling (BiM) in the construction industry, like e.g. the 5D-initiative of ENCORD, but much more research is needed.

Another important future research area is the development of new high-performance multi-functional components (with or without active solar energy conversion) for the building skin which can be produced effectively with industrialized processes that also include the planning, installation and maintenance in order to reduce the life-cycle-costs.

9 Acknowledgements

The author thanks his wife Ruth for very much support, encouragement and for helping to find the time to write this thesis.

References

References with authorship or co-authoship of Tilmann E. Kuhn

[1] EN 14500 *Blinds and shutters - Thermal and visual comfort - Test and calculation methods*, European Standard, May 2008. The author is member of the committee CEN/TC33/WG3/TG5 and has contributed to develop this standard.

[2] EN 14501 *Blinds and shutters - Thermal and visual comfort - Performance characteristics and classification*, European Standard, 2005. The author is member of the committee CEN/TC33/WG3/TG5 and has contributed to develop this standard.

[3] F. Frontini, S. Herkel, T. E. Kuhn, P. Strachan, G. Kokogiannakis, *Implementation of a new bi-directional solar modelling method for complex facades within the ESP-r building simulation program and its application*, conference paper IBPSA Building Simulation 2009, University of Strathclyde, Glasgow, Scotland, 27th - 30th July 2009.

[4] K. Fath, J. Stengel, W. Sprenger, H. R. Wilson, F. Schultmann, T. E. Kuhn, *A method for predicting the economic potential of (building-integrated) photovoltaics in urban areas based on hourly Radiance simulations*, http://dx.doi.org/10.1016/j.solener.2015.03.023

[5] ISO/CD 19467, *Thermal performance of windows and doors - Determination of solar heat gain coefficient using solar simulator* International Organisation for Standardisation, Geneve, Switzerland, 2015 The author is member of the committee ISO/TC163/SC1/WG17 and has contributed to develop this standard.

[6] S. Jordan, J. Hafner, T. E. Kuhn, A. Legat, M. Zbašnik-Senegačnik *Evaluation of various retrofitting concepts of building envelope for offices equipped with large radiant ceiling panels by dynamic simulations* Sustainability, 2015, http://www.mdpi.com/2071-1050/7/10/13169

[7] S. Jordan, J. Hafner, T. E. Kuhn, A. Legat, M. Zbašnik-Senegačnik *indoor environment in retrofitted offices equipped with radiant ceiling panels*, paper-ID: 1289-2015, accepted for publication in GRADEVINAR, the Journal of Croatian Association of Civil Engineers, 2015.

[8] T. E. Kuhn, C. Bühler, W. J. Platzer *Evaluation of overheating protection with sun-shading systems*, Solar Energy Vol.69 (Suppl.) Nos. 1-6, pp. 59-74, 2000. http://dx.doi.org/10.1016/S0038-092X(01)00017-2

[9] T. E. Kuhn, J. Wienold, *Solar control* Contribution to the Conference Tall buildings and Transparency in Stuttgart, Germany, October 5-7, 2003, http://www.ctbuh-stuttgart.de/

[10] T. E. Kuhn, *Solar control: A general evaluation method for facades with venetian blinds or other solar control systems to be used 'stand-alone' or within building simulation programs*, Energy and Buildings, Vol 38, Issue 6, pp. 648-660, June 2006. http://dx.doi.org/10.1016/j.enbuild.2005.10.002

[11] T. E. Kuhn, *Solar control: Comparison of two new systems with the state of the art on the basis of a new general evaluation method for facades with venetian blinds or other solar control systems*, Energy and Buildings, Vol 38, Issue 6, pp. 661-672, June 2006. http://dx.doi.org/10.1016/j.enbuild.2005.10.001.

[12] T. E. Kuhn, *Sonnenschutz: Eine generelle Bewertungsmethode - auch für zwischenliegende Systeme - und zwei neue Behänge*, Bauphysik, Vol 29 (2007), Heft 1, pp. 63-71, 2007. http://dx.doi.org/10.1002/bapi.200710012

[13] T. E. Kuhn, S. Herkel, et al. (2011). *Solar control: A general method for modelling of solar gains through complex facades in building simulation programs*, Energy and Buildings 43(2011): 19-27 http://dx.doi.org/10.1016/j.enbuild.2010.07.0158.

[14] T. E. Kuhn, Calorimetric determination of the solar heat gain coefficient *g* with steady-state laboratory measurements, Energy and Buildings, 2014. http://dx.doi.org/10.1016/j.enbuild.2014.08.021

[15] T. E. Kuhn, H. R. Wilson, J. Hanek, M. Santamouris Ra_{out-in}: *Color rendering of objects in the room seen from the outside* accepted for publication in Energy and Buildings, 11.2.2016.

[16] Ch. Maurer, Th. Baumann, M. Hermann, P. Di Lauro, S. Pavan, L. Michel, T. E. Kuhn, *Heating and cooling in high-rise buildings using facade-integrated transparent solar thermal collector systems*, Proceedings of Building Simulation 2011: 12th Conference of International Building Performance Simulation Association, Sydney, 14-16 November 2011.

[17] Ch. Maurer, T. E. Kuhn, *Variable g value of transparent façade collectors*, Energy and Buildings, Vol. 51, pp. 177-184 (2012).

[18] N. Sack, T. E. Kuhn, Andreas Beck, *final report of the German national research project REGES with the title "Development of a reference method for calorimetric g-value measurements of transparent and translucent building components"*, i.f.t. Rosenheim, Fraunhofer ISE and ZAE Bayern, 2001. http://www.baufachinformation.de/literatur/Forschungsvorhaben-REGES/2007049008923

[19] M. Santamouris (Editor) and Nicol F., Roaf S., Akbari H., Voss K., Kuhn T. E., Nitz P., Herkel S., Wall M., Hellström B., Kolokotroni M., Pfafferott J., Walker-Hertkorn S., Sanner B. and Erell E., *Advances in passive cooling*, Earthscan, August 2007, 284 pages, ISBN: 9781844072637

[20] W. Sprenger, H. R. Wilson, T. E. Kuhn, *Electricity yield simulation of the building-integrated photovoltaic system installed in the main building of the Fraunhofer Institute of Solar Energy Systems (ISE)*, submitted for publication to Solar Energy, 2015

[21] H. R. Wilson, J. Hanek, T. E. Kuhn *Solarer Transmissionsgrad einer PC-Stegplatte - Auswirkung verschiedener Gewichtungsspektren*, internal communication, Fraunhofer ISE, 2014

[22] H. R. Wilson, J. Hanek, T. E. Kuhn *Optical Characterisation of Concrete for Heat Island Mitigation, solar reflectance index (SRI) of concrete*, CPI - Concrete plant international - 5, 2015 www.cpi-worldwide.com

Patents for solar control systems and other facade components, invented or co-invented by the author of this document

[23] U. Clauss, T. E. Kuhn, EP 1417393 B1, *flat structure to be used as solar control device*, European Patent, 2001

[24] H.-P. Baumann, R. Brunkhorst, T. E. Kuhn, EP1243743,*slat for a venetian blind*, European Patent, 2002

[25] T. E. Kuhn, US 9051771 B2,*solar control device with angular selective transmittance, with or without PV-elements*, United States Patent, 2006; European Patent EP 2 041 388 B1.

[26] M. Hermann, T. E. Kuhn, WO2008000236, *partially transparent solar collector with solar control functionality*, international patent, 2006

[27] T. E. Kuhn, M. Hermann, EP2047055,*partially transparent solar control system*, European patent, 2007

[28] T. E. Kuhn, P. Nitz, Ch. Meyer, WO2009074280 A1 *venetian blind with translucent and opaque parts*, International patent application, 2007

[29] Ch. Maurer, M. Hermann, P. Di Lauro, T. E. Kuhn, M. Bauch EP2587182, *solar control system, venetian blind with integrated solar thermal collector based on heat pipe technology*, European patent application, 2011

[30] N. Nestle, A. Daiss, K. , R. Noerenberg, J. M. Szeifert, E. Khazova, A. Loeffler, T. E. Kuhn, Ch. Maurer, Th. Pflug, J. Wienold, A. Glueck, WO2014114563, *Construction element having a controllable heat-transfer coefficient u*, International patent application, 2013

General references

[31] AFNOR experimental standard on *Solar and light transmission coefficients of complete windows with or without solar protection devices*, presented by the association francaise de normalisation (AFNOR) in 2014.

[32] O. Aschehoug, S. Aydinli, J. Christoffersen, G. Courret, I. Edmonds, R. Jakobiak, M. Kischkoweit-Lopin, M. Klinger, E. Lee, L. Michel, J.-L. Scartezzini, S. Selkowitz, (ed.): *Daylight in Buildings*, IEA SHC Task 21/ECBCS Annex 29. LBNL Report Number: LBNL-47493. http://gaia.lbl.gov/iea21/

[33] ASTM E1980-11, *Standard Practice for Calculating Solar Reflectance Index of Horizontal and Low-Sloped Opaque Surfaces*,

[34] P. Berchtold, IPB Ing. Büro für Energie + Gebäudetechnik, 6060 Sarnen, Switzerland, *Private communication.*

[35] D. M. Berson, F. A. Dunn, M. Takao, *Phototransduction by retinal ganglion cells that set the circadian clock*, Science, 295(5557):1070-3, Feb. 2002, http://dx.doi.org/10.1126/science.1067262

[36] BINE themeninfo I/2011, U. Heinemann, H. Weinländer, D. Gintars, *Insulation through vacuums - high performance thermal insulation for building envelopes and windows.* ISSN 1610-8302, FIZ Karlsruhe, 2011.

[37] BINE themeninfo I/2002, P. Nitz, A. Wagner, *Schaltbare und regelbare Verglasungen*, ISSN 1610-8302, 2002. FIZ Karlsruhe, 2002.

[38] L. Brotas, J. Wienold, *Solar reflected glare affecting visual performance*, 8th Windsor Conference, London, April 2014.

[39] A. P. Brunger, L. E. West, *Measurement of SHGC and U-value of windows with insect screens*, Published 1999 by CANMET Energy Technology Centre, ISBN 10 0662274644, 1999.

[40] B.Bueno, L. Norford, J. Hidalgo, G.Pigeon, *The urban weather generator*, Journal of Building Performance Simulation, August 2012, DOI:10.1080/19401493.2012.718797

[41] F. Chen, S. K. Wittkopf, Summer condition thermal transmittance measurement of fenestration systems using calorimetric hot box, Energy and Buildings, Vol. 53, pp. 47-56, 2012

[42] CIE 13.3-1995, *Method of Measuring and Specifying Colour Rendering Properties of Light Sources* , 1995 ISBN 978 3 900734 57 2

[43] F. Chen, S. K. Wittkopf, P. K. Ng, H. Du, *Solar heat gain coefficient measurement of semi-transparent photovoltaic modules with indoor calorimetric hot box and solar simulator*, Energy and Buildings Vol. 53, pp. 74-84, 2012

[44] Clauss Markisen GmbH, *s_enn, Sonnenschutz aus Edelstahl*, http://clauss-markisen.de/CM-Broschuere-s-enn.pdf

[45] R. D. Clear, *Discomfort glare: What do we actually know?*, Lighting Research and Technology April 2013 vol. 45 no. 2, pp. 141-158, DOI: 10.1177/1477153512444527, http://lrt.sagepub.com/content/45/2/141

[46] *D3.1.2 Prototype for transparent thermal collector for window integration*, deliverable report of the European research project Cost-Effective, www.cost-effective-renewables.eu, 2011. http://www.cost-effective-renewables.eu/includes/images/Publications/Files/6c449715a9306252d04344c05969c1ac.pdf

[47] *D4.1.2 Integrated Concepts - Construction Aspects*, deliverable report of the European research project Cost-Effective, www.cost-effective-renewables.eu, 2012. http://www.cost-effective-renewables.eu/includes/images/Publications/Files/0791734e07bacdacbb4e2c44a7e8c77e.pdf

154

[48] A. Dama, *Angular dependency of optical properties and energy performances of glazing and solar shading devices for windows and facades*, Politecnico di Milano, Dipartimento di Energetica, Dottorato di Ricerca in Energetica XVI ciclo, Milan, Italy, Anno Accademico 2003-2004.

[49] A. Gonzales-Pardo, J. Gonzales-Aguilar, M. Romero Alvarez, *Analysis of glint and glare produced by the receiver of small heliostat fields in building facades. Methodology applicable to conventional central receiver systems*, Solar Energy XXX, 2015

[50] K. Blümel, E. Hollan, A. Jahn, M. Kähler, R. Peter, *Entwicklung von Testreferenzjahren (TRY) für die Klimaregionen der Bundesrepublik Deutschland.* Scientific report of the Institute for Geophysical Sciences Technical University Berlin. BMFT-FB-T- 86-051, July 1986.

[51] C. Bühler, *Mikrostrukturen zur Steuerung von Tageslichtströmen*, Inaugural-Dissertation zur Erlangung des Doktorgrades der Fakultät für Mathematik und Physik der Albert-Ludwigs-Universität Freiburg, (PHD-Thesis), May 2003.

[52] LBNL Window & Daylighting Group, *Complex Glazing Database (CGDB)*, http://windows.lbl.gov/software/cgdb, 2015

[53] J. Clarke et. al, *Energy Simulation in Buiding Design*, second ed., Butterworth-Heinemann, 2001. see also *ESP-r whole building simulation model*, http://www.esru.strath.ac.uk/Programs/ESP-r.htm.

[54] DIN 5034, Tageslicht in Innenräumen Teil 1-6, German standard, 2007

[55] J. A. Duffie, W. A. Beckman, *Solar Engineering of Thermal Processes* Wiley-Interscience Publication, 1991.

[56] DOE-2 *is a widely used and accepted building energy analysis program that can predict the energy use and cost for all types of buildings*, http://www.doe2.com/.

[57] EnergyPlus, U.S. Department of Energy, *EnergyPlus Energy Simulation Software 8.1.0*, http://apps1.eere.energy.gov/buildings/energyplus/

[58] EN 410 *Bestimmung der lichttechnischen und strahlungsphysikalischen Kenngrößen von Verglasungen. Glass in Building - Determination of luminous and solar characteristics of glazing.* German Version EN 410:2011.

[59] DIN EN ISO 11664-1, Colorimetry - part1: CIE standard colorimetric observers, international Standard, January 2007

[60] EN 12464-1, *Light and lighting - Lighting of work places - Part1: Indoor work places*, January 2011.

[61] , EN 12898, *Glass in building - Determination of the emissivity*, European standard, 2001

[62] EN 13363, *Solar protection devices combined with glazing - Calculation of total solar energy transmittance and light transmittance. Part 1 with simplified calculation method, Part 2 with detailed calculation method.*, DIN EN 13363-2:2005-06, DIN EN 13363-1:2007-09.

[63] EN 13561 *External blinds and awnings - performance requirements including safety*, European Standard, 2015.

[64] EN 13659 *Shutters and external venetian blinds - performance requirements including safety*, European Standard, 2015.

[65] EN 15251 *Indoor environmental input parameters for design and assessment of energy performance of buildings addressing indoor air quality, thermal environment, lighting, and acoustics*, International Organisation for Standardisation, Geneve, Switzerland, December 2007.

[66] R. G. Foster, I. Provencio, D. Hudson, S. Fiske, W. de Grip, M. Menaker, *Circadian photoreception in the retinally degenerate mouse (rd/rd)*, Journal of Comparative Physiology A, 169(1), pp. 39-50, July 1991, http://dx.doi.org/10.1007/BF00198171

[67] M. S. Freedman, L. R. J. Lucas, B. Soni, M. von Schatz, M. Munoz, Z. David-Gray, R. Foster, *Regulation of mammalian circadian behaviour by non-rod, non-cone, ocular photoreceptors*, Science, 284:502-4, 1999.

[68] F. Frontini, S. Herkel, T. E. Kuhn, *Evaluation of a new method for solar control calculation in the ESP-r building simulation program*, submitted for publication to Energy and Buildings, 2009.

[69] F. Frontini, *Daylight and solar control in buildings: general evaluation and optimization of a new angle selective glazing façade* Dissertation, scuola di dottorato di ricerca, Politecnico di Milano, 2009
ISBN 3-8396-0238-6 (978-3-8396-0238-6)

[70] *Basis for the GS-testing of visual display terminals EK1-ITB 2000:2015*, 1.1.2015

[71] **GUM** JCGM 100:2008 *Evaluation of measurement data - Guide to the expression of uncertainty in measurement*, Joint Committee for guides in metrology (JCGM member organizations: BIPM, IEC, IFCC, ILAC, ISO, IUPAC, IUPAP and OIML), 2008

[72] L. Heshong, *Daylight metrics. PIER Daylighting Plus Research Program* final project report, prepared for the California Energy Commission, CEC-500-2012-053, 387 pages, February 2012

[73] ISO 9050, *Glass in Building - Determination of light transmittance, solar direct transmittance, total solar energy transmittance, ultraviolet transmittance and realated glazing factors*, International Organisation for Standardisation, Geneve, Switzerland, second edition 2003-08-15.

[74] ISO 15099, *Thermal performance of windows, doors and shading devices - Detailed calculations*, International Organisation for Standardisation, Geneve, Switzerland, November 2003.

[75] ISO 15469, *Spatial distribution of daylight - CIE standard general sky*, International Organisation for Standardisation, Geneve, Switzerland, February 2004.

[76] ISO 7730, *Ergonomics of the thermal environment. Analytical determination and interpretation of thermal comfort using calculation of the PMV and PPD indices and local thermal comfort criteria. Deutsche Fassung EN ISO 7730:2005, Berichtigungen zu DIN EN ISO 7730:2006-05*, International Organisation for Standardisation, Geneve, Switzerland.

[77] ISO 9241-303, *ergonomics of human-system interaction - Part303: requirements for electronic visual displays*, international ISO standard, November 2011.

[78] , J.-S. Kang, T.-J. Kim, G.-S. Choi, S.-E. Lee, Development and evaluation of SHGC measurement system for cooling energy saving in buildings, Advanced Materials Research, Vol 689, pp. 176-179, 2013

[79] J. Karlsson, A. Roos, *Modelling the angular behaviour of the total solar energy transmittance of windows*, Solar Energy, 69, 4 (2000).

[80] N. P. Ketema, T. B. Saafir, G. Tosini, , Reviews in endocrine & metabolic disorders, Vol. 10, Issue 4, pp. 271-278, 24.9.2009, doi: 10.1007/s11154-009-9120-x The author manuscript can be found on the US national library of medicine: http://www.ncbi.nlm.nih.gov/pmc/articles/PMC2848671/

[81] J. H. Klems, *Net energy performance measurements on electrochromic skylights*, Energy and Buildings, Vol 33, pp. 93-102, 2001.

[82] C. Kurayama, H. Ishidumi, M. Uwanori, 41002 Study on Test Method for Thermal Performance of Window System : Part 1 Trial Test Apparatus of Solar Heat Gain Coefficient, NII Electronic Library Service, ISSN 1341450X , http://ci.nii.ac.jp/naid/110006566358#article, 2001

[83] Bund-Laender-Arbeitsgemeinschaft fuer Immissionsschutz (LAI), *Hinweise zur Beurteilung und Minderung von Lichtemissionen*, Beschluss der LAI vom 13.9.2012.

[84] W. Lorenz, *A glazing unit for solar control, daylighting and energy conservation*, Solar Energy Vol.70 No.2, pp. 109-130, 2001.

[85] D. L. Marinoski, S. Güths, R. Lamberts. *Development of a calorimeter for determination of the solar factor of architectural glass and fenestrations*, Building and Environment Vol. 47, pp. 232-242, 2012

[86] Ch. Maurer, *Theoretical and experimental analysis and optimization of semi-transparent solar thermal façade collectors*, Dissertation, ISBN: 978-3-8396-0395-6, Fraunhofer Verlag, 2012.

[87] Ch. Maurer et. al. g-Wert-tracker - Outdoor-Charakterisierung von Fassadenkollektoren und BIPV
http://www.ise.fraunhofer.de/de/geschaeftsfelder/solarthermie/themen/thermische-solaranlagen/projekte/laufende-projekte/g-wert-tracker

[88] N. Moghbel, *New model for VDT associated visual comfort in office spaces*, Dissertation, Department of Architecture, Karlsruhe Institute of Technology (KIT), 19.4.2012

[89] P. Moon, D. E. Spencer, Illumination from a non-uniform sky. Illumination Engineering 37, pp. 707-726, 1942.

[90] NFRC 201-210, *Procedure for Interim Standard Test Method for Measuring the Solar Heat Gain Coefficient of Fenestration Systems Using Calorimetry Hot Box Methods*, NATIONAL FENESTRATION RATING COUNCIL, Greenbelt, MD 20770, USA, 2010

[91] Nitz P. M. *Optische Vermessung und Modellierung thermotroper Systeme*, Ph.D.-thesis, University of Freiburg, 1999.

[92] T. Oke, *Boundary layer climates*, London: University paperbacks methuen, 1987.

[93] OPTICAD *Optical Analysis Program*, Opticad Corporation, 511 Juniper Drive, Santa Fe (NM), 87501 USA.

[94] R. Perez, P. Ineichen, R. Seals, J. Michalsky, R. Stewart, *Modeling of daylight availability and irradiance components from direct and global irradiance*, Solar Energy 44 (5) (1990) 271-289.

[95] R. Perez, R. Seals, J. Michalsky, *All-weather model for sky luminance distribution - preliminary configuration and validation*, Solar Energy 50 (3) (1993) 235-245.

[96] J. Pfafferott, *Enhancing the Design and Operation of Passive Cooling Concepts*. Fraunhofer IRB Verlag, Stuttgart, 2004.

[97] , L. Vandaele, P. Wouters, *EU research project PASSYS: The passys services: summary report*, Belgian Building Research, ISBN:90-802301-1-1, 1993

[98] W. J. Platzer, *Energetische Bewertung von Transparenter Wärmedämmung* Fraunhofer ISE Study TOS4-WJP-9705-E01, June 1997.

[99] Platzer W. J., *Solare Transmission und Wärmetransportmechanismen bei transparenten Wärmedämmaterialien*, Inaugural-Dissertation zur Erlangung des Doktorgrades der Fakultät für Physik der Albert-Ludwigs-Universität Freiburg, 1988.

[100] W. J. Platzer, *The ALTSET project. Measurement of angular properties for complex glazings.* proc. of the 3rd int. ISES Europe Solar Congress, Copenhagen, Denmark, 19-22 June 2000.

[101] C. F. Reinhart, O. Walkenhorst, *Dynamic RADIANCE-based daylight simulations for a full-scale test office with outer Venetian Blinds*, Energy and Buildings, 33:7 pp. 683-697, 2001. DOI:10.1016/S0378-7788(01)00058-5

[102] C. F. Reinhart, J. Mardaljevic, Z. Rogers, *dynamic daylight performance metrics for sustainable building design*, Leukos Vol. 3, pp. 7-31, July 2006.

[103] C. F. Reinhart, M. Andersen, *Development and validation of a radiance model for a translucent panel*, Energy and Buildings Vol. 38(7), pp. 890-904, 2006.

[104] A. Roos, J. Karlsson, P. A. van Nijnatten, M. G. Hutchins, P. Polato, E. Nichelatti, M. Montecchi, F. Olive, C. Anderson, *Angular dependent optical properties of coated glazings - validation of two predictive algorithms*, SPIE-Conference, published in proceedings volume 4458, November 2001. http://dx.doi.org/doi:10.1117/12.448261

[105] A. Roos, P. Polato, P.A. van Nijnatten, M.G. Hutchins, F. Olive, C. Anderson, *angular-dependent optical properties of low-e and solar control windows - simulations versus measurements*, Solar Energy 69 (suppl. 6) (2001) 15-26.

[106] J.L.J Rosenfeld, W.J Platzer, H van Dijk, A Maccari, *Modelling the optical and thermal properties of complex glazing: overview of recent developments*, Solar Energy 69 (suppl. 6) (2001) 1 - 13

[107] J.L.J. Rosenfeld, Proc. of the 8th International Meeting on Transparent Insulation Material, Freiburg, Germany, 1996. It is difficult to get the paper, therefore it has been put with the permission of the author on the Fraunhofer ISE web-site: http://www.ise.fraunhofer.de/downloads/pdf-files/paper/paper-rosenfeld

[108] M. Santamouris (Editor), D: N. Asimakapoulus, V. D. Asimakapoulus, N. Chrisomalli-dou, N. Klitsikas, D. Mangold, P. Michel, A. Tsangrassoulis, *Energy and Climate in the Urban Built Environment*, Routledge Taylor and Francis, 2001, ISBN 978-1-873936-90-0

[109] C. Schierz, P. W. Schmits, *Evaluation zur Störung der Anzeigen von LCD-Bildschirmen durch die Beleuchtung = study on the evaluation of disturbing illumination on LCD computer screens)*, by order of the German employers liability insurance association VBG, March 2012.

[110] W. M. M. Schinkel, 1980. Natural convection in air-filled enclosures. Ph. D Thesis, Delft University of Technology. ISBN 90 6231 079 6 soft-bound edition.

[111] Siegel R. und Howell J., *thermal radiation heat transfer*, 4th ed., 2002. Taylor and Francis.

[112] Simpson, J. R., McPherson, E. G., *The effects of roof albedo modification on cooling loads of scale model residence in Tucson, Arizona*, Energy and Buildings, 25 (2), pages 127-137, 1997

[113] H. Sinnesbichler, M. Kersken, G. Haag, Errichtung einer Versuchseinrichtung für energetische, feuchtetechnische und strahlungsphysikalische Untersuchungen an neuartigen Dachsystemen und transparenten Außenkonstruktionen, public final report of the national German research project Nr BMWi-0327240F, 2012

[114] F. Schmidt, U. Krüger, S. Wolf, *Applikationen der ortsaufgelösten Licht- und Farbmessung*, conference "LICHT 2004",19.-22.09.2004, Dortmund http://www.technoteam.de/apool/tnt/content/e6009/e6310/e6076/pb_download6295/TTBV_TUI_Licht2004_ger.pdf

[115] W. Sprenger, *electricity yield simulation of complex BIPV Systems* , PH.D. Thesis, Delft University of Technology, 2013, ISBN: 978-3-8396-0606-3.

[116] P. Strachan, *Addition of Blind/Shutter Control to Transparent Multi-Layer Constructions and Other Improvements to the Solar Routines of ESPsim*, ESRU Occasional Paper, available online as http://www.esru.strath.ac.uk/Documents/90/strachan_solar_mods.pdf

[117] TRNSYS *The Transient Energy System Simulation Tool*, http://www.trnsys.com/

[118] TAS Thermal Analysis Software, http://www.harvardthermal.com/

[119] US Environmental Protection Agency, *Reducing Urban Heat Islands: Compendium of Strategies - Cool Pavements*, 2005, http://www.epa.gov/heatisland/resources/pdf/CoolPavesCompendium.pdf

[120] P. Tregenza, *Subdivision of the sky hemisphere for luminance measurements*, Light. Res. Technol. 19 (1987) 13-14.

[121] Two-Dimensional Building Heat-Transfer modeling software developed at Lawrence Berkeley National Laboratory (LBNL) California, US. http://windows.lbl.gov/software/therm/therm.html

[122] Waldram P. J., *A standard of daylight illumination of interiors*, Illumination Engineering, 2:469, 1909.

[123] O. Walkenhorst, J. Luther, C. F. Reinhart, *Dynamic annual daylight simulations based on one-hour and one-minute means of irradiance data*, Solar Energy Vol. 72(5), pp. 385-395, 2002

[124] Warema Renkhoff GmbH, *Project report about the Main Tower Frankfurt am Main, Germany*, Dok-Nr 999553.12.2008, 2008

[125] G. Ward, R. Shakespeare, *Rendering with RADIANCE. The art and science of lighting visualization*, Morgan Kaufmann publishers, 770p., 1998

[126] Wienold, J., Christoffersen, J.: *Evaluation methods and development of a new glare protection model for daylight environments with the use of CCD cameras*, Energy and Buildings, vol. 38 (2006), p. 743-757.

[127] Wienold, J., *glare caused by reflections of solar panels*, 12th European Lighting conference, Luxeuropa, Krakow, September 2013.

[128] Wilson H. R. W.: *solar control coatings for windows*, EUROMAT ´99 functional materials, vol. 13 (2000), p. 221-233, WILEY-VCH, ISBN-3-527-30254-9.

[129] WIS 1.0. and 2.X β-Versions of the *Advanced Windows Information System*. WIS Steering Committee coordinated by TNO Buiding and Construction Research Delft (NL). Distributed by Energy Research Group University College Dublin. http://erg.ucd.ie/wis/wis.html

[130] H. R. Wilson et. al., *INTERCOMPARISON OF TRANSMITTANCE AND REFLECTANCE MEASUREMENTS OF LIGHT-SCATTERING AND PATTERNED GLASS WITH SPECTROPHOTOMETERS AND INTEGRATING SPHERES*, Internat. Commission on glass technical committee T10, www.icg-tc10.org, 2009

[131] WINDOW 6.3 *is a publicly available computer program for calculating total window thermal performance indices (i.e. U-values, solar heat gain coefficients, shading coefficients, and visible transmittances)* http://windows.lbl.gov/software/window/window.html.

[132] G. Wyszecki and W. S. Stiles, em Color science: concepts and methods, quantitative data and formulae, second edition, ISBN 0-471-39918-3 Wiley Classics Library Edition, 2000).

[133] F. H. Zaidi, J. T. Hull, S. N. Peirson, K. Wulff, D. Aeschbach, J. J. Gooley, G. C. Brainard, K. Gregory-Evans, J. F. Rizzo, C. A. Czeisler, R. G. Foster, M. J. Moseley, S. W. Lockley, *Short-Wavelength Light Sensitivity of Circadian, Pupillary, and Visual Awareness in Humans Lacking an Outer Retina*, Current Biology 17, pp. 2122-2128, 18. Dec 2007, http://dx.doi.org/10.1016/j.cub.2007.11.034